Development of advanced carbon/glass fibre based hybrid composites

Ashok Rajpurohit

PSL UNIVERSITÉ PARIS

THÈSE DE DOCTORAT
DE L'UNIVERSITÉ PSL

Préparée à MINES ParisTech

Development of advanced carbon/glass fibre based hybrid composites

Développement de matériaux composites hybrides avancés à partir de fibres de verre et de carbone

(Confidentielle jusqu'au 28.05.2025)

Soutenue par
Ashok RAJPUROHIT
Le 29 Mai 2020

Ecole doctorale n° 621
Ingénierie des Systèmes, Matériaux, Mécanique, Énergétique

Spécialité
Sciences et génie des matériaux

Composition du jury:

Christophe BINETRUY Professeur des universités, École Centrale de Nantes	*Président*
Richard BUTLER Professor, University of Bath	*Rapporteur*
Josep COSTA Professor, University of Girona - UdG	*Rapporteur*
Frédéric LORTIE Maître de conférences, INSA Lyon	*Examinateur*
Vicky SINGERY Ingénieur R&T, Chomarat Group	*Examinateur*
Sébastien JOANNÈS Chargé de recherche, Mines ParisTech	*Examinateur*
Lucien LAIARINANDRASANA Directeur de recherche, Mines ParisTech	*Directeur de thèse*

MINES ParisTech | PSL

I dedicate this dissertation work to the following …

My *Gurus* and to the all mighty creator *Lord Brahma*,
My late grandfather *Daata Shri Mansingh ji*, my beautiful grandmother, *my Dhai*,
My beloved mother *Jashodadevi*, my pillar of strength my father *Narayansingh ji*,
My siblings *Anuja* and *Harish*
and
My lovely wife *Rekha*.

I dedicate this work and my journey towards achieving this feat to a special person, a father-figure in my life, my late uncle *Swargiya Shri Sanwalsingh ji*, for that I know, he would have been the happiest person to see me achieve what I have today …

गायत्री मंत्र

ॐ भूर्भुवः स्वः ।
तत् सवितुर्वरेण्यं ।
भर्गो देवस्य धीमहि ।
धियो यो नः प्रचोदयात् ॥

Gayatri Mantra

We meditate on the glory of the radiant sun,
may he illuminate our intellect and lead us on to the righteous path.

Rig Veda (Mandala 3.62.10)

भगवद् गीता

कर्मण्येवाधिकारस्ते मा फलेषु कदाचन।
माकर्मफलहेतुर्भूर्मा ते सङ्गोस्त्वकर्मणात्॥

Bhagavad Gita

You have the right to work, but never to the fruit of work. You should never engage in action for the sake of reward, nor should you long for inaction. Perform work in this world, Arjuna, as a man established within himself - without selfish attachments, and alike in success and defeat.

Gita (2.47)

Funding

The research presented in this thesis was done within the framework of the FiBreMoD project and has received funding from the European Union's Horizon 2020 research and innovation programme under the Marie Skłodowska-Curie grant agreement No 722626.

Acknowledgements

The research work presented in the current thesis would be impossible without the support of numerous individuals. It is my pleasure to convey my gratitude and humbly acknowledge everyone who directly or indirectly contributed to this PhD work.

First of all, I would like to express my heartfelt gratitude to my supervisors at Centre des Matèriaux, Mines ParisTech. I thank Prof. Lucien Laiarinandrasana and Dr. Sébastien Joannès for their valuable time, insights, unconditional and unceasing support enabling successful completion of this work in time. Though having a workplace far away from the materials center they made sure my doubts and questions were all answered adequately in time bound manner. I also thank Philippe Sanial and Dr. Vicky Singery, my supervisors at Chomarat for posing their trust in me and providing me the freedom to undertake my experiments in a busy industrial setup.

I am also grateful to the external members of my supervisory and examination committee: Prof. Richard Butler, Prof. Josep Costa, Prof. Christophe Binetruy and Dr. Frédéric Lortie; their input and feedback was indispensable in increasing the quality of this PhD thesis.

I would like to gratefully acknowledge European Union's H2020 funding and thank the coordinators of the FiBreMoD project, Dr. Larrisa Gorbatikh and Prof. Yentl Swolfs for making sure the project was steered and guided successfully .

My colleagues at Chomarat and Mines ParisTech were helpful in many ways to enable me complete this work. I would like to thank my colleagues Claude, Geatan and Julie for helping me with their expertise in fabrication of composites and for fruitful discussions; Gilles, Rapahele and Helene for assisting me with characterization of composite materials at Chomarat Lab; and Jean-Christoph and Julie for fruitful discussion and their assistance in characterization studies in the lab during my stay at Mines ParisTech. I acknowledge support of each and every technician, working in Chomarat's carbon workshop specially, Laurent, Sebastien, Nicolas, Willy and Gaetan, as without them the fabrication of reinforcements and process optimization would not have been possible. I thank Jean-Michel, Thomas, Marine, Jerome, Fabienne, Olivier, Sylvain, Thibault, Nadege, Justine, Simon, Betty, Christophe, Damien,

Pascal and all the project managers and colleagues in the R&D department at Chomarat for their constant encouragement, sharing laughs and for the nice time spend together. I thank each one of my colleague at Chomarat for making me feel home even when we did not share a common language to communicate.

I thank all my fellow PhD scholars in the FiBreMoD project for the great time and discussions we had together. I specially express my thanks to Jan, Faisal, Lorenzo, Arsen, and Francisco, with whom I collaborated during my PhD work and learned from them.

I want to thank all friends I made in India, Germany and France and who have stayed with me during thick and thin. Without naming anyone out of fear of missing uncountable names, I thank each one of them for being there for me when I felt alone.

I am grateful to have in my life, my brother Harish, sister-in-law Bhakti, my sister Anuja, my brother-in-law Radheyshyam ji, my cousins Karan and Ghevarsingh. Since childhood we have grown together, discovering the meaning of life and making the most of it. Very special thanks to my wife Rekha for the courage, motivation and love that she has given me during the whole process. I commend her courage and support. I specially want to thank her and my in-laws Shri Narayansingh ji, Prem ji, Ravi ji and the extended family for being there for me and taking care of our children Rudraksh and Bharti during my absence.

I also want to remember my nephews Medhansh and Rudransh, my nieces Ishita and Ishani; my son Rudraksh and daughter Bharti. Watching them grow helped me and motivated me to grow professionally; their laughs were constant reminder for me and it made me realise how beautiful life is.

Lastly and most importantly, I cannot finish without saying how grateful I am to my parents Shri Narayansinghji and Shrimati Jashodadevi. I wish to thank them for their infinite love, support and encouragement throughout my whole life. I am what I am now because of them and for that, I love them so much. I have no words to acknowledge the sacrifices they made and the dreams they had to let go, just to give me a shot at achieving mine.

Table of contents

List of figures

List of tables

Chapter 1

Introduction

Introduction

L'utilisation de nouveaux matériaux et produits innovants dans divers domaines d'application à un effet important sur la croissance économique ainsi que sur la vie de la population. L'un des principaux défis technologiques et scientifiques pour les ingénieurs composites est de développer de nouveaux matériaux structurels résistants et allégés pour des applications exigeantes telles que l'aéronautique, l'automobile ou l'éolien. Les designers ont à disposition de nombreuses fibres et résines qui leur permettent de concevoir des matériaux composites hautes performances tout en prenant en considération le critère de coût. En général, si une pièce composite est soumise à un chargement complexe (par exemple une combinaison de traction, flexion et un couplage flexion/traction comme dans le ski) et doit satisfaire plusieurs performances, l'utilisation d'un renfort conventionnel ne sera pas appropriée. Pour de telles applications, les composites hybrides sont la combinaison optimale car ils sont une solution efficace pour augmenter la contrainte à la rupture ou améliorer d'autres propriétés tout en réduisant les coûts. Cette thèse a pour but de comprendre le comportement mécanique et l'effet synergique que permet de tels matériaux composites hybrides soumis à différentes conditions de chargement. L'objectif est de développer de nouveaux renforts hybrides unidirectionnels à différents niveaux d'hybridation, pli à pli, nommé inter-plis, fil à fil, nommé intra-pli et fibre à fibre, nommé intra-fil (voir figure 1.2) et d'étudier plus en détail les performances mécaniques de ces composites par rapport à des composites de références non-hybrides ; lors de sollicitations en traction, en compression et en flexion.

Le rapport de thèse est divisé en sept chapitres. Le chapitre 1 est une introduction générale et définit le but et les objectifs des travaux de recherche décrits dans les 5 chapitres suivants (chapitres 2 à 6). Chaque chapitre ayant ses propres axes de recherche (voir Table 1.1). Les interactions et le workflow sont représentés schématiquement dans la figure 1.3. Le dernier chapitre de cette thèse, le chapitre 7, est un résumé global qui inclut les conclusions ainsi que des suggestions d'ouverture pour des travaux futurs.

1.1 General introduction

The global composites end product market is expected to reach an estimated $114.7 billion by 2024 as reported by Lucintel [94] in 2019. Market and Market report in 2017 and Zion Market research of 2019 among others agree in predicting an estimated cumulative average growth rate (CAGR) of 8.2 % up to 2024 [98, 174]. Hence the future of the global composites market looks very attractive with opportunities in transportation, construction, wind energy, pipe and tank, marine, consumer goods, electrical and electronics, aerospace, sports and leisure. Increasing demand for lightweight materials in the aerospace, defence and automotive industry; corrosion and chemical resistant materials demand in construction, pipe and tank industry; electrical resistivity and high flame retardant materials demand in electrical and electronics industry have been identified as major contributing areas for driving this growth. Emerging trends which have a direct impact on the dynamics of the industry, includes, the development of low-cost carbon fibres, high-performance glass fibre, rapid cure resin system and recent trends in hybridization of composite materials. Hence, in the world of composite materials, it is absolutely essential to keep an eye on technology and market trends in raw materials and end use applications. From emerging newer generation of raw materials to design and manufacturing innovations, the pace of continuous innovation and change in the industry is quite remarkable.

Companies across industries have shown an increased interest in thermoplastics in recent years, including car manufacturing companies such as BMW and Audi, and aircraft manufacturers such as Boeing and Airbus. Mordor Intelligence [104] reports that, the thermoplastic composites industry is predicted to grow at a CAGR of 5.29 % between 2018 and 2023. Similarly, the trends in light weighting and low cost composite manufacturing using thermoset resins can be observed in most parts of the world across industries. The demand for carbon fibre reinforced polymers (CFRP) was 125.500 t in 2018 but it is expected to reach 141.500 t in 2019, following a sustained CAGR of more than 10 % reports AVK [12]. This trend follows the same growth pattern previously experienced by composites with other reinforcements such as glass fibres.

Usage of alternative material systems and products in various application fields, in general, has a huge effect on the sustainable world's economic growth as well as people's life as a whole. In an advanced society like ours we all depend on composite materials in some aspect of our lives. Naturally occurring materials such as wood and bones are composite materials, while man-made composites have also been used in several applications since thousand of years, for example, straw and natural fibres in bricks and laminated woods, etc. Fibre reinforced polymer composites are finding ever increasing end uses not only in conventional applications but also in newer high technology as well as high volume applications in the last

Fig. 1.1 Prospective applications for carbon/glass hybrid composites

couple of decades. There is a steady increase in usage of fibre composite materials, both in terms of number of applications for these materials in a wider application field and also in the variety of fibre systems and resin systems that are available to the composite material designers. Designers are always looking for high specific strength, high specific stiffness, enhanced dimensional stability, enhanced energy absorption, corrosive resistance as well as reduced cost while selecting the material systems for a typical composite application.

Composites developed using a single reinforcing material such as carbon may not be suitable for an application if it has to undergo complex loading conditions (such as combination of tensile, bending and bending–torsion coupling, for example, Skiis) during its service life. Hybrid composite materials hence prove to be an optimum solution for such typical applications shown in Fig. 1.1, as they offer an effective way of increasing ultimate failure strain and enhancing some of the other properties while reducing the cost of the developed advanced composite material system. For hybrid composites, it is hypothesised that an effective method of improving the ultimate failure strain, damage tolerance and impact properties of high modulus fibre composites such as carbon composites, is by adding some percentage of low modulus fibres like E-glass or Kevlar in the composites. Such an arrangement would lead to possible decrease in in-plane strengths of hybrid composites

compared with those of high modulus fibre composites. By combining two or more types of fibres, it is possible to club advantages of both the fibres while simultaneously mitigating their less desirable properties for a specific application. Normally one of the fibres in hybrid composites is high modulus, low elongation (LE) or and high cost fibre such as carbon or boron and the second fibre is usually low modulus or high elongation (HE) fibre like E-glass or Kevlar. The LE fibre provides the stiffness and load bearing qualities, whereas the HE fibre makes the composite more damage tolerant and keeps the material cost low.

Carbon and glass fibres is the most popular fibre reinforcements choice for fibre hybrid composites owing to their relevance in multiple application areas. The continuous innovation in materials and designs therefore provides a series of challenges and opportunities for the whole composite manufacturing process chain. Carbon fibre manufacturers are developing new generation of low cost fibres, while glass fibre manufacturers are focusing on glass fibres with improved performance. The textile/preforming and composite manufacturing technologies further needs to be adapted to the production of the final composite for a specific end use. Owing to the drawbacks of existing toughening strategies, extensive over-designing of carbon composites and the strong need for new lightweight materials with improved toughness, reduced costs and having better balance of different mechanical properties, the research interest in fibre hybrid polymer composites using carbon and glass reinforcements has been widely increasing.

1.2 Background and motivation

One of the major technological and scientific challenge for the composite engineers is the development of new stronger as well as tougher lightweight structural materials and design concepts for complex applications such as in aircraft, automotive structures and large wind turbine blade structures. Several fibre types and resin systems are available to the designers who aim to achieve composite product properties such as high specific strength, high specific stiffness, enhanced energy absorption as well as reduced cost for a certain application field. But, in general, if a composite undergoes different loading conditions during its service life and has to satisfy multiple performance conditions, then the composite made from a conventional single reinforcement system may not prove to be suitable. For example, carbon fibre composites have been commercially used in the development of skies, and these composites are also used in manufacturing of spar-caps which is one of the main structural element of wind blades. In these two applications, carbon fibre is a material of choice as it is lighter and stiffer. But on the other hand, the exceptionally stiff carbon reduces the pleasure

of skiing, the fibres have lower failure strain and hence breaks earlier when loaded, and these fibres are costly and hence less competitive in high volume applications.

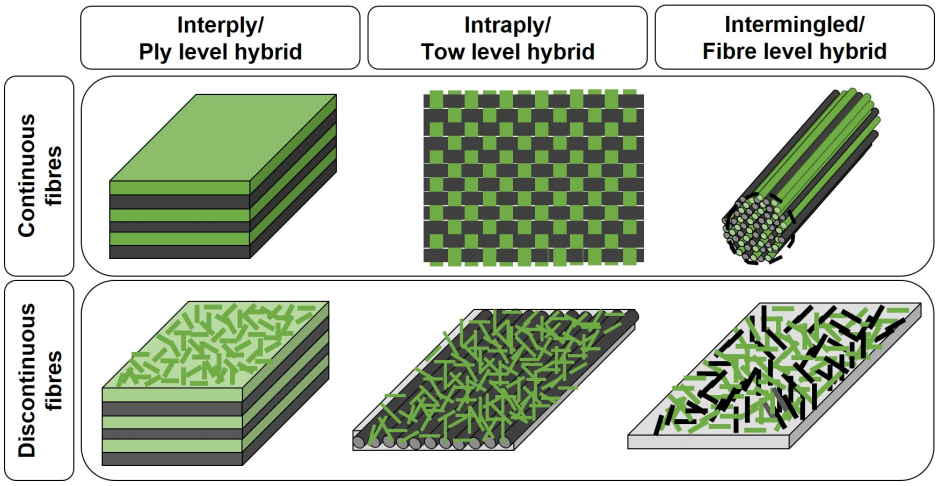

Fig. 1.2 Overview of hybrid configurations at different levels of hybridization

For several such performance based applications, a compromise in one or several properties is rendered essential, and considering this, the hybrid composites prove to be a desired solution, as they offer an effective way of increasing ultimate failure strain and enhancing some of the other properties while reducing the cost of the developed advanced composite material system. In fact, one of the greatest benefits of fibre-reinforced composites over other materials is their potential for design optimisation. Furthermore, not being restricted to a single fibre type expands this design envelope even further. Hybrid composites are therefore a logical evolution towards even more design freedom and hence more possibility for performance optimisation and cost reduction. Hybrid composites have been used for various structural applications due to their enhanced mechanical performance over their non-hybrid counterparts. For fibre hybrid composites, as seen in Fig. 1.2 depending on the way the individual constituents are brought together, there are three major fabrication configurations: interply hybrids or ply level hybrids, intraply hybrids or tow level hybrids and intermingled hybrids or fibre level hybrids. Plenty of investigations, both experimental methods and computational models have been attempted to understand the mechanical behaviour of hybrid composites in tension, compression, flexion, and other mechanical modes [88, 143, 103]. Several studies have been reported on hybrid composites demonstrating combination of different technical polymeric fibres such as carbon, glass and aramid; metal fibres, mineral fibres and natural fibres [88, 148, 120].

The majority of previous work on fibre hybrid composites mainly focuses on the mechanical behaviour and the failure of interply hybrids, while little work has been conducted

on intraply hybrid structures. Work on fibre to fibre hybrids, or so called intermingled hybrid composite for structural applications has been rarely reported. Also, previous studies predominantly rely either on studies on unidirectional composites or those bi-directional composites made out of woven fabric structures. The aim of this study is to develop novel unidirectional hybrid fabrics and their composites with different hybrid configurations, namely, interply, intraply and intermingled; and further investigate the mechanical performance of these composites with respect to reference homogeneous non-hybrid composites, specifically in tensile, compression and flexural loading conditions.

"Fibre-hybrid composites" are the category of hybrid composites which contain two or more fibre types (synthetic fibre with another synthetic fibre or synthetic fibre with natural fibre or synthetic fibre with metallic fibres) embedded in a common polymer matrix. Utilisation of this advanced material system for actual industrial application is still in its nascent stage. This challenge to develop industrial usage of fibre hybrid composites can only be met through an understanding of the relationships between materials architecture, microstructure and mechanical response in complex loading conditions for specific applications. This, hence necessitates development and optimisation of all the process steps in a composite manufacturing process chain, from fabric manufacturing to development of composite processes and further characterization of developed composite coupon samples.

1.3 Aims and objectives

In 2016, European Union's Horizon 2020 research and innovation programme under the Marie Sklodowska-Curie grant agreement initiated funding for the project FiBreMoD, i.e. Fibre Break Models for Designing Novel Composite Microstructures and Applications. The FiBreMoD project aims to train 13 such researchers to become multi-talented and interdisciplinary researchers that will be highly coveted in the field of composites. The researchers worked on one or several aspects so as to fulfil the common goal of the project, that is, to advance state-of-the-art composite failure models to reach the required levels of accuracy and develop advanced and industry-friendly characterization techniques for measuring the required input data. The goal is to enable prediction of composite failure behaviours for new generation of composites by developing new concepts for modelling and prediction and also enabling the experimental validation of these models by actually developing the composites and characterising its mechanical performance.

As a part of the FiBreMoD program, the overall research objective of the reported work in this thesis is to develop novel advanced hybrid carbon and glass based reinforcements and composites and to understand effect of hybridization through the mechanical behaviour

Table 1.1 Summary of the objectives of the five chapters of results.

Chapter	Aims and objectives
Chapter 2	(1) To characterise tensile properties of glass and carbon fibres using conventional and automated single fibre tensile (SFT) test method, and (2) understanding the effect of textile processing on the strength and strength distribution of carbon and glass fibres
Chapter 3	(1) Optimisation of spreading process for glass fibres, and (2) understanding the spreading behaviour of commingled rovings and simultaneous glass and carbon spreading to manufacture novel hybrid reinforcements hybridised at intraply and intermingled configuration
Chapter 4	(1) Development and characterization of novel hybrid interply and intraply textile reinforcements, (2) fabrication, process optimisation and characterization of hybrid composites, (3) physical, mechanical and damage characterization of composites under tensile, compressive and flexural loading conditions, and (4) understanding hybrid/synergistic effect and balance of mechanical properties for carbon and glass composites hybridised in interply and intraply configuration
Chapter 5	(1) Fabrication, process optimisation and characterization of intermingled hybrid composites made using commingled and spread tape reinforcements, (2) physical, mechanical and damage characterization of composites under tensile, compressive and flexural loading conditions, and (3) understanding hybrid/synergistic effect and balance of mechanical properties for carbon and glass composites hybridised in intermingled configuration
Chapter 6	(1) Development of novel thin intraply reinforcements using carbon and glass rovings, (2) translaminar fracture toughness characterization (using multiple data reduction techniques) for hybrid composites and reference carbon and glass composites, and (3) evaluating hybrid effect for thin-ply carbon and glass fibre based intraply hybrid composites

characterization of the developed composites. The research focuses on key mechanical properties such as tensile behaviour, compression behaviour, flexural behaviour and fracture toughness behaviour for potential applications of these hybrid composites in structural applications in the field of wind energy, sporting goods and automotive. To understand hybrid effect at different levels of hybridization, a series of novel unidirectional (UD) textile reinforcements are developed and the processes are optimised for the same. Using these reinforcements, sets of composites are fabricated to enable the characterization of the mechanical behaviour of these composites in the identified loading conditions. Analysis of key process steps and their optimisation also form a critical part of the reported work. To

successfully achieve the overall objective, this thesis is divided into five chapters of results, each with their own research objectives. Table 1.1 summarises the objectives of each of these five chapters.

1.4 Thesis outline

The thesis is divided into seven chapters. Chapter 1, the chapter in which we currently are, provides a general introduction and defines the aims and objective of this research. Chapter 2, 3, 4, 5 and 6 deals with separate topics woven together in order to achieve the overall goals of the work. These chapters have their own set of challenges, therefore, each of these five chapters includes an introduction, an individual discussion on state of the art and literature review, descriptions of the manufacturing techniques and test methods, experimental results and their discussion, and a conclusive summary of the key findings for that chapter.

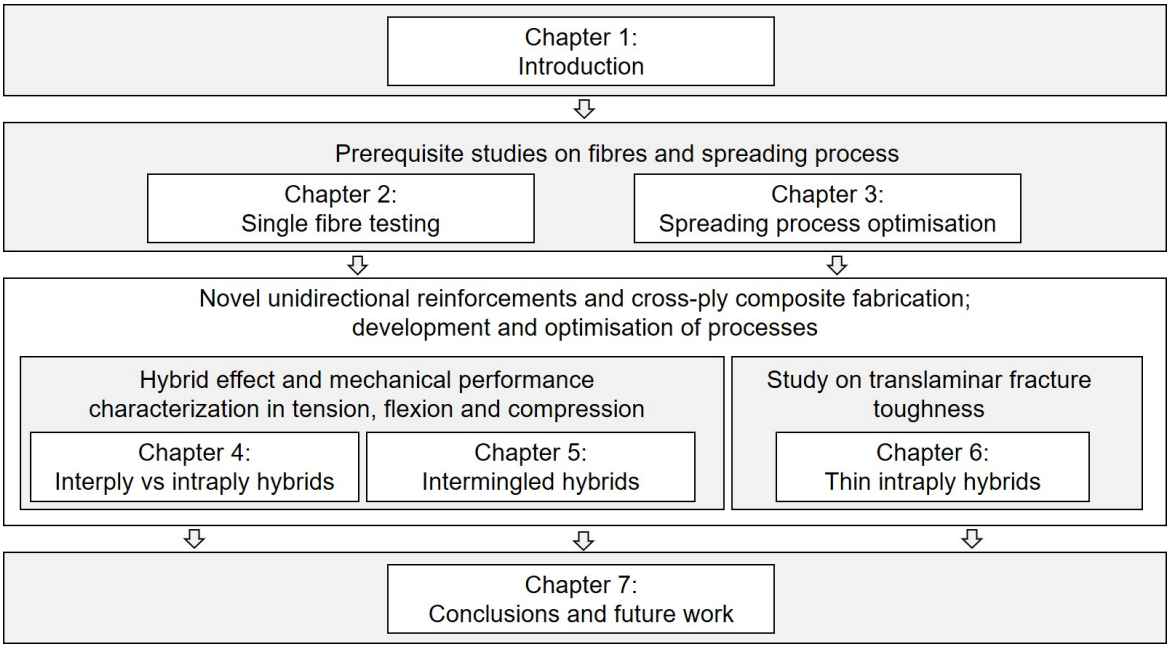

Fig. 1.3 Schematic overview of the chapters and the work flow in the thesis

Chapter 2 provides an essential insight in the textile manufacturing process (multiaxial technology, commingling) and its effect on the strength and strength distribution of input raw material i.e. the fibres. It provides an understanding on the input parameter; the single fibre strength, that needs to be used in the prediction and modelling tools. Chapter 3 discusses the textile process of spreading and its optimisation so as to develop new generation of thin-ply composites reinforcements using carbon, glass and their combinations. On the basis of the

results from Chapter 3, intermingled hybrid composites are fabricated and characterised in Chapter 5 to understand the hybrid effect in intermingled (fibre-level) hybrids vis-à-vis results for hybrid effect in interply (ply-level) and intraply (tow-level) hybrids from Chapter 4. Furthermore composites with different hybrid microstructure were developed using the thin-ply reinforcements to understand the translaminar fracture toughness behaviour of intraply hybrid composites in Chapter 6. The interaction between the chapters is schematically presented in the Fig. 1.3.

The final chapter, Chapter 7 of this thesis provides an overall summary and conclusion of this research as well as the suggestions for future work.

Chapter 2

Experimental investigations on single fibre tensile tests

Investigations expérimentales autour des essais mono-filamentaires

Ce chapitre traite de la caractérisation expérimentale à l'échelle mono-filamentaire et discute notamment des propriétés obtenues lors d'essais de traction sur fibres unitaires. Les défis que cela représente pour des fibres de verre et de carbone, une dizaine de fois plus fines que des cheveux, sont présentés. Afin d'étudier et comprendre l'effet des procédés textiles sur la résistance des fibres, une analyse statistique des performances en traction mono-filamentaires a été réalisée sur des fibres T700S pour le carbone et E-CR Advantex pour le verre. Cette étude permet également de statuer sur les données « fibres » à considérer lors des simulations multi-échelles : les données issues de la bobine sont-elles représentatives de celles des fibres situées au sein d'un renfort textile ? L'accent est mis sur le traitement statistique de ce grand nombre de données et la nécessité de quantifier finement les incertitudes.

Ainsi, l'introduction du chapitre est suivie d'une section sur l'état de l'art (Section 2.2) des fibres techniques et de leur caractérisation mécanique. La Section 2.3 décrit en détail les matériaux fibreux utilisés à différentes étapes de la transformation textile ; la caractérisation sur fibre unitaire est également développée dans cette section. Enfin, la Section 2.4 examine les résultats des tests mono-filamentaires, leur importance et leurs implications pour toutes les fibres testées aux différents stades de la transformation textile.

Les conclusions de cette étude sont présentées en Section 2.5. De par leurs diamètres très fins, les résultats sur les fibres de carbone font apparaître la conséquence d'une « présélection ». Une partie de la population des fibres est en effet inaccessible car les fibres les plus fragiles sont cassées lors de l'extraction, les données sur leur résistance ne sont donc pas connues. La rigidification des fibres de carbone lors de l'essai de traction peut également être observée, ce qui n'est pas le cas pour les fibres de verre. Il peut être conclu que les écarts observés sur les distributions à rupture aux différents stades des transformations textiles ne sont pas significatifs. Les procédés étudiés n'endommagent que très peu les fibres et les données obtenues plus facilement sur bobines peuvent être exploitées à des fins de simulation.

2.1 Introduction

This chapter describes the experimental characterisation and results of fibre properties obtained through single fibre tensile tests. In this chapter, solutions and recommendations to overcome some of the difficulties in the single fibre testing are proposed. For T700S carbon fibres and E-CR Advantex glass fibres, a scientific and statistical evaluation is made available for the designers and manufacturers to understand and confirm the effect of textile processes on the single fibre strength and its distribution. This chapter also answers the so far unanswered question, if in simulations it is ideal to use fibre input data for fibre strength from the as received raw bobbin or from the intermediate textile product such as a fabric preform. Emphasis in the chapter is also given to understand the uncertainties in the automated characterisation of the single fibre strengths and how it affects the strength and Weibull parameters.

This chapter is divided into five sections. The introduction of the chapter is followed by a section on the state of the art (Section 2.2) on technical fibres and their characterisation using single fibre tests. This section also describes in detail the issues with single fibre characterisation and the process of analysing the single fibre tests by utilising suitable statistical distributions. It discusses in short the textile process of conversion of a roving/tow into a non-crimp fabric. Section 2.3 describes in detail, the fibre materials used from various textile processing stages. Emphasis in this section is laid on the actual process steps for experimental characterisation using single fibre tests. Finally Section 2.4 discusses the results of single fibre tests, their significance and implications for all the fibres tested at different processing stages and test conditions. Conclusion of the study is reported in Section 2.5. The schematic overview of the experimental and scientific section of this chapter is presented in Fig. 2.1.

2.2 State of the art

Variability in the performance of composite materials arises mainly from the variability in constituent properties, fibre distribution, structural geometry, loading conditions and also manufacturing process. For numerous applications exploiting high performance composite materials, in-service safety and reliability assessment is a key challenge for engineers [135]. Composite materials made using technical fibres such as carbon, glass and aramid fibres are ideally used for structural applications such as in automotive, aerospace and defence applications, and their performances depend largely on the mechanical behaviour of its constituents and especially on the strength of technical fibres which it is made of. Fibres

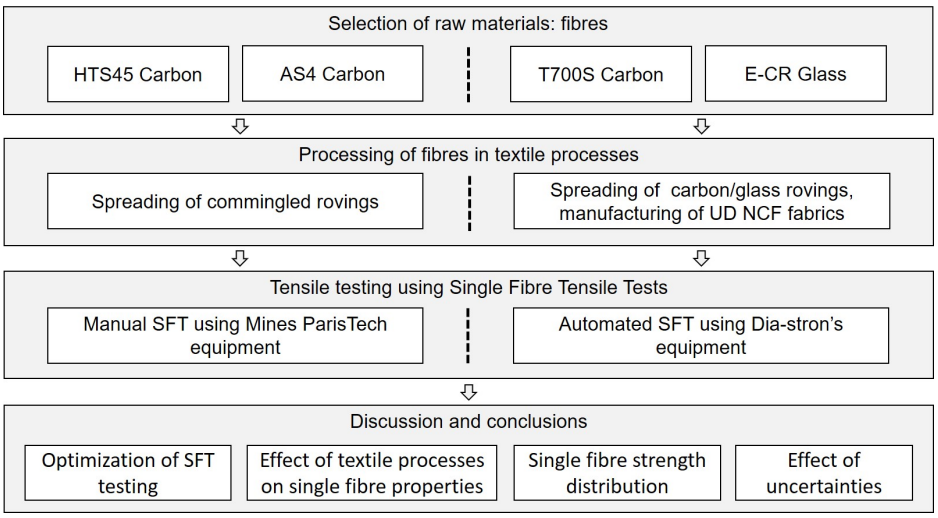

Fig. 2.1 Schematic overview of the experimental (Section 2.3) and scientific (Section 2.4) sections of this chapter.

are the principal load carrying component of composite structures and their characteristics significantly influence the effective mechanical and damage properties of the composites fabricated from it. Researchers have been working on simulation and modelling tools to understand and predict the failure behaviour of composites for many years. It is essential that the simulation or modelling tools are provided with accurate input parameters. One of the most important input parameters for composite modelling tools is fibre strengths and its distribution; and correctly capturing fibre strength statistics and failure kinetics is crucial. It can be safely said that, the success of a stochastic model for predicting strength of composite materials depends largely on how accurately the input parameter such as single fibre tensile strength is measured [25, 146, 147]. In most of the micromechanical analysis techniques the mean or average properties are used, but the variation of properties can also have significant effect on the simulated results. Hence, it is absolutely essential that the statistical information such as the distribution of a particular property around its mean value be also taken into consideration for detailed micromechanical analysis [25, 70].

Fibre strength information is essentially used by both the composite designers and manufacturers of textiles and composite materials. For reinforcement manufacturers it is important that the single fibres in their roving contribute to a maximum extent in the strength of the composites. The objective of the textile manufacturers is to avoid misalignments, avoid fibre breakages such that no deterioration in the strength of the fibre population occurs during the processing of fibres from roving stage to the textile semi finished product stage. It is essential for the textile manufacturer to make sure that the processes and process parameters used to manufacture a specific semi finished product using the raw bobbin (as received

rovings) do not affect the fibre strength and its distribution. If in the process of manufacturing the textile, excessive heat, vibration or friction deteriorates the single fibre strength, then, modification in process parameters or the process itself can be considered. Further, it is important for designers to understand the reliability of a composite product. This is usually done by simulating the strength of the product using the known strengths of its constituent fibres from the bobbin. Hence for successfully predicting the performance and reliability of composite product it is absolutely essential to know the strength of the fibres and its confidence bounds.

Characterisation of single fibres is always challenging owing to their micron level fibre diameter and that the mechanical test is very time consuming and requires a great deal of manual intervention. Despite great progress in characterisation techniques including introduction of automated test equipment's [69, 83], many obstacles still remain to obtain accurate fibre strengths and distributions. Several previous studies have acknowledged these difficulties in accurately obtaining fibre strength data [106, 153, 109]. In the current work solutions and recommendations to overcome some of the difficulties in the single fibre testing are proposed. For T700S carbon fibres and E-CR Advantex glass fibres, a scientific and statistical evaluation is made available for the designers and manufacturers to understand and confirm the effect of textile processes on the single fibre strength and its distribution. This work answers the so far unanswered question, if in simulations it is ideal to use fibre input data for fibre strength from the raw bobbin or from the intermediate textile product such as a fabric preform. Emphasis in the current work is also given to understand the uncertainties in the automated characterisation of the single fibre strengths and how it affects the strength and Weibull parameters.

2.2.1 High performance fibres

Owing to their low density, high strength and modulus, advanced fibre reinforced composites have become critical components for modern aircraft and aerospace vehicles. The characteristics have also contributed to the application of advanced composites in other fields, from automotive components, wind energy to electronics to recreation products in sports and leisure. With lowered production costs, a vast expansion of their applications to many other areas is possible, making them of even greater economic importance. Development of all these new product and applications fields have arisen due to use of newer generation of cost effective fibre materials in the form of high performance fibres such as carbon, glass and aramid among other fibres.

Carbon filaments were first produced in the 19^{th} century by the pyrolysis of cellulosic fibres and they were used as experimental filaments for the first trials of electric light bulbs.

The carbon–carbon bond being the strongest in nature and it was expected that such fibres would prove to be a valuable structural material. But, for carbon fibres made from cellulosic fibres with poorly organised atomic structure had just 24 % carbon by weight and hence were not as stiff as they were expected to be. The commercial production of carbon fibres made from polyacrylonitrile (PAN) began in the 1960's and today they have become the most widely used form of carbon fibre. The first industrial uses for PAN-based carbon fibres were in the aerospace and sports goods fields. While aerospace industry has adopted carbon fibre composites as a major structural material, latest generation of planes, such as the Airbus A380 and Boeing 787, use around 35 t of carbon fibre reinforced plastics (CFRP) for each aeroplane to reduce weight, to get better mileage and to improve passenger comfort.

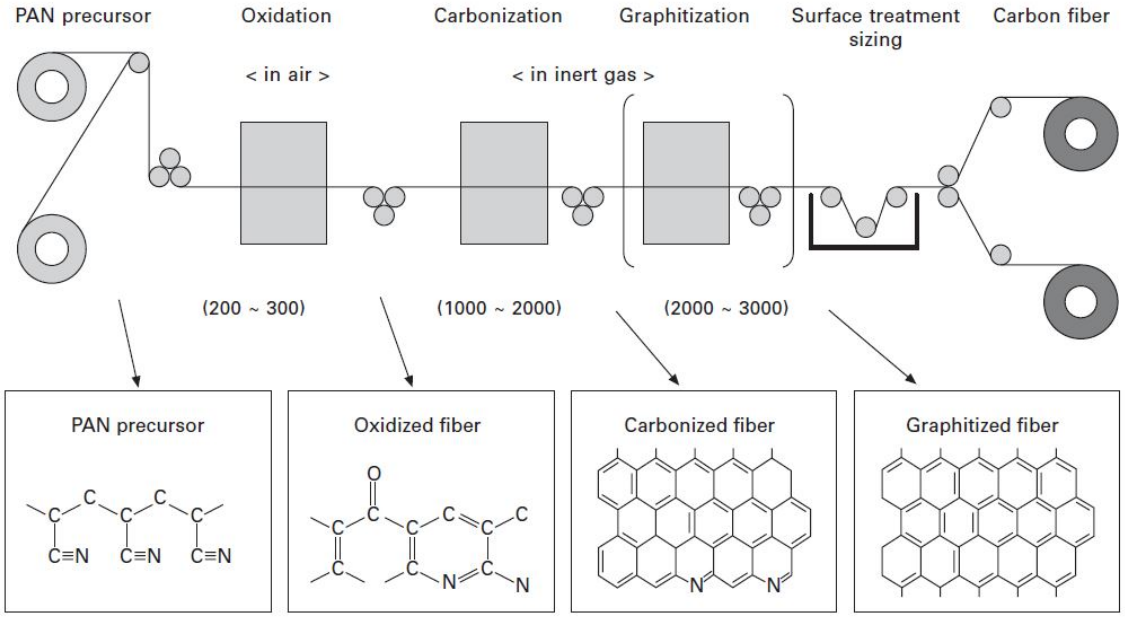

Fig. 2.2 Processing steps and parameters for PAN-based carbon fibres [100].

Based on the type of precursor used (PAN or Pitch based) and the parameters of processing of the precursor at several stages (temperatures in carbonization or graphitization steps), phase/medium of processing at various stages as well as the type of surface treatment as seen in Fig. 2.2, the properties of carbon fibres; their strength, stiffness and diameters can vary in a wide range.

Unlike carbon fibres, glass fibres a type of inorganic fibre have been known for centuries but the use of these kind of fibres in technical applications started only in early 19^{th} century. Contradicting the general definition of high performance fibres, the glass fibre has an isotropic three-dimensional network structure and is not crystalline. The main constituent of glass is silica (SiO_2) and depending on the proportion of silica and other constitutes the glass fibre can

be made into several types, those with enhanced electrical properties, or corrosion resistance, etc. Silica melts at very high temperature and it rapidly crystallises on solidification, both these factors pose a difficulty in processing of glass. A typical schematic representation of a typical continuous filament fibre glass production process is depicted in Fig. 2.3. The molten glass will normally flow out of the bushing under the force of gravity into fibres on the order of 1 mm diameter. The final diameter of the glass fibre is a strong function of the tension applied to the fibre as it is being drawn. Tension increases with lower glass temperatures (higher glass viscosity) and with higher pull speeds. Both temperature and pull speeds are process variables that are adjusted to obtain the desired fibre diameter and hence the mechanical properties of the glass fibre.

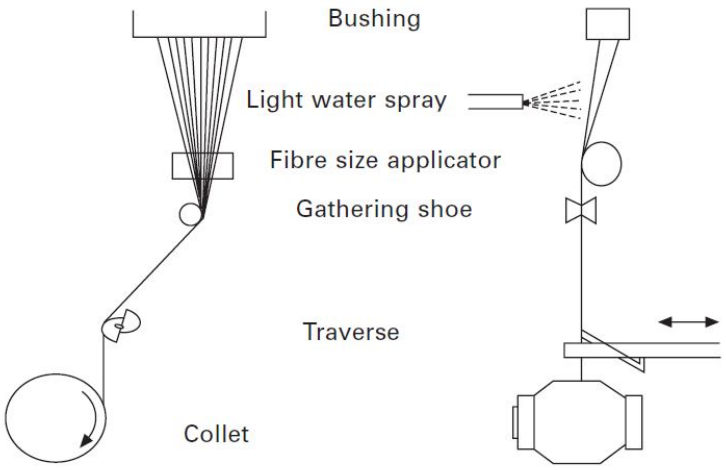

Fig. 2.3 Schematic of melt spinning process for glass fibre production [81].

For glass fibres, the tensile modulus is a function of the chemical forces operating within the amorphous network and tensile strength is a function of composition. Like carbon for glass too, the strength is not the fundamental material property because it depends heavily on the presence of defects and flaws within the structure [16, 173].

2.2.2 Characterisation of technical fibres

Characterisation of technical fibres in general includes many fibre characteristics such as physical, electrical, optical, thermal, chemical and magnetic properties of the fibre material. The interest of the current study is characterising the tensile properties of the fibres. The most popular methods through which the tensile properties of technical fibres can be characterised are: (1) the single fibre tests [44], (2) bundle tests [31] and (3) fragmentation tests [37] and the schematic of the test methods are presented in Fig. 2.4. The single fibre test is the most

straightforward but a very tedious and time-consuming process for testing fibres. With the bundle test method, a bundle of fibres or rovings is tested by applying a load and observing the behaviour of the bundle as a whole. This bundle fibre test is simple to conduct but the analysis of the single fibre properties from this test is not very straightforward. The bundle fibre test for technical fibres is generally performed on the fibre bundle which is embedded in resin. The fibre fragmentation test usually embeds a single fibre inside a polymer matrix and the composite is tested to determine the parameters for fibre strength distribution. Each kind of method for characterisation has its own limitations. Taking into consideration the limitations, the classical single fibre testing process still appears to be one of the most reliable means of characterising fibres or exploring their morphology. The individual steps in single fibre testing, however, leave scope for improvement. If the existing problems could be solved, the efficiency of the processes could be significantly improved.

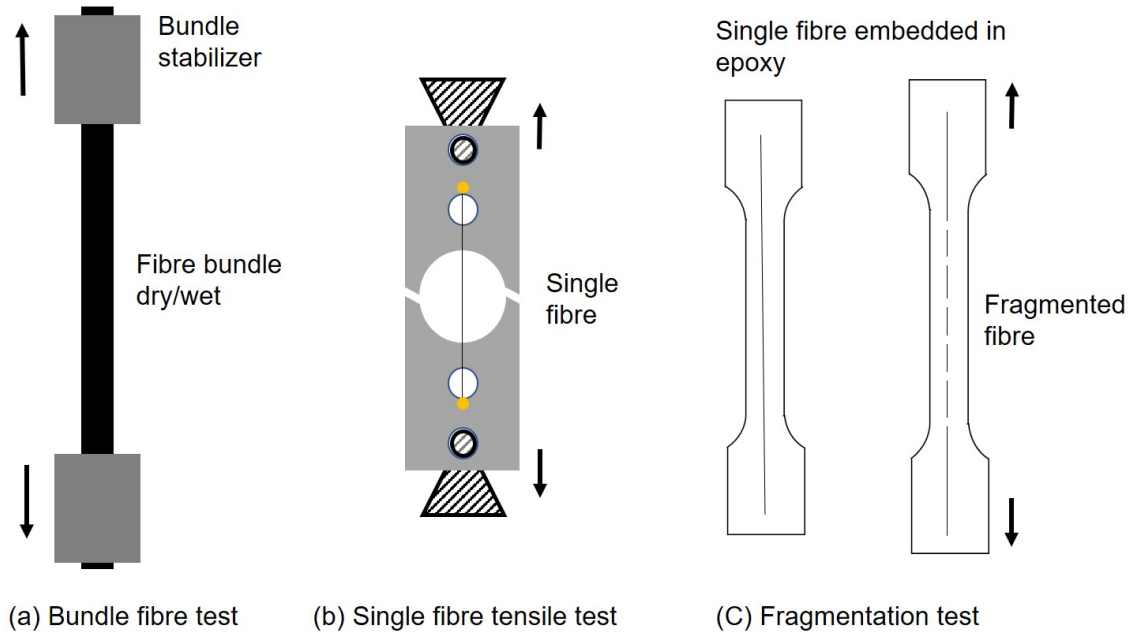

Fig. 2.4 Schematic of popular tests for characterisation of technical fibres.

Tensile strength for the fibres is expressed in terms of stress (σ), particularly the ultimate or break stress as it allows the comparison between different fibres or same fibres with different fibre fineness. Stress (σ) is defined as the force (F) applied to the sample divided by the cross-sectional area of the fibre (A) and having diameter (d) assuming the fibre to be circular.

$$\sigma = F/A \tag{2.1}$$

$$\text{where, } A = \pi \times d^2/4$$

Technical fibres such as glass or carbon fibres typically do not elongate very much during the tensile testing process, though they have variability in initial cross-section throughout its length they specifically do not experience a significant change in cross-sectional area due to tensile testing. Also these fibres do not yield and so have a linear stress-strain curve. The modulus of elasticity (E) or Young's Modulus is a measure of the stiffness of the fibre and as a first approximation for fibres with strain <5 %, it can be determined from the slope of the stress-strain curve. Experimentally, the modulus is calculated by dividing the ultimate breaking stress by the strain (ε) for the fibre as in the equation below.

$$E = \sigma/\varepsilon \tag{2.2}$$

For technical fibres, reporting accurate properties is very critical for considering its utility in several structural applications. The assumption of circular cross-section is in general valid for carbon and glass fibres, but the assumption of linearity of the stress strain curves for these fibres can be critical for carbon fibres. Diameter data is also important as it affects the value of the determined stress and through it, the value of the elastic modulus and fibre strength. Therefore, it is also essential that the diameter measurements be as accurate as possible.

2.2.3 Fibre strength distribution

Strength of a technical fibre cannot be just expressed in terms of its mean value and its standard deviation. The fibres such as carbon and glass fibres are brittle fibres and along their physical structure they tend to posses some regions where they are weaker. This means, when these fibres are loaded the fibre tends to break at these weaker places and hence the probability of failure of the fibre depends on the probability of existence of such weaker regions. One can hence based on weak-link theory, logically say that the shorter fibres will have higher strengths, as the probability of finding a weak region (or flaw) for shorter lengths is lower. This kind of size dependency in fracture mechanics was first explained by Griffith [54], he concluded the size dependency is based on the microscopic flaws in the material. Weibull model [163] is an approximation of the weak-link process which is well suited if enough defects or weak places are considered in the material. Todinov [154] further proved that the Weibull distribution predicts correctly the probability of failure locally initiated by flaws if and only if the probability that a flaw will be critical is a power law or can be approximated by a power law of the applied stress.

The standard 2-parameter based Weibull probability distribution (P) for fibre strength is defined as:

$$P(\sigma_f) = 1 - exp\left(-\left(\frac{L}{L_0}\right)\left(\frac{\sigma_f}{\sigma_0}\right)^m\right) \tag{2.3}$$

where, L is the characteristic gauge length, L_0 is the reference gauge length, σ_f is the fibre strength, σ_0 is the scale parameter and m is the shape parameter or Weibull modulus [163].

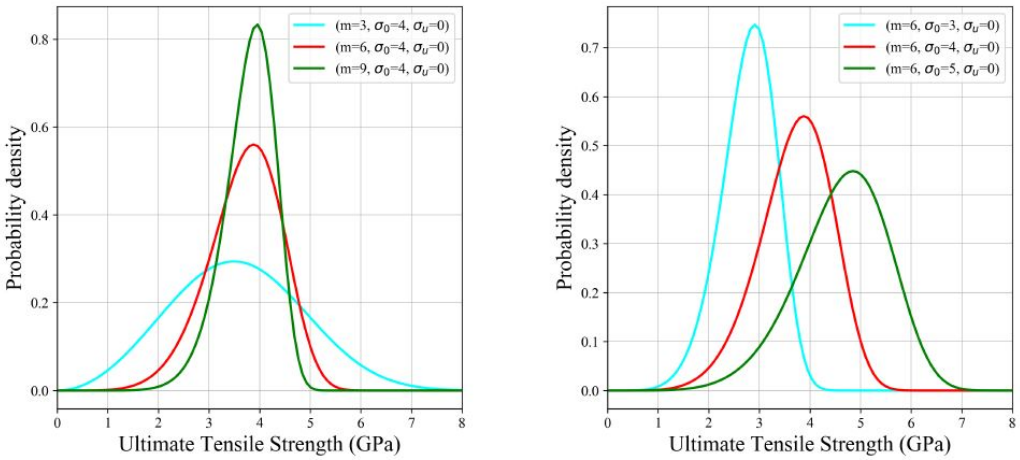

(a) Effect of shape parameter (m)

(b) Effect of scale parameter (σ_0)

Fig. 2.5 Effects of the shape (m), scale (σ_0) on a 2-parameter Weibull distribution [68].

Majority of strength models uses this as standard Weibull distribution, where the scale parameter σ_0 represents the strength at which 63.2 % of the fibres will fail, while, the Weibull modulus m determines the scatter around the average value. As seen in Fig. 2.5, a large Weibull modulus indicates a narrow distribution, which corresponds to little scatter in the fibre strength. This distribution assumes that the cross-sectional area of the fibre is constant along the length before and during the loading. This distribution also assumes the value of the threshold stress (σ_u in 3-parameter Weibull distribution) to be zero, where, σ_u is the minimum stress value below which the failure probability is Zero. It is important to note that for most experimentally generated data sets for single fibres, a lower limit on fibre strengths is observed, however, this can also be probably due to experimental limitations.

$$P(\sigma_f) = 1 - exp\left(-\left(\frac{L}{L_0}\right)\left(\frac{\sigma_f - \sigma_u}{\sigma_0}\right)^m\right) \tag{2.4}$$

It is experimentally very difficult to reliably measure or to prove that the minimum strength of the fibre is σ_u and hence most of the researchers consider the minimum strength of the fibre to be zero, thus converting the original 3-parameter Weibull distribution Eq. 2.4 to the standard 2-parameter standard Weibull distribution as in Eq. 2.3. The effect of this assumption on the tensile strength can easily be evaluated with the help of simulation but experimentally it is still not proved if the threshold exist and what is the value of the threshold.

As the modelling of composite materials is at micro scales, the Weibull distribution also needs to be extrapolated to short gauge lengths which is not very accurate as the

assumptions such as constant failure strain at any gauge lengths are no longer valid for very short gauge lengths. This extrapolation can yield $\sigma_{(0,2)}$ which is corresponding strength at the extrapolated gauge length $L_{(0,2)}$ with respect to the measured $\sigma_{(0,1)}$ at the gauge length equal to $L_{(0,1)}$ as in the equation below:

$$\sigma_{(0,2)} = \sigma_{(0,1)} \left(\frac{L_{(0,1)}}{L_{(0,2)}} \right)^{(\frac{1}{m})} \tag{2.5}$$

Modified Weibull distributions have also been reported in the literature. Eqs. 2.3 and (2.4) represent uni-modal Weibull distribution and hence assumes there is only one type of flaw in the population. But this may not be true for technical fibres such as carbon and glass; and that the flaws may be originating at different processing and handling stages [153]. Bi-modal distribution which is the most popular multi-modal distribution can be represented in the following form:

$$P(\sigma_f) = 1 - exp\left(- \left(\frac{L}{L_0} \right) \left(\frac{\sigma_f}{\sigma_{(0,x)}} \right)^{m_x} - \left(\frac{L}{L_0} \right) \left(\frac{\sigma_f}{\sigma_{(0,y)}} \right)^{m_y} \right) \tag{2.6}$$

where, $\sigma_{(0,x)}$ and $\sigma_{(0,y)}$ are the scale parameters, and m_x and m_y are the Weibull moduli for the first and second flaw population, respectively. This distribution is very difficult to use if no evidence of two types of defects are existing and in that case, for each fibre tested, one has to classify the failure break due to either defect type.

Similarly, a power law accelerated Weibull distribution is also reported [162] by adding the term α in the Eq. 2.3 in such a way that, using $\alpha = 1$ in this new Eq. 2.7 reduces it to the original Eq. 2.3.

$$P(\sigma_f) = 1 - exp\left(- \left(\frac{L}{L_0} \right)^{\alpha} \left(\frac{\sigma_f}{\sigma_0} \right)^{m} \right) \tag{2.7}$$

Curtin [34] proposed the "Weibull of Weibulls" distribution assuming that the strength distribution along a fibre follows the standard Weibull distribution. Based on this Weibull distribution, a characteristic strength at a certain length L can be calculated for each fibre. He then assumed that the characteristic strengths of each fibre are different and also follow a Weibull distribution. Deriving inspiration from Berger and Jeulin [17], Islam et al. [70] proposed a truncation parameter to represent single fibre strength data set thereby demonstrating a Truncated Weibull distribution. Several other types of distributions have also been reported but not all of them are based on solid theoretical background. In the current work we used a 2-parameter Weibull distribution for the comparative studies.

2.2.4 Issues with single fibre tensile (SFT) test

Despite great progress in characterisation techniques, many obstacles remain to obtain accurate fibre strengths and most studies have reported the difficulty in obtaining fibre strength data which can accurately represent the entire fibre population for each application. Standard SFT involves the following steps as per the ASTM D3822 (for natural and man-made fibres), C1557 (for ceramic, glass or carbon fibres) and ISO 11566 (for carbon fibres) test procedures [10, 9, 72]: (1) Preparation of the sample, (2) measurement of the diameter, and (3) tensile testing. For a manual SFT test, the steps can be schematically represented as in Fig. 2.6. SFT though being the best possible alternative for fibre characterisations, it however has its limitations: complex sample preparation, misalignments, lengthy and time-consuming process, limited gauge length and prone to errors because of major human intervention [70, 146, 147] are some of them. The characterisation of fibres through SFT is hence challenging, but it is the only feasible option to obtain fibre strength data to be fed into the micro-mechanical models and was thus used in the present study.

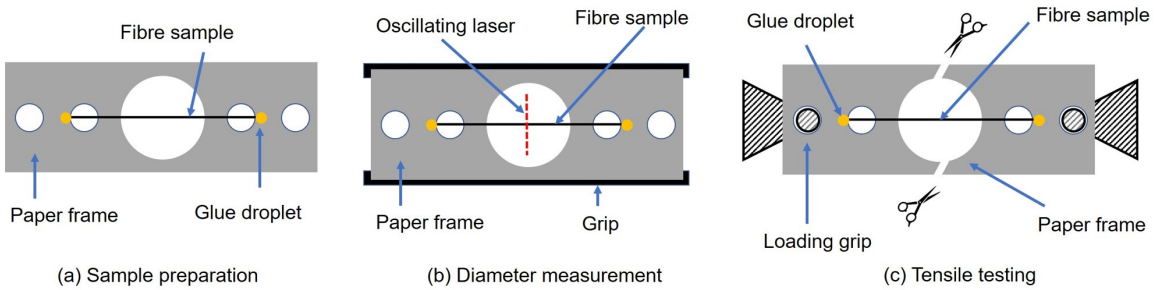

Fig. 2.6 Schematic of manual single fibre testing process steps.

2.2.4.1 Preparation of sample

As the name suggests, the sample preparation for single fibre testing essentially involves extraction of a single fibre from a bunch of fibres called rovings or from a textile semi-finished product such as fabrics or mats. It is the most critical step, owing to the time consumed and manual intervention required in it. Absolute care here is essential that no unnecessary stress is applied on the fibres that may eventually damage or break them, hence not letting one to test that fibre [153, 70]. The cohesion between fibres can be reduced to simplify the extraction process by treating the bunch of fibres with a solvent such as ethanol or by using static discharge methods. In the sample preparation process, there is lot of human intervention and every interaction adds to the uncertainty and bias because of preselection i.e. failure of fibre sample before testing. This step is tiresome and time consuming, hence

the prime reason which limits the number of tests that can be made for a sample population. Apart of inherent variability in the fibres, several issues (preselection, misalignment and incorrect gauge length, etc.) that exist in single fibre testing (both manual and automated process) originates from this step.

2.2.4.2 Measurement of fibre diameter

The most widely used methods for measuring diameter for technical fibres have been: (1) optical microscope method, (2) scanning electron microscope (SEM) method, and (3) laser scanning method. It has been found that the SEM method produces high-quality fibre images for diameter estimation, but it is impractical to use for fibres that are also needed to be tested for strength. The same problem exists for diameter measurements using optical microscopy, but it is an alternative low cost and lesser time-consuming method. Diameter measurement using optical microscopy proves to be problematic for transparent fibres such as glass, since accurate boundary of fibre is hard to locate and this leads to high uncertainty in the measurement. Laser diffraction system (LDS) is a very practical method for determining opaque fibre diameters that are also to be tensile tested [48, 115]. Although LDS is the best possible method for opaque fibres such as carbon, it is not always the best choice for transparent fibres like glass for which people have used Laser scanning micrometer (LSM) principle. The LDS and LSM methods are beneficial also because they require very little preparation specific to diameter measurement and they provide the possibility to measure diameters at several hundred points along the length and continuously along the cross-sectional surface.

2.2.4.3 Tensile testing

Tensile testing of single fibres can be done using a universal tensile testing machine which can operate at very low load and displacement levels. Commercial tensile test equipment are available, while there are also in house developments of tensile testing equipment such as one from Bunsell and Hearle [24]. Most of the modern tensile test equipment's such as Diastron's LEX820 / LDS0200 system, the pre-tensioning of the specimen to be tested is done so as to straighten the fibre and the corrected gauge length is further used for stress and strain calculation. The manual method of SFT sometimes do not provide the opportunity for misalignment correction and gauge length correction. The major difference between the manual SFT and automated SFT can be attributed to this step of fibre testing owing to barely minimum human interference during this step in automated SFT tests.

2.2.5 Textile non-crimp fabrics

An ideal composite material is one which is made using unidirectional tapes, placed by hand or by robot and consolidated in an autoclave, has ideal fibre placement and the best local mechanical properties due to the unidirectional (UD) microstructure of the reinforcement. One such reinforcement is a "prepreg" (pre-impregnated unidirectional textile sheet), but as we know, the manufacture of composite parts using prepregs has its own limitations and is cumbersome, costly and not suitable for high volume production. Prepregs also have a limited shelf life. Composite parts can also be produced using out-of-autoclave manufacturing processes, which uses dry reinforcement in the form of woven fabrics, is relatively cheap and takes advantage of easy handling of large stacks of the fabric. The use of woven fabrics pose several limitations among them the crimp is the most prominent one. Due to crimp the fibres deviate from their ideal directions, create resin rich zones and affect adversely several mechanical properties [92]. Hence the challenge to create a reinforcement which would combine unidirectional fibres while imparting structural integrity, ease of handling and drapeability. This long-standing challenge faced by designers of composite material to combine a perfect placement of the reinforcing fibres with easy, inexpensive, automated manufacturing of the composite part is answered by using so called non-crimp fabrics (NCFs) [129].

NCFs are a type of engineered fabric used to reinforce polymeric composites that are made up of multiple layers or fibres stitched together. The most used NCFs are bi-axial, triaxial and quadraxial fabrics, where the fibre tows are straight and with different orientations (0, 45, 90 degrees) to provide multidirectional properties. The combination of multiple layers of fibres, stacked in just one fabric, leads to faster and cheaper preforms production processes than single layer based processes. NCF reinforced composites generally fare superior in its mechanical properties compared to other dry fibre reinforced forms as the tows are not crimped or woven and they also posses better delamination resistance and impact strength. The excellent conform-ability of bi-axial fabrics under convex-concave deformation conditions (though not better than woven fabrics) is caused by a slippage of the fibre tows as there is no joints that restrict this movement. This is why the use of NCF is rapidly growing in aircraft, automotive, wind energy and other complex structural components.

The fabrication of a warp knitted NCF fabrics for high performance applications essentially involved two steps as seen in Fig. 2.8: (1) spread tape manufacturing and (2) layup and stitching. Spread tape manufacturing is a critical step where the individual rovings are spread and brought together to produce a uniform tape, normally 10 inches wide (but can be adjusted to any other width) wound on a metal beam. These beams are further mounted on the multi-axial machines, where different heads, lay the spread tapes on the conveyer belt in

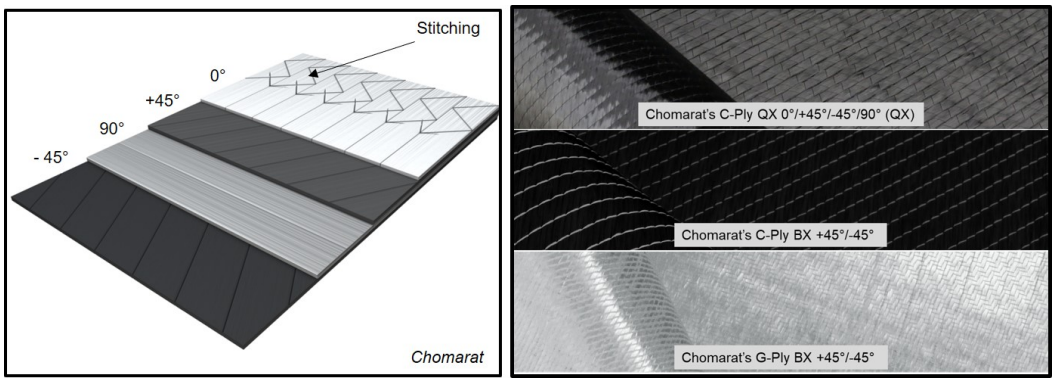

Fig. 2.7 Schematic set-up of a multi-axial warp-knitted non-crimp fabric and pictures of non-crimp fabrics.

different directions as per the requirement as seen in Fig. 2.7. The conversion process from bobbin to spread tape introduces lot of stresses on the fibres, due to friction and abrasion at the guides and at the vibrating bars in the mechanical spreading zone. Introduction of heat in the range of 100 to 180 °C is also essential for softening the sizing and facilitating the spreading process. Further the laid layers of spread tape are consolidated by stitching the layers together; stitching also caused friction and fibre breakages depending on the type of fibres and stitching parameters used. It is possible that the process of conversion from bobbin to fabric causes lot of fibre breaks and may affect the fibre strength distribution in the textile material. No study as of now has reported the effect of these textile processes on the tensile strength and the strength distribution of the fibres.

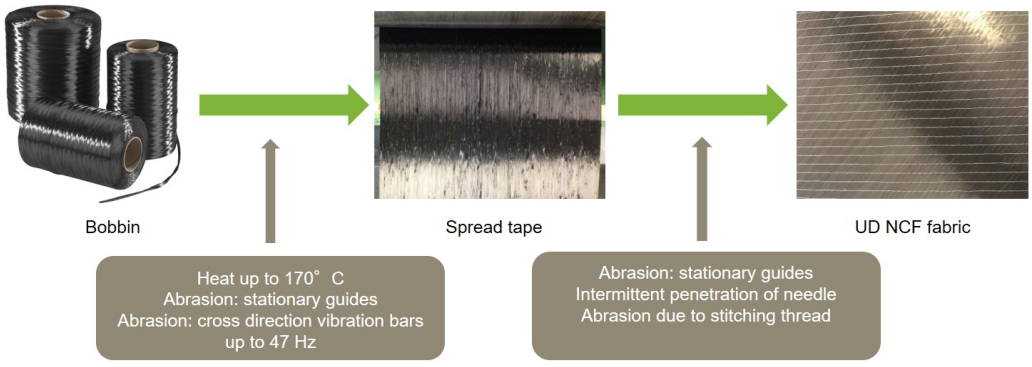

Fig. 2.8 Conversion process from bobbin to NCF fabric and associated factors that can cause fibre breakages.

2.3 Experimental materials and methods

2.3.1 Materials

In the current work, the idea was to characterise the tensile strength of the fibres using single fibre tensile tests. Considering the end uses in structural applications, in sports and leisure, the carbon fibres in the form of high strength T700S fibres and glass fibres in the form of Advantex E-CR glass were identified. The T700S rovings were procured from Toray Europe, while the E-CR Advantex glass fibre rovings were procured from Owens Corning. These two fibres were selected for a detailed study on effect of textile processes on the tensile strength and Weibull parameters of the fibres. Apart from this a pre-study on single fibre strengths of carbon fibres from commingled rovings and their spread tapes was conducted using a manual SFT. The commingled rovings were procured from two different suppliers, Supplier A and Supplier B. Supplier A roving contained HTS45 carbon fires from Toho Tenax Europe GmbH, while the Supplier B roving contained aerospace grade AS4 carbon fibres from Hexcel Corporation. The properties of single fibres for the selected carbon and glass fibres relevant to the current and following chapters as reported in the technical data sheets of the manufacturer is presented in the Table 2.1 below.

Table 2.1 Mechanical properties of fibres as provided by the manufacturer in their technical data sheets.

Property	Units	HTS45 Carbon fibres	AS4 Carbon fibres	T700S Carbon fibres	Advantex E-CR Glass fibres	PPG E-Glass fibres
Density	[g cm^{-3}]	1.77	1.79	1.76 - 1.84	2.62	2.58
Fibre diameter	[µm]	7	7.1	7	17	14
Tensile strength	[MPa]	4500	4433	4510	2400	2290
Tensile modulus	[GPa]	240	231	221 - 240	81	72
Failure strain	[%]	1.8	1.8	1.9	4.9	–

Using the above mentioned carbon, glass and commingled rovings, spread tapes and UD fabrics were developed on a multi-axial machine. Further tensile tests were also performed on the fibres that were extracted from the spread tape and the fabrics respectively.

2.3.2 Experimental methods

2.3.2.1 Sample preparation

For HTS45 and AS4 fibres tested using a manual SFT test, bunch of fibres with length of about 50 to 60 mm were cut out from the original roving or spread tape. The bunch was then immersed in a dish containing ethanol to remove the cohesion and stickiness in the

fibre. Single fibres were extracted from the fibre bundles and fixed on the paper frame at two points separated by a distance of 30 mm (the selected gauge length) using an epoxy based adhesive/glue (as can be seen in Fig. 2.9) which was allowed to cure overnight. Care was taken to maintain the gauge length, tautness of the fibres and orientation of the fibres as these parameters affected the final test results. For T700S carbon and E-CR glass fibres tested using automated process, the preparation of the sample involved similar steps. Instead of paper frame, fibres were mounted using a fast curing glue on plastic tabs (as seen in Fig. 2.9) which were separated from each other by the distance equal to the gauge length. The plastic tabs were then mounted on a cassette which could hold a set of 20 to 50 samples. The geometry of tabs was such that it provided a "well" where the glue droplet could be used to fix the fibre, the "centre notch" in the tab also maintained the orientation of the fibre and did not allow misalignment.

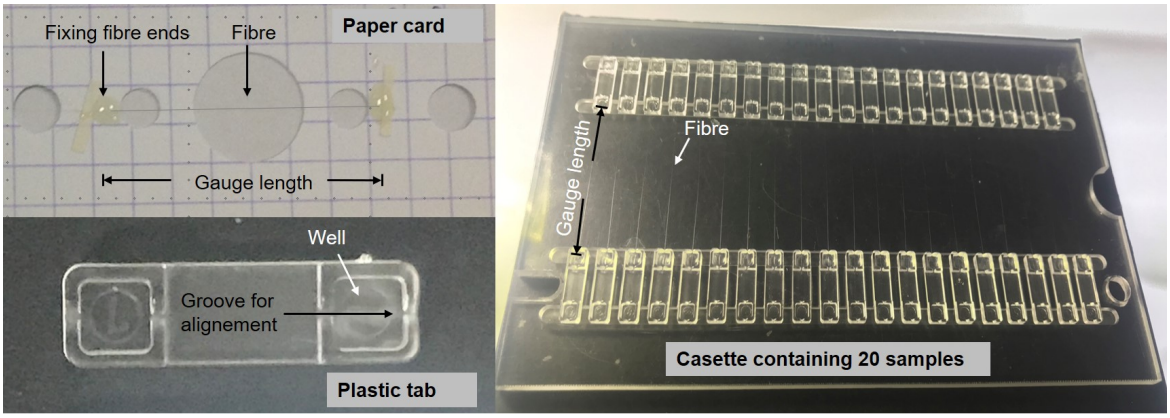

Fig. 2.9 Sample preparation for single fibre tensile tests.

2.3.2.2 Diameter measurement

For the pre-study that was conducted on the commingled rovings, the diameter measurements on carbon fibre were done on a Mitutoyo system (LSM500) on the principle of Laser Scanning Micrometer (LSM). Each sample that was prepared manually on a paper tab was used individually to measure diameter on three different points along the test gauge length. The average of three measurements of diameter along the length for each test was used for calculating the tensile strengths and modulus for that measured fibre using the manual single fibre test.

For the automated single fibre tests, the diameters for carbon fibres were measured using the automated Laser Diffraction System (LDS) which worked in coordination with the Diastron's LEX820 / LDS0200 system of measurement. The LDS0200 is designed for direct,

non-contact diameter measurements. The measurement principle is based on laser diffraction which enables diameter measurements down to a few microns with accuracy and least count of 0.01 µm. On the other hand, the diameter for each glass fibre tested was measured using the LSM principle on Dia-stron's FDAS770 system. The LSM system for the glass fibres is also not ideal as the transparency affects the diameter measurements, it is found that depending on the glass fibre types used, the LSM system underestimated the diameter by 10 to 20 %. To accurately determine the diameter, for calculating the tensile strengths of glass fibre, additional diameter measurements were done using Scanning Electron Microscopy (SEM).

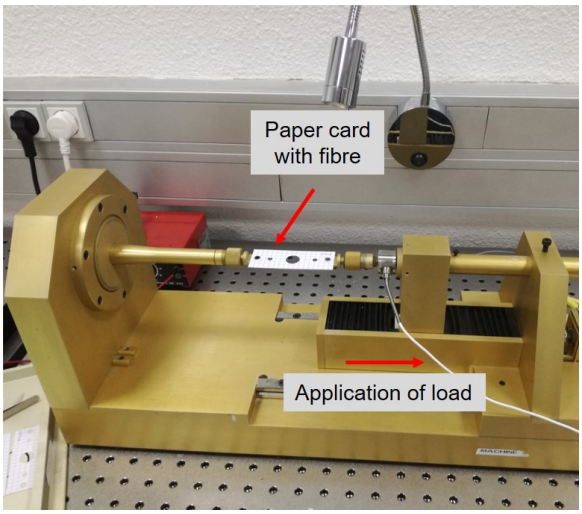

(a) Manual SFT.

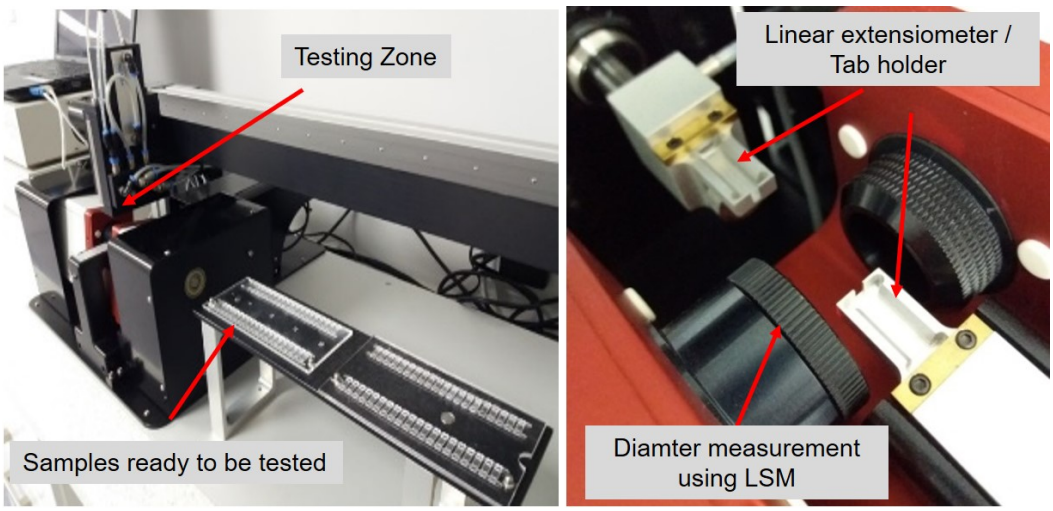

(b) Automated SFT, LEX and LDS system from Dia-stron.

Fig. 2.10 Diameter and tensile testing equipments used.

2.3.2.3 Tensile testing

The tensile tests on the carbon fibres from the commingled rovings were done using the manual single fibre testing equipment developed by Bunsell and Hearle [24] and has improved over the years at MINES ParisTech (seen in Fig. 2.10a). The equipment provided the load and extension values for each test and using the diameter values that were separately obtained as described in section above, the tensile strengths were further manually calculated for each fibre using Eqs. 2.1 and (2.2). About 60 fibres were tested for each fibre type using manual method.

The automated SFT test setup from Dia-stron was used for all the other single fibre tensile tests. For carbon fibre tests the setup consisted of LEX820 / LDS0200 system, where LEX820 is a high resolution extensometer developed for fine fibre applications (Fig. 2.10b). As already informed for glass fibres the diameter measurements were done using LSM instead of LDS0200 used for carbon fibres. The fibre samples were tested at 30 mm gauge length and at a constant loading rate of 1 mm min^{-1}. A pretension of 0.1 g was applied before the start of the test to correct the gauge length. Further, certain number of tests were also done at different gauge lengths (4 mm, 12 mm and 20 mm) to measure the system compliance. A software in the form of "UvWin 4.2.4" was used to visualise the output from the Dia-stron's test setup. Parameters for tests and the analysis methods could be easily edited within the software and it enabled automatic data correction for system compliance. For each fibre type about 100 fibres were tested, which makes the results in this work as one of the most extensive data set for single fibre testing of the fibres.

2.4 Results and discussions

2.4.1 Measurement of diameter

It is well understood that accurate measurement of tensile strength required accurate measurements of diameter for each tested fibre. For carbon fibres the diameter measurements were carried out using LDS and LSM measurement system. Optical microscopy and SEM have their own limitations as reported in Section 2.2.4. The results from diameter measurements for carbon and glass fibres tested can be seen in Fig. 2.11. For glass fibres, it was already known that the LSM system tends to underestimate the fibre diameter owing to the transparency of glass fibres. For this reason, additional measurements using SEM images were done and a correction factor was applied to the diameter measurements obtained using the LSM, further the corrected diameter values were used in the strength calculations. For E-CR glass the average diameter measured using LSM was 14.82 µm, while the average

diameter for measured using SEM was 16.76 µm. Hence the LSM system of measurement underestimated the glass fibre diameter by about 12 %.

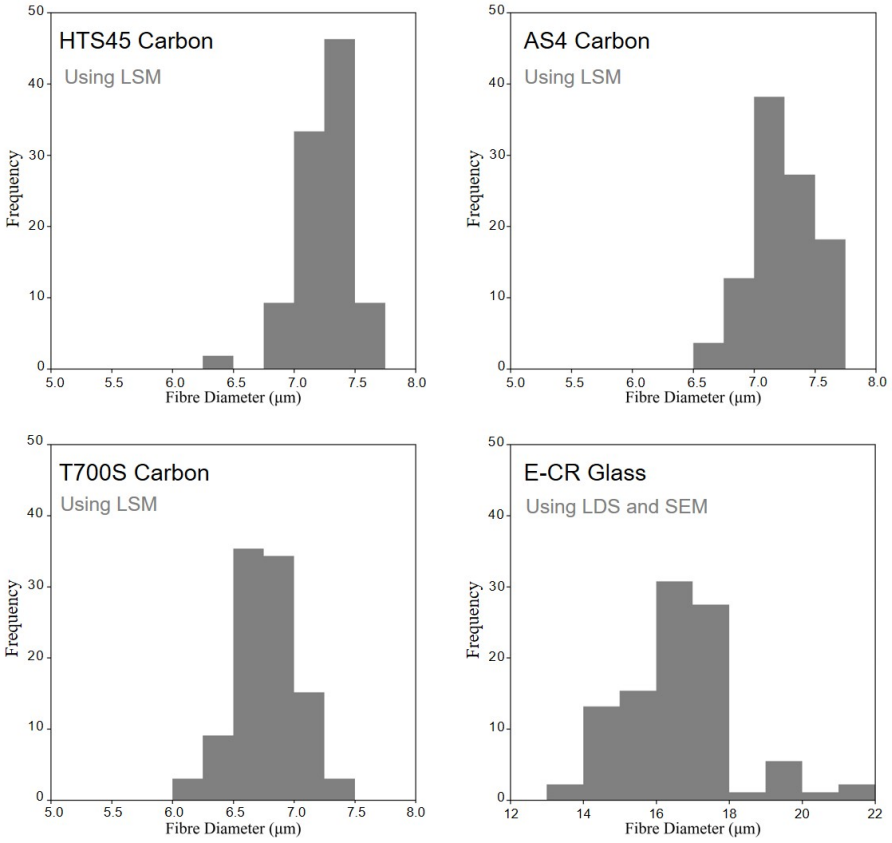

Fig. 2.11 Histogram of diameters measurements for different fibres.

The carbon fibre diameter was near accurately measured by both the LSM and LDS systems. The average diameter values for T700S, HTS45 and AS4 fibres were observed to be, 6.8 ± 0.04 %, 7.2 ± 0.05 % and 7.2 ± 0.06 % respectively. Here and hereafter in this chapter the values after ± represent the standard deviation at 90 % confidence level obtained using guide for uncertainty measurement [55]. It can be also seen that the LDS system underestimated while the LSM system overestimated the diameter values when compared to the diameter values provided by the fibre manufacturer's in their technical data sheets. The mean diameter for E-CR glass was found to be 16.8 ± 0.31 %. Among all fibres, the coefficient of variation of diameter is the highest for E-CR glass fibres (10.6 %) while for all the carbon fibres it is in between 3 to 4 %

2.4.2 Measurement of compliance

For automated SFT, compliance was calculated by testing each type of fibre at 3 different gauge lengths. The compliance for each specimen was plotted against the gauge lengths, the measured compliance is the addition of compliance of the system and the compliance of the specimen. System compliance was separately measured for glass fibres, as the fibres and their interaction with the curing adhesive tends to change the initial system compliance. This measured compliance is linearly dependent on the length of fibre and the independent term related to the compliance of the system. For carbon fibres and for glass fibres the system compliance was found to be $0.06\,\mathrm{mm\,N^{-1}}$. On the other hand, for the same type of fibres, at different processing stages, the system compliance as expected did not change significantly. The system compliance for T700S carbon and E-CR glass is presented in Fig. 2.12

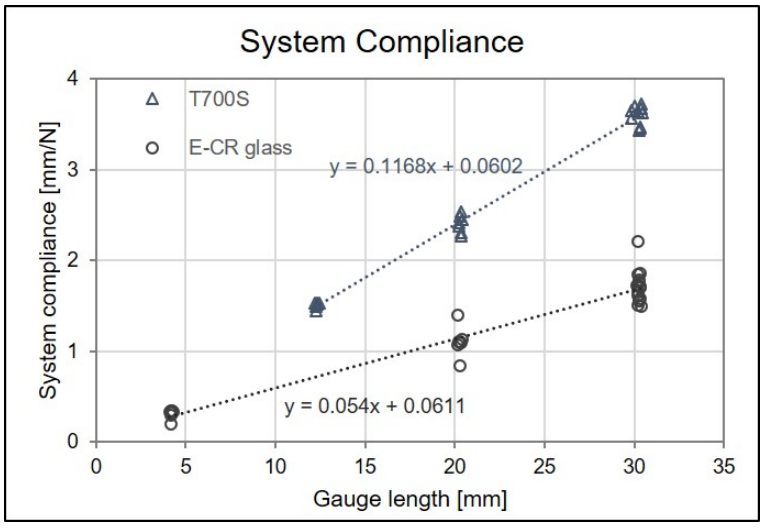

Fig. 2.12 Determination of system compliance for carbon and glass fibres.

2.4.3 Tensile properties

Typical tensile stress–strain curves for carbon fibres HTS45, AS4 and T700S and E-CR glass fibres obtained from single fibre tensile testing are presented in Fig. 2.13. For the carbon fibres, though the stress applied to the specimens seems almost linearly proportional to the strain until failure, but slight non-linearity still is observed. The non-linearity and dependence of stress on the strain in the fibres is explored in Section 2.4.4.

The average tensile strength, failure strain, modulus and diameter for fibres tested are presented in Table 2.2. The strength values for same fibres reported in the technical data sheets (Table 2.1) by the manufacturers are different than those measured. This difference

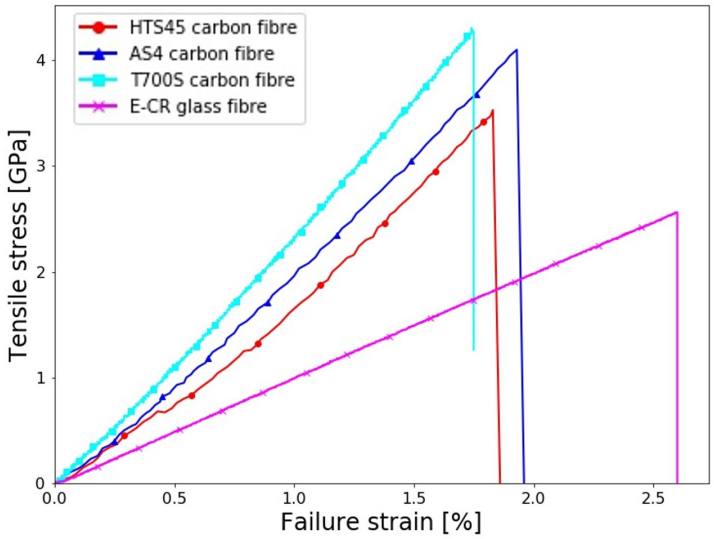

Fig. 2.13 Representative stress vs. strain curves for fibres tested in single fibre tensile test.

in strengths can be attributed to the use of a bundle fibre test in industrial setup which tests fibres embedded in a resin with longer gauge lengths. The values in the brackets represent the standard deviation.

Table 2.2 Properties of fibres tested in single fibre tests.

Fibre	State	Fibre diameter [μm]	Tensile strength [GPa]	Failure strain [%]	Tensile Modulus [GPa]	N° of tests
HTS45	Commingled (A)	7.24 (0.22)	3.38 (0.60)	1.62 (0.27)	-	55
	Commingled (M)	7.16 (0.22)	3.46 (0.61)	1.62 (0.27)	-	55
AS4	Commingled	7.22 (0.25)	3.59 (0.66)	1.72 (0.32)	-	55
	Spread tape	7.41 (0.26)	3.37 (0.61)	1.63 (0.32)	-	54
T700S	Bobbin	6.76 (0.25)	3.45 (0.64)	1.45 (0.23)	211 (16)	96
	Spread tape	6.82 (0.30)	3.45 (0.77)	1.42 (0.26)	215 (17)	112
	Fabric	6.76 (0.31)	3.52 (0.66)	1.48 (0.25)	216 (15)	102
E-CR glass	Bobbin	16.8 (1.77)	2.06 (0.48)	2.61 (0.57)	82 (5)	92
	Spread tape	16.5 (1.40)	1.98 (0.45)	2.32 (0.51)	88 (6)	100
	Fabric	17.0 (1.21)	1.95 (0.50)	2.49 (0.62)	81 (6)	97

* For HTS45, (A) and (M) stands for the tensile properties measured using average diameter and minimum diameter. ** Values in the brackets ( ) are the standard deviations for that property.

2.4.3.1 Study on HTS45 carbon fibre

Initial study on HTS45 was conducted using manual SFT test method. HTS45 fibres were extracted from the commingled roving from Supplier A. Diameter measurements on HTS45 fibres was done at 3 points along the gauge length for each fibre to be tested. The stress

in the fibres was calculated using Eq. 2.1 using two different values of diameter and hence the cross sectional areas. In the first case, average value of 3 diameter values along the length was used for stress calculation, while, in the second case, assuming that the fibre failure occurring at the thinner region of the fibre diameter, the minimum diameter value measured was used for stress calculation. It was found that the average tensile strength for the premier case was 3.38 ± 0.13 GPa while for the latter case was 3.46 ± 0.15 GPa. The Weibull shape parameter and scale parameter (m and σ_0) were not significantly different either. It has to be noted difference in the mean values of the average diameters for the fibres (7.24 ± 0.05 µm), and that of the minimum diameters of tested fibres (7.16 ± 0.06 µm) was also not significant. One of the reason there was no significant difference in strengths for the two cases can be originating from the fact that diameter measurement is done at only 3 places and not continuously throughout the length of the fibres, and a weak place (thinnest diameter) could lie outside the three measured points. It is also possible that the weakest point corresponds to a void inside the fibre which has no effect on the apparent cross-section of the fibre. The Weibull plots for the measured tensile strengths along with 95 % confidence range is presented in Fig. 2.14a.

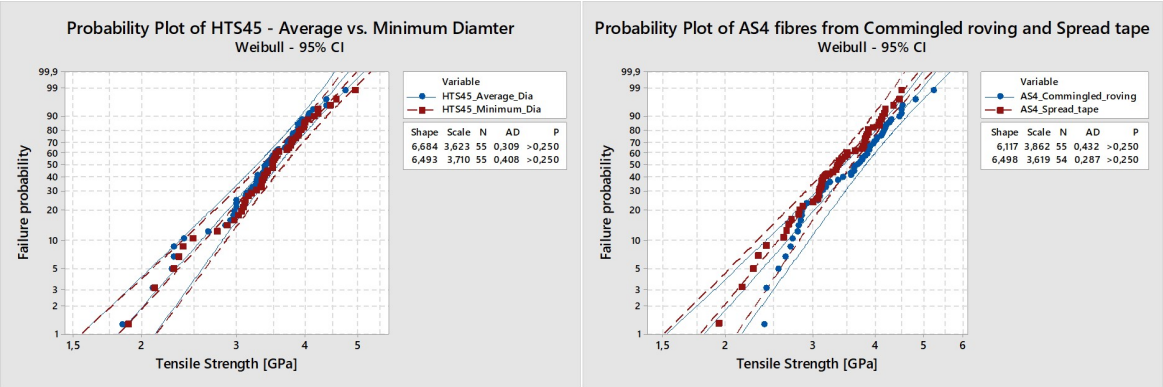

Fig. 2.14 Weibull plots for (a) HTS45 and (b) AS4 carbon fibres from different states.

2.4.3.2 Study on AS4 carbon fibre

AS4 carbon fibres from Supplier B commingled roving, were tested at two different states: (1) fibres extracted from a commingled roving, (2) fibres extracted from a spread tape made using the commingled roving. For this pre-study it was found that the average strength measured for fibres extracted from the spread tape (3.37 ± 0.14 GPa) was lower than that of the fibres extracted from the commingled roving bobbin (3.59 ± 0.15 GPa), and the scale parameters were observed to be 3.62 GPa for fibres from spread tape and 3.86 GPa for fibres from the bobbin respectively as seen in Fig. 2.14b. This difference in scale parameters is not

significant and could be because of difference in average diameters recorded for the fibres extracted from the spread tape (7.41 ± 0.06 µm) when compared to that from the bobbin (7.22 ± 0.06 µm). This difference in the average diameters observed for the two are not statistically significant owing to the uncertainties in the measuring process itself. Hence for critical studies it is rendered very important to correctly measure the diameter for the tensile tests to make right conclusions. This pre-study provided the basis for the study of tensile behaviour and the distribution of tensile strengths for the same fibre at various processing stages using an automated SFT test.

2.4.3.3 Effect of textile processes on tensile strength of T700S carbon and E-CR glass fibres

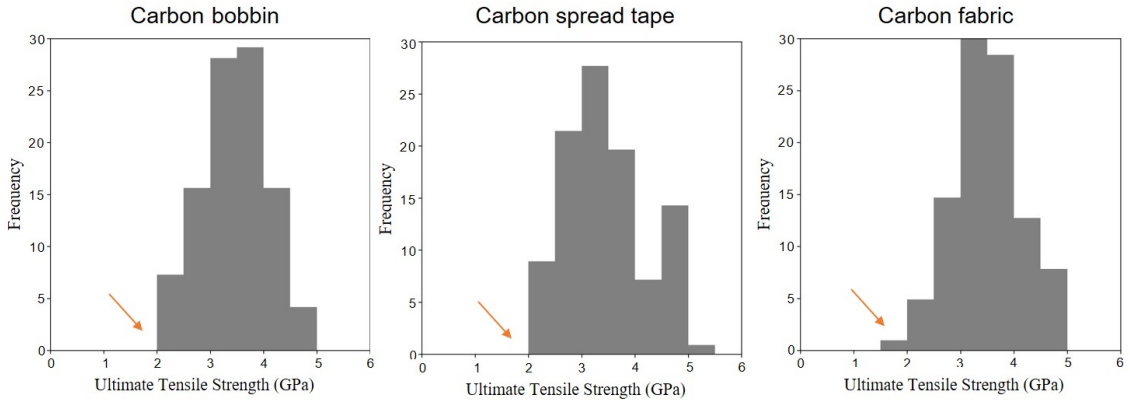

(a) For T700S carbon.

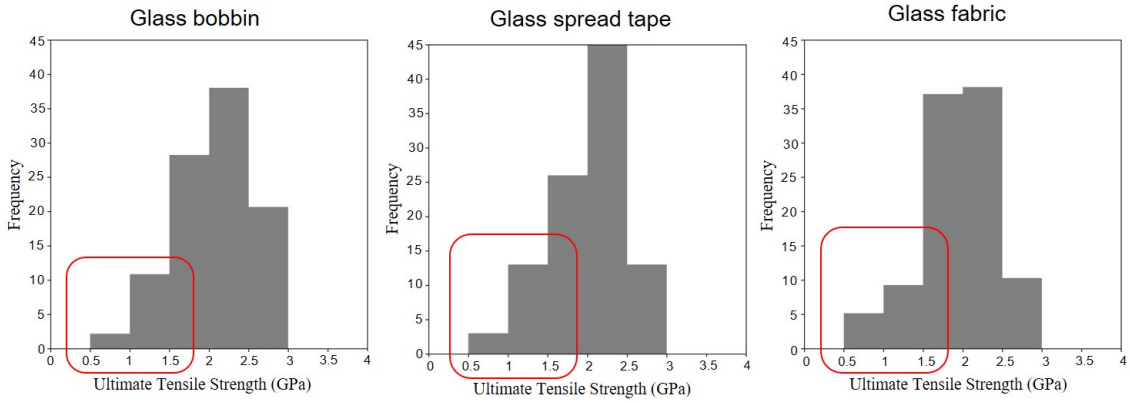

(b) For E-CR glass.

Fig. 2.15 Histogram representing the fibre strength distributions.

As mentioned earlier, the success of a model to correctly predict properties of a composite, it is essential that the model is fed with right input parameters. Fibre strength and its

distribution is one of the most important input parameter for modelling. Though the fibre from the as-received bobbin passes through several processing stages before finally becoming a part of the composite, it is still not confirmed by a detailed research work if the fibre strength or distribution of fibre from the as-received bobbin remains the same throughout these processes. For this study, the results for tensile properties and the Weibull parameters are generated from about 100 fibres for at each processing stage. This is inline with the recommendation from Berger and Jeulin [17] who reported that 30 tests are not enough for tensile testing using single fibre tests and Thomason [153] who suggested a minimum of 80 SFT tests are necessary to confidently estimate the Weibull parameter of a data set.

For T700S carbon fibres, as expected the average failure strains and the stiffness at the 3 processing stages were not very different as can be seen in Fig. 2.2. The average tensile strengths of the fibres from bobbin was 3.45 ± 0.13 GPa, while for the fibres extracted from spread tape and fabrics showed a strength of 3.45 ± 0.14 GPa and 3.52 ± 0.13 GPa respectively. That means, considering the inherent variation in the tensile strength for carbon fibres itself, the change in tensile strength because of the effect of textile processes was significantly lower. Similarly for E-CR glass, the tensile strengths for fibres from bobbin, spread tape and fabric were 2.06 ± 0.10 GPa, 1.98 ± 0.09 GPa and 1.95 ± 0.13 GPa respectively. A slight trend of reduction in average tensile strength here is observed and it can be attributed to the fibre breakage and weakening of fibres happening during processing of glass fibres. The broken fibres could also be noticed on the surface of the spread tape roll produced by the spreading process. Though it has to be noted that this trend is not statistically significant.

For T700S fibres and E-CR glass fibres the histograms of the fibre strength data at various processing stages is presented in Fig. 2.15a and Fig. 2.15b respectively. Typical breaking force for a high strength carbon fibre is 0.15 N, considering this, several researchers have reported a preselection effect for carbon fibres [153, 70]. For T700S carbon fibres obtained from the bobbin, spread tape and the fabric a fibre preselection effect can be observed in the current study. For all the 3 sets of carbon fibres, no fibre showed a strength $<$2 GPa. For glass though the preselection effect is not prominent, as the fibres with strengths as low as 0.5 GPa were tested. Glass fibres in general can sustain higher loads than carbon and hence the possibility of fibre failure during extraction and sample preparation is lower. This has been also found in the practical experience reported in Section 2.4.5.

2.4.4 Strain dependency of stiffness

Carbon fibres shown evidence of nonlinear elastic behaviour and this has been observed by several researchers [34, 15]. As can be seen in Fig. 2.16a, for a typical carbon T700S

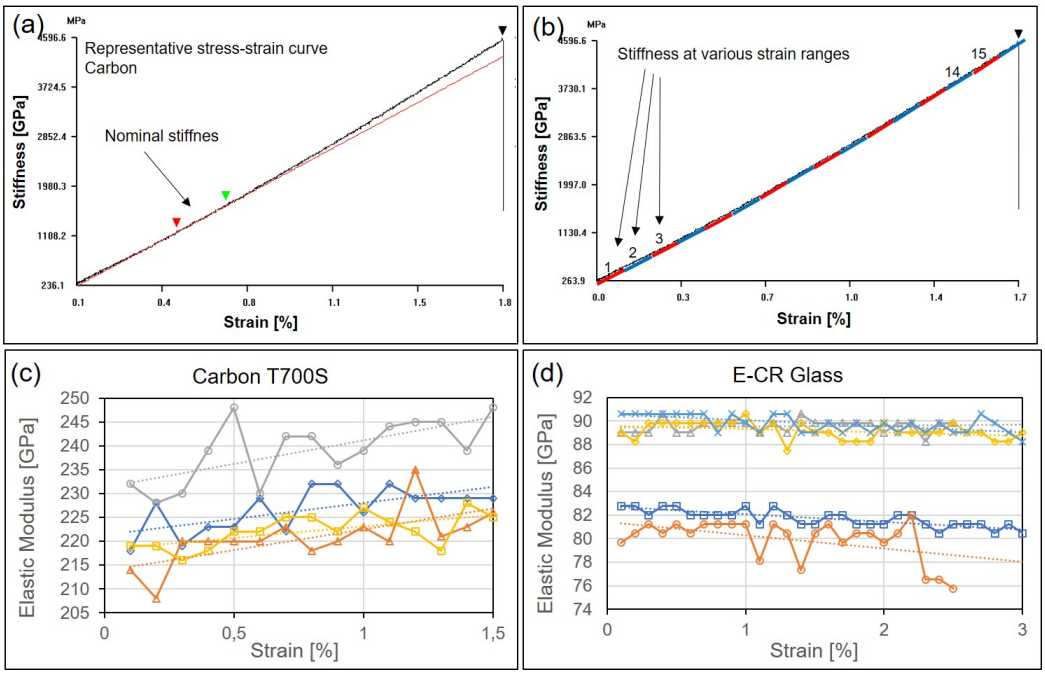

Fig. 2.16 Strain induced changes in stiffness of carbon and glass fibres

fibre the stiffness of the fibre tends to increase after a certain strain level. This increase is quantified by measuring the stiffness of the same fibres between various strain levels. For example for a carbon fibre with failure strain of 1.5 %, the strain region was divided into 15 sections each corresponding to 0.1 % increase in the strain as shown in Fig. 2.16b. Using this method, modulus vs strain is plotted as shown in the bottom row of Fig. 2.16. It can be seen that for carbon fibres, there is a clear trend of increase in the stiffness at higher strain levels. This strain dependence was earlier reported by Beetz Jr [15], in their study on a different carbon fibre they reported around 20 % increase in stiffness per percent increase in strain. In the current work, for T700S carbon fibres this increase was found to be about 3 % to 6 %. This observation of stiffening can be explained by a strain-induced increase in the fibre preferred orientation. For T700S fibres in the current work, the degree of strain induced stiffening was significantly lower than that observed by Beetz Jr [15] in 1982; one of the reason for this observation is that the modern generation of high performance carbon fibres posses higher orientation of microfibrillar structure than the fibres produced more than three decades ago. While for glass fibres, the stiffness tends to slightly reduce on increase in the strain. For glass fibres the strain dependence of stiffness is not reported in earlier studies and it is found in the current work this dependence is insignificant, with about 2 % reduction in stiffness per unit percentage increase in strain. This phenomenon of strain dependency of stiffness violates the initial assumption of linearity of stress-strain curve for different types

of fibres and hence should be taken into account when modelling the strength of composite materials using Weibull input parameters.

2.4.5 Effect of uncertainties

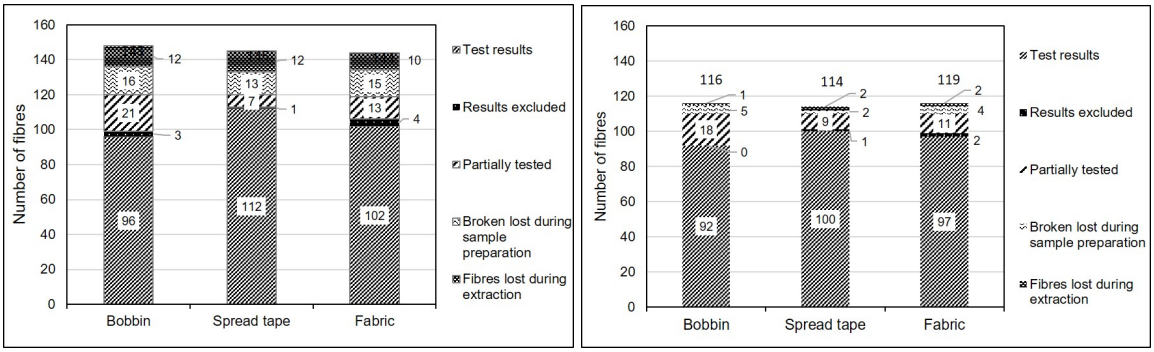

(a) For carbon fibres. (b) For glass fibres.

Fig. 2.17 Experimental observations from identification of fibre to the tensile testing.

In the current tests, the observation of uncertainties is reported not only at the testing stage but right from that stage of fibre identification and extraction. Care is taken to account for each fibre in the test that was identified for testing and record if the fibre went though all the steps until the final analysis of the results. As can be seen in Fig. 2.17, for example for all the T700S carbon tests from the bobbin, from about 148 fibres identified to be tested, the analysis of results includes only 97 fibre test results. The rest of the fibres except the 97 fibres that were used in analysis, could be broadly categorised in three groups: (1) fibres not tested because of pre-selection, (2) lost or not tested due to manual errors, and (3) not tested or partially tested due to testing machine issues.

Overall, it is observed for an average 100 carbon fibre results, about 142 fibres were identified to be tested and for glass 100 fibre test results could be obtained by just identifying about 120 fibres from bunch of all fibres. That means the number of fibres in the three categories mentioned above for glass fibres are significantly lower for glass fibres than for carbon fibres and one of the reason for it is the higher breaking loads for glass fibres. For both carbon and glass fibres, among the three processing stages, at bobbin stage it was observed that more number of fibres were lost or partially tested in the tests and this can be attributed to the higher number of weaker fibres in the bunch and to presence of higher amount of sizing on the fibres at bobbin stage.

The reason it was thought to track the fibres from extraction stage to the testing stage was to understand if the final results for the tests are influenced by factors such as pre-selection.

These figures not only are important to quantify the uncertainties in the results that are generated from the single fibre tests, but also, to understand the limitations in the current process of automated single fibre testing.

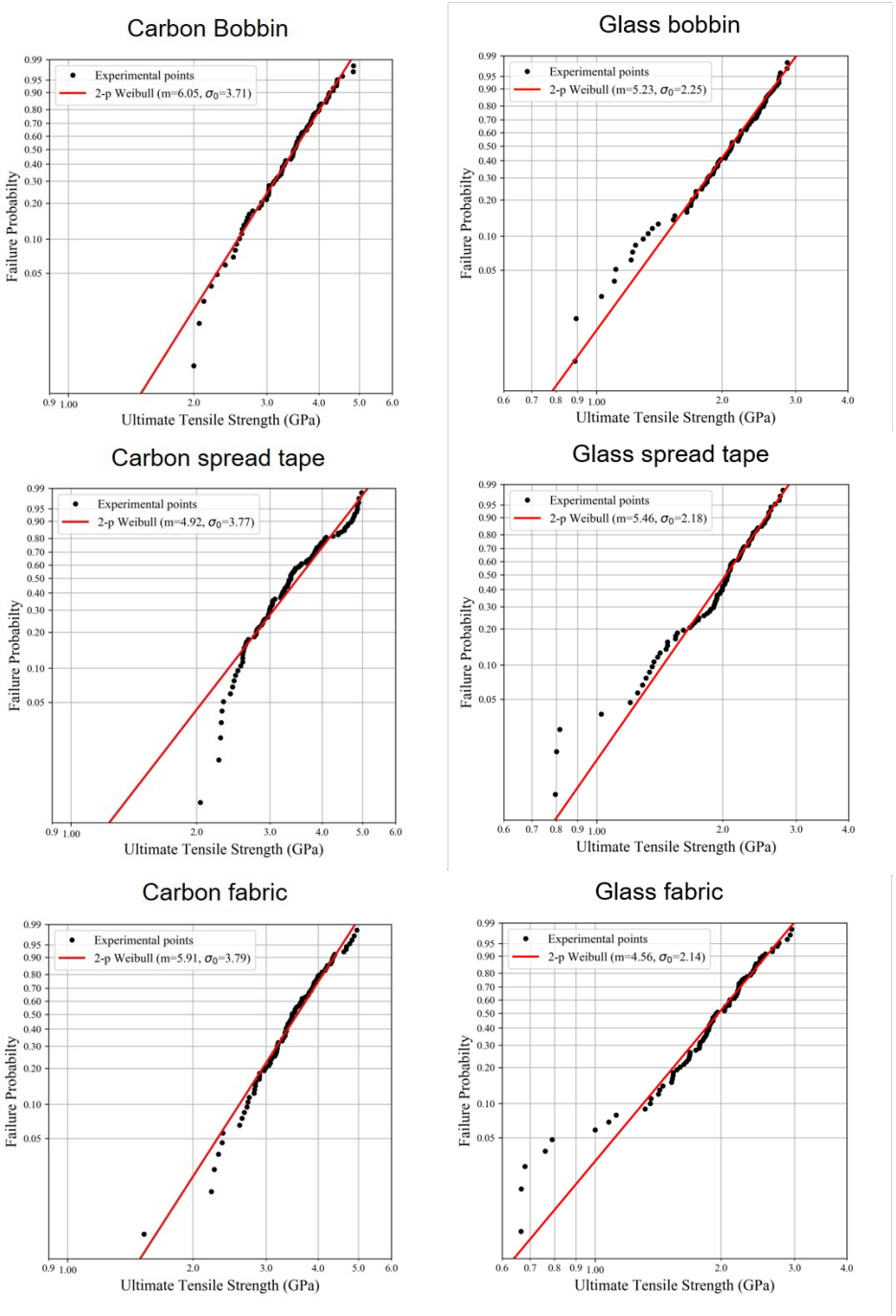

(a) For T700S carbon. (b) For E-CR glass.

Fig. 2.18 2-Parameter Weibull distribution for fibre strength data.

2.4.6 Statistical distribution

The 2-parameter Weibull distribution for the strengths obtained for T700S carbon and E-CR glass fibres at various stages of processing is presented in Fig. 2.18a and Fig. 2.18b respectively.

The Weibull shape factor for T700S fibre from bobbin, spread tape and fabric is found to be 6.05, 4.92 and 5.91 respectively. This difference in the shape parameter is not statistically significant considering the inherent variation in fibre carbon fibre property and the uncertainties in the single fibre test procedure. The scale parameter for T700S at different process stages from bobbin to fabric shows a slight trend of improvement with σ_0 = 3.71 GPa, 3.77 GPa and 3.79 GPa respectively, hinting at breakage of low strength fibres during the processing but the effect is not very significant. Islam et al. [71] also demonstrated in their studies on T700S carbon fibres, that the experimental uncertainties in single fibre testing can lead to a variation of ± 1 in Weibull shape parameter (m) and ± 0.5 GPa in Weibull scale parameter (σ_0).

Similarly for E-CR glass fibre, Weibull shape parameter for fibres from bobbin, spread tape and fabric is observed to be 5.23, 5.46 and 4.56 respectively, while the scale parameter is observed to be 2.25 GPa, 2.18 GPa and 2.14 GPa respectively with a slight positive trend. Like carbon fibre, the shape parameters for glass fibres from three stages does not show a significant difference.

For T700S the experimental points show deviation from the 2-Parameter distribution line at the lower strength regions, this can be attributed to the confirmed preselection effect in the carbon fibres. For E-CR glass, the 2-Parameter does not fit the experimental points from lower to middle regions, this may be because of multiple flaw populations. The only way to confirm this is to analyse each fibre break separately and further observe and classify the type of flaw for each fibre break.

2.5 Conclusion

This chapter investigated the potential and challenges of SFT tests using an automated SFT equipment from Dia-stron. Several different types of carbon fibres and E-CR glass fibres were characterised at different processing stages and test conditions. Using the analysis of the results and observations made during testing of the fibres, following conclusions can be drawn from this work.

- Automated testing equipment from Dia-stron can potentially be used for testing of technical fibres and lead to better understanding the single fibre properties by eliminating the present limitations in the manual test method and equipment.
- Diameter and tensile strength for fibres was found to be 7.24 µm and 3.38 GPa for HTS45 carbon; 7.22 µm and 3.59 GPa for AS4 carbon; 6.79 µm and 3.45 GPa for T700S carbon fibres, while for E-CR glass fibre diameter and strength were measured to be 16.8 µm and 2.06 GPa respectively.
- Accurate diameter measurement is the key for accurate tensile strength measurements; though Laser Diffraction Method is best suited for carbon fibres, for glass fibres the system underestimates the fibre diameter. For more accurate strengths, continuous measurement along the whole gauge length is essential, though it still may not be able to detect cross sectional variations due to internal voids/flaws.
- Carbon fibres shows preselection effect and there exist weaker fibres which could not be tested as they were broken during extraction from the rovings.
- Strain induced stiffening of fibres can be observed for carbon fibres but the effect is not significant for glass fibres.
- Incorporating uncertainties, preselection effect and strain induced stiffening for carbon fibres can lead to better understanding of fibre properties for modelling and designing of composites.
- Glass fibres has very low preselection effect. The number of fibres not tested due to fibre extraction, mounting and testing uncertainties is comparatively lower for glass fibres than carbon fibres.
- The Weibull shape factor for T700S fibre from bobbin, spread tape and fabric is found to be 6.05, 4.92 and 5.91 respectively. This difference in the shape parameter is not statistically significant considering the inherent variation in fibre carbon fibre property and the uncertainties in the single fibre test procedure.
- For E-CR glass fibres, Weibull shape parameter for fibres from bobbin, spread tape and fabric is observed to be 5.23, 5.46 and 4.56 respectively, while the scale parameter is observed to be 2.25 GPa, 2.18 GPa and 2.14 GPa respectively with a slight positive trend.

- Carbon and glass behave differently, for example for carbon, in the spread tape, the spread of tensile strengths is maximum while for glass fibres from spread tape, the spread of strength values is minimum.

Chapter 3

Investigations on fibre spreading process and its optimisation for glass fibres

---

Etude du procédé d'étalement de fibre et optimisation pour les fibres de verre

Ce chapitre se concentre sur la technologie d'étalement des fibres techniques telles que le carbone et le verre. Les deux objectifs spécifiques de ce chapitre sont : (1) l'optimisation du processus d'étalement des fibres de verre, et (2) la compréhension du comportement à l'étalement des mèches préalablement comélées ainsi que l'étalement simultané de fibres de verre et de carbone pour fabriquer des renforts hybrides fibre à fibre. Les résultats de cette étude sont ensuite mis en application pour fabriquer des renforts hybrides intra-fils en utilisant le procédé d'étalement. Ces renforts et les composites sont ensuite utilisés au chapitre 5 afin de comparer les propriétés mécaniques des composites hybrides réalisés à l'aide de la technologie d'étalement par rapport à ceux réalisés à partir de fils comélés.

Ce chapitre est divisé en cinq sections. L'introduction est suivie d'un état de l'art (Section 3.2) sur la technologie d'étalement et la technologie multi-axiale (NCF – Non Crimp Fabric). Cette section fait aussi un état de la littérature sur le comportement mécanique des hybrides fibre à fibre (intra-fil) réalisés à partir de fils comélés et d'hybrides plis fins. La Section 3.3 décrit les matériaux fibreux utilisés ainsi que le procédé et les paramètres d'étalement. La Section 3.4 examine les résultats obtenus à partir du plan factoriel de Taguchi et détaille les conclusions obtenues pour les fibres de verre.

Les conclusions de l'étude sont présentées à la Section 3.5. Il a été observé que les paramètres de la zone d'étalement tels que la fréquence de vibration, la température, l'embarrage et la vitesse ont un effet significatif sur le comportement d'étalement des fibres de verre. L'effet des interactions entre les paramètres est aussi significatif pour un étalement optimal de ces fibres. Cette configuration optimisée a été utilisée pour fabriquer une nouvelle génération de plis fins en fibres de verre ainsi que des renforts hybrides verre/carbone intra-plis et intra-fils. L'étude expérimentale sur les stratifiés à base de fils comélés a conclu que l'étalement de ces fils était contre-productif car cela génère une quantité élevée de casses des fibres en raison de la torsion inhérente à la structure de la mèche comélées.

3.1 Introduction

This chapter is a preliminary study that focuses on spreading technology for technical fibres such as carbon fibres. The two specific aims of this chapter are: (1) Optimisation of spreading process for glass fibres, and (2) understanding the spreading behaviour of commingled rovings and simultaneous glass and carbon fibres spreading to manufacture reinforcements hybridised at fibre level. The outcomes from this study are further utilised to manufacture intermingled hybrid fabrics using spreading process and these reinforcements are used in Chapter 5. This enables comparison of mechanical properties of fibre level or intermingled hybrid composites manufactured using spreading technology vs those using commingled rovings. Further the results from Chapter 3 and Chapter 5 provides the overall balance of mechanical properties of hybrid composites characterised at all three levels of hybridization as described in Fig. 1.2.

This chapter is divided into five sections. The introduction of the chapter is followed by a section on the state of the art (Section 3.2) in spreading technology and non-crimp manufacturing process. Further this section discusses the mechanical behaviour of intermingled hybrids reported in the literature for commingled rovings and thin-ply hybrids. Design of Experiments technique relevant for process optimisation is also reported in this section. Section 3.3 describes in detail, the fibre materials used along with the process and process parameters of spreading technology. Taguchi method of Design of Experiment is introduced as it will be used for the current study in this section. Section 3.4 discusses the results obtained from the Taguchi's factorial design and conclusions are made on the spreadability of selected glass fibres. Factors with maximum effect on spreading process are identified and new generation of fibre level hybrids are fabricated for future use in Chapter 5 and Chapter 6. Conclusions on the factorial designs using Taguchi Method and spreadability of E-CR glass fibres are presented in Section 3.5. The schematic overview of the experimental and scientific section of this chapter is presented in Fig. 3.1.

3.2 State of the art

3.2.1 Non-crimp fabric composites – NCF

For composite manufacturing processes a variety of reinforcements can be used. Commonly used fibre types include several varieties of carbon, glass and aramid fibres with a diverse range of mechanical properties as described in Chapter 2. Most composite applications are based on use of glass fibres (general purpose E-Glass and high strength glass fibres) as reinforcement due to their desirable price-performance ratio. Glass or carbon fibre based

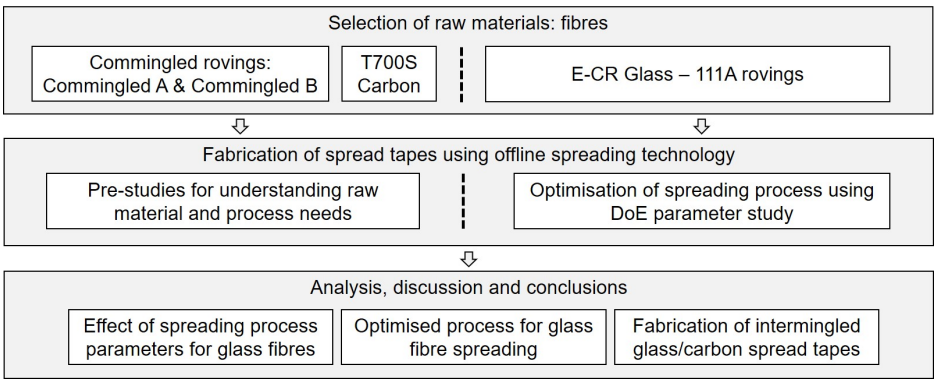

Fig. 3.1 Schematic overview of the experimental (Section 3.3) and scientific (Section 3.4) sections of this chapter.

textile reinforcements can be manufactured by weaving, braiding, knitting, stitching, and by using non-woven techniques. Each manufacturing technique has its own advantages and disadvantages in terms of specific composite properties and the selection can be made based on the end-use. Three-dimensional woven, braided fabrics are those kinds of reinforcements that can be directly used without preforming process, as near-net shape preforms can be produced with these technique. Woven fabrics, as seen in Fig. 3.2 has fibre undulation and crimp, while, NCF's differ from woven fabrics as they have no or little crimp and that multiple unidirectional fibre layers are brought together by stitching them with a fine polymeric fibre thread. Owing to its structure, non-crimp fabrics are also referred to as Multiaxial Multiply Fabrics sometimes.

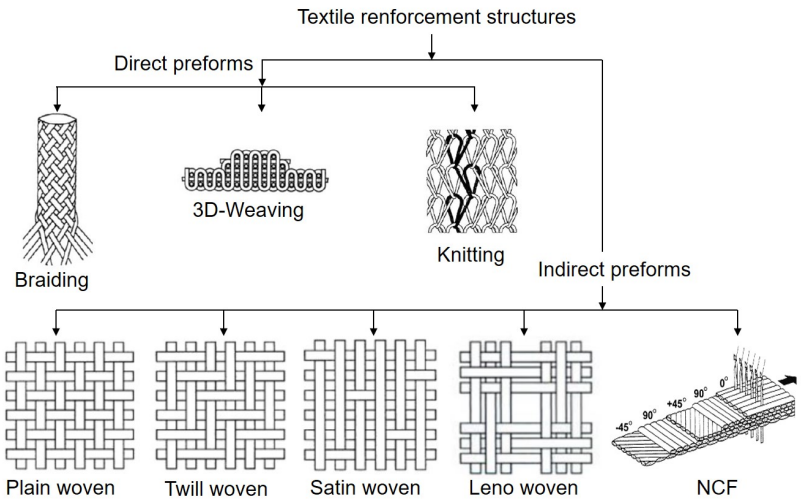

Fig. 3.2 Textile structures for composite reinforcements.

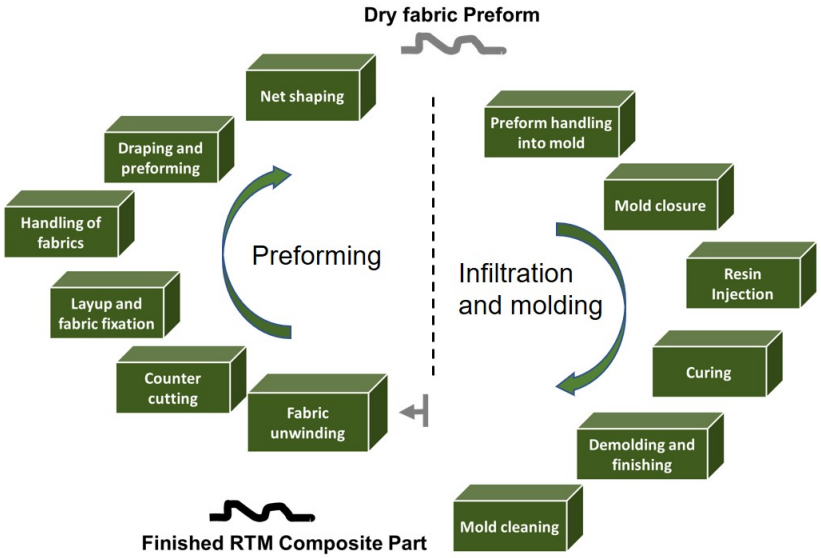

Fig. 3.3 Schematic of resin transfer moulding process based on sequential preforming.

The NCF composites show some reduction in performance as compared to those derived from prepregs mainly because of the fibre misalignment's and resin rich pockets caused because of irregularities due to stitching, also called as "fish eyes". Regardless of that, the main reasons for the industry to use NCF composites instead of either prepregs or woven fabric based laminates are the economical benefits. Studies have reported about 35 % reduction in cost for composites manufactured using NCF's and a liquid composite moulding processes when compared to conventional prepreg and autoclave process systems [18]. These non-crimp fabric composites are generally made using a liquid composite moulding process such as Resin Transfer Moulding (RTM) whose process steps are schematically depicted in Fig. 3.3. Manufacturing parameters associated to both the preform and composite manufacturing are important for the final performance of the composite. Important parameters for the preform manufacturing are, fibre type used, inter-tow gap, stitch tension, stitch type, stitch density and stitch material. Important parameters, besides the matrix properties, associated with the composite manufacturing process are different for each manufacturing technique.

3.2.1.1 Non-crimp fabrics

The manufacturing technique for non-crimp fabric, also called as multiaxial technology is attractive due to small amounts of material wastage, reduced production time and virtually unlimited shelf life which results in lower production costs. Typically this production technique can produce unidirectional, biaxial, triaxial and quadriaxial fabrics of carbon or

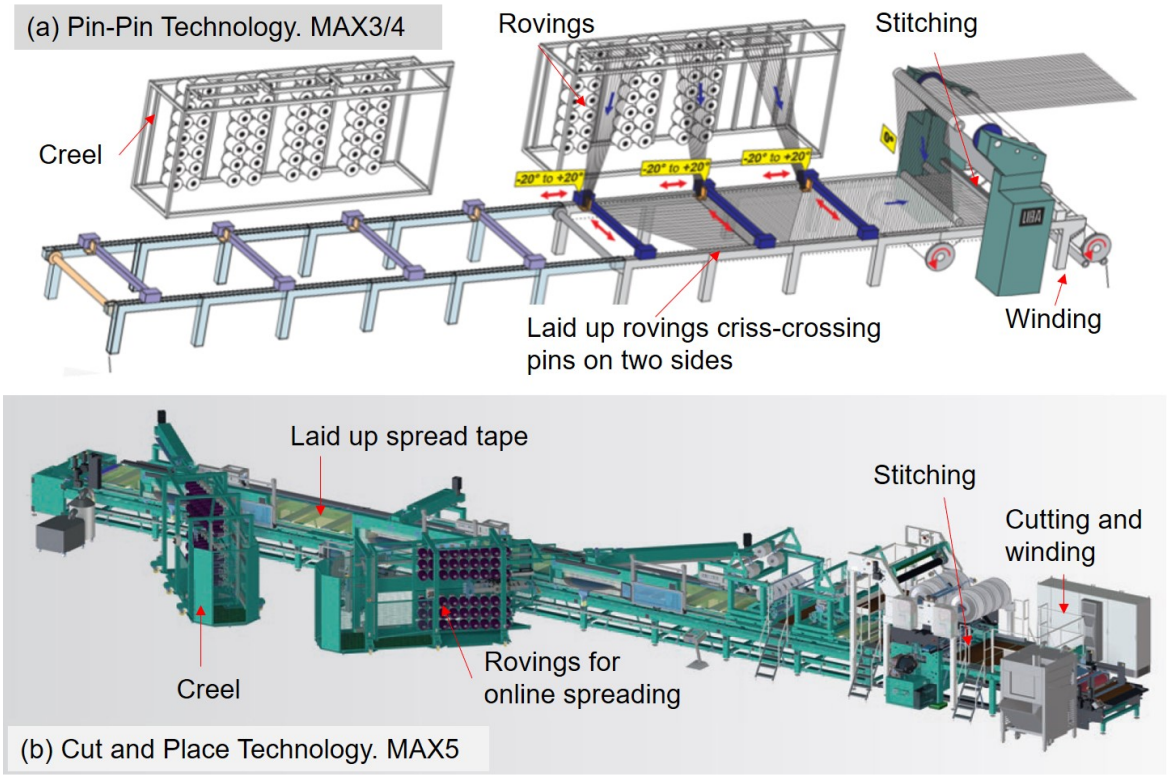

Fig. 3.4 Schematic of the multiaxial technologies (a) Pin-Pin, MAX3/4 and (b) Cut and Place, MAX5, from LIBA/KM (www.karlmayer.com).

glass fibre using polyester (PET) or polyamide (PA) as stitching yarns. Non-crimp fabrics can trace their early steps to the marine industry and they were first manufactured in the 80s. A schematic figure of the production of NCF preforms and the image of the machine in production is presented in Fig. 3.4. As of now there are two different forms of fabrication of non-crimp fabrics manufactured and used: (1) Standard NCF (without spreading) (Pin-Pin Technology), and (2) Spread tape NCF's with spreading (Cut and Place technology). Spread tape NCF's in general have greater uniformity along the width and thickness, while enabling lower areal weights as can be seen in pictures shown in Fig. 3.5. The standard NCF process schematically presented in Fig. 3.4a, has bobbins as the input materials, and the layup units directly unwinds the rovings from the bobbins and criss-crosses the pins on both sides of the conveyer belt, creating a uniform sheet of rovings in desired orientation. Further this stack of multiple layers is than stitched in the warp knitting zone to make the NCF. On the other hand the modern spread tape NCF's, an intermediate step is essential where multiple rovings are brought together to manufacture a homogeneous tape, called spread tape, which is then cut and laid in specific orientations and stitched together. It has to be noted that this intermediate step of spread tape manufacturing can be done online as seen in Fig. 3.4b

or offline as shown in Fig. 3.7a in LIBA's offline spreading system. The steps involved in multiaxial fabric manufacturing is diagrammatically presented in the Fig. 3.6.

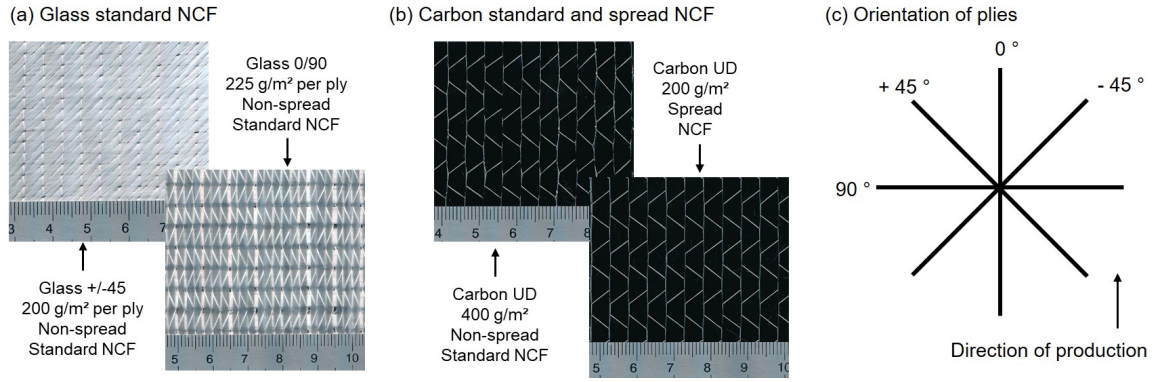

Fig. 3.5 Photos of NCF fabrics (a) glass fibre NCF's, (b) carbon fibre NCF's and (c) standard orientation of NCF's.

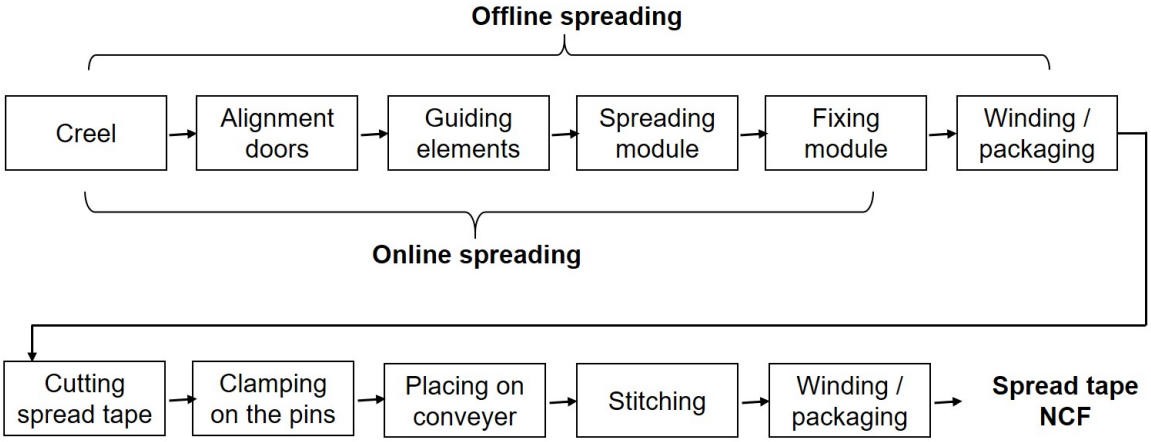

Fig. 3.6 Steps for fabrication of spread tape NCF fabrics.

Researchers are also investigating development of new generation of textile reinforcements to assist the preform manufacturing process while considering the process economy. Such new generation of textile reinforcements includes development of hybrid reinforcements in which different fibre materials (e.g. glass, carbon and/or aramid fibres) are combined to optimise the performance and cost of the reinforcement to the required component. Recent generations of multiaxial technologies, such as MAX5 from LIBA also enables online (or offline) tow spreading capability and accurate placements so as to produce a quadriaxial fabric with areal weight as low as $200\,\mathrm{g\,m^{-2}}$ using carbon fibres. It has to be noted that spread tape NCF production using glass fibres is rarely reported.

3.2.2 Fibre spreading technology

Fibre spreading technology and their NCF's offer several advantages as composite reinforcements:

- enable thin plies to be fabricated and provides additional design freedom in terms of ply orientations [133, 131]
- thin plies provide enhanced mechanical properties for similar weights as reported by Tsai and others [133, 3, 26]
- spreading enables use of coarser/heavier rovings such as 24 K or 50 K to produce finer fabrics and hence warrant economic gains [86, 128, 134]

The spreading process in recent years has been identified as a key element to using heavy tow fibres for aerospace applications. There are several ways to spread different kinds of fibres, a detailed overview of these processes, studies and patents is presented by Singery [134] in her thesis. These processes can be divided into active or passive spreading methods and some of them include a combination of both. For the active methods, energy is used to spread the roving, for example the use of an airflow (pressure or suction) in a small gap or the transfer of ultrasonic waves and vibrations into the filaments. The passive methods only use tension and a constant movement over different geometries like spreading bars, convex or other geometrical guiding elements.

Broadly the patents on spreading can be divided into 4 sections:

- based on static mechanical techniques (US 7 536 761 B2, EP 0 972 102 B1),
- based on pneumatic techniques (EP 0 837 162 B1, EP 2 213 775 B1, EP 2 436 809 B1 and EP 1 548 166 B1),
- based on dynamic mechanical techniques (US 04 959 895, EP 0 302 449 A2), and
- others diverse techniques and combinations (EP 0 467 313 A1, FR 2 618 456 and FR 2 148 729).

In the current work with objective to optimise the parameters for spreading of glass fibres and to understand the extent of spreadability of selected glass fibres, the offline spreading technology from LIBA (type UD 60006) is used. The method of spreading here is mechanical using transverse vibrations as described in Fig. 3.7b. The schematic of this offline spreading machine is presented as in Fig. 3.7a. Being the focus of the current work, details of the machine set-up and parameters are discussed in Section 3.3.

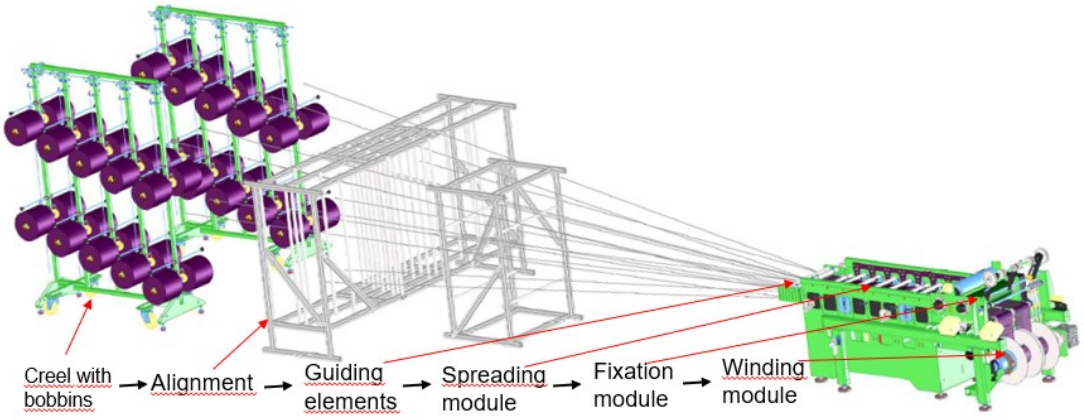

(a) Schematic of the offline spreading technology from LIBA

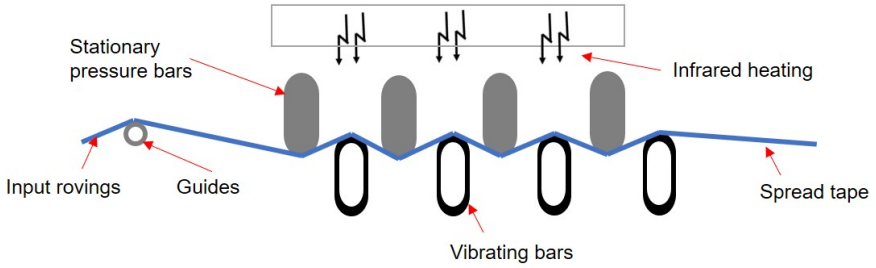

(b) Description of spreading module

Fig. 3.7 Offline spreading machine and spreading module from LIBA. (www.karlmayer.com).

3.2.3 Intermingled hybrids

Intermingled fibre hybrids have two different fibres hybridised at fibre level, i.e. these kind of hybrids have the highest dispersion. Commingling is one of the most widely used process for such hybridization, while, fibre level hybrid by spreading technology is not reported in literature till today. Spread tape manufacturing is a cost intensive process and has been widely used for very specific fibres such as heavy tow carbon fibres which are in general significantly cheaper than finer tows. For almost all of the fibre level hybrid studies reported, thermoplastic fibres are the most widely used fibres along with either carbon or glass fibres. Commingled yarns consist of reinforcing filaments or fibres and the matrix component integrated into the yarn structure in form of powder, staple fibres, filaments, or split-films. The commingling process over the years have been used in textile processing for a wide range of reasons such as, developing a core sheath yarn for functionalities such as moisture uptake and comfort, to develop economic alternatives of a costly yarn, to combine low strength natural fibre with a technical fibres and to develop hot press moulded thermoplastic composites among others. Manufacturing of the composite part from such textile preforms for example directly

in a hot press is possible without any separate impregnation process has been of interest for composite engineers [32]. Extensive studies are also reported in which researchers combine fibres such as glass or carbon (continuous or discontinuous) with other thermoplastic fibre to produce a commingled yarn textile product which can be used in composite production using hot press methods [148, 139]. The traditional commingling technologies are based on air-texturing, dref-spinning, core spinning and twisting. These processes in-principle mixes fibres either by blowing air through or surface friction or by simply twisting methods. These processes typically lead to a dispersion that is not on the fibre level, but more on the yarn level. Fig. 3.8 shows a typical microstructure of commingled yarns.

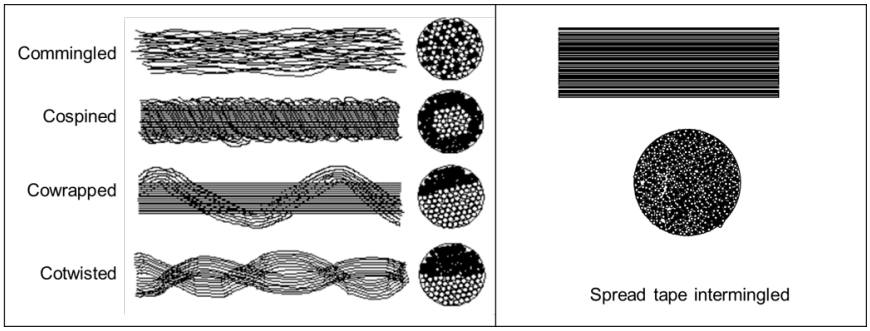

Fig. 3.8 Different kinds of fibre level hybrid textile structures

Commingling of two technical fibres such as carbon and glass together is challenging; a potential disadvantage here is that it can introduce damage to the fibres, which reduces the strength and the possible synergies that may arise because of hybridization. Several solutions to avoid such kind of damage has been looked upon by researchers, for example, Mäder et al. [95] proposed spinning the polymer fibres while commingling and Yu et al. [170] proposed process such as aligned discontinuous composites. The problem with these techniques is that these are not applicable to two technical fibres or for continuous fibre reinforcements. Advantage of combining technical fibres such as carbon and glass at fibre level is that these reinforcements then can be used in several of the liquid composite moulding processes. Hybrid effect in composites is hypothesised to be highest in composites where the dispersion is highest, but proofs are not available as manufacturing of these highly dispersed hybrids is not easy.

As of today, processes such as tow spreading for spread tape and NCF manufacturing; and commingling have reached a certain maturity for non-hybrid composites, these advancements open new opportunities for hybrid composites specifically for those fibre level hybrids (intermingled hybrids), which were earlier seldom reported. While spreading of carbon fibres is reported and commercially available, spreading of glass is studied for the first time on commercial spreading technology. It is expected that the optimised process for glass

fibres will further widen the applicability of hybrid reinforcements and composites for newer applications using technologies such as RTM. The current work explores the very first study of commingled hybrids and spread tape intermingled hybrid composites using carbon and glass fibres in Chapter 5. The current chapter explores the possibility of fabrication of a new type of carbon/glass intermingled hybrid fabrics through fibre spreading process.

3.2.4 Design of Experiments

It is very important to plan and conduct experiments to obtain enough and relevant data so that the science behind the observed phenomenon can be inferred and understood. Similarly, for optimising a process planning of experimental techniques is vital to correctly infer and optimise the process. In textile processes like any other process three techniques for planning and conducting experiments are widely used: (1) trial and error approach, (2) Design of Experiments (DOE), and (3) robust DOE using the Taguchi approach. Trail and error is the simplest method and it is based on performing a series of experiments each of which gives some understanding of individual factors. It requires recording observations and measurements after every experiment so that analysis of observed data will allow one to decide what should be done next, i.e. which parameters should be varied and by how much. Many times such series do not progress much as negative results often discourage or not allow a selection of parameters which ought to be changed in the next experiment. This kind of experimentation is cost effective and largely depends on the experience of the experimenter. In this kind of experimentation, the interaction of factors is ignored and the data is also often insufficient to draw any significant conclusions; the objective of the optimisation generally still remains unsolved.

Design of Experiments on the other hand is a well planned set of experiments, in which all parameters (also called factors) of interest are varied over a specified range also called as levels), is a much better approach to obtain systematic data. Due to extensive and systematic experimental work this set of experiments ought to give desired results. It can be "Full Factorial Design" meaning a fully crossed design but one can also apply other space filling techniques which can improve the efficiency: Random, Fractional Factorial, Latin Hypercubes, Halton, Sobol, etc. The number of experiments and resources (materials, time and costs) required are prohibitively large. Sometimes the experimenter performs a subset of the complete set of experiments to save on the material, time and experimentation costs. The analysis for such subset is not very easy (though it may be easy for the mathematician/statistician) and thus effects of various parameters on the observed data are not readily apparent. In many cases, particularly those in which some optimisation is required, or some

specific problem such as improving the quality of manufactured products is to be solved, then, dedicated methods such as Taguchi is preferred.

Dr. Genichi Taguchi of Nippon Telephones and Telegraph Company, Japan has developed a technique based on orthogonal array of experiments which provide much reduced variance for the experiment with optimum setting of the process control parameters. Thus coming together of Design of Experiments with optimisation of control parameters to obtain best results is achieved in the Taguchi Method. Taguchi designs are based on prior selection of the most likely interactions, whereas in standard fractional factorial designs, the interactions are selected later on, after the initial results from the designed experiments have been analysed. The way in which interactions are selected clearly differs between the two approaches. Orthogonal Arrays (OA) provide a set of well balanced (minimum) experiments and Taguchi's Signal-to-Noise ratios (S/N), which are log functions of desired output, serve as objective functions for optimisation, help in data analysis and prediction of optimum results. This technique has been widely used in different fields of engineering to optimise the process parameters and to determine the impacts of different parameters within the combination of design parameters. Thus the integration of Design of Experiment with parametric optimisation of process is achieved in the Taguchi method further providing desired results. The Taguchi Method treats optimisation problems in two categories, (1) a static problem, which involves determining the best control factor levels so that the output is at the the target value, and (2) a dynamic problem, which involves an additional signal input apart from the control factors that directly decides the output. In this chapter a static method is used where the desired result refers to the target spreadability of glass fibre in a fibre spreading process. The details of experimental plan is described in the Section 3.3.

3.3 Experimental study

3.3.1 Materials

Advantex Glass, a boron-free corrosion resistant E-CR glass fibre was used for the primary optimisation study of the fibre spreading process. This glass has similar mechanical behaviour to standard E-Glass and has superior corrosion resistance. 111A, 1200 tex (with approximately 2000 fibres in the cross-section), direct rovings containing these fibres were procured from Owens Corning. The glass fibres that are commercially available exist in the form of an internally unwound package called spools as shown in Fig. 3.9.

A short study to understand spreading behaviour of commingled rovings was also accomplished. Commingled A and Commingled B rovings were obtained from Supplier A and

Supplier B who used their proprietary commingling process to manufacture their carbon/glass hybrid commingled rovings. The Supplier A rovings contained HTS45 carbon, 12 K (approximately 800 tex) and E-Glass, 2×300 tex from Toho Tenax Europe GmbH and PPG industries respectively. While the Supplier B roving contained 2×24 K (approximately 1600 tex), AS4 carbon fibres and 1200 tex 111A E-CR Glass, from Hexcel Corporation and Owens Corning respectively.

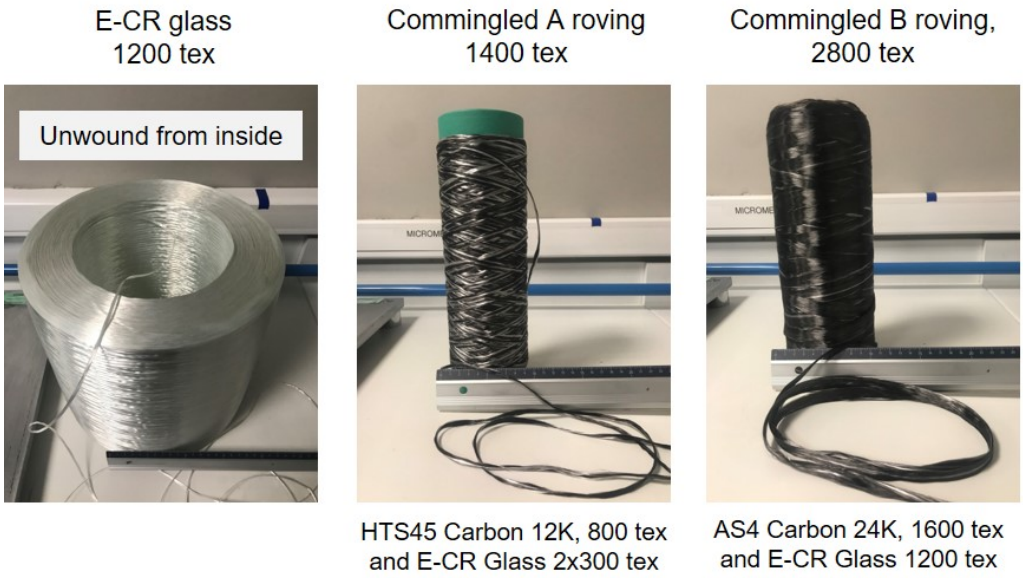

Fig. 3.9 Pictures of glass rovings and commingled rovings used in the spreading study.

3.3.2 Methods and means

The objective of the thesis is to study the hybrid effect and mechanical behaviour of carbon/glass hybrid composites hybridised at ply, yarn and fibre levels. For fibre level hybridization we identified two forms of textile processing, commingling and hybridising through simultaneous spreading of carbon and glass. Before we reach to a step where the simultaneous hybrids can be fabricated, it was essential to fill the gap in the current state of the art, this gap referred to spreading of glass fibres. Spreading technology have been used for carbon fibres recently to manufacture thin-ply fabrics with economical and heavier tows. In this process the width of input rovings is increased and its thickness is reduced, so as to create a tape like form for each roving, when such rovings are joined side by side, it produces a spread tape as seen in Fig. 3.10. This technology has not been studied for glass fibres. The main reason for this is the fact that cost of glass fibres in some cases are approximately one tenth of the carbon fibres, and unlike carbon fibres, finer glass rovings do not significantly

differ from heavier rovings in terms of their costs. But spreading technology can assist in the fabrication of fibre level reinforcements and owing to this, glass fibre spreading has received renewed interest. Also, glass fibres with higher strength are currently developed for composite applications and these glass fibres sometimes cost in the range for carbon fibres, hence spreading of these fibres also have received interest from the applications developers for composite materials.

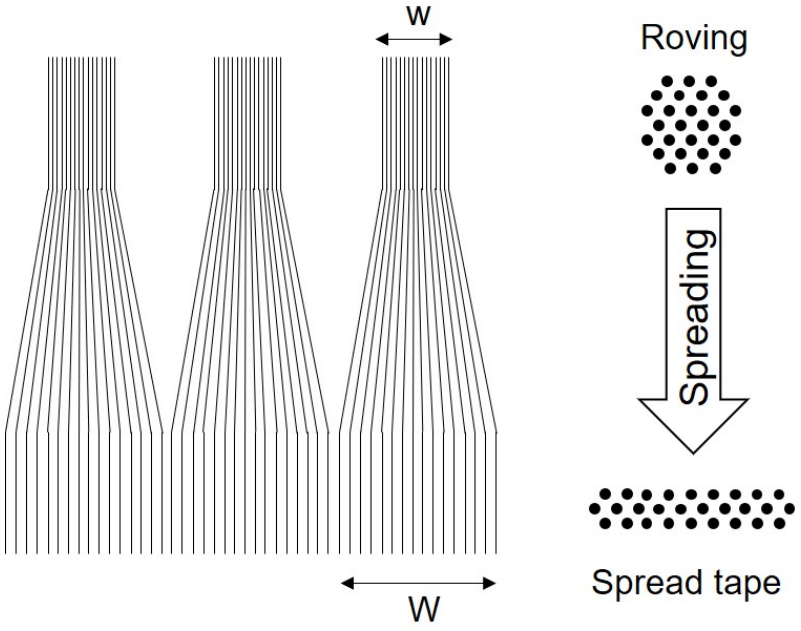

Fig. 3.10 Schematic of fibre spreading.

In this chapter we report the first ever study on glass fibres to optimise the fibre spreading process parameters. The objective is also to evaluate maximum spreadability of the selected glass fibres. The spreadability of a fibre roving is defined by the Eq. 3.1:

$$\text{Spreadability } (\%) = 100 \times \frac{\text{Tow width after spreading - Tow width on the bobbin}}{\text{Tow width on the bobbin}} \tag{3.1}$$

The measure of spreadability was identified as the quantitative criteria for optimising the spreading process, while qualitatively, the broken fibres, gaps on the surface were looked upon vis-à-vis ideal spread tape (Fig. 3.10) to explore the effect of processing parameters. A "Zero Point" of the technology was established based on the parameters already optimised for carbon fibres [134]. Further important parameters were identified and varied for a range to understand its effect on spreadability, finally, the optimal configuration for the maximum spreading limit was identified through Design of Experiments technique.

During the experimental trials, 10 rovings were spread and analysed at the same time, the rovings were arranged parallel, next to each other with a regular space in between them before spreading. Further using digital imaging, widths of these 10 rovings after spreading were measured using image analysis tool to ensure reliability and faster analysis [134]. For every parameter setting, about 25 photographs of spread tows were taken every 15 s by a Canon EOS 1100D SLR 12MP camera with EF-S DC III, 18 to 55 mm, F / 3.5 to 5.6 lens specifications. The camera was positioned on a support to repeatedly capture photographs of the 10 rovings after they appeared from spreading zone. The point of photography along the process was chosen (Fig. 3.11) so that there is enough space to put the camera, the brightness is correct (enough light without reflection) and the rovings are flat, horizontal and on the same level to avoid distortion during the image analysis.

Fig. 3.11 Image recording setup for spread tow width measurement.

This camera was controlled from a computer using DSLR Remote Pro multi-camera software developed by Breeze Systems Software. It is able to control one or two cameras simultaneously or independently and provides possibility of adjusting the camera settings directly from the computer. The camera is programmed to take pictures of the area of interest automatically, as per requirement, hence avoiding any human interference, which may affect the quality of images and thereafter their analysis.

To analyse images captured during experimental tests, ImageJ software was used[1]. The software is developed by National Institute of Health (USA) and allows for the most image analysis operations such as display, thresholding, processing, applying filters, measurement

[1]ImageJ an open to use software in public domain for image processing, using the JAVA programming language, running on both Windows, Mac or Linux and can be downloaded at: http://rsbweb.nih.gov/ij/download.html.

etc. Furthermore the software allows for possibilities of additional functionalities by means of user developed macros and plugins. To automate the image analysis for the current work, a plugin developed by Singery [134] was used, the details of the plugin can be found in her PhD thesis [134]. The basic steps involved with this analysis were as follows:

- Convert set of images into a stack in ImageJ
- Define region of interest (ROI)
- Transform pixels of this color image to gray-scale
- Applying a predefined threshold value for the ROI to differentiate fibre and non-fibre region
- Scan the ROI area "pixel by pixel" and "line by line" to determine the number of rovings and their widths in pixel
- Convert pixels to mm scale, using the predefined conversion scale (measured by capturing a ruler along with one of the image in the set)

An example of the original and processed image is provided in Fig. 3.12. For a set of pictures captured for an experimental trial, one additional picture was captured by introducing a physical mm scale at the same level as in the rovings in the region of interest. This picture was used to calibrate the pixels to length units for all the measurements in the set of pictures. The "bands" in the image refers to the spread tow width while the gaps refer to width in between two tows. The software also enables micro-gap measurement, where smaller and finer gaps could also be measured. The plugin can also analyse a spread tape, instead of the spread rovings, but this is out of scope for the current work.

As mentioned earlier, apart from the above mentioned optimisation study, short studies on spreading behaviour of commingled rovings have also been carried out. As commingled rovings are already considered to be a fibre level hybrid, but the homogeneity of mixing of carbon and glass is not very significant, it was hypothesised that spreading can improve the dispersion of carbon and glass compared to that in the original commingled rovings. In the end, using optimised parameters, fibre level hybrids were manufactured by simultaneous spreading of carbon and glass fibres. The results of commingled roving spreading and the simultaneous carbon/glass spreading are presented in Section 3.4

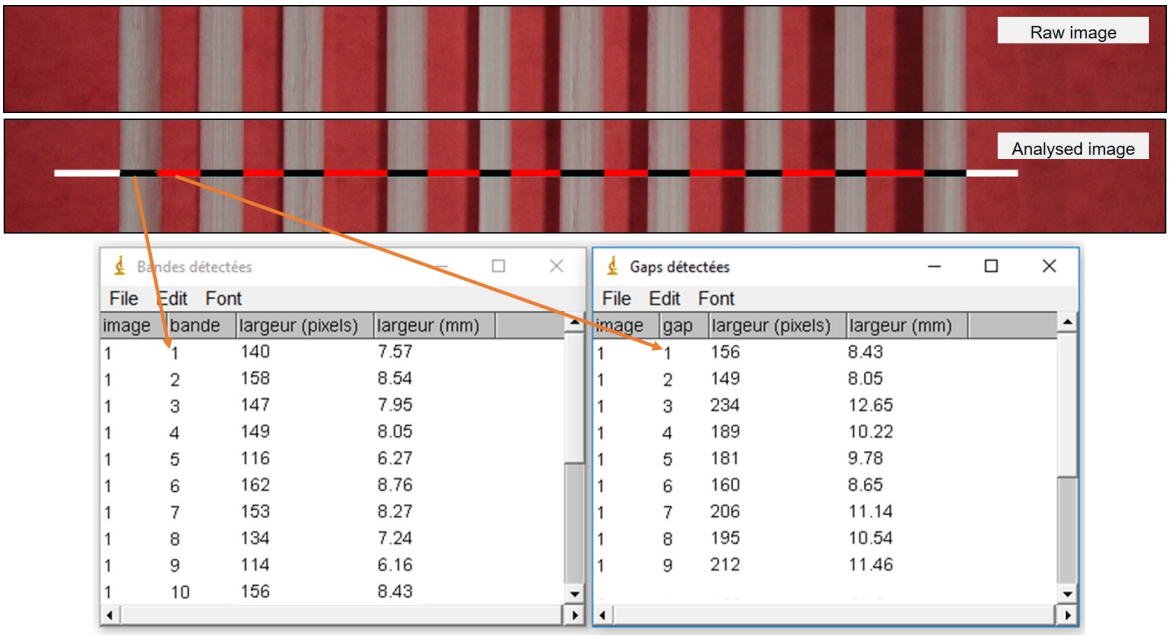

Fig. 3.12 Measurement of spread tow width using Image analysis.

3.3.3 Design of experiments

For the process optimisation study for fibre spreading process, there are a lot of parameters that needs to be optimised. Further these parameters can have a range of values. For a full experimental optimisation, the number of experiments required and the costs associated with it are huge, rendering this option non viable. Hence, in this study, a factorial experimental plan was defined keeping into mind the following points:

- Studying the most important factors only
- Perform a minimum number of experiments with maximum precision
- Model the response, characterising a process

It is to be noted here that, the interaction effect among the selected parameters was not prioritised in this study, as previous studies by Singery [134] reported that the interaction effects among the selected factors in spreading process is not significant. To fulfil these criteria, we used Taguchi's technique for solving optimisation problem and to study the parametric influence on responses.

In the current experimental design, "control factors" are the parameters that will be studied and "levels" are the values that a factor can take during the tests. "Response or quality characteristic" corresponds to the quantity measured at the output, in our case, the width at the end of spreading is the response of the experiment for a factor and level combination.

In order to apply the Taguchi method for the present investigation, eight steps have been followed as seen in the flowchart in Fig. 3.13 and the details of the study are described in Section 3.4.1.

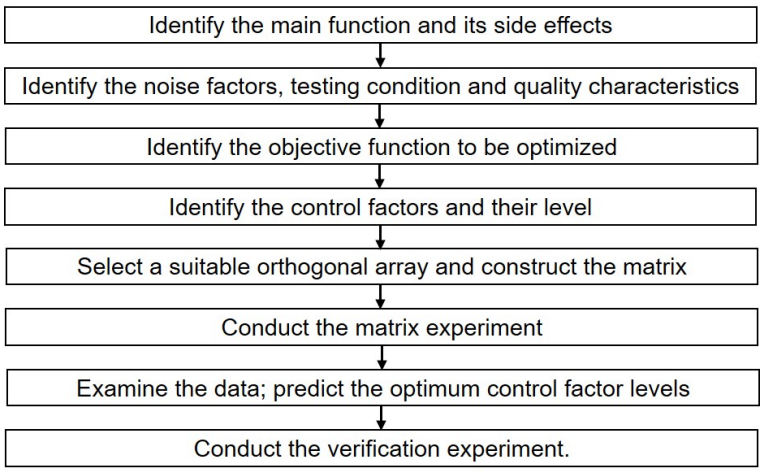

Fig. 3.13 Steps involved in parameter optimisation using Taguchi's method.

The analysis of the results obtained by conducting the experiment was organised and carried out using Minitab, a statistics package developed at the Pennsylvania State University. Statistical analysis software such as Minitab automates calculations, allowing the user to focus more on the analysis of data and the interpretation of results. In the Minitab 18, analysis of Taguchi's L9 orthogonal array with 3 levels is not straightforward, and it does not provide any hint on the interaction effect, hence a Generalised Linear Model is used for the analysis. Both Generalised Linear Models and Least Squares Regression investigate the relationship between a response variable and one or more predictors. A practical difference between them is that Generalised Linear Model techniques are usually used with categorical response variables, while, Least Squares Regression is usually used with continuous response variables. Least Squares minimises the sum of squared errors to obtain maximum likelihood estimates of the parameters. Generalised Linear Models obtain maximum likelihood estimates of the parameters using an iterative re-weighted least squares algorithm. The Generalised Linear Models in general can include interaction and polynomial terms, crossed and nested factors, and fixed and random factors.

3.4 Results and discussions

3.4.1 Optimisation of glass fibre spreading process

As mentioned earlier, most glass fibre bobbins are commercially available in the form of spools and that the rovings has to be unwound from inside the spool. The problem with using these packages is that internal unwinding adds twists in the rovings which is detrimental to spreading and that a positive and uniform control of tension in the rovings is not possible. Such bobbins can be used in external unwinding fashion, but it requires a special bobbin holder and the creel which can sustain the heavy weight of glass tows and their sizes. One such creel enabling tension control and external unwinding for glass fibre spools has been recently developed by Texmer [2], a single bobbin holder can be seen in Fig. 3.14. As replacing the whole creel with such holders is not possible and is very cost intensive, in the current experiments the existing spools were first converted from an internal unwound package to an external unwound package. This involved a single bobbin holder as in Fig. 3.14, from which roving was unwound from outside and rewound on a standard 3 inch card board core, which can be universally used on most of the existing creels including the one for the used LIBA spreading machine. The rewound package was assessed to be suitable for spreading operation and that no twist addition was found in the rewound bobbing when compared to the original bobbin.

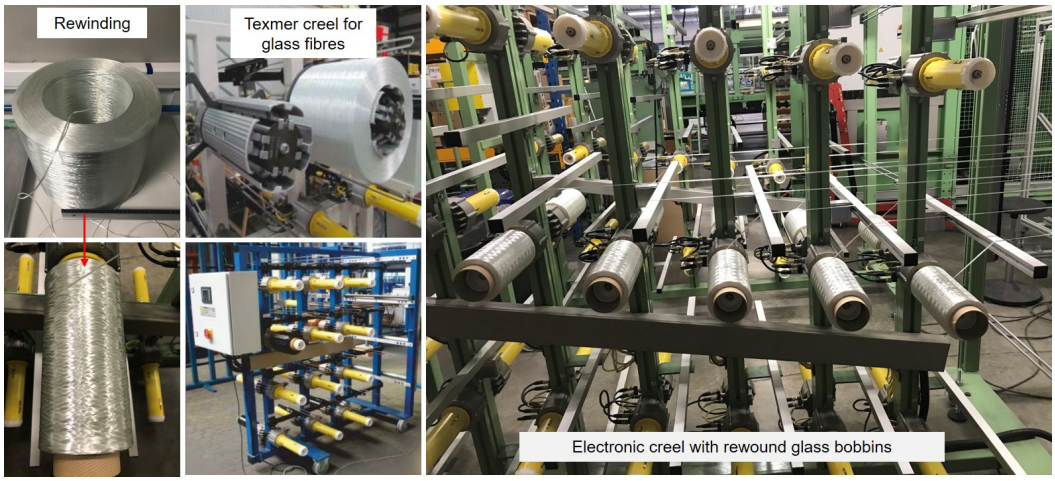

Fig. 3.14 Glass fibre rewinding and creel for the spreading machine.

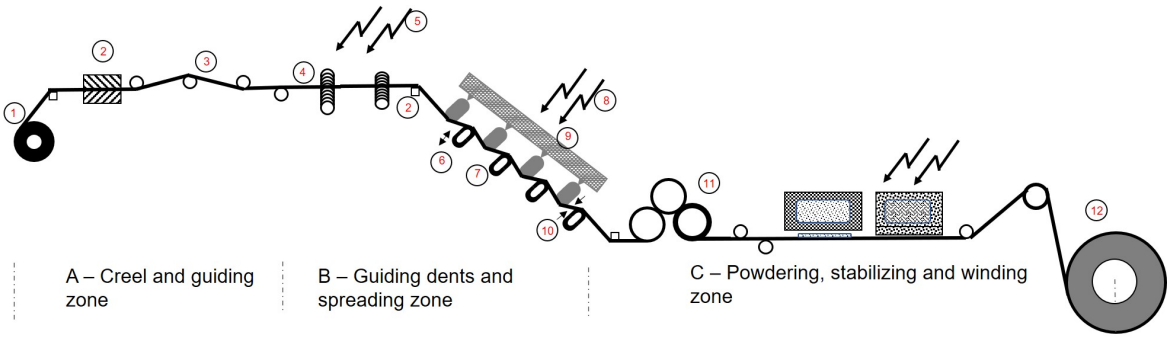

1 – Bobbin tension	2 – Alignment flaps	3 – Guides, and spacing	4 – Dents and spacing
5 – Temperature at dents	6 – Vibration traverse	7 – Vibration frequency	8 – Temperature at spreading
9 – Number of bars	10 – Depth of bars/pressure	11 – Winding pressure	12 – Production speed

Fig. 3.15 Schematic of the spreading process and important process parameters.

3.4.2 Parameter optimisation

The schematic of the offline spreading process is presented in Fig. 3.15. The main function for the study was parameter optimisation for spreading of glass fibres. There are several parameters marked from 1 to 12 that can affect the main function. Apart from these the uncontrollable factor such as initial width of the rovings, twist in the rovings, moisture and humidity in the surroundings, etc., can also affect the response, these are noise factors. On contrary to carbon fibres, for glass fibre bobbins the twist is not commercially mentioned by the manufacturer, also the unwinding of glass rovings from inside adds twist to the roving. After listing the control and the noise factors, decisions on the factors that significantly affect the performance were ascertained and only those factors were taken into consideration in constructing the matrix for experimentation. All other factors were considered as noise factors. The width of the tow after spreading was the quality characteristic to be observed during the study and the objective function of larger-the-better was selected. The factors and their levels were decided for conducting the experiment were based on a brain storming session with a group of people with expertise on spreading and also based on the "Zero Point" established for carbon fibre spreading. The factors and their levels are shown in Table 3.1.

Out of the four factors selected, three of them (Frequency, Temperature and Depth) were from the heart of the process, i.e. the spreading zone. While one factor each from input side (the bobbin Tension) and output side (the production Speed) was identified to be studied. Owing to limitations in number of experiments that could be done, only Speed was considered as a factor in the current study, though Tension as a factor has a significant

[2] www.texmer.de

Table 3.1 Selected factors and their levels for the parameter optimisation study.

Factors	Levels		
	1	2	3
Frequency [Hz]	15	30	45
Temperature [°C]	RT	100	150
Speed [m min^{-1}]	2	4	8
Depth [units]	2	4	6

effect on spreading as reported by Irfan et al. [67] and Singery [134]. The interaction effect between frequency and speed was identified to be interesting but was not considered in the experimental plan for two reasons: (1) limiting number of experiments and (2) Singery [134] reporting insignificant interaction effect for carbon fibres. The P-Diagram for the experiment and the selected L_9 (3^4) orthogonal array is presented in Fig. 3.16.

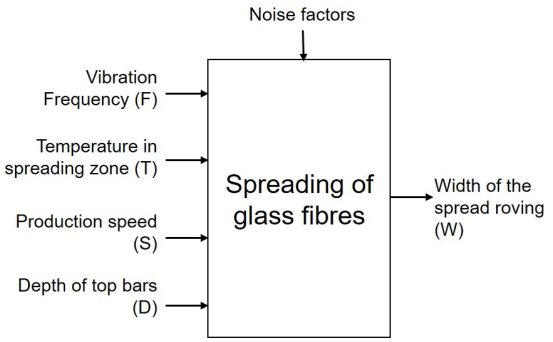

Experimental Run	Frequency (F) (Hz)	Temperature (T) (°C)	Speed (S) (m/min)	Depth (D) (Unites)
1	15	RT	2	2
2	15	100	4	4
3	15	150	8	6
4	30	RT	4	6
5	30	100	8	2
6	30	150	2	4
7	47	RT	8	4
8	47	100	2	6
9	47	150	4	2

Fig. 3.16 P-Diagram and the L_9 orthogonal array used for the study.

The parameters Frequency, temperature and speeds were directly changed from the control panel, while altering the depth of the top bars was not direct. It has to be noted that the change in depth of top bars, directly affects the tension in the fibres, it increases surface contact of the fibres with the bars (vibrating and non-vibrating). Though the depth cannot be directly reported in the length scales, the depth in the experiments was altered by addition of "spacer rings" as can be explained in Fig. 3.17

In accordance with the selected orthogonal array (Fig. 3.16), experiments were conducted with their factors and their levels as mentioned in Table 3.2. The experiments in the plan were conducted randomly (with trial sequence t01-t09) and 10 rovings were used for each measurement to account for the variations that may occur due to the noise factors. For each experiment the machine was allowed to run for 5 min before the spread tow measurement begins and that for each run, measurements were done at least 24 times at a gap of 15 s

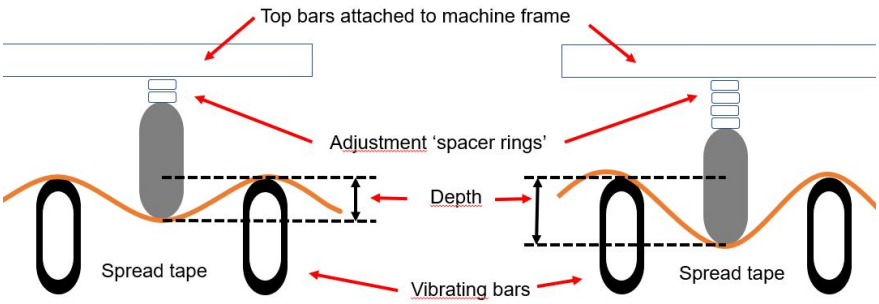

Fig. 3.17 Depth setting of top bars in the spreading zone.

between each measurement. The width of roving after spreading was measured as explained in the Section 3.3 and the representative samples of analysed pictures for some of the experimental tests with lowest and highest widths is presented in Fig. 3.18.

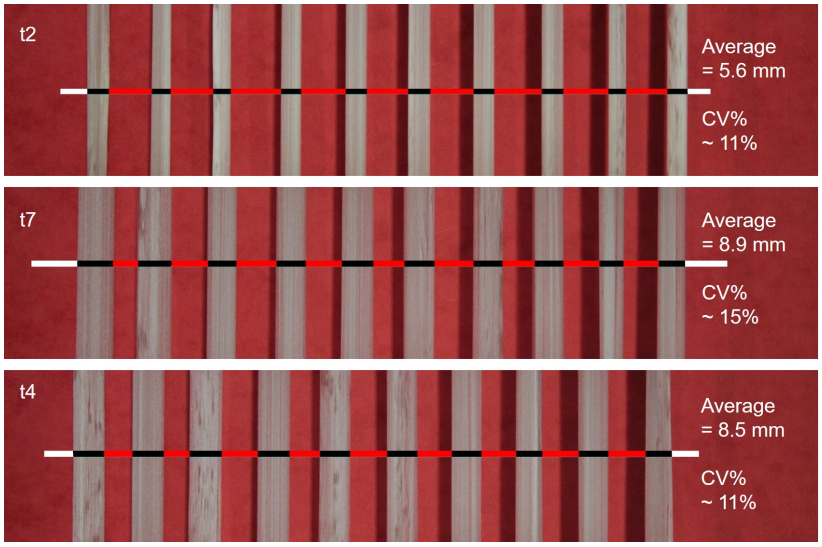

Fig. 3.18 Measurement of spread tow width for representative samples from different experimental trials.

Table 3.2 shows the measured values of widths of rovings after spreading obtained from different experiments. All the experiments were considered to be valid as there were no excessive broken fibres or degradation of the rovings observed on the surface of the rovings.

For analysis using Generalised Linear Model in Minitab, the data set was processed to include same number of observations/responses for each experiment. The common minimum number of photographs for each test which had all the roving measurements recorded without any fault or micro-gaps, were selected to be analysed for all tests. In the analysis we used the average roving widths for 8 central rovings in 12 photographs for each experimental run. The

Table 3.2 Experimental matrix and results

Experiment No.	Trial sequence	Frequency F [Hz]	Temperature T [°C]	Speed S [m min^{-1}]	Depth D [units]	Average width [mm]	Standard deviation	Coefficient of variation [%]
1	t02	15	RT	2	2	5.6	0.6	10.9
2	t06	15	100	4	4	7.7	0.9	12.0
3	t05	15	150	8	6	7.6	1.0	13.1
4	t03	30	RT	4	6	6.5	0.9	13.0
5	t08	30	100	8	2	6.4	0.7	10.6
6	t07	30	150	2	4	8.9	1.4	15.1
7	t01	47	RT	8	4	6.1	0.8	12.6
8	t04	47	100	2	6	8.5	1.0	11.3
9	t09	47	150	4	2	6.9	0.8	11.5

two edge rovings were not taken into the analysis as the two edge rovings practically do not have constant tension like for the central rovings and the variation of widths for edge rovings was higher than that measured for central rovings. The histograms for the spread tow widths for different trials is presented in Fig. 3.19a. It was observed that though the distribution of widths for each experiments was symmetric but probably the distribution was not a Normal (Gaussian) distribution for some of them. This was confirmed by the Normal probability plots as shown in Fig. 3.19b. It was seen that for some of the trials the distribution of widths was not Normal, nevertheless, as asymmetries were not too strong, we could use statistical functions like ANOVA (Analysis of Variance) with appropriate precautions.

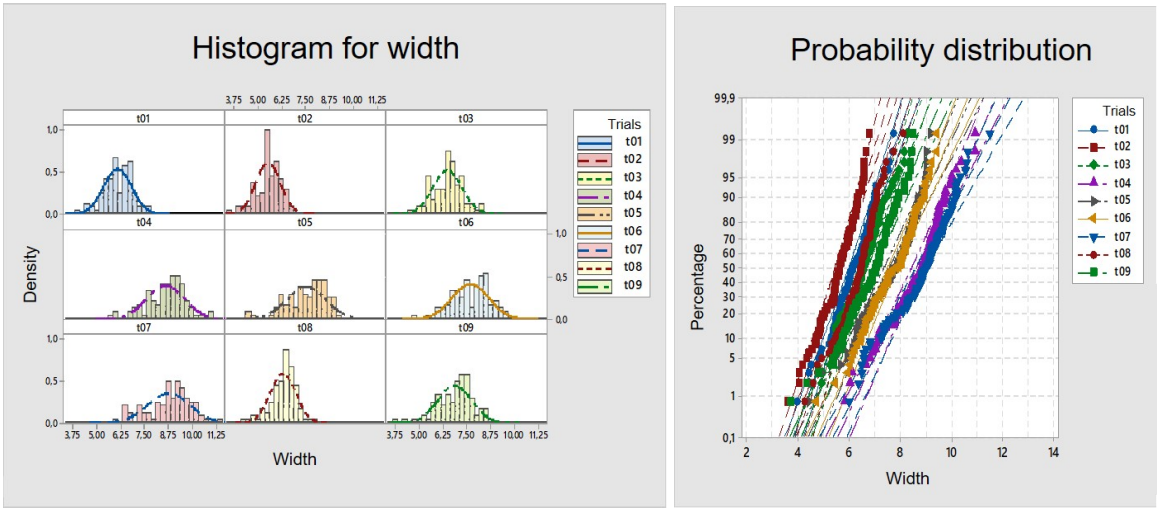

(a) Histotogram (b) Normal probability plot

Fig. 3.19 Histogram for widths for different trials and their Normal probability plots.

Boxplots for the width of spread tow for all the tests showed (Fig. 3.20a) that the abnormality of the width data was prominent on the left side and that there is a large overlapping between trials. The abnormality on the left side of box-plot can be explained by

the twist that might be present in the as received glass fibre rovings (Fig. 3.21). Regardless of the parameter combinations used, spreading of an already twisted roving will not yield significant increase in the width of the roving. Some of the abnormality in the width data hence can be explained by the differences in the rovings themselves as explained by the box plot for just roving N° 4 values in each trial in Fig. 3.20b.

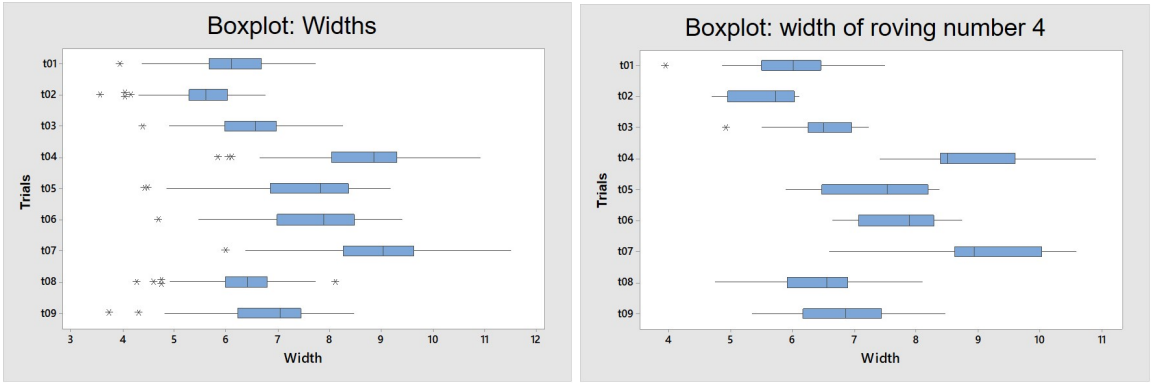

(a) Boxplot: width all trials

(b) Boxplot: width for roving 4

Fig. 3.20 Box plots demonstrating abnormality in the roving width distribution (a) for all trials and (b) for a single roving position.

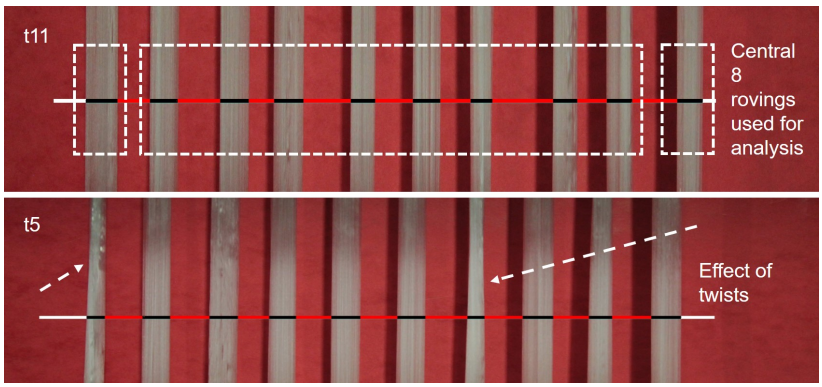

Fig. 3.21 Initial widths and twists in the rovings as an uncontrolled / noise factor

Owing to a large overlapping between the distributions plots for the trials, it can be concluded that the parameters variation can not explain all the width variation in the rovings after spreading. In other words variation in width occurring due to “External variation” (due to studied parameters, trials) is significant, but the “Internal variation” variation (inside Trials, due to the noise and uncontrolled parameters such as twist or initial roving widths) is also large enough.

Further plotting a multivariate plot for width as a function of tests (Fig. 3.22a) and width as a function of Tests and Roving Position (Fig. 3.22b) shows that the roving position has

a little impact on the mean and the variance of Width. Roving position did not show a significant effect on relative impacts of the studied parameters and for each roving position same pattern of change in average width was observed for all trials. No interaction between roving position and parameters changes is observed.

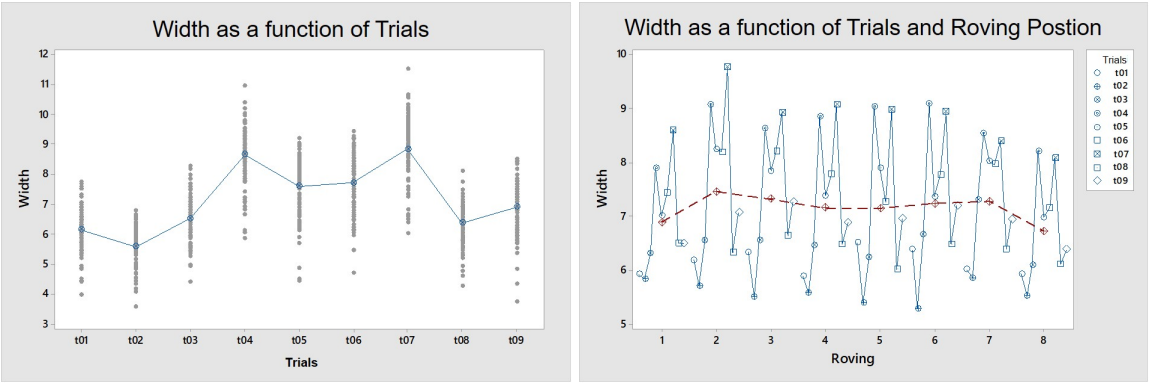

(a) Width as a function of trials (b) Width as a function of trials & roving position

Fig. 3.22 Multivariate charts (a) Width as a function of trials and (b) Width as a function of trials and roving position.

As reported, width did not follow Normal distribution in all the trials, but, for all trials it was symmetric enough to use ANOVA. In the study for effect of trials (global parameters) on the width we used the condition of not equal variances, the inequality of variance was confirmed by the "Test for equality of variance". One-way ANOVA for mean widths for each trial (global parameter) suggest that the global parameters have significant effect on the mean width of the spread roving with R-square value of 59.5 % (Fig. 3.23). This means, the global parameter variation (Trials) explains about 60 % of the width variation. It was observed that the Residuals are not Normal, that means that uncontrolled parameters have an impact on the Width and this impact of uncontrolled parameters, between 0 % and 40 %, can come from the roving. As also described in Fig. 3.22 the multivariate charts that the roving as an uncontrolled variable has a significant impact. Further digging the effect of roving, we studied effect of trials (global parameters) on individual rovings, instead of using average for all 8 rovings, we observed using ANOVA, the global parameters have significant effect on the mean width of each individual roving with R-square value for all the 8 rovings between 51 to 80 %. This again confirms that the effect of uncontrolled parameter in the form of roving is significant and prompts further study on this factor.

The Design of Experiment analysis to study the main effects of the selected factors on width was done by using Generalised Linear Model. For the initial analysis, interaction effects between the factors was not considered. It was found that all the four selected parameters (Frequency, Temperature, Speed and Depth) are statistically significant and they

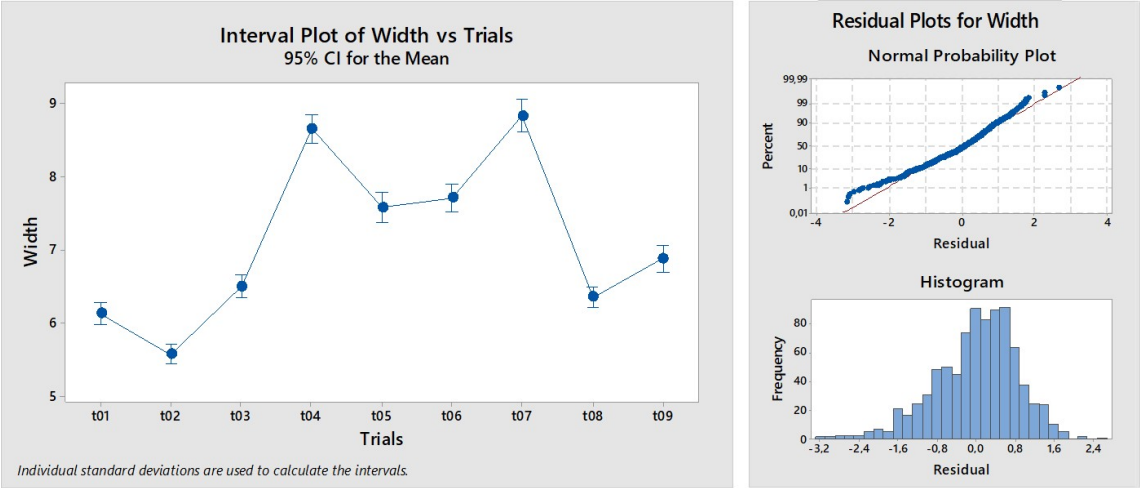

Fig. 3.23 One-way ANOVA: Width as a function of Trials.

explain about 51 % of the Width variation (Fig. 3.24a). As also observed for the ANOVA for global parameters, here too the residuals are not Normal. The main effects for the mean widths for different factors can be seen in Fig. 3.24b. It can be concluded from the main effect plots, that the Frequency, Temperature and Depth, from Level 1 to Level 3 had a positive effect on width, while for Speed the effect was negative. For the selected levels, Temperature had the highest effect and high temperatures led to higher widths. The effect of increase in speed was nearly linear, with increase in speed reducing the widths of the spread tow. From Fig. 3.24a, it can be concluded that among the selected factors, the Temperature followed by Depth of the top bars and Speed of production were the three most important factors affecting the width. The effect of Frequency was also significant, but the effect is observed to be small compared to other factors.

Considering no interaction, the regression equation for the analysis can be given in the form of:

$$\begin{aligned} \text{Width} = {} & 5.057 + 0.00827 \times \text{Frequency} + 0.013753 \\ & \times \text{Temperature} - 0.1546 \times \text{Speed} + 0.3265 \times \text{Depth} \end{aligned} \tag{3.2}$$

This regression equation quantifies the relationship between a response variable (Width) and one or more control factors. Regression also enables future predictions or indications of past behaviour for a process based on the selected levels of one or multiple factors. When second order interaction effect is considered for the Design of Experiment, then the General Linear Model again concludes significant effects for all the 4 selected factors. Apart from this, three second order interaction factors, namely, Frequency$\times$Temperature, Frequency$\times$Speed and Temperature$\times$Speed are identified to have significant effect on the Width of the spread rovings as it can be seen in Fig. 3.25a and Fig. 3.25b. It is to be noted that if the interactions

General Linear Model: Width versus Frequency; Temperature; Speed; Depth

Analysis of Variance

Source	DF	Adj SS	Adj MS	F-Value	P-Value
Frequency	1	10,09	10,090	10,75	0,001
Temperature	1	453,36	453,359	482,84	0,000
Speed	1	128,50	128,502	136,86	0,000
Depth	1	245,59	245,588	261,56	0,000
Error	859	806,56	0,939		
Lack-of-Fit	4	141,06	35,265	45,31	0,000
Pure Error	855	665,50	0,778		
Total	863	1644,10			

Model Summary

S	R-sq	R-sq(adj)	R-sq(pred)
0,968995	50,94%	50,71%	50,39%

Regression Equation

Width = 5,057 + 0,00827 Frequency + 0,013753 Temperature - 0,1546 Speed + 0,3265 Depth

(a) Summary

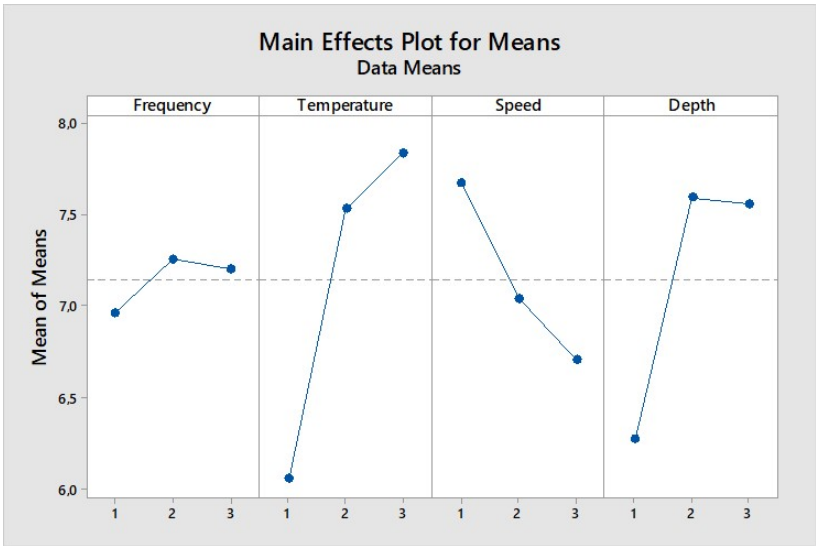

(b) Main effect plot

Fig. 3.24 General Linear Model: Width versus Frequency; Temperature; Speed; Depth without interaction effect, (a) Summary and (b) Main effect plot

are considered then the otherwise low effect observed for Frequency is negated and it becomes second important factor following the Temperature. Furthermore, all the interaction effects are more significant and more important than the two individual factors, namely, Speed and Frequency. This confirms that for glass fibres the interaction parameters are more important

in the vibration zone for spreading of glass fibres while this interaction effect is not significant for carbon fibres as reported by Singery [134]. The inclusion of interaction effect brings the R-square value close to 60 % which is similar to the one obtained using the One-way ANOVA for the trials.

Considering the effect of interaction, the regression equation for the analysis can be given in the form of:

$$\begin{aligned}\text{Width} = {} & 0.412 + 0.2722 \times \text{Frequency} + 0.06290 \times \text{Temperature} + 1.076 \\ & \times \text{Speed} - 0.3524 \times \text{Depth} - 0.001416 \times (\text{Frequency} \times \text{Temperature}) \\ & - 0.03565 \times (\text{Frequency} \times \text{Speed}) - 0.004469 \times (\text{Temperature} \times \text{Speed})\end{aligned} \tag{3.3}$$

For the analysis with or without interaction effects, the optimal parameters are identified to be: Frequency = 30 Hz ; Temperature = 150 °C; Speed = 2 m min^{-1} and Depth = 4 units (spacer rings). Theoretically leading to a response (width) of 8.36 mm for the first case (without considering interaction effects) and 8.90 mm for the second case (considering interaction effects).

The mean tow widths calculated can be correlated to the spreadability of the fibres for selected parameters through Eq. 3.1. The spread tow width for individual rovings for the selected fibre-parameter combination can also be correlated to the areal weight that can be achieved for the actual spread tape using those fibre-parameter combination by using Eq. 3.4, where the textile unit "Tex" represents weight in grams of 1000 meters of roving.

$$\text{Areal weight (g/m}^2) = \frac{\text{Roving count (in Tex) / 1000}}{\text{Spread tow width (in m)}} \tag{3.4}$$

Hence for the optimised parameter combination using Eqs. 3.2, 3.3 and 3.4, the optimum spread tape that can be fabricated using the optimised vibration module in the spreading process is 135 to 145 g m^{-2}. There are several other parameters for the spreading process which directly impact the spreading behaviour and those factor needs to be worked upon in future to reach maximum spreadability for glass fibres (identified in Fig. 3.15). It is also important in future studies to consider the noise factors; characterisation of twists in the roving, initial roving widths, bobbin placements on creel, guides and angles, etc., to accurately modelling the spreading behaviour.

3.4.3 Effect of complementary element

In the experimental trials mentioned above though the bobbin tension on the creel was identified an important factor, it was not used as a variable factor in the studies. The bobbin tension was set to 150 cN as a constant parameter for all the experiments. As concluded in

General Linear Model: Width versus Frequency; Temperature; Speed; Depth

The following terms cannot be estimated and were removed:
Frequency*Depth; Temperature*Depth; Speed*Depth

Analysis of Variance

Source	DF	Adj SS	Adj MS	F-Value	P-Value
Frequency	1	48,57	48,571	62,34	0,000
Temperature	1	145,33	145,332	186,53	0,000
Speed	1	20,34	20,343	26,11	0,000
Depth	1	13,97	13,969	17,93	0,000
Frequency*Temperature	1	30,28	30,278	38,86	0,000
Frequency*Speed	1	44,91	44,914	57,65	0,000
Temperature*Speed	1	18,05	18,053	23,17	0,000
Error	856	666,93	0,779		
Lack-of-Fit	1	1,43	1,431	1,84	0,175
Pure Error	855	665,50	0,778		
Total	863	1644,10			

Model Summary

S	R-sq	R-sq(adj)	R-sq(pred)
0,882680	59,43%	59,10%	58,70%

Regression Equation

Width = 0,412 + 0,2722 Frequency + 0,06290 Temperature + 1,076 Speed - 0,3524 Depth
- 0,001416 Frequency*Temperature - 0,03565 Frequency*Speed
- 0,004469 Temperature*Speed

(a) Summary

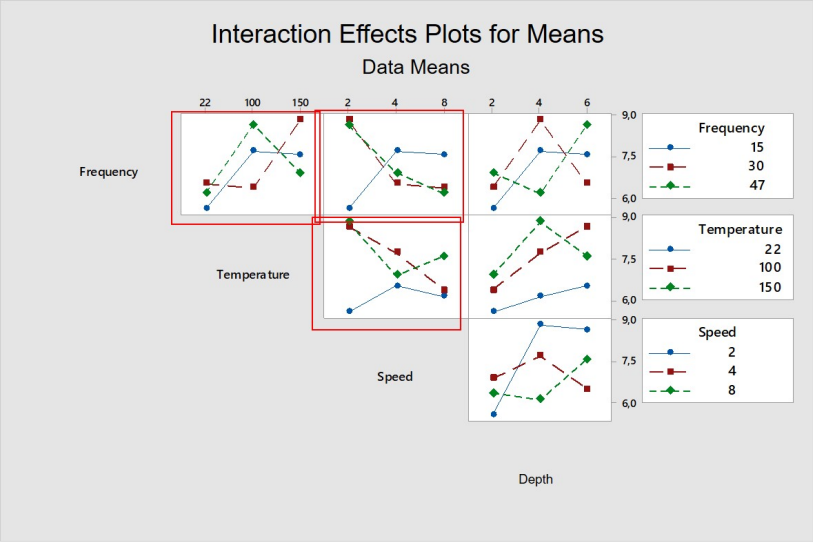

(b) Interaction effect plot

Fig. 3.25 General Linear Model: Width versus Frequency; Temperature; Speed; Depth with interaction effect considered, (a) Summary and (b) Interaction effect effect plot

the initial experiments, a lot of variation occurs in the spread roving widths, a majority of it can be traced back to the initial bobbin quality (twists, uniformity, etc.). Tension is not just a principal factor but also is an important factor that can affect the spreading through its interaction with other parameters. Apart from the tension applied through automatic electronic motors on the creel the guiding elements can also be used to increase tension in the rovings. The S-Guide element that can be seen in Fig. 3.26 is one such newly designed guide which serves multiple purposes: (1) applying additional tension, (2) to maintain a twist free state in the roving, (3) adjust the width of the final spread tape, and (4) initiate and assist in lateral spreading [67]. Two experiments using two paths as represented schematically in Fig. 3.27b and Fig. 3.27c were conducted to study if the spread roving width is altered by use of S-Guide and if the effect is significant.

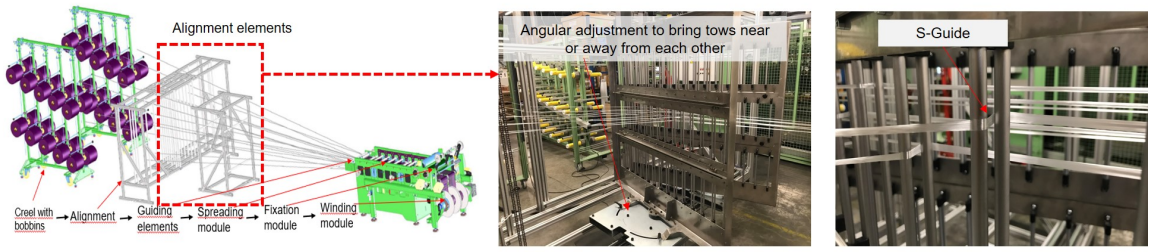

Fig. 3.26 Photographs of the complementary S-guides between creel and spreading zone.

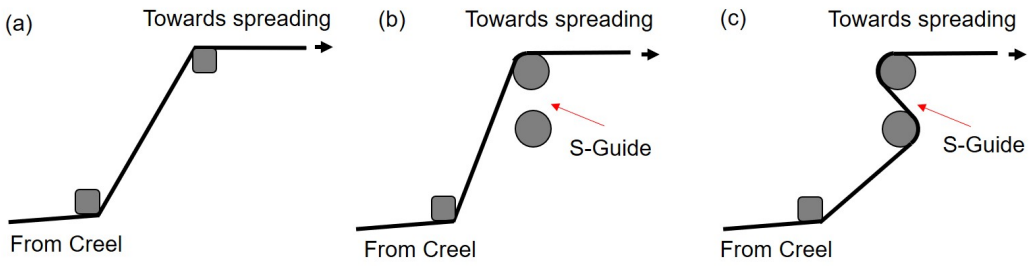

Fig. 3.27 Schematic of first guiding elements from creel to spreading zone: (a) Using square profiles, (b) and (c) Using S-guide with modified paths.

The average value of spread tow width obtained for the experiment using the S-Guide was 8.1 mm while the average value of width without using S-Guide was 7.6 mm. Representative picture from the two experiment analysed using ImageJ is presented in the Fig. 3.28.

The difference between the mean widths obtained with or without S-Guides was concluded to be significant and this was confirmed by Mood's Test for significance of median and the T-Test for significance of mean. The summary of results from T-Test is presented in Fig. 3.29.

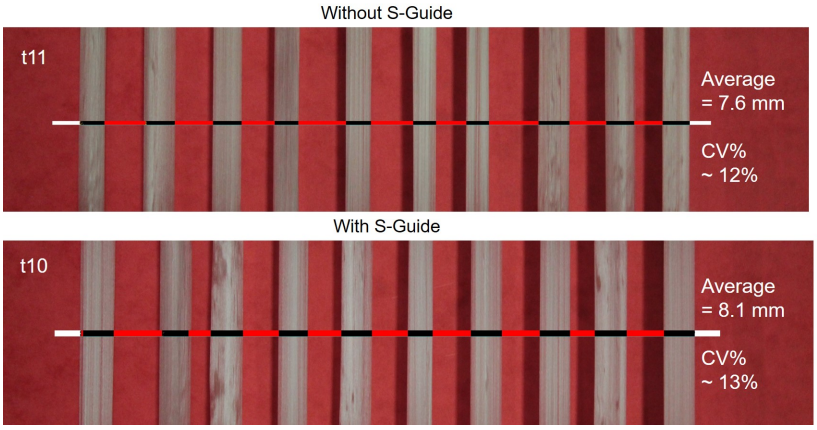

Fig. 3.28 Representative image of spread roving experiment without and with using of S-Guide.

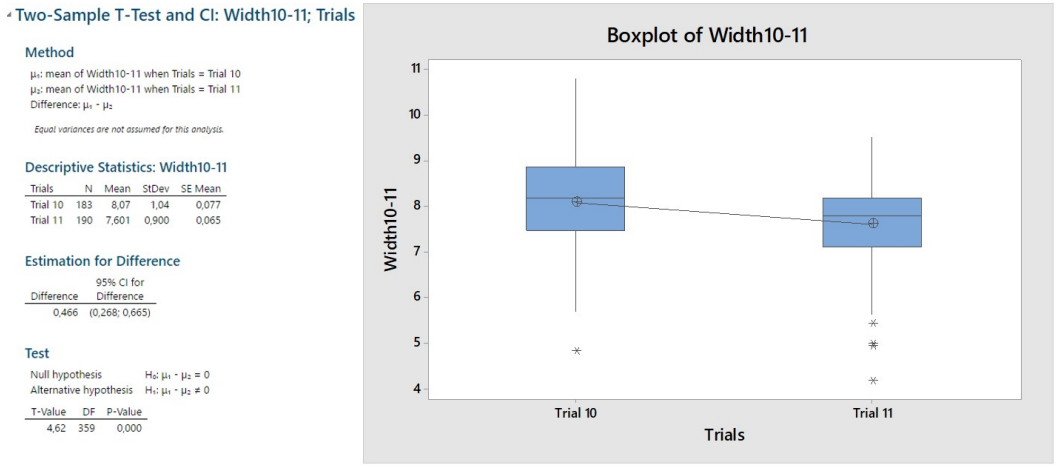

Fig. 3.29 T-Test for significance of mean for experiments with and without using S-Guide.

It can hence be concluded in the study, that complementary guiding elements such as S-Guide significantly effect the spreading behaviour apart from efficiently guiding the roving through its path without twist addition. Further as a validation study using the experimental parameters from experiment 10, in the regression equation obtained in Eq. 3.3; the theoretical spread tow width obtained is 7.5 mm, while experimental value obtained was 8.1 mm and that the difference between the theoretical width and the experimental value is not statistically significant.

3.4.4 Commingled fibre spreading

Commingled yarns are hybrid structures in which two different materials in the form of fibres are mixed to form continuous-filament yarns. Current technologies for commingled

yarns/roving manufacturing are far away from delivering even a near perfect intermingling between the two fibres. This is specially true for commingled rovings with two technical fibres such as glass and carbon. As can be seen in microscopic images (Fig. 3.30) of two of the commingled rovings used in this work; these are currently best form of commingled rovings one can develop today. As can be seen, the commingling form in this can be said to be "side-by-side" coinciding with the "co-wrapped" or "co-twisted" forms reported in Fig. 3.8.

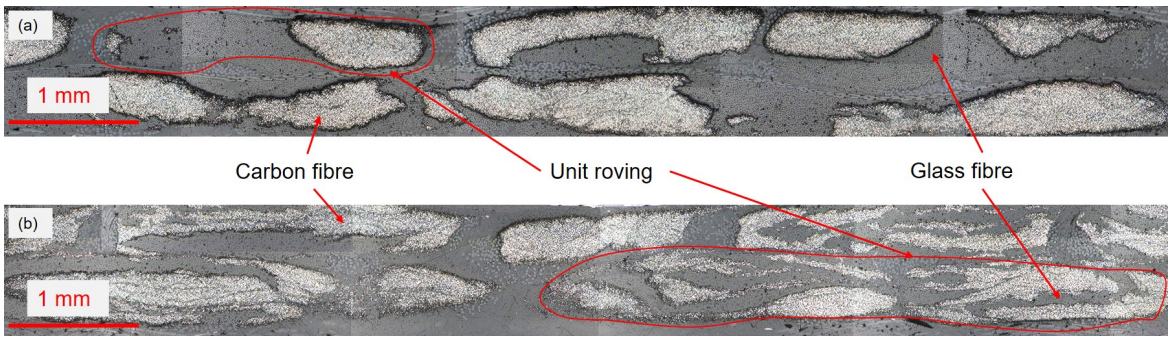

Fig. 3.30 Cross section of carbon/glass commingled rovings used for the study: (a) Commingled A rovings and (b) Commingled B rovings.

1400 tex commingled roving from Supplier A and 2800 tex commingled roving from Supplier B were used on the online spreading machine. The process technology of online-spreading is not very different from offline spreading except that an intermediate spread tape is manufactured and directly used for NCF manufacturing, hence bypassing the winding and unwinding steps for spread tapes as presented in Section 3.2. The objective was: (1) to understand if spreading of the commingled roving is feasible and to what extent for the selected rovings, and (2) develop spread tape hybrids using commingled rovings. Using the expertise from the fibre spreading process for carbon fibres (generated at Chomarat) and glass fibres expertise from the current work, optimum parameters were discussed and set as "Zero Point" for spreading of commingled rovings.

In the existing spreading setup, the spreading occurs through two specific processes: (i) vibrating action of spreading bars (Fig. 3.7b) (ii) mechanically induced spreading by guides and tension [67]. Maximum contribution to spreading out of the two concepts is brought by the vibrating bars. For Supplier A rovings, the commingling process involved bringing together of a carbon and glass tow in a closed air-jet nozzle, where pressurised jet of air is introduced causing the filaments from the two rovings to mingle together. It was observed, that a slight twist (in the range of 2 to 5 twists per meter) is also introduced in the process to bind the filaments together. Both this characteristics of the roving itself hampers the possibility of any spreading of the fibres. As can be seen in Fig. 3.31, the commingling causes uneven tension in the filaments inside the roving, the twists do not

allow vibration induced spreading, and the mingling and twists resists spreading and hence causes fibre breakages excessively. The spread tape hence produced is not coherent and is counterproductive because of excessive fibre breakages.

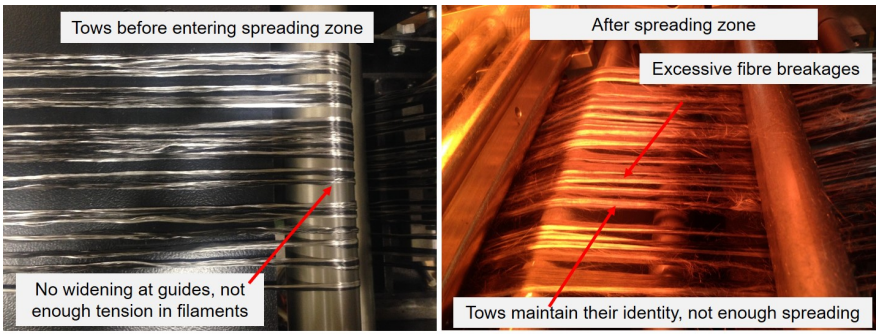

Fig. 3.31 Spreading of commingled rovings procured from Supplier A.

Commingled process for Supplier B rovings did not include introduction of a pressurised air-jet and it had a limited twist introduction. The Supplier B technology just involved bringing together of the two or more than two rovings and introducing a slight twist to bind all the filaments together. The carbon and glass rovings had parallel fibres in side-by-side fashion with barely minimum twist. Though the twist was limited, the spreading operation for these rovings caused fibre damage on the surface contact with vibrating bars. Though this damage was minimised by altering parameters specially in the spreading zone, hence reducing the mechanical friction, but this would further lead to minimising the spreadability for these fibres. In the pictures in Fig. 3.32, the spread tape had areal weight of 250 $\mathrm{g\,m^{-2}}$ can be seen. For less harsh spreading parameters, the areal weight for uniform spreading will be higher than 250 $\mathrm{g\,m^{-2}}$, which makes the spreading process less interesting for the application, while adding considerable cost to the fabrics.

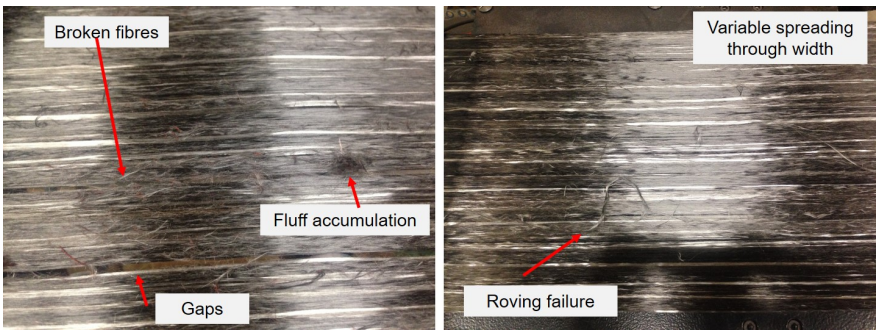

Fig. 3.32 Spread tape manufacturing using commingled roving from Supplier B.

Hence for both the selected commingled rovings, it was concluded that developing an intimately mixed hybrid by spreading the commingled rovings is not an ideal choice and there

are several limitations, some of which cannot be mitigated. Though uniform spread tapes in some case can be produced, but the fibre breakages and higher areal weights, makes the process not interesting and unfavourable. In Chapter 5, the commingled rovings are used to manufacture unidirectional fabrics through Malimo Technology of fabric manufacturing and a comparative study is hence reported for the mechanical properties achieved by commingled roving fabric composites and spread tape fabric composites.

3.4.5 Development of thin ply fabrics, hybrid fabrics using spreading

Using the optimised parameters obtained from the study on 1200 tex glass fibres reported in the earlier part of this section and considering the limitations for spreading of commingled rovings, a plan for fabricating hybrids using simultaneous spreading of carbon and glass fibres was devised. As a first step in this direction, the objective was set to manufacture a uniform spread tape with best possible mixing of T700S carbon 12 K (approximately 800 tex and 24 000 fibres) and E-CR glass fibres (1200 tex) (approximately 2000 fibres) in its cross section. The areal weight optimisation lay outside the scope of this study.

For simultaneous spreading of two fibre (carbon and glass), a couple of preliminary questions needed to be answered first. These questions were: (i) what initial parameters for spreading should be used?, (ii) should a single guide dent/comb (Peigne) at the back be used for both fibre types? and (iii) should carbon fibres lay on the top of glass or vice-versa? The study begun with initial parameters that were identified for an ideal carbon fibre spreading and the results from the optimisation study for glass fibres. The parameters were finally stabilised suiting best for both carbon and glass for simultaneous spreading as reported in Table 3.3. Other parameters that were not so vital were also maintained constant.

Table 3.3 Parameters for initial study of simultaneous carbon and glass spreading.

Creel and guide zone	Guiding dent and spreading zone	Powdering, stabilising and winding zone
Bobbin tension: 150 cN Alignment flaps: 25° S-Guide: Yes Guides after flaps: 4 bar	Guide dents: 1Front, 1Back Temperature-dents: 100 °C Vibration traverse: 3 mm Vibration Frequency: 30 Hz Spreading Temp: 150 °C Depth: 4 spacer rings	Winding pressure: 2 bar Powdering: 4 g m^{-2} Stabilising: 180 °C Production speed: 2 m min^{-1}

For the very first test, after the dents, the fibres were passed between the four stationary (top) and four vibrating bars (bottom) as seen in Fig. 3.7b. It was observed that the

spreading and intermingling in this case was worst of all, and that the two fibre types slid besides each other avoiding mingling and this intern also constrained the roving from the neighbours and hence affecting spreading. A novel approach here was applied in terms of position of spreading bars and modified path for both fibre types in spreading as schematically represented in Fig. 3.33c.

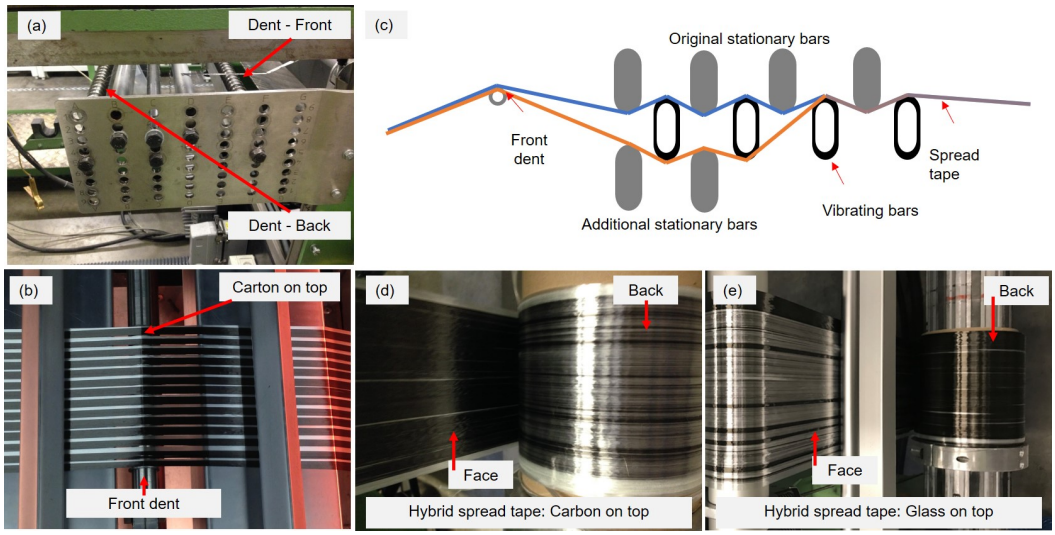

Fig. 3.33 Simultaneous spreading of carbon and glass fibres: initial study.

For the initial tests we used a common dent for both the fibre types, with carbon fibre laid on the top of glass fibre in the dents. In this configuration, it was observed that the carbon fibres, though spread to an extent, they lay on the top of glass fibre and did not enter the glass fibres. Instead of entering the bottom layer of spread fibres, over the period of time, the fibres slide over in the dent and lay side by side (Fig. 3.33b). Similarly when the glass fibres are brought on the top of carbon fibres, the effect of top fibres not entering the bottom fibres still exist (3.33d-e). This behaviour demonstrated that it is in best interest of simultaneous spreading to separate the set of fibres until the fibres are introduced in the spreading zone. The glass on top or carbon on top did not produce significant difference in terms of commingling effect, but glass on the top was slightly better option for spreading for glass fibres.

One of the important factor identified for this non-intermingling behaviour can be the tension in the rovings. As for both the rovings the tension is uniform, none of them offers a chance for the other to penetrate between their fibres. As of now, the electronic creels do not offer the possibility where then tension in each bobbin or set of bobbins can be independently controlled. This aspect of effect of uneven tensions for two fibre types can be interesting and can be looked upon in the future studies.

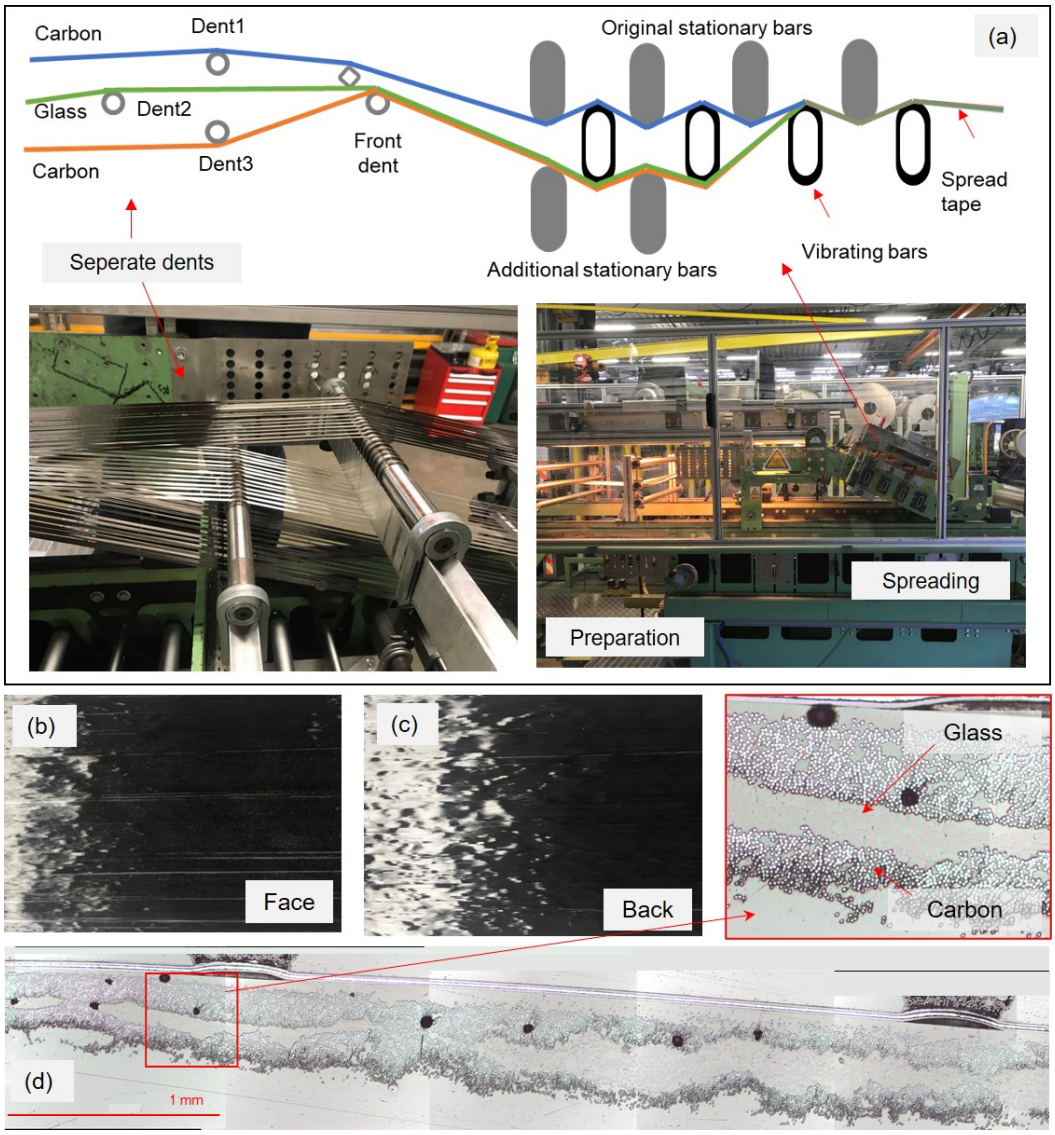

Fig. 3.34 Simultaneous spreading of carbon and glass fibres: final study.

For a simultaneous spread tape fabric, that is supposed to be used in Chapter 5, the condition of a hybrid ratio of 0.62 was to be maintained. For this it was necessary to use carbon and glass roving number in the proportion of 2:1. Hence in the final experiment, considering the experience of individual denting from previous experiment, three guide dents were used (see Fig. 3.34a). The fabrics developed using these modified techniques and parameters produced the first of its kind, dry intermingled carbon/glass hybrid with highest degree of dispersion. Scanned images of fabrics and the microscopic cross section of un-compacted single layer of the fabric is presented in Fig. 3.34d.

3.5 Conclusion

This chapter investigated the spreading of E-CR glass fibres on the spreading machine for the first time. Following conclusions can be made from the study:

- The existing online or offline fibre spreading processes though designed for carbon fibres can also be used for spreading of glass fibres.
- All the four parameters studied, the Frequency, Temperature, Depth and Speed have significant effect on the spreading behaviour of glass fibres. While interaction effect has not been very critical for carbon fibres, it is critical to study the interaction effect for glass fibre spreading.
- Ignoring interaction, the temperature in the spreading zone and depth of spreading bar are critical factors for spreading of glass fibres.
- The optimised spreading parameters are: Frequency- 30 Hz, Temperature- 150 °C, Speed- 2 m min^{-1} and Depth- 4 units. This parameters yield a tow width of 8.9 mm per tow and an areal weight of 135 g min^{-1} for the spread tape.
- Though only four parameters were studied in the initial work presented in this chapter, it is essential in future to consider several other factors in the process chain which can affect the spreadability. Apart from the currently used Taguchi Method, use of other statistical tools such as Response Surface Model (RSM) and Space Filler DoE's should be explored for process and quality optimisation.
- Study on commingled rovings concluded that spreading of commingled rovings is counterproductive as it causes lot of fibre breakages due to inherent twist in the commingled roving structure.
- Spreading process optimisation for simultaneously spreading carbon and glass fibres in the standard spreading process was studied. While the tow-level (intraply) hybrids with carbon and glass were successfully fabricated, fibre-level hybrids with higher dispersion still needs more investigation and optimisation of the process.

Apart from manufacturing carbon/glass hybrids using spreading process, this strategy of hybridisation can be used to manufacture hybrids using different varieties of carbon fibres and open a vast possibilities in fibre hybrid composites and their applications.

Chapter 4

Mechanical performance of interply and intraply hybrids

Performances mécaniques des hybrides inter-plis et intra-plis

L'objectif de ce chapitre est de développer de nouveaux renforts hybrides unidirectionnels et leurs composites avec deux configurations hybrides différentes, à savoir, inter-plis et intra-plis (voir figure 1.2). Les performances mécaniques de ces composites en traction, compression et flexion sont étudiées et sont comparées aux performances des composites de référence non hybrides. Cela a permis de tirer des conclusions sur le comportement à la rupture de ces composites, l'effet de l'hybridation pour les configurations sélectionnées, l'équilibre des différentes propriétés mécaniques et la pertinence des hybrides développés pour des applications spécifiques légères et structurelles.

La Section 4.2 de ce chapitre est un état de l'art sur les composites hybrides, leur comportement mécanique et l'effet de l'hybridation. Cette section détaille également les types de renforts et leurs domaines d'application. La Section 4.3 décrit les fibres, les configurations textiles utilisées et l'accent est aussi mis sur les étapes du procédé de fabrication des composites par RTM. Enfin, la Section 4.4 étudie les résultats obtenus à partir des tests des composites hybrides et non hybrides dans différentes conditions de chargement et l'effet de l'hybridation est caractérisé pour les hybrides inter-plis et intra-plis développés.

Les conclusions de l'étude sont présentées dans la Section 4.5. La contrainte à la rupture en traction pour l'hybride inter-pli révèle un effet d'hybridation positif de +7,4%, tandis qu'il montre un effet négatif de -6,4% en compression. L'hybride intra-pli avec alternance de trois mèches de carbone et trois mèches de verre démontre des performances mécaniques supérieures à tous les autres hybrides ; des effets synergiques de +17,8% et +39,6% en résistance à la traction et à la compression sont observés pour cette configuration hybride. Les résultats montrent que différentes stratégies d'hybridation peuvent être exploitées pour équilibrer le coût et les performances des composites pour les applications structurelles et légères. Des données quantitatives sont fournies pour les propriétés mécaniques des composites pour chaque condition de chargement.

4.1 Introduction

This chapter describes the fabrication of novel unidirectional hybrid carbon and glass based textile reinforcements and composite manufacturing using a liquid composite moulding process. The aim of this chapter is to develop novel unidirectional hybrid fabrics and their composites with different hybrid configurations, namely, interply and intraply (see Fig. 1.2); and further investigate the mechanical performance of these composites with respect to reference homogeneous non-hybrid composites, specifically in tensile, compression and flexural loading conditions. Conclusions are drawn on the failure behaviour of these composites, hybrid effect in selected configurations, on the balance of different mechanical properties and the suitability of developed hybrids for specific light-weighting and structural applications.

Section 4.2 in this chapter investigates and reports in detail the current state of the art in hybrid composites, their mechanical behaviour and their hybrid effect. This section also explores the reinforcement types and their application areas in composite materials. Section 4.3 describes in detail, the fibre materials and the textile configurations used. Emphasis in this section is laid on the composite manufacturing process steps using Resin Transfer Moulding (RTM). Specifics of quality check procedures and testing methods is presented in this section. Finally Section 4.4 discusses the results obtained from the testing of the hybrid and non-hybrid composites in different loading conditions. The significance and implications of the tests are discussed and the hybrid effect is characterised for the fabricated interply and intraply hybrids. Conclusions of the study is reported in Section 4.5. The schematic overview of the experimental and scientific section of this chapter is presented in Fig. 4.1.

4.2 Review of the literature

Several fibre types and resin systems are available to the designers who aim to achieve composite product properties such as high specific strength, high specific stiffness, enhanced energy absorption as well as reduced cost for a certain application field. But, in general, composites made from a single reinforcing material may not be suitable if it undergoes different loading conditions during its service life and has to satisfy multiple performance conditions. A compromise in one or several properties is rendered essential in such cases, and considering this, the hybrid composites can prove to be a better solution for such applications. In fact, one of the greatest benefits of fibre-reinforced composites over other materials is their potential for design optimisation. Furthermore, not being restricted to a single fibre type expands this design envelope even further. Design freedom for composite materials is not only reflected in the choice of fibres and matrices, but also in aspects such as the fibre orientations,

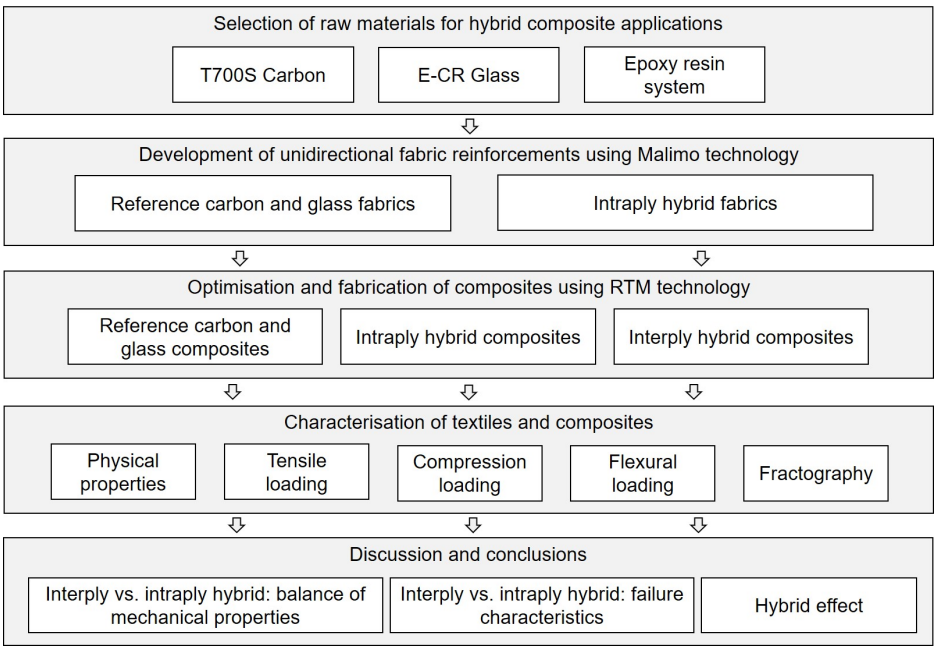

Fig. 4.1 Schematic overview of the experimental (Section 4.3) and scientific (Section 4.4) sections of this chapter.

stacking sequence and preform types. Hybrid composites are therefore a logical evolution towards even more design freedom and hence more possibility for performance optimisation and cost reduction. Hybrid composites have been used for various structural applications due to their enhanced mechanical performance over their non-hybrid counterparts [88, 143].

The term “hybrid composites” is generally used to describe a composite system either; with two or more than two types of fibres, or two types of resin, or their combinations, or a combination of fibres and metals, but this thesis is restricted to hybrid composites containing two types of reinforcing fibres in a common matrix, such composites are also called “fibre hybrids” or “fibre hybrid composites”. In this thesis the terms hybrid composites or fibre hybrid composites are used interchangeably and both mean composites utilising two or more fibre types in a common matrix. For fibre hybrid composites depending on the way the individual constituents are brought together, there are three major fabrication configurations (see Fig. 1.2): interply hybrids or ply level hybrids, intraply hybrids or tow level hybrids and intermingled hybrids or fibre level hybrids. The subsections that follows in this chapter discusses the current state of the art in hybrid composite reinforcements, the hybrid and synergistic effect, mechanical properties and failure characteristics of hybrid composites. Experimental work on hybrid composites being the focus of the current work is discussed in detail the current and succeeding chapters, state of the art in modelling and simulation work on the hybrid composites is though introduced in Section 5.2.3 but not discussed in detail.

4.2.1 Synergistic effect

As the definition of composites suggests that these are the materials made from two or more constituent materials with significantly different physical or chemical properties that, when combined, produce a material with characteristics different from the individual components. Extending this concept, when combining two or more types of reinforcement components can produce synergistic effects. These synergistic effect appear in different materials systems and performance characteristics. As a general definition, synergistic effects can be defined either as properties that are better than expected or the occurrence of behaviour that is not present in either of the constituent materials.

4.2.1.1 Definition: Hybrid effect

Hybrid effect is termed as a synergistic effect on the stress-strain response on mechanical loading of hybrids over non-hybrid composite. Hayashi [58], in 1972 first reported that the failure strain of the carbon fibre layers in a carbon/glass hybrid composite was 40 % higher than in the reference carbon fibre composite. Later, several researchers showed the existence of this effect of higher failure strain in a hybrid composite. The earlier studies showed remarkable synergistic effects in several hybrid combinations and the effect ranged typically from 10 to 50 % [23, 116, 176, 97, 169, 112, 171]. Based on work by Hayashi [58], the initial definition of hybrid effect was formulated and gained significant attention. This definition defined the hybrid effect as the apparent failure strain enhancement of the low-elongation fibre in a hybrid composite compared to the failure strain of a low-elongation fibre-reinforced non-hybrid composite. This definition is schematically illustrated in Fig. 4.2a. This failure strain is often affected by stress concentrations at the grips, while this stress concentration effect is smaller in hybrid composites it is higher for non-hybrid composites such as carbon composites. This may cause over estimations of the hybrid effect. For calculation of hybrid effect using this definition hence requires accurate determination of the failure strain of the reference carbon fibre composite.

Further, Summerscales [138] in 1983 and Fischer and Marom [45] in 1987 defined hybrid effect in such a way that it could capture more features to understand effect of hybridisation. This definition of hybrid effect was based on the deviation of a property from Rule of Mixture (RoM), as is schematically depicted in Fig. 4.2b. This definition based on RoM can also be applied to mechanical properties other than failure strain. Application of this definition though is not completely straightforward and has its own challenges. For example, the RoM is not necessarily linear for all properties, it is bi-linear for tensile and compressive strength [97], i.e. for these cases the property is dominated by one fibre type up to a certain hybrid

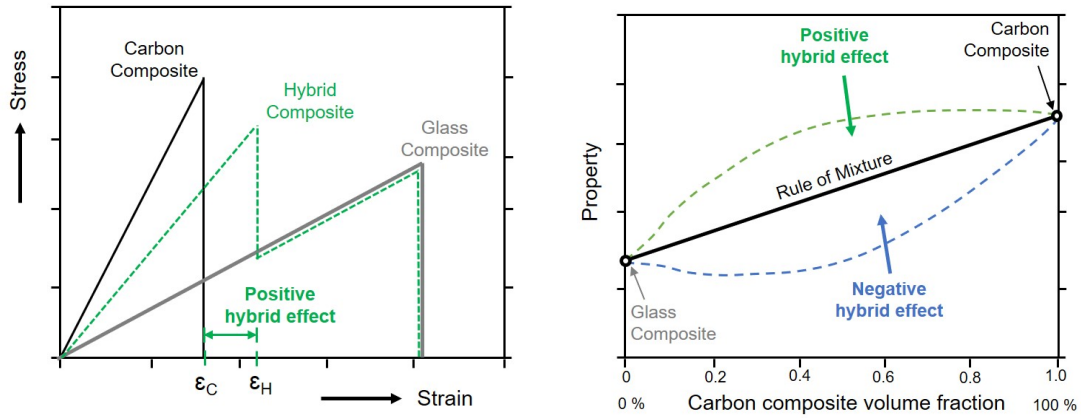

Fig. 4.2 Illustration of the definitions of the hybrid effect for C/G hybrid composite: (a) apparent failure strain enhancement in hybrid composite, and (b) property deviation from RoM.

ratio and by the other for higher ratios. For carbon/glass hybrid in the current work the b-linear RoM and hybrid effect calculations are explained in Appendix A. Further for the application of the second definition a certain composition parameter is necessitated and choosing and further calculating a right one is vital. As suggested by Phillips [117, 116], the relative volume fractions of the low-elongation and high-elongation composites are a good choice, but experimentally determining this is challenging. Finally, even though the second definition is more general, it still does not work for composite properties in flexural loading, which for the hybrid effect calculation needs to also include the classical laminate theory and hence complicates the prediction of hybrid effect in such complex loading conditions.

4.2.1.2 Hypotheses: Hybrid effect

Though there were contradictions in some of researchers about the hybrid effect owing to the way in which the effect is determined or the composition parameter that is selected; the belief in the surprising failure strain enhancement of the LE fibre gradually increased when more experimental data became available. Larger experimental data also provided for convincing hypotheses which could explain the hybrid effect. As of today, three different hypotheses for the hybrid effect have been coined based on: i) residual stresses, ii) changes in the damage development leading to final failure of the hybrid composite, and iii) dynamic stress concentrations. The identified hypotheses have been applied to unidirectional hybrid composites in either the interply or intraply configuration but these can be extended to

multidirectional composites, as their failure, although more complex, still coincides with failure of fibres in the loading direction.

When two different types of fibres are combined together in a common matrix, it is possible that there are residual shrinkage stresses present in the system as the combined fibres and the resin has different thermal contraction. For example, if carbon fibres with coefficient of thermal expansion (CTE) between -1×10^{-6} to $1 \times 10^{-6}\,\mathrm{K}^{-1}$ is combined with glass fibres with CTE between 5×10^{-6} to $10 \times 10^{-6}\,\mathrm{K}^{-1}$, then, as the resin is in the curing stage and still in liquid form, the glass fibres tends to increase its length while carbon fibres nearly maintains its length. Now, when the resin is completely cured and cooled down, the glass fibres will try to shrink, but the cured resin prevents this from happening. Hence, a force equilibrium is established, putting compressive stresses on the carbon fibres and tensile stresses on the glass fibres. In this hypothesis, these compressive stresses counteract the applied stress and increase the apparent failure strain of the carbon fibres. This effect of residual stress though cannot fully explain the hybrid effect as pointed out by Zweben [176], Bunsell and Harris [23] and Manders and Bader [97]. The two types of experimental results that point out that some other effects are also responsible for hybrid effect are the ones where the hybrid effect is as high as 50 % [88, 143] and the ones where carbon fibres are combined with aramid fibres which have a negative CTE, which as per this hypothesis should produce negative hybrid effect, but actually produces positive hybrid effect as reported by Zweben [176].

When compared to a non-hybrid composites, the failure in the hybrid composite takes place differently. The development of failure in unidirectional composites in general takes following steps. When loaded in tension, the strain is the same in all fibres when all the fibres are intact. Further, on increase in strain, the first fibre will break and locally lose its load carrying capacity, however, this does not lead to composite failure. After the first fibre break, the surrounding matrix is loaded in shear and transfers stress back onto the broken fibre, which will recover its full load carrying capacity a certain distance from the fracture location. But, the neighbouring fibres will be subjected to stress concentrations and locally take over the additional load caused by the broken fibre. As reported by Nedele and Wisnom [107] and Swolfs et al. [142] these stress concentrations on neighbouring fibres are typically in the range of 5 to 15 % in the plane of the fibre break and rapidly decrease with increased distance from this fibre break plane. The stress concentrations lead to an increased failure probability in the neighbouring fibres. When the strain is further increased, this increased probability will lead to the development of clusters of broken fibres. If one of these clusters grows large enough and reaches a certain critical size, then that cluster will grow in an unstable manner and lead to final failure of the composite. For hybrid composites the presence of two different

fibres can interfere with this damage development process at several stages. The hybridisation affects the stress concentrations and stress recovery, it may hinder the development of critical clusters and increase the critical cluster size and cause size scaling effect. Failure strain of conventional composites increases with decreasing the sample size [33, 164], this can also cause increase in the failure strain of hybrid composites when compared to the reference low-elongation composite.

Hedgepeth and Van Dyke [59] pointed out that, when a fibre breaks the load on that fibre is locally relaxed and the fibre springs back, this further creates a stress wave travelling along each fibre, causing a temporary increase in the stress concentration. He used a shear lag approach to prove that the dynamic stress concentrations are 15 to 27 % higher than the static stress concentrations. Xia and Ruiz [167] predicted the dynamic stress concentration factors to be 20 % higher in glass fibre composites than in carbon fibre composites.

4.2.2 Failure characteristics and stiffness of hybrid composites

4.2.2.1 In tensile loading

For carbon glass hybrid composites, Hayashi [58] first reported that the failure strain of the carbon fibre layers in a carbon/glass hybrid composite was 40 % higher than in the reference carbon fibre composite. Further failure strain enhancement of above 100 % was reported by Aveston and Sillwood [11]. Manders and Bader [97], Bunsell and Harris [23] and Zweben [176] confirmed that the hybrid effect exists but cautiously pointed out that the thermal effect could only account for about 10 % of the hybrid effect and that for full hybrid effect there are other supporting mechanisms apart from the thermal effect taking place because of hybridisation. Diao et al. [38] recently reported a negative hybrid effect of 8 % in commingled T700-IM7 carbon/carbon hybrid composite compared to the reference IM7 carbon fibre composite. This decrease was attributed to surface damage introduced by the commingling process. Pandya et al. [113] reported a hybrid effect of 36 % and 90 % for a carbon/glass hybrid composite and they also suggest putting the carbon fibre layers as inner plies rather than outer plies for better hybrid effect. They achieved a gradual failure in tension for hybrids, but still used the ultimate failure strain to calculate the hybrid effect. Though this does not conform to the definition of hybrid effect based on the apparent failure strain enhancement of the low elongation composite, but it was not possible to deduce the hybrid effect using the proper definition using their data. You et al. [169] reported a hybrid effect of 9 to 33 % in unidirectional carbon/glass hybrids and concluded highest hybrid effect was when the fibres were well dispersed. Zhang et al. [171] hybridised woven glass and carbon fibre and found improvements in failure strain, ranging between 10 % and 31 %. The

failure of the carbon fibre layers coincided with final failure of the hybrid composite and no further load carrying by the glass fibre layers was observed. Though longitudinal tensile modulus of hybrid composites has been shown to obey a linear RoM, according to many researchers [58, 23, 138, 45], Ren et al. [125] reported a higher modulus for intralayer than for interlayer unidirectional carbon/carbon hybrids. They also observed a small but negative hybrid effect by combining two different types of carbon fibres in a single composite. The tensile strength for intralayer hybrids was observed to be higher than for interlayer hybrids, demonstrating that increased dispersion leads to better mechanical performance in hybrid composites. Kretsis [88] analysed literature data prior to 1987 and clearly demonstrated that the hybrid effect increased with decreasing LE fibre content. He added a vital caveat for interpreting the literature data gathered from work 2 to 3 decades ago that the hybrid effect observed will have been influenced by factors such as poor quality carbon material (with lower failure strain) and improper testing and measurements. For both tensile and compression tests [165] and Swolfs et al. [143] have reported difficulties in measuring the baseline tensile failure strain of a high strength unidirectional composite against which the strain at failure of the hybrid is compared to determine the hybrid effect.

4.2.2.2 In longitudinal compression loading

The longitudinal compression behaviour of a composite is one of the most critical mechanical properties, however, there are only few studies on the compressive properties of hybrid composites. These studies report compression behaviour of mostly interlayer hybrid composites [161, 64, 63]. Wang et al. [161] revealed from the experimental results, that the compression modulus for hybrid composites increases linearly with the increase of carbon fibre content, following the RoM. The C/G hybrid ratio is regarded as the decisive factor for the compression modulus of hybrid composites. Positive mixing effect was confirmed to exists in compression strength for interlayer and intralayer hybrid composites in their studies. Hwang and Mao [64] studied the compression properties of interlayer hybrid composites, and revealed that an increase in glass fibre content in hybrid composites can decrease the compressive strength. A similar conclusion can be confirmed by Yerramalli and Waas [168] who studied a C/G hybrid composite cylinder. Pandya et al. [113] investigated the compression loading of a carbon and glass woven hybrid composite and presented a positive synergy in compression strength and failure strain for both interply configurations with carbon layers on outside and glass on outside in layup configuration. Ikbal et al. [65] found for unidirectional composites that the compressive strength of an intralayer hybrid structure is a bit better than that of an interlayer hybrid structure. Reports on the mechanical properties of intralayer

C/G hybrid composites are limited; especially, little work has been done on the compression properties of intralayer hybrid.

4.2.2.3 In flexural loading

Behaviour of composites in flexural loading is highly dependent on the layup, as the longitudinal stress at the neutral line is zero, but increases when moving away from that line. Hybrid composites yield additional possibilities to optimise the mechanical performance by not only changing the ply angles, but also by changing the material type of each ply. This also makes the flexural properties of hybrid composites more difficult to interpret than the tensile properties. Just like the tensile modulus, the flexural modulus can be predicted rather well. While simple RoM apply to tensile moduli, the classical laminate theory is commonly used to predict flexural moduli. Dong et al. [42] obtained experimental flexural strengths for carbon/glass intralayer hybrids, which are 40 % and 9 % higher than the full carbon and full glass reference composites. The achieved strength for the hybrids was higher than the values predicted by both finite element analysis and classical laminate theory. Giancaspro et al. [51] reported that glass fibre composites failed on the tension side, while carbon fibre composites failed mainly on the compression side near the loading nose owing to the poor transverse compressive properties of carbon fibres. Adding carbon fibres on the tension side of glass fibre composites hence increased the flexural strength, while this was not the case when they were added on the compressive side. Dong et al. [42], Dong and Davies [40, 41], Giancaspro et al. [51] and Sudarisman et al. [137] in all these studies concluded that an optimal level of glass fibre exists to achieve maximum flexural strength and that addition of glass fibre in the compressive side yields a higher flexural strength for hybrid composite. Dong and Davies [40] further reports that the highest flexural strength in carbon/glass hybrids was achieved at a relative content of 12.5 % of glass fibres, all of which are placed on the compressive side. Further conclusion was made that a symmetric layup is hence not the optimal design for a hybrid composite that will be subjected to flexural loads. Chamis et al. [29] showed that combinations of high-modulus graphite/S-glass/epoxy matrix composites exist which yield intraply hybrid laminates with the ‘best’ balanced properties: for example, 100 %increase in impact resistance and 35 %increase in tensile and flexural strengths, with no reduction in modulus compared with graphite fibre/epoxy matrix composites. Wang et al. [160] concluded for UD composites that for intraply hybrid composites, the C/G hybrid ratio plays a dominating role in the bending failure. The bending failure of intraply hybrid composites occurs in advance since carbon fibre are located in each layer; the failure process shows a multi-stage fluctuating decline and the decline slows down as carbon fibre content increases.

For interlayer hybrids the study reports early failure when carbon fibre layer is present on the compression side of the test specimen.

From the above mentioned reports in this Section 4.2.2 it can be summarised that the factors identified to be influencing the bulk of hybrid effect studies are: relative volume fractions, elastic properties of the fibres, ratio of failure strains for the two fibres, fibre strength distribution of low elongation fibres, type of matrix used and the dispersion for the fibres (microstructure) in the composite cross section.

4.2.2.4 Fracture toughness and impact properties

Apart from the benefits arising because of synergistic effects and the cost advantage, fibre hybrid composites have found their way into research and industries for the specific advantages it offers in terms of its toughness, impact and fatigue properties. While the state of the art has greatly advanced since the start of fibre hybridisation for high-performance composites for tensile or flexural loading; but other more complex loading conditions received less attention and are lacking a solid understanding. This is especially true for impact and toughness properties as pointed out by recent review papers [88, 143]. Swolfs et al. [141] in their studies reported a positive hybrid effect o 40 % in the penetration impact resistance for hybrid carbon/glass composites with glass on the outside, when compared to the RoM behaviour. González et al. [53] like Swolfs et al. [141] found at least one of their hybrid composite having Compression-after-impact (CAI) better than the glass or carbon reference composites. While Naik et al. [105] reported better compression properties for carbon on the outside configuration for CAI strength; they reported in [112] that placing E-glass layers in the exterior and carbon layers in the interior provides higher ballistic impact behaviour. Considering these publications, there is a strong need for developing a clear understanding of how the change in layup causes a change in performance.

In the literature published on fracture toughness; Ortega et al. [111, 110] and Swolfs et al. [141] are found to be among the few studies reporting translaminar fracture toughness for carbon/glass interply hybrid composites. Details of other work on fracture toughness for hybrid composites explored and presented in Section 6.2.2. For these complex loading conditions, some authors report conflicting data for the effect of certain parameters and hence more in-depth investigations as well as more advanced modelling tools are required to be developed to understand the mechanisms and the hybrid effects.

4.2.3 New materials and processing of hybrids

4.2.3.1 Fibre types

In the section above, the mechanisms controlling synergistic effects for mechanical properties are reported, these synergistic effect though is different for different fibre material and reinforcement types and their combinations. Apart from the mechanical synergies mentioned above it is also essential to understand how different fibres and matrices fail and how those mechanisms can interact. For example for a carbon glass hybrid with relatively lower carbon Fibre Volume Fraction, though there is no hybrid effect in failure strain enhancement, but pseudo-ductility effect can be observed even when both carbon and glass are brittle fibres on their own [35, 170]. Depending on selection of fibres and matrix systems, thermal and electrical conductivity, damping behaviour or electromagnetic properties can also be enhanced because of hybridisation. Fibre selection is a challenging task itself for hybrid composite materials. It is not just the two fibre type and synergistic effects of their combination which is important, but balance of other mechanical properties for a specific application role is equally important. For example, for a specific application, where partial carbon fibres are replaced by glass fibres, the flexibility and failure strain can be enhanced because of hybridisation, but this might lead to reduction in the strength property because of presence of glass fibres on the exterior of the laminate [40].

Development of new improved fibres have a major role to play in the fibre hybridisation. Recently, newly developed carbon fibres with superior mechanical properties and consistency are commercially available, for example, Toray's T1100G a carbon fibre for primary aircraft structure offers a superior balance of stiffness (324 GPa), strength (6600 MPa) and failure strain (2.2 %) [155]. Similarly, S-2 has emerged as a cost-effective alternative as glass fibre which is suitable for ultimate tensile and impact performance [1]. A brief review of manufacturing process for carbon and glass fibres can be referred to in Section 2.2.1.

High performance polymer fibres such as aramid and ultra high molecular weight polyethylene have been explored in several composites and hybrid applications for their impact and ballistic characteristics [43, 114]. Polypropylene and carbon hybrids have also been explored for specific applications [140, 101]. Last two decades hybrids with a number of natural fibres specifically for composite applications have been vastly studied, the reason here apart from balancing mechanical properties is to impart sustainability and cost advantage to the final product [108]. Researchers and industries alike have explored hybrid composites with metal fibres enabled because of the developments of metal drawing technologies [27]. Many of these polymeric, natural and metal fibres are playing a role in advances of hybrid

composites but these are not very relevant to the current work and hence are not discussed in this section.

4.2.3.2 Resin systems

For fibre hybrid composites where multiple type of fibres are embedded in a common matrix, resin selection is an important decision. Unlike conventional composites where resin system choice was solely based on the application, in hybrid composites there are other parameters such as compatibility to the multiple fibre type, functionality, assistance to the hybrid effect, etc., which are important to understand. The choice of a thermoplastic matrix (such as polyester or polypropylene) or a thermoset matrix system (such as epoxies or vinyl-ester) has strong implications on the manufacturing route, but also on the matrix and hence composite properties. While thermoplastic matrices have faster processing times, with advantages of recyclability and improved toughness, the thermoset matrices have better strength and stiffness properties and easier processing routes due to their viscosity.

Mechanical properties of matrix contributes to the overall composite stiffness, but this contribution is small in the fibre direction for most fibre types. This contribution of matrix properties in the transverse direction and voids in the matrix is though very significant for a unidirectional composite as it directly affects the failure behaviour and damage propagation [126]. In off-axis loading, for example, the ratio of transverse fibre stiffness over matrix stiffness ratio determines the magnitude of the stress concentrations around the fibres. This stress concentration together with the matrix strength and fibre/matrix interface strength will determine the onset of damage and composite strength [30].

Matrix selection in conventional non-hybrid composites has been explored with aim to obtain better composite properties and advanced functionalities such as electrical conductivity, fire resistance, etc. It is observed in the literature that, the matrix selection in fibre-hybrid composites has received relatively little attention, hence care should be taken to ensure the chemical and processing compatibility and the interfacial bonding of the resin with fibre-types used in hybrid composites.

4.2.3.3 Reinforcement systems

Regardless of the fibre material, reinforcements are available in various forms to serve a wide range of processes and end-product requirements. Reinforcement materials can be designed with unique fibre architectures and be preformed depending on the product requirements and manufacturing process and can be in the form of a roving, milled fibre, chopped strands, continuous, chopped or mat. In technical literature, there is a wide range of terms for

the production technologies for different kinds of fabrics. As the focus of current chapter and work is on non-crimp fabrics, other fabric forms such as woven or chopped mats are not discussed in this section. Unidirectional reinforcements including tapes containing the fibres all aligned parallel in one direction and in non-crimped fashion provides the highest mechanical properties. Composites using unidirectional tapes or sheets have high strength in the direction of the fibre. Unidirectional sheets are thin and multiple layers are required for most structural applications. Typical applications for unidirectional reinforcements include highly loaded designed composites, such as aircraft or automotive components. Non-crimp fabrics are most widely used reinforcements and are best suitable for processes such as pultrusion, RTM and other Liquid Composite Moulding processes using dry reinforcements. Detailed review of non-crimp fabric manufacturing and the RTM process can be referred to in Section 2.2.5, 3.2.1 and 3.2.2.

Spreading and thin ply technologies recently have proved to be effective strategy to achieve good dispersion allowing strong interactions between fibres and can lead to synergistic effects for the initial failure strain in tension. Wisnom et al. [165] reported a hybrid effect of up to 20 % for a 29 µm thick carbon fibre ply surrounded by thicker glass ply in interply configuration. Conventional thin ply reinforcements have several advantages, most vital among them are: (1) greater versatility in optimising stacking sequence, (2) delay of onset of damage, and suppression of delamination, and (3) higher compressive and fatigue properties. These advantages of thin-ply can be extended to the newer generation of hybrid composites too by carefully selecting the fibre and reinforcement format. Hybrid textile technologies have also gained interest where quasi-UD fabrics in the form of either woven or non-crimp fabrics can be produced by utilising a very low quantity of weft yarn in the cross direction. Balanced fibre-hybrid fabrics along with recently developed spread tow hybrid fabrics both woven [21] and non-crimp fabrics [131, 128] are commercially available as well.

Fabrics with commingled rovings [139] and aligned discontinuous fibre fabrics [170] are two other interesting trends in hybrid reinforcement technologies. As the thesis focuses on continuous fibre hybrids only, hence, discontinuous mat production is not of interest in this thesis, the details of commingling and spread tape technology is discussed in details in Chapter 3 and Chapter 5.

4.2.4 Applications

Hybrid composites are relatively common in industrial and sports applications. In most case the primary use is linked to performance improvement and imparting functionality; while in some cases hybridisation is primarily for economic reasons. Some of the application examples where hybridisation has imparted functionality are: imparting conductivity by

addition of carbon fibres [99], imparting insulation and protection from galvanic corrosion by adding of glass fibre layers [132], using metal meshes for air crafts for electromagnetic shielding against lightening strikes [159], adding natural fibres for vibration damping and energy dissipation in bicycle frames [46] and introduction of aramid layers on the top to improve fibre resistance [87]. Hybridisation has been explored also taking into consideration the environmental effect, for example it causes reduction in use of carbon fibres which require about 5 times more energy to produce when compared to glass fibres [166]; other example is use of natural or thermoplastic polymeric fibres which are sustainable and has lower environmental effects [120].

Manufacturers in general are often secretive about mentioning the technical reason for fibre-hybridisation. For example many of the surfboards and ski manufacturers advertise use of carbon, glass or their hybrids as reinforcement and skin material for their products, but the exact technical advantages it can offer is not very openly spelt out. It can be inferred from literature studies that adding carbon fibre to glass fibre increases stiffness and strength, which implies that a thinner skin is required. On the same lines, masts for sailboats use carbon/glass hybrid to achieve the dual objective of low cost and improved impact performance. Hybrid composites in competitive sports such as tennis, squash and badminton can help in extending the design freedom, provide more control over stiffness, and can be made more aerodynamic and lighter in weight. The most important reason for fibre hybridisation though for these applications is that hybridisation helps to improve the damping properties thus it reduces drastically the probability for fatigue and repetitive strain injuries. Exactly for similar reasons, hybrid composites have been used for bicycle frames as it can improve rider comfort and reduce fatigue. Additionally, the hybrid frame with either steel or other polymeric fibres offers better vibration damping and reduces the risk of splinters harming the rider in case of an accident. Externally, carbon parts are covered by layer of aramid to avoid fragmentation of carbon fibres in occurrence of a crash, further on the inside, carbon aramid hybrids for example for seats provide highest impact performance.

The efficiency of wind energy generation and its cost efficiency is directly linked to the length of the wind blade. The load carrying beam also called as spar and the aerofoil, are the two most important components of a wind blade and both of them are made of glass fibre composites. To make longer blades a shift to carbon fibre composites is required; such a shift could save about 20 to 30 % of the direct weight saving compared to a glass fibre composite blade, indirectly though the weight savings would be higher but of course increase in costs make this alternative not very interesting. Manufacturers are therefore shifting towards carbon/glass fibre-hybrid composites for offshore wind blades which are longer and larger. The record for the longest blade is currently held by LM Windpower, with their 107 m long

blade [93] and the most vital contributor to this feat was use of carbon/glass hybrid spar caps. There are also several challenges in terms of fibre hybridisation for Wind turbine blades as they have complex loading conditions during their operation and performance of these hybrid materials are poorly understood for such multiple loading conditions. Considering these specific industrial needs, this chapter and the thesis altogether focuses on hybrid fabrics and composites application in the areas of sporting and leisure goods and wind energy applications.

4.3 Experimental materials and methods

4.3.1 Materials

Based on the prospective end uses for the hybrid textile reinforcements in structural applications in wind energy, sports and leisure, the carbon fibres in the form of high strength T700S fibres and glass fibres in the form of Advantex E-CR glass were identified. T700S carbon fibres have excellent processing ability and are widely used in high tensile applications like pressure vessels, recreational and industrial products. Glass rovings with commercial name 111A Type 30 made from Advantex glass fibres possesses excellent mechanical and electrical properties of traditional E-Glass with the acid corrosion resistance of E-CR-Glass. The T700S rovings were procured from Toray Europe, while the E-CR Advantex glass fibre rovings were procured from Owens Corning. These two fibres were selected and used for a detailed study on effect of hybridisation (at ply-level, tow-level and fibre-level) on the mechanical properties of the developed composite materials. Carbon 24 K (approximately 1600 tex and 24 000 fibres) and glass 1200 tex (approximately 2000 fibres) rovings were utilised to fabricate unidirectional hybrid intraply fabrics in different configurations. Finer rovings in the form of 12 K carbon and 600 tex glass were used for reference fabrics so as to achieve similar C/G ratio and areal weights in the interply hybrids when compared to the intraply hybrid configurations. The sizing on both carbon and glass fibres were compatible to the used epoxy resin system; though no additional information on exact chemical formulation is publicly available.

A commercially available epoxy system from Huntsmann Advanced Materials GmbH in Switzerland was used and it consisted of Araldite LY 564, a low viscosity epoxy resin and Aradur 2954, a cycloalophatic polyamine hardener. This system is used in wide range of applications in industrial composites owing to its suitability for various production processes. Properties of these fibres and cured matrix from their technical data sheets are provided in Table 4.1.

Table 4.1 Properties of the constituents at room temperature from technical data sheets.

Property	Units	T700S Carbon	E-CR Glass	*LY 564 and Aradur 2954
Density	[g cm^{-3}]	1.76 - 1.84	2.62	1.1
fibre diameter	[µm]	7	17	-
Tensile strength	[MPa]	4510	2400	71 - 77
Tensile modulus	[GPa]	221 - 240	81	2.5 - 2.6
Failure strain	[%]	1.9	4.9	4.5 - 5.5

*Neat resin properties measured for the used processing and curing conditions is presented in Appendix B.

4.3.2 Manufacturing methods

4.3.2.1 Reinforcement manufacturing

Unidirectional reference carbon and glass fabrics along with intraply hybrids were developed using Malimo UD stitching technology. Rovings from the creel were guided through the reed with specific density suiting the required areal weight. Further a stabilisation fabric was introduced in the stitching zone, where this uniform stack of reinforcing fibre and the stabilisation fabric was stitched together in a tricot stitching pattern using 170 dtex Polyester threads. The stabilisation fabric used here was a light woven fabric with an areal weight of 42 g m^{-2} made from fine glass yarns as can be seen in Fig. 4.3b. The process parameters along with stabilisation and stitch parameters for all the fabrics were maintained uniformly. The developed fabrics were further quality checked to confirm the compositions of the technical fibre, stitching thread and stabilisation fabrics. Photographs of the developed fabric reinforcements can be seen in Fig. 4.3.

4.3.2.2 Composite fabrication

Composite plates were fabricated using epoxy-RTM process. The preforming and RTM parameters were selected considering the behaviour of the fabrics and that those were kept constant for all the composites fabricated. Preforms were made by laying fabric layers in required orientation sequentially on the aluminium preforming table. A cross-ply, symmetric layup $[0/90/0]_S$ consisting of 6 layers was used for all composites except for interply hybrid I1 where the layup consisted of total 12 alternating glass and carbon layers $[0_G/0_C/90_G/90_C/0_G/0_C]_S$ and had similar hybrid ratio like intraply hybrids. In thickness direction, the fabric placement was randomised so that the carbon or tow blocks in all layers did not fall exactly on the corresponding tow blocks. The width of individual fabrics was lower than the preform size and hence multiple fabrics were placed precisely side by side for each layer. After each layer is laid down a fine layer of epoxy preforming powder

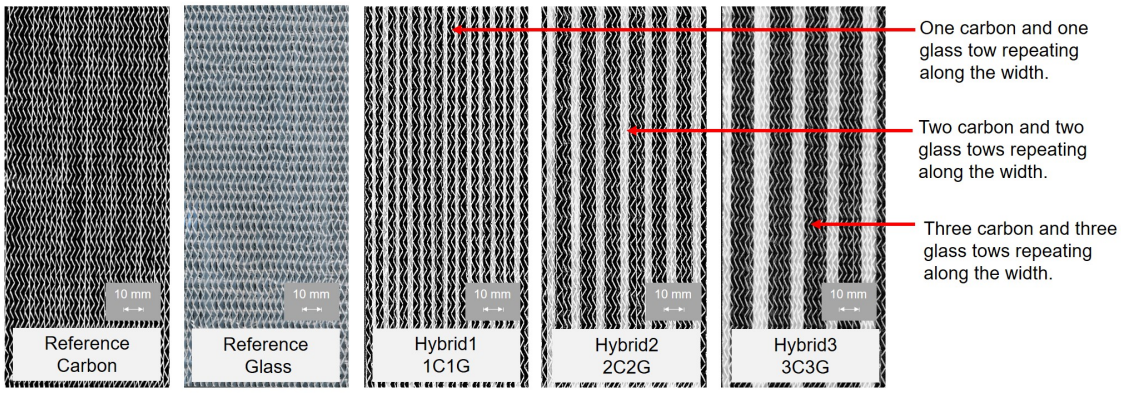

(a) Developed fabrics

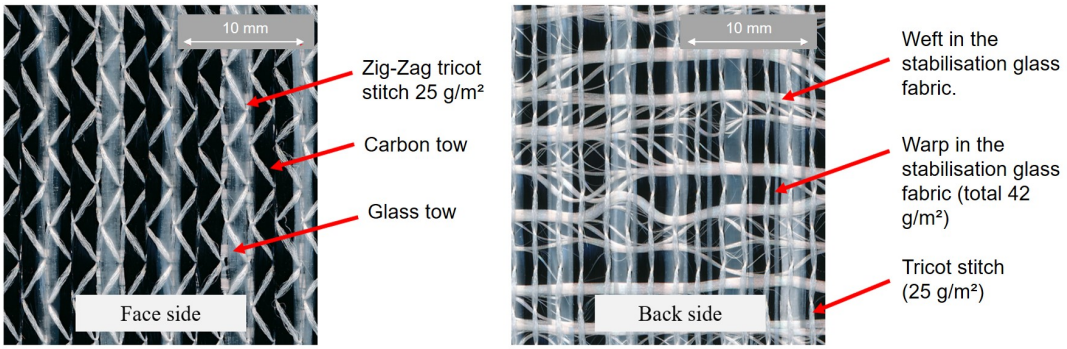

(b) Zoomed in picture for fabric - Hybrid1, 1C1G tow dispersion.

Fig. 4.3 Photographs of developed reference and hybrid fabric reinforcements.

(Epikote 05390 from Hexion Inc.) is applied on the edges coinciding the final net shape of the preform as shown in Fig. 4.4a. The stack was then vacuum sealed to 0.3 bar and heated to 80 °C for 10 min to activate the binder and consolidate the layers together. After cooling down the preform stack was net shaped to the final mould/part dimensions using roller knife and rested into the cleaned lower mould (Fig. 4.4b).

The lower mould (500 mm × 500 mm) contains a line injection channel on one end and 3 exit ports on the opposite end. On the remaining two sides a silicon packing was applied in a very fine gap between the preform edge and the mould cavity to avoid “race tracking”. The closed mould was then placed into the pneumatic press which applied a pressure of about 16 bars and heated the mould to a temperature of 60 °C. Vacuum of 0.9 bar was applied to remove the air from the preform and the mould cavity. Pre-mixed and degassed resin was then injected in the mould cavity at 2 bar initially and later the pressure was increased up to 6 bar. The curing cycle for all composites is schematically presented in Fig. 4.4d. Finally, the composite plate was demoulded after cooling and the edges and the resin channel cut off from the plate.

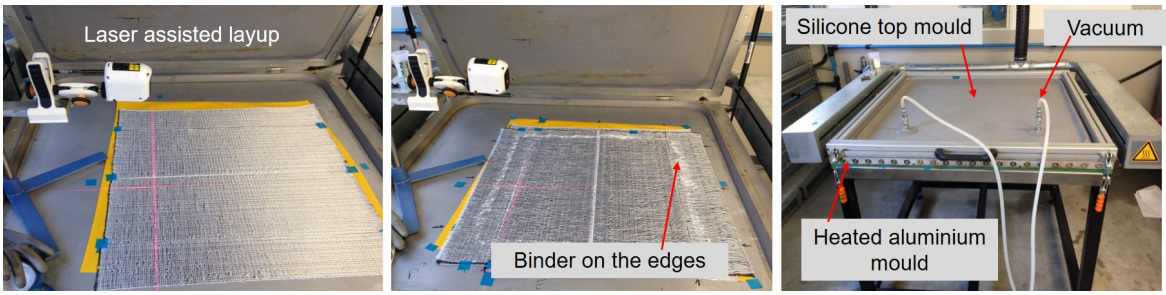

(a) Preforming

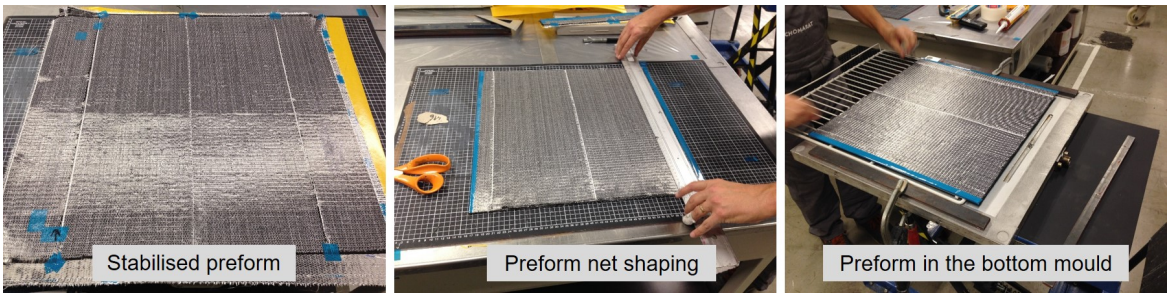

(b) Net shaping

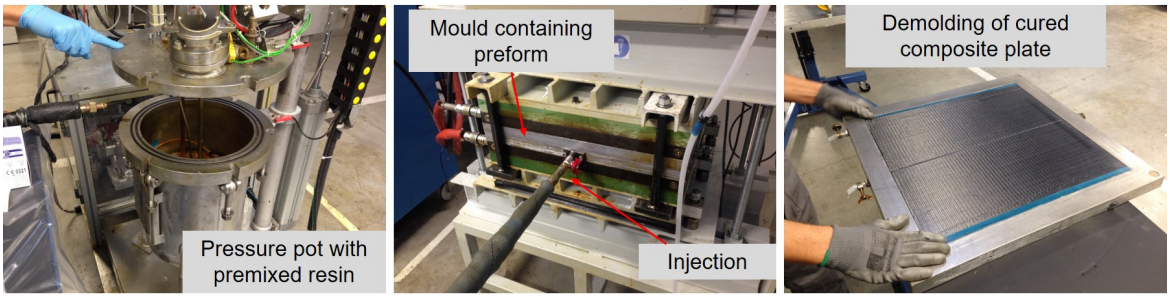

(c) Infiltration and curing

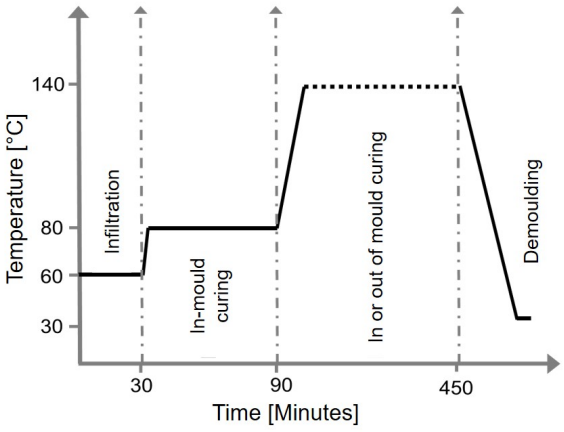

(d) Curing cycle

Fig. 4.4 Composite manufacturing using RTM process.

Three sets of composites (1) reference composites, R1 and R2, (2) intraply hybrid composites, H1, H2 and H3, and (3) interply hybrid composite I1, were manufactured. The details of manufactured composites and their physical properties along with the Fibre Volume Fraction (FVF) is summarised in the Table 4.2.

Table 4.2 Overview of manufactured composites.

	Composite name	Fabric used	Number of layers	Layup sequence	Thickness [mm]	Density [$g\,cm^{-3}$]	FVF [%]
Reference	R1	Ref Carbon	6	$[0/90/0]_S$	1.8	1.5	49.4
	R2	Ref Glass	6	$[0/90/0]_S$	1.2	1.8	47.1
Intraply	H1	Hybrid1 (1C1G)	6	$[0/90/0]_S$	2.6	1.6	51.3
	H2	Hybrid2 (2C2G)	6	$[0/90/0]_S$	2.6	1.6	54.1
	H3	Hybrid3 (3C3G)	6	$[0/90/0]_S$	2.6	1.6	51.8
Interply	I1	Ref Carbon & Ref Glass G	12 (6+6)	$[0_G/0_C/90_G/90_C/0_G/0_C]_S$	3.1	1.6	50.4

4.3.3 Characterisation of textile and composites

4.3.3.1 Physical properties of textiles

Physical properties of fabrics were characterised and these are presented in Table 4.3 and the pictures demonstrating the tests are presented in Fig. 4.5. The fabric parameters such as thickness and areal density were measured so as to confirm the quality and comparability of the fabrics. The composition of the constituents of the fabrics were characterised by unravelling and dismantlement individual components of the fabrics. Coverage and the stitching parameters were identified by image analysis of high-resolution pictures of the fabrics scanned using a Canon 9000F Mark II scanner.

Table 4.3 Physical properties of the manufactured fabric reinforcements.

Property	Units	Ref Carbon	Hybrid1	Hybrid2	Hybrid3	Ref Glass
Thickness at 400 g load	[mm]	0.6	0.7	0.8	0.8	0.5
Thickness at 28 kg load	[mm]	0.4	0.6	0.6	0.5	0.3
Areal density	[$g\,m^{-2}$]	327	520	516	521	260
Coverage	[%]	95	98	98	99	88
Stitch gauge	[stitches/inch]	10.1	9.8	9.7	9.6	9.9
Stitch pitch	[stitches/inch]	3.2	3.2	3.2	3.1	3.2

Permeability measurements were carried out on a stack of 4 fabrics by utilising a vegetable oil as a fluid medium with a known viscosity and measuring the time required to reach a certain flow length (500 mm) at a vacuum pressure of 0.9 bar. The setup for permeability measurement is presented in Fig. 4.6. The permeability was further calculated using a modified form of Darcy's law described in an equation form for x-direction as below:

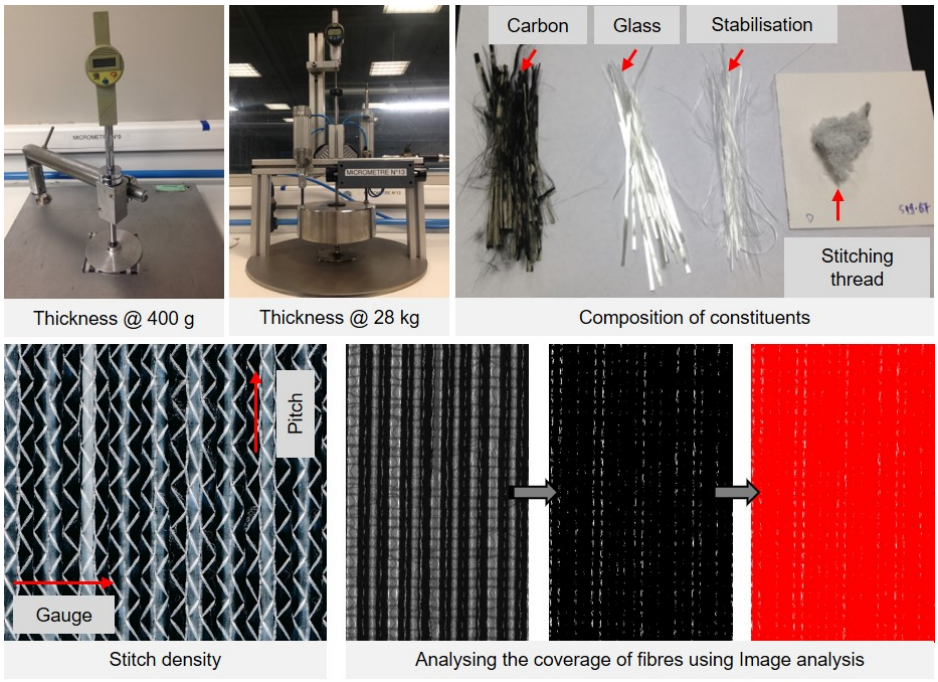

Fig. 4.5 Physical property test for reinforcement fabrics.

$$V = \frac{Q}{A} = \frac{k}{\eta} \times \frac{dp}{dx} \tag{4.1}$$

Where, V is the resin flow front velocity, Q is total amount of flow, A is total cross sectional area for fluid flow, k is the permeability of the textile preform, dp/dx is the pressure gradient and η is the viscosity of the fluid.

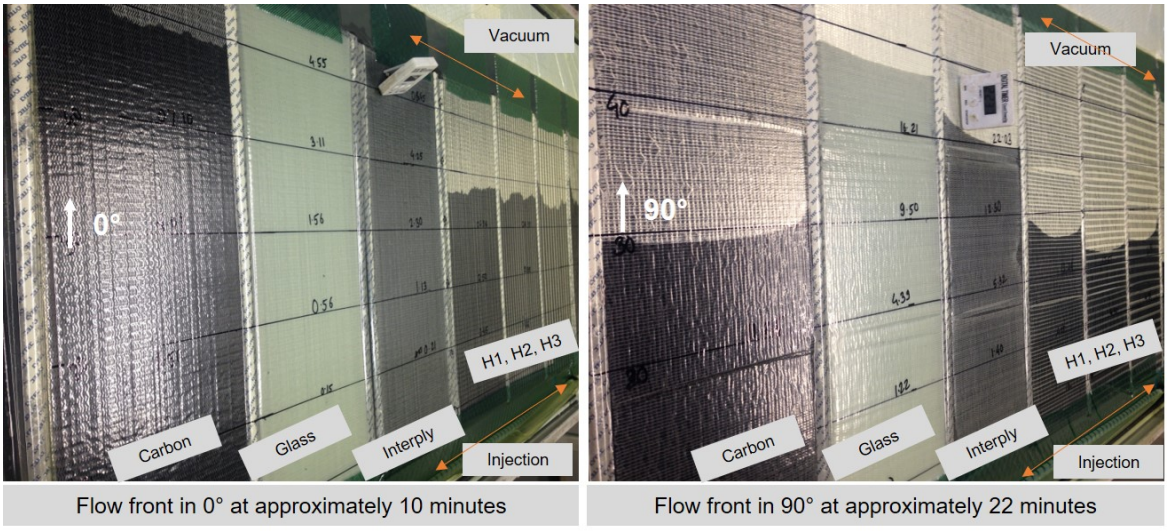

Fig. 4.6 Permeability tests on reinforcement fabrics.

4.3.3.2 Physical properties of composites

For composites, thickness was measured using micrometer screw gauge and the densities of the composites were measured using buoyancy method as per the ASTM standard D3800-16 [6]. While standard test method for Fibre Volume Fraction (FVF) estimation does not exist for hybrid composites, a modified form of burn-off test was developed. For individual components (carbon, glass and epoxy), Thermogravimetric Analysis was carried out to understand the weight loss for each constituent as a function of time and temperature. It was observed that quick burning-off in limited time did not cause significant weight loss in carbon and glass while the resin is vaporised completely. Finally, pre-weighted composite coupon samples were introduced in a preheated muffle furnace at 550 °C for 30 min, the residue was then weighted and the Fibre Volume Fraction was calculated using ASTM standard D-3171 [5]. This method underestimated (<5 %) the FVF when compared to the test method based on Acid Digestion, but for comparability and ease of use, the method based on burn-off was used for all composites in this work. Optical microscopy was carried out on composite coupons using Ziess AX10 Lab.A1 Microscope with a magnification limit from 50× to 1000×. Infiltration quality and void content was ascertained by analysis of images and measuring the area of voids in the total surface area of composite cross section.

4.3.3.3 Tensile properties

Quasi-static tensile tests were conducted using a Universal Testing Machine (UTM) from Instron using a load cell with maximum capacity of 100 kN and a wedge type mechanical grip. The tensile properties (ultimate tensile strength, failure strain and modulus) of the fabricated composites were measured according to ISO 527-4 standard [73]. A minimum of 5 specimens were tested for each composite and the schematic of specimen dimensions is presented in Fig. 4.8. The loading step was controlled with a cross-head speed of 2 mm min^{-1}. The selected cross-head speed resulted in the strain rate in the range of 10^{-4} to 10^{-5} s^{-1} for all types of composites. For each specimen, four rectangular glass fibre reinforced composite end-tabs were bonded at the gripping portions using a cold hardening high-performance epoxy resin. The strain in the composite was measured using optical strain gauge setup, namely, Advanced Video Extensiometer attached to the Instron UTM as seen in Fig. 4.7. The AVE measures the strain in real time and communicates the strain to the Instron machine in real time with no post processing required. The ultimate tensile strength was determined using the stress-strain curve and the tensile modulus was determined by calculating the slope of the initial linear portion of the obtained curve. For some samples Digital Image Correlation

was also conducted to compare the strain obtained by the digital imaging system and the optical strain gauge.

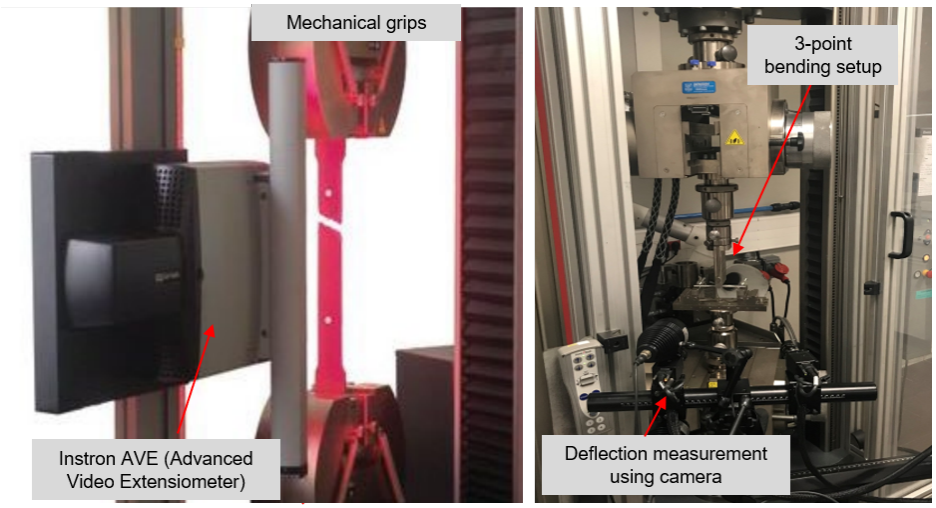

Fig. 4.7 Tensile and flexural testing set-up for tested composites.

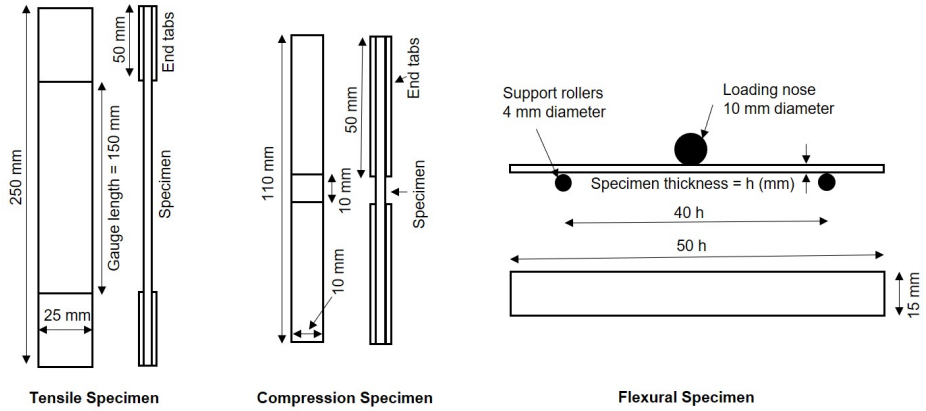

Fig. 4.8 Specimen dimensions for test samples in tensile, compression and flexural tests.

4.3.3.4 Compression properties

Quasi-static longitudinal compression tests were performed using ISO 14126 standard [75] an Instron Universal Testing Machine with 100 kN load-cell. Cross-head speed was set to 1 mm min^{-1}. A minimum of 5 specimens were tested for each composite and the schematic of specimen dimensions is presented in Fig. 4.8. For each specimen, four rectangular glass fibre reinforced composite end tabs were bonded at the gripping portions barring the 10 mm $\times$ 10 mm central test region as seen in Fig. 4.9. The strain in the composite was

measured using a DIC setup and image analysis. Full-field measurements were carried out using Baumer TXG20 camera (1/1.8" sensor size, 1624×1236 pixels, 8-bits) fixed on a balanced and stabilised tripod. A region of interest was selected in central region of test zone barring the edges. Analysis of images was done according to the specifications of the VIC-3D 2013 software. Computation of 3D displacement fields was performed by discretizing the region of interest in 21×21 pixel squares, with a distance of 7 pixels between two successive square centres. For compression samples, two cameras were used to look at two different regions of interest in compression specimen while the strain measurements were calculated from the DIC of face side of samples, the pictures of side camera were used to understand the fracture behaviour. The measured strain from DIC was than related to the load elongation data from the UTM and the stress-strain curves were plotted using the obtained data sets. The ultimate compressive strength was determined using the stress-strain curve and the modulus in compression was determined by calculating the slope of the initial linear portion of the obtained curve.

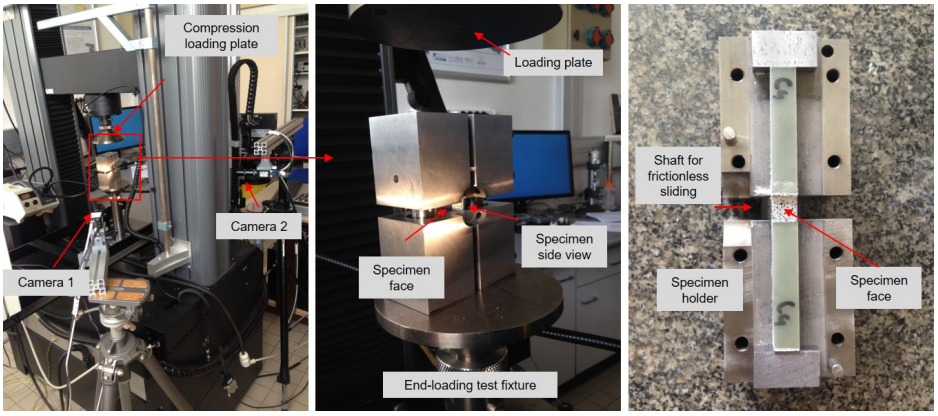

Fig. 4.9 Compression testing set-up for tested composites.

4.3.3.5 Flexural properties

The flexural tests were performed in a three-point bending mode using ISO 14125 standard [74] on an Zwick/Roell UTM with 10 kN load-cell. A minimum of 6 samples were tested for each configuration and the width of the specimens was selected to be 15 mm and for specimen thickness of h, the length of the test specimen for carbon and hybrid composites was fixed to 50 $\times$ h mm, for glass composites the length was 30 $\times$ h mm as seen in figure Fig. 4.8. The loading nose had a diameter of 10 mm while the support rollers had diameter of 4 mm and the distance between the two support rollers was set to be 40 $\times$ h mm for carbon and hybrid composites while it is 20 $\times$ h mm for glass composites. The loading nose

lowered at a displacement rate of 2 mm min^{-1}. The strain measurements were obtained by the deflection provided by the camera and digital image correlation setup see in Fig. 4.7. The flexural strength (σ_{fl}) and flexural strain (ε_{fl}) of the tested composites were calculated according to the following equations.

$$\sigma_{fl} = \frac{3FL}{2bh^2} \tag{4.2}$$

$$\varepsilon_{fl} = \frac{6sh}{L^2} \tag{4.3}$$

where, L represents the support span length and F is the maximum flexural load. b and h are the specimen dimension and thickness and s is the measured deflection. The flexural modulus (E_{fl}) is calculated by measuring the slope of the linear portion (between strain values of 0.05 % and 0.25 %) of the flexural stress-strain curve.

4.3.3.6 Fractography

The fractured samples were further analysed at macroscopic and microscopic level to understand typical fracture behaviour of the composites in different tests. Scanning Electron Microscopy using Nova NanoSEM 450 from FEI was performed to observe the fracture surface of the broken samples. The specimens were coated with 3 to 5 nm of Gold/Palladium (Au/Pd) to ensure good conductivity and inhibit specimen charging. The fractured samples were cut straight near the fracture location using a diamond saw. Optical microscopy was carried out using Zeiss AX10 Lab.A1 equipment with a magnification range from 50× to 1000×.

4.4 Results and discussions

4.4.1 Physical properties of textiles and composites

The fabric structural parameters such as thickness and areal weight for each fabrics showed an insignificant standard error and the coefficient of variation recorded for each tests was <5 %. This confirms the fabrics manufacturing process robustness. Among the three intraply hybrid fabrics, apart from the dispersion of tows no other fabric parameter is significantly different. The stitching parameters for all reference and hybrid fabrics were successfully maintained constant and hence its influence on the composite properties is same for all the reinforcements (See Table 4.3).

Thickness at different loads along with the permeability are essential parameters that influence the composite manufacturing process steps such as preforming and infiltration. Technically infiltration of glass fibre reinforcement, for the same volume fraction, is easier that carbon fibre reinforcement. This comes from the fact that glass fibre diameter is more than twice of the carbon fibre. As expected, Fig. 4.6 shows that permeability of all UD fabrics in 0° is higher than that in 90° direction owing to the assistance from capillary effect; and Fig. 4.10 demonstrates highest permeability for glass fibre reinforcements followed by interply reinforcements. As seen in Fig. 4.10 while have three intraply hybrids with different cross-sectional microstructure shows same permeability (around 3.1×10^{-11} m^2); the interply hybrid with alternate carbon and glass layers shows the permeability equal to 11.4×10^{-11} m^2 which is higher than the permeability of reference carbon fabrics (6.7×10^{-11} m^2). It has to be noted that the reference carbon fabrics show higher permeability than intraply hybrids this is because of the finer areal weight of reference fabrics and its lower coverage percentage (See Fig. 4.3.

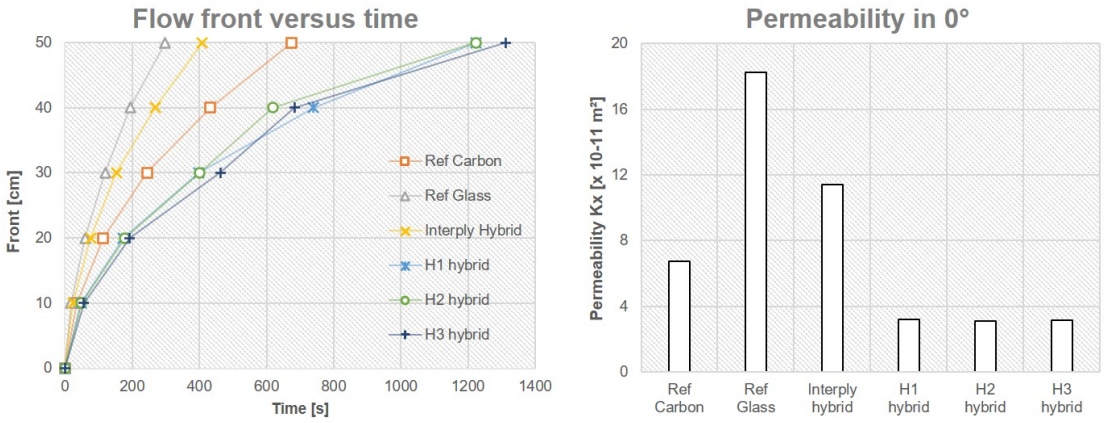

Fig. 4.10 Flow front and measured permeability of fabrics in 0° direction.

FVF and density of fabricated composite panels were evaluated to ensure the quality consistency of every composite specimen prior to subsequent mechanical tests. The density measurements and the fibre content from the burn-off tests are as presented in Table 4.2 and it can be seen the FVF for all composites are comparable. Besides this, the RTM process used, proves to be a very reliable and robust process to manufacture composites. Optical microscopy images suggested presence of no major voids and the void content on an average was <0.75 % in the samples. It is also apparent that, by introduction of glass fibres in the fabrics and composite layup, the density of subsequent composite increases. Stitched image showing the overview of cross-section for H1 intraply hybrid composite can be seen in Fig. 4.11a and a zoomed-in magnified image is presented in Fig. 4.11b. Composite volume

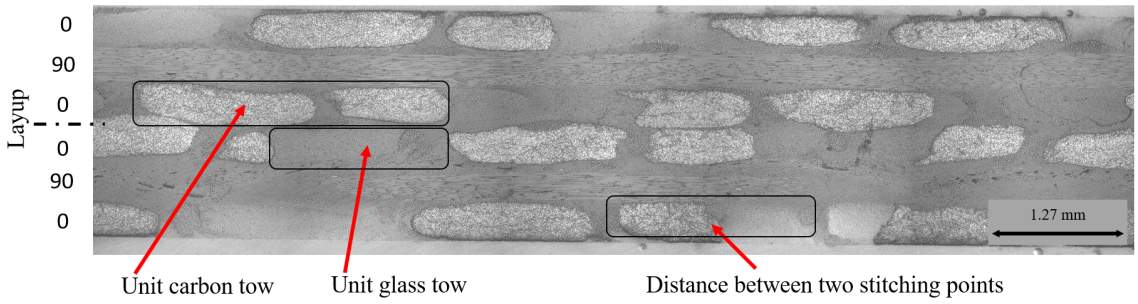

(a) Overview of cross-section

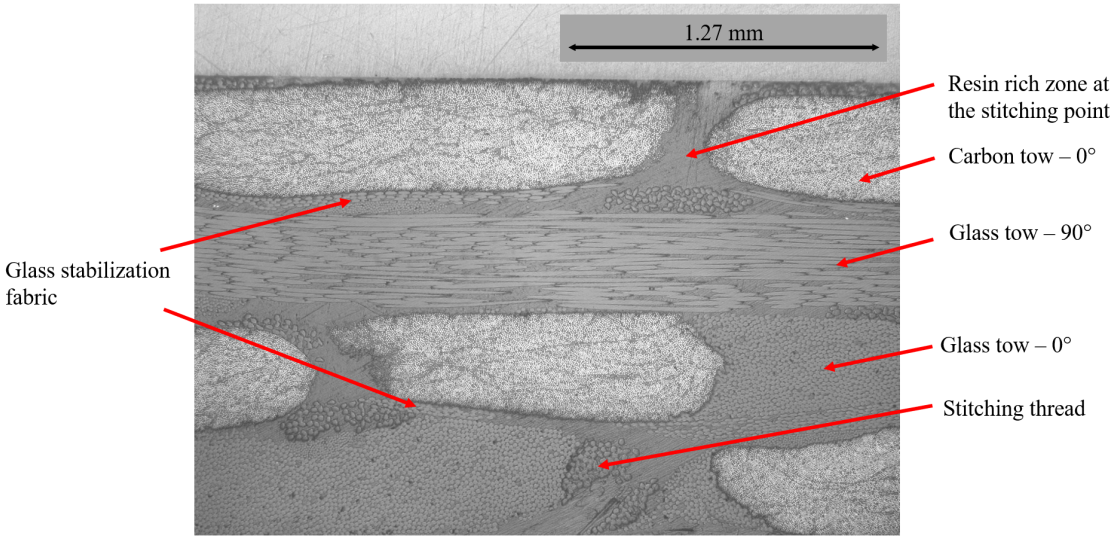

(b) Zoomed-in

Fig. 4.11 Optical microscopy images of H1 intraply hybrid composite: (a) overview of the cross-section, and (b) zoomed-in.

fraction (V_c) or hybrid ratio defined as the ratio of volume of one of the constituents (here, carbon) of the hybrid composite to the volume of hybrid composite was 0.62 for the hybrid composites. Selection of this hybrid ratio was influenced by the final end use for such hybrids in structural or semi-structural applications. This was also limited by the linear densities of the carbon and glass fibre tows used in the study.

4.4.2 Tensile properties

4.4.2.1 Stiffness

The stiffness for three intraply hybrid composites H1, H2 and H3, are not significantly different and their mean stiffness values are 60.8 GPa, 59.3 GPa and 60.5 GPa respectively.

Table 4.4 Tensile properties of composites along 0°; mean values for properties and standard deviation associated with 90 % confidence level are presented.

Composites	Ultimate tensile strength σ_t [MPa]	Ultimate failure strain ε_t [%]	Tensile modulus E_t [GPa]
R1 - Ref carbon	1165 (± 43)	1.70 (± 0.04)	69.8 (± 2.1)
H1 - Intraply (1C1G)	935 (± 58)	1.60 (± 0.10)	60.8 (± 3.0)
H2 - Intraply (2C2G)	964 (± 43)	1.67 (± 0.10)	59.3 (± 1.2)
H3 - Intraply (3C3G)	1024 (± 49)	1.67 (± 0.09)	60.5 (± 2.0)
I1 - Interply	898 (± 44)	1.82 (± 0.10)	50.2 (± 0.8)
R2 - Ref glass	587 (± 20)	2.74 (± 0.13)	21.8 (± 0.5)

These values suggest there is no effect of tow dispersion on the stiffness of intraply hybrid composites (Fig. 4.12a). Several researchers [58, 45, 88] earlier showed that the tensile modulus for hybrid composites obey a linear Rule of Mixtures, but most of the reported studies were on unidirectional composites. For cross ply layup like in the current study the transverse direction reinforcements where Rule of Mixtures are not linear and often less accurate can influence the Young's modulus in longitudinal directions. The intraply hybrids show a positive deviation in the Young's modulus when compared to that obtained from linear RoM while, I1 (50.2 GPa) demonstrates stiffness nearest to the theoretically obtained value (51.5 GPa) using the linear RoM. Positive deviation from Rule of Mixtures for hybrid composites have been also reported by Ren et al. [125] and Taketa [149]. It is found that the tensile modulus of the intraply hybrid composites are significantly higher than that of the interply hybrid composites. This may be attributed to better dispersion of high modulus carbon and low modulus glass fibres in the intraply hybrids than that in interply. Higher dispersion leads to a better load transfer from fibres to fibres in the intraply composites.

4.4.2.2 Failure characteristics

The hierarchy of tensile strength is as follows: [R1 - Reference carbon composite] $>$ [H3 $\approx$ H2 and H1 Intraply hybrid composite] $>$ [I1 - Interply hybrid composite] $>$ [R2 - Reference glass composite].

The hierarchy of ultimate tensile strain is as follows: [R2 - Reference glass composite] $>$ [I1 - Interply hybrid composite] $>$ [H3 - H2 and H1 Intraply hybrid composite] $\approx$ [R1 - Reference carbon composite].

The hierarchy of tensile strength for all composites follow a trend similar to that of tensile stiffness, the difference being that H1, H2 and H3 do not show similar strengths, but they showed identical modulus. The failure strain as expected is highest for glass fibre composite

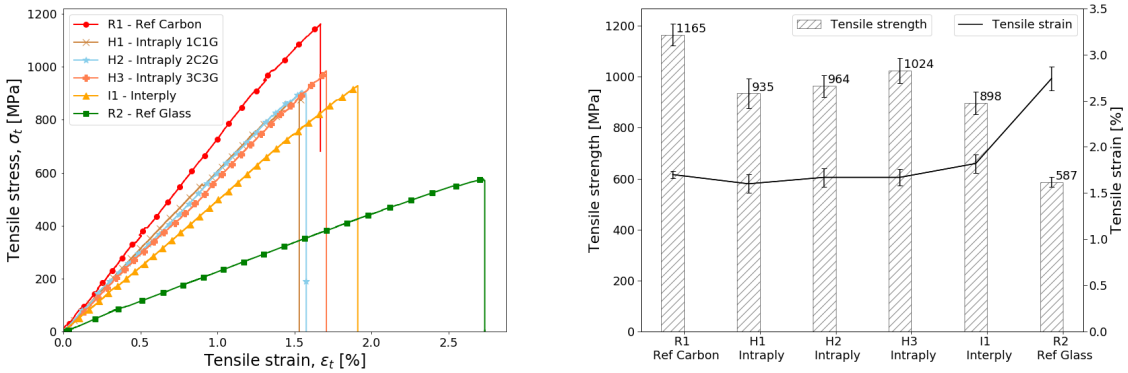

(a) Tensile stress - strain plot

(b) Tensile failure characteristics

Fig. 4.12 Tensile properties of composites along 0°: (**a**) Stress-strain plot (**b**) Failure characteristics. (In (a) representative curves with failure characteristics closer to the average values reported in Table 4.4 for each composite type are presented.).

R2. For I1 on contrary to the stiffness and strength properties, its tensile failure strain lies higher in the hierarchy than the three intraply hybrids H1, H2 and H3.

The failure strain of interply hybrid composite I1 is more than that of intraply hybrids H1, H2 and H3. In other words, for the same hybrid ratio, the hybrids made by combining carbon and glass on a ply by ply basis gives higher tensile failure strain than the tow by tow hybridised composites. For interply hybrid composite I1, the carbon layers are sandwiched between glass layers, hence, possible damage evolution in carbon layers during tensile loading is constrained because of surrounding glass layers, resulting in carbon layers withstanding more strain before failure of the layer. This phenomena is as also reported by Pandya et al. [113] and Swolfs et al. [143]. Even though the intraply hybrids H1, H2 and H3 has a significant proportion of high elongation glass fibre in its structure they tend to not affect the failure development in the carbon fibres in the exterior layers as they are not sufficiently constrained and hence show no improvement in the failure strain when compared to the reference carbon composites. Kretsis [88] in his review paper analysed literature data prior to 1987 and clearly demonstrated that the hybrid effect increased with decreasing high modulus fibre content. Swolfs et al. [143] further suggested caution in interpreting the failure strain enhancements reported earlier, as the studies reported $-66\,\%$ to $+166\,\%$ failure strain enhancements; which is unrealistic. Multiple reasons can be identified for these unrealistic values, like, improper testing of reference carbon composites or low quality carbon fibres during earlier times.

The tensile strength for interply and intraply hybrids falls in between the values for the two reference composites R1 and R2 (1165 MPa and 587 MPa respectively). The tensile strength

for Interply hybrid I1 is 898 MPa and it is lowest among the hybrids. An improvement in the tensile strength of intraply hybrids is observed as the carbon and glass tows are blocked together in the intraply hybrids from 935 MPa for H1 to 964 MPa and 1024 MPa for H2 and H3 respectively (Fig. 4.12b). This improvement in the strength for the intraply variants can be attributed to the effect of hybridisation and the changes in their failure behaviour. Among the hybrids, the intraply hybrids H1, H2 and H3 has tensile strength 4.1 %, 7.4 % and 14.0 % higher respectively than the interply hybrid I1. Ikbal et al. [66] reported higher strength for interply hybrids for unidirectional composites, though in their studies the difference between interply and intraply was about 5 % for strength and 2 % for modulus which is not very significant and can be influenced by several processing and testing parameters. In the current study, higher dispersion of carbon and glass fibres in the intraply configuration, leads to better load transferring from fibre to fibre and hence demonstrate higher strengths when compared to interply composite I1. It is to be noted that for hybrid specimens the width of the specimen was sufficient to include at least one repeat unit of textile and that in thickness direction the placement of carbon and glass tows was random. The edge effects for hybrid specimen were similar to the reference specimens and their influence on damage was not studied in the scope of current work.

4.4.3 Compression properties

4.4.3.1 Stiffness

Table 4.5 Compressive properties of composites along 0°; mean values for properties and standard deviation associated with 90 % confidence level are presented.

Composites	Ultimate compressive strength σ_c [MPa]	Compressive strain ε_c [%	Compressive modulus E_c [GPa]
R1 - Ref carbon	492 (± 22)	0.98 (± 0.09)	52.5 (± 2.0)
H1 - Intraply (1C1G)	484 (± 40)	1.00 (± 0.19)	45.9 (± 3.1)
H2 - Intraply (2C2G)	515 (± 13)	0.97 (± 0.09)	52,7 (± 2.6)
H3 - Intraply (3C3G)	535 (± 36)	1.12 (± 0.06)	51.3 (± 8.2)
I1 - Interply	388 (± 16)	0.91 (± 0.08)	45.3 (± 2.5)
R2 - Ref glass	316 (± 30)	1.29 (± 0.18)	25.0 (± 3.5)

For the developed composites the hierarchy of compressive modulus is as follows: [R1 - Reference carbon composite $\approx$ H2 and H3 - Intraply composite] $>$ [H1 - Intraply composite $\approx$ I1 - Interply hybrid composites] $>$ [R2 - Reference glass composite].

Last column in Table 4.5 provides the mean values ($\pm$ standard deviation associated with 90 % confidence level) for compressive modulus for each composite type. It can be seen that

the hybrid composites H2 and H3 have a comparable compressive stiffness to the reference carbon composite R1 (see Table 4.5 and Fig. 4.13a). When compared to the theoretical stiffness (42.1 GPa) calculated using Rule of Mixture (using the stiffness's of R1, R2 and hybrid ratio of 0.62), configurations H1 (45.9 GPa) and I1 (45.3 GPa) do not show significant difference in longitudinal compression. Hence interply hybrid I1, shows to obey a linear Rule of Mixture for both tensile and compressive modulus while the intraply hybrid H3 shows a positive deviation in both the cases. Among hybrids the intraply H1 has the highest ratio (1.32) of tensile to compression modulus which is same for R1, while it is lowest (1.11) for I1 interply hybrid.

4.4.3.2 Failure characteristics

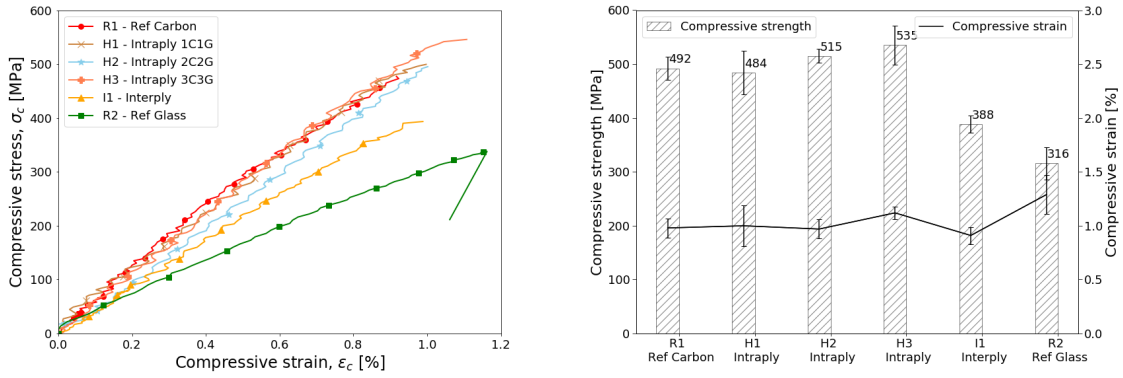

(a) Compressive stress - strain plot

(b) Compressive failure characteristics

Fig. 4.13 Compression properties of composites along 0°: (**a**) Stress-strain plot (**b**) Failure characteristics. (In (a) representative curves with failure characteristics closer to the average values reported in Table 4.5 for each composite type are presented.).

The hierarchy of compressive strength is as follows: [H3, H2 - Intraply hybrid composite] > [R1 - Reference carbon composite] > [H1 - Intraply hybrid composite] > [I1 - Interply hybrid composite] > [R2 - Reference glass composite].

The hierarchy of ultimate compressive strain is as follows: [R2 - Reference glass composite] > [H3 - Intraply hybrid composite] > [[R1 - Reference carbon composite ≈ H2 and H1 Intraply hybrid composite] > [I1 - Interply hybrid composite].

I1 had the highest failure strain in tension; on the contrary in compression the I1 hybrid made by combining carbon and glass on a ply per ply basis gives lower failure strain than placing carbon and glass tows in the individual fabric. This behaviour of I1 in compression (and hence its lower compressive strength behaviour) can be attributed to multiple factors:

(1) the I1 composites have more number of ply interfaces as it has twice the number of layers, (2) I1 has low modulus glass fibres in the exterior of the layup, this makes it more susceptible to the local buckling (initiated during or after delamination) occurring during longitudinal compression test. Delamination in I1 composites was prominently observed and in compressive loading I1 did not assist a gradual failure behaviour like in tensile loading. Though the specimen width in compression (for H2 and H3) was lower than the repeating unit cell width in the fabrics, the standard deviation for strength and failure strain does not show a significant difference from other composites. The failure strain for intraply hybrids are equal to or higher than the reference carbon composite and this is attributed to better load transfer between the fibres due to dispersion of carbon and glass fibres in the cross-section.

The compressive strength values for the interply I1 (388 MPa) falls in between the values for the two reference composites, but the compressive strengths for intraply hybrids H1, H2 and H3 are very similar or slightly higher than that for reference carbon composite R1. Such a trend for interply hybrid bi-directional composites was reported by Pandya et al. [113]; while Ikbal et al. [65] and [66] reported a trend of about 60 % reduction of compressive strengths for hybrids when compared to reference carbon composites for unidirectional composites. It is important to mention that precise measurement of reference composites is consequential to interpret the change for hybrids, and this is more difficult for unidirectional composites than for the current work on multidirectional composites. For intraply hybrids though the face of specimen contained carbon and glass rovings side by side, the strain during compression observed through DIC was uniform over the width. Further, the final failure on face and sides show failure of both carbon and glass tows in compression and then through other mechanisms such as delamination and buckling as seen in Fig. 4.14 for H1 composite specimen.

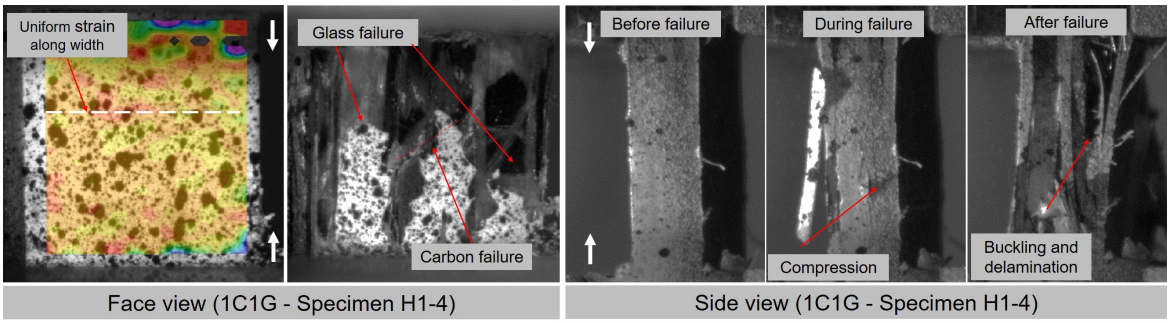

Fig. 4.14 Pictures from camera setup during compression tests: DIC measurements on face side, fracture observation on the thickness of specimens.

When compared to the reference composite R1, the strength of hybrid composites H2 and H3 show an increase of 4.6 % and 8.6 % respectively while I1 shows a reduction of 21.2 %

respectively. The improvement in compressive performance in intraply hybrids over interply can be explained by the fact that the glass fibre tow blocks provide protection to carbon fibre tow blocks against buckling. As also observed during tensile loading, a gradual improvement in compressive strength (484 MPa, 515 MPa, and 535 MPa for H1, H2 and H3) for intraply hybrids is observed as the carbon and glass tows are blocked together in the intraply hybridisation, as can also be seen in Fig. 4.13b.

4.4.4 Flexural properties

4.4.4.1 Stiffness

For the developed composites the hierarchy of flexural modulus is as follows: [R1 - Reference carbon composite] $>$ [H3 $\approx$ H2 $\approx$ H1 - Intraply hybrid composites] $>$ [I1 - Interply hybrid composite] $>$ [R2 - Reference glass composite]. The trend of modulus in flexion is similar to that of in tension. The stiffness in flexion for all the three intraply hybrid composites H1, H2 and H3, are not significantly different and their mean stiffness values are similar to that in tensile loading (See Table 4.6 and Fig. 4.15a). These values suggest there is no effect of tow dispersion on the stiffness of intraply hybrid composites. The stiffness of interply hybrid I1 in comparison to R1 and H1 is about 41.2 % and 21.9 % lower respectively. Unlike in tension and compression, a simple RoM cannot be applied to predict the properties of hybrid composites.

Table 4.6 Flexural properties of composites along 0°; mean values for properties and standard deviation associated with 90 % confidence level are presented.

Composites	Ultimate flexural strength σ_{fl} [MPa]	Flexural strain ε_{fl} [%]	Flexural modulus E_{fl} [GPa]
R1 - Ref carbon	909 (± 37)	1.30 (± 0.09)	78.6 (± 1.7)
H1 - Intraply (1C1G)	798 (± 31)	1.47 (± 0.34)	59.2 (± 2.0)
H2 - Intraply (2C2G)	794 (± 31)	1.36 (± 0.06)	60.8 (± 1.6)
H3 - Intraply (3C3G)	825 (± 29)	1.46 (± 0.12)	58.6 (± 1.6)
I1 - Interply	563 (± 5)	2.07 (± 0.53)	46.2 (± 0.6)
R2 - Ref glass	572 (± 29)	2.91 (± 0.24)	27.4 (± 0.8)

4.4.4.2 Failure characteristics

The hierarchy of flexural strength is as follows: [R1 - Reference carbon composite] $>$ [H3 and H1 $\approx$ H2 Intraply hybrid composite] $>$ [R2 - Reference glass composite] $\approx$ [I1 - Interply hybrid composite].

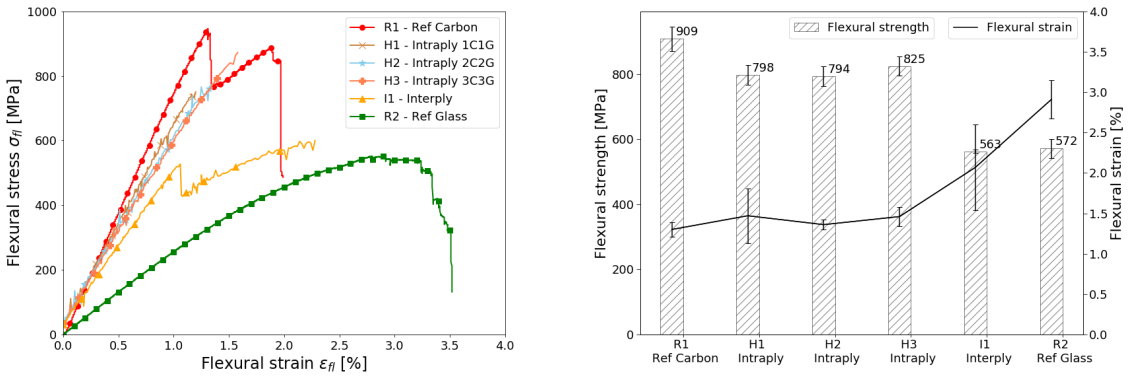

(a) Flexural stress - strain plot

(b) Flexural failure characteristics

Fig. 4.15 Flexural properties of composites along 0°: (**a**) Stress-strain plot (**b**) Failure characteristics. (In (a) representative curves with failure characteristics closer to the average values reported in Table 4.6 for each composite type are presented.).

The hierarchy of flexural strain is as follows: [R2 - Reference glass composite] > [I1 - Interply hybrid composite] > [H3 - H1 and H2 Intraply hybrid composite] > [R1 - Reference carbon composite].

It is observed that the reference glass fibre composite R2 has the highest failure strain (2.91 %). Similar to failure strain behaviour in tensile loading, interply hybrid I1 having failure strain of 2.07 % is highest among all hybrids. Two important reasons for this are: (1) glass fibres have better transverse compression property and that it resists the composite failure on the compressive side, and (2) glass fibre has a higher failure strain hence can strain more on the tension side during flexural test, hence, glass fibres in exterior play a supportive role during the flexural testing of interply hybrids. For intraply hybrid composites, the carbon fibre tows on the exterior are not sufficiently constrained by high strain glass layers. It is observed that the initiation of failure in these hybrids is because of compressive stresses near the loading nose, which cause the crushing effect on carbon tow to cause failure. Further as the load increases the stress is transferred to the layers adding delaminations and compressive stresses in other layers. Hence these composites, H1, H2 and H3 has relatively lower ultimate failure strain (29 to 35 % lower) than the hybrid composite I1. It may be also noted that in flexural loading, percentage gain in failure strain for hybrid composite I1 is significantly higher than percentage loss in flexural strength when compared to R1 composite and for intraply hybrids this difference is very low and can be considered as negligible.

The flexural strength for Interply hybrid I1 is 563 MPa and it is lowest among all the composites. This could be because of excessive delaminations during the flexural loading in these composites and that a glass layer is present on the tension side of the flexural loading.

The intraply hybrids H1, H2, H3 has a flexural strength of 798 MPa, 794 MPa and 825 MPa respectively. Owing to a similar damage/failure behaviour, blocking of multiple carbon and glass tows (tow dispersion) in intraply hybrids shows no significant difference in the flexural strength (as seen in Fig. 4.15b), here flexural strength of H1, H2 and H3 are nearly similar, H3 being just 3.6 % higher than H2. Among the hybrids, the intraply hybrid H1, H2 and H3 have significantly higher flexural strength (41 to 46 % higher) than the interply hybrid I1.

4.4.5 Fractography

During tensile loading it is observed that the reference composites R1 and R2 failed suddenly in a catastrophic failure, though the cracking noise could be heard during the entire duration of test for both composites. All carbon samples broke yielding two separate pieces or sometimes three pieces because of secondary failure induced by the shock of rapid elastic recovery. Glass composite R2 still had some unbroken rovings which would connect the two pieces across the tensile failure line. Hybrid composites also failed catastrophically and this catastrophic failure in them can be attributed to a higher proportion of carbon fibres in the hybrid composite structure. Macroscopic observations show that the three intraply hybrid samples show very similar kind of failure surface. The failure tends to show that as the strain increases the carbon fibre fail first (seen in Fig. 4.16a), causing stress concentrations and matrix cracking in adjoining regions, as the strain increases a whole carbon fibre bundle (tow) fails.

The catastrophic tow failure causes longitudinal splitting of carbon tow from the specimen and large-scale pullout in adjoining regions further leading to composite failure. The glass fibre tow in the hybrid ply at the surface here can be clearly seen broken and delaminated from the surface in Fig. 4.16b. The area of damage (and delamination for glass tows) witnessed for these intraply hybrid composites is higher than that for reference and interply composites (see Fig. 4.16b). For interply I1 carbon ply fails catastrophically on reaching the maximum stress and further this failure of carbon ply leads to the catastrophic failure in the glass plies. Interlayer delamination can also be prominently in all hybrids though for these composites secondary failure was not observed.

All the samples loaded in longitudinal compression show catastrophic failure, but no samples were observed to be completely separated into two halves. It is observed that the load applied at two ends concentrate at the center of the test zone. As the load increased, for interply hybrids, the failure catastrophically occurred by forming a major crack at the central plane and enlargement of this crack into a though the thickness crack as seen in Fig. 4.17b. For intraply hybrids, the failure was similar for all the three types. Delamination between the layers was more prominent and larger failure surface was noted specifically for intraply

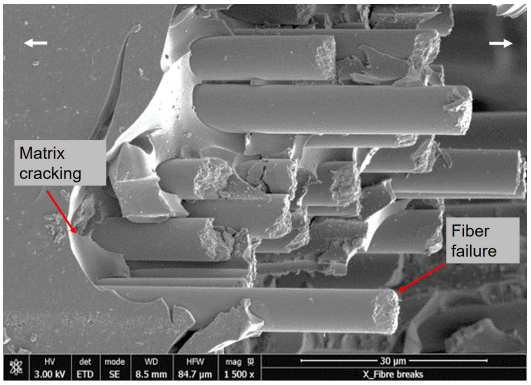

(a) Fibre break and matrix cracking

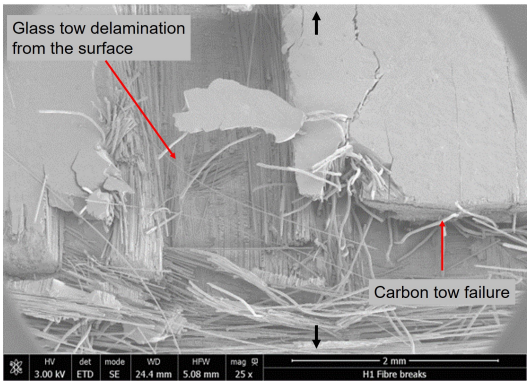

(b) Glass tow break and delamination

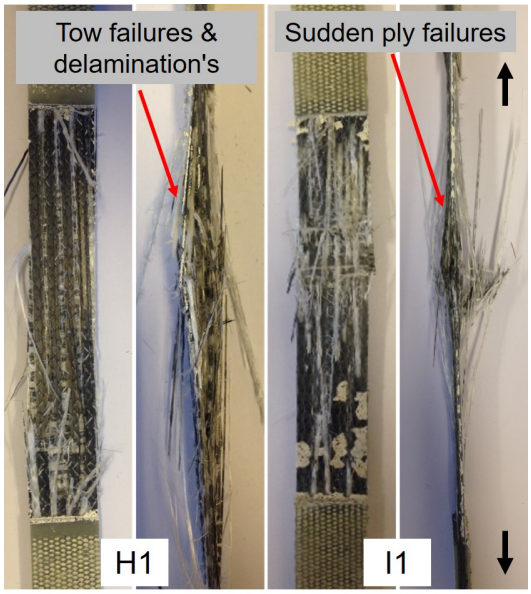

(c) Failure H1 and I1 composite specimens

Fig. 4.16 Fractography of failure of composites in tensile loading.

hybrids (seen in Fig. 4.17a and Fig. 4.17c) because, the two fibres in the same layer had a very different failure strain.

The flexural stress of carbon fibre composites R1 shows a stepped decline at the beginning of failure, and then it rises again slowly until the sample fails again with a significant stress drop catastrophically. For R1 and all the hybrids, the transverse compressive stress decreases gradually from the upper layers (loading nose side) to the lower layers, and a larger compressive failure zone is observed for the top layers for all the composites. Due to lower transverse modulus and the lower failure strain of carbon fibre, once the loading reaches the failure strain of carbon fibre, the upper layer fails. As the loading continues delaminations are introduced in the upper layers instantly along with the compressive stress transferred

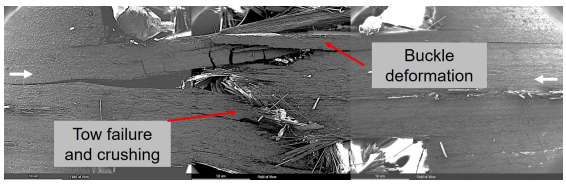

(a) Typical failure H3

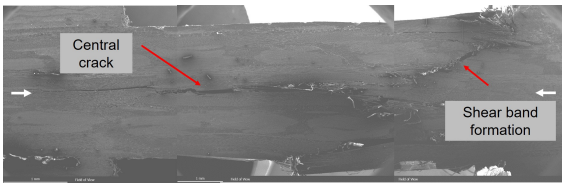

(b) Typical failure I1

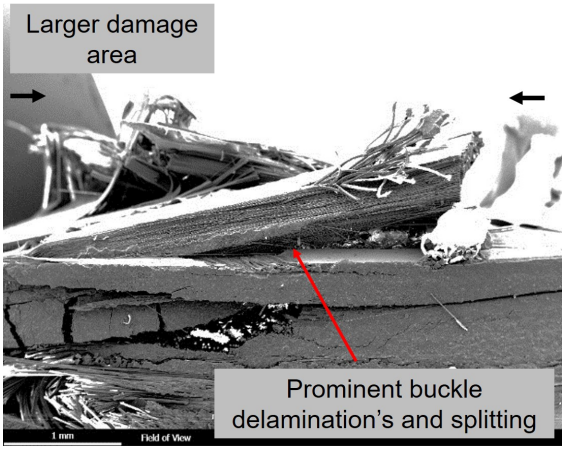

(c) Typical failure H3 - zoomed-in in the failure zone.

Fig. 4.17 Fractography of failure of composites in compressive loading.

to layers below, which leads to propagation of fracture zone to the lower layers gradually, finally leading to final failure.

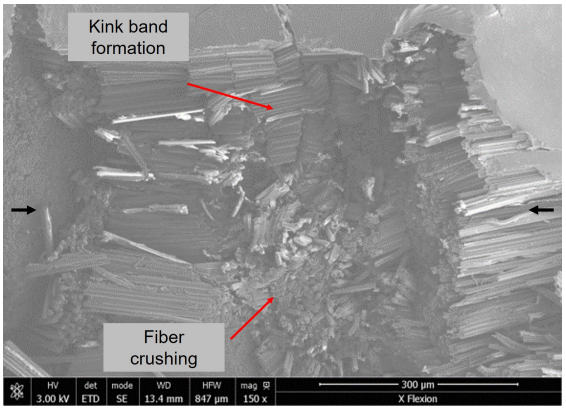

(a) Kinking and microbuckling

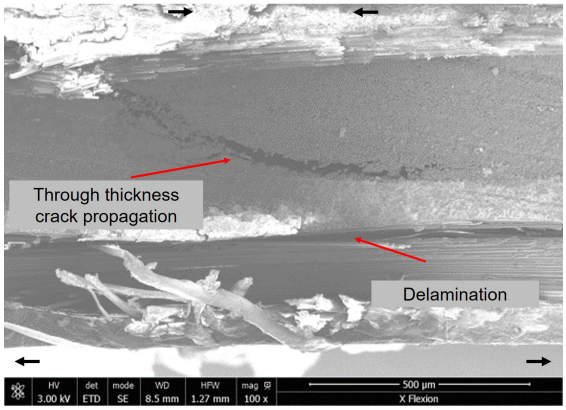

(b) Delamination and crack propagation

Fig. 4.18 Prominent failure modes in flexural loading of tested composites.

It is observed that the most common failure mode is kinking or microbuckling at the compression side, which can be found in all three intraply hybrid composite specimens (Fig. 4.18). Failure in tension on the other side of loading was not observed for carbon reference com-

posite and intraply hybrid composites. For intraply hybrids, for example in H1, through the thickness crack and delamination plays major role in the flexural failure apart from the compression failure on the top. While for interply I1 the tensile failure along with delamination is very much prominent and that the failure occurs too early at comparatively lower loads. The details of failure modes of all composite types are summarised in Table 4.7. The interply hybrids also showed a two-step failure and a significantly lower flexural strength in the stress-strain curve, this was because of their laminar structure with glass layer in the exterior (tension side) of the composite. As also reported by Dong et al. [42]; the glass layer in tension side generally deteriorates the flexural strength and modulus. They also report in [40] that a symmetric layup like in the current interply composites are not the optimal design for the hybrid composites that are subjected to flexural loads.

Table 4.7 Composites and their failure modes in flexural tests.

Composite	Failure
R1 – Ref carbon	fibre buckling and kinking on compression side
H1 – Intraply hybrid	fibre buckling, delamination through thickness, and carbon tow delamination on surface
H2 – Intraply hybrid	fibre buckling in compression side, only for carbon tows
H3 – Intraply hybrid	fibre buckling in compression side, only for carbon tows; interlaminar shear
I1 – Interply hybrid	fibre buckling in compression, larger delamination and shear, failure in tension. Complex.
R2 – Ref glass	fibre buckling on compression side, delamination

4.4.6 Hybrid effect

4.4.6.1 Improvement in failure strain

The failure strain in tension, compression and flexion normalized to the failure strain of low elongation reference carbon composites in respective loading conditions is presented in the Fig. 4.19. It can be derived from Table 4.4 and Fig. 4.19a that in tensile loading there is a slight negative hybrid effect or no hybrid effect for intraply hybrid composites while the interply hybrid composite I1 shows a positive hybrid effect of $+7.4\,\%$. Similarly, for compressive loading conditions the intraply hybrids H1 and H2 showed no hybrid effect; while the intraply hybrid H3 showed a positive hybrid effect of about $+14.0\,\%$. Opposite to its behaviour in tension, the ply per ply hybrid I1 in compression shows a negative hybrid effect of $-6.4\,\%$, as seen in Fig. 4.19b and this can be attributed to the number of layers, complex failure mode and prominent delaminations.

In flexural loading, failure strains of all the composites normalized to the failure strain of reference carbon composite is presented in the plot Fig. 4.19c. All hybrid composites show a positive hybrid effect in the flexural loading conditions. The highest positive hybrid effect of

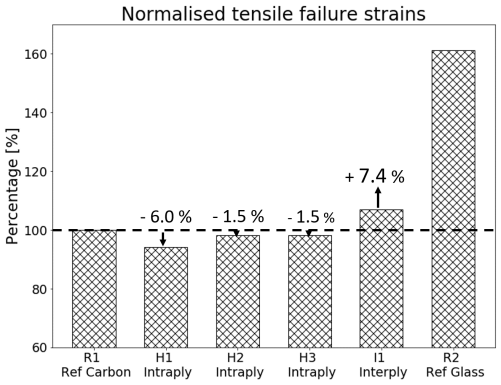

(a) Tensile failure strain

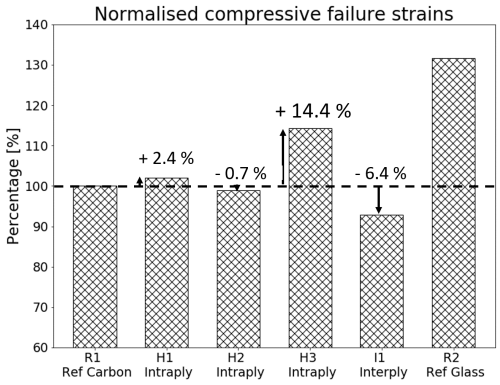

(b) Compressive failure strain

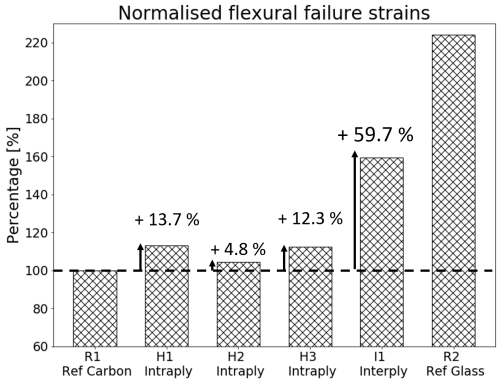

(c) Flexural failure strain

Fig. 4.19 Hybrid effect in failure strain for interply and intraply composites: Failure strains normalised to failure strain of carbon composite in different loading conditions.

about +59.7 % is demonstrated by I1 interply hybrid composite. The intraply hybrids also show positive hybrid effect of about 4.8 % for H2 and about 13.7 % and 12.3 % respectively for H1 and H3 composite.

4.4.6.2 Deviation from Rule of Mixtures

Tensile and compressive strength of hybrid composite as a function of carbon composite volume fraction (V_c) is presented in Fig. 4.20a and Fig. 4.20b respectively. These figures are plotted based on mechanics of materials approach to strength under quasi-static loading along the 0° direction. Here lines AB and BC represents the strength of the hybrid composite as per bi-linear RoM for different carbon composite volume fractions (V_c). It has to be noted that line AB represents the RoM when the strength property is dominated by glass fibres, typically for lower carbon composite volume fractions and line BC represents the

RoM for composite with larger carbon composite volume fraction. When the volume fraction of carbon composite is zero then it represents reference glass fibre composite R2, whereas volume fraction of carbon composite equal to one represents reference carbon fibre composite R1. Point B in Fig. 4.20a, is the strength where the bi-linear rule of mixture lines meet and was found to be corresponding to the carbon composite volume fraction, $V_c = 0.15$. The details of these calculations can further referred to in Appendix A. Experimentally obtained mean strength values for hybrid composites H1, H2, H3 and I1 are denoted by H1, H2, H3 and I1 respectively in Fig. 4.20

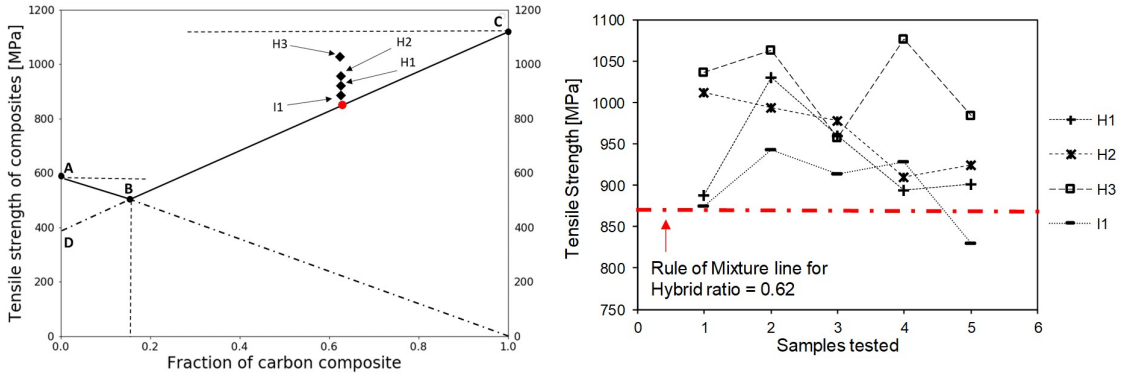

(a) Hybrid effect in tensile strength testing

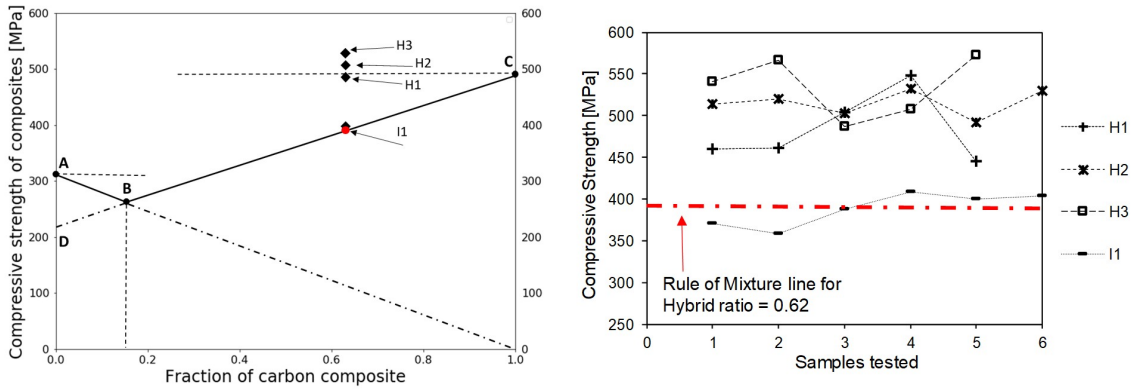

(b) Hybrid effect in compressive strength testing

Fig. 4.20 Synergistic hybrid effect on strength for interply and intraply hybrid composites under quasi-static loading.

The tensile strength obtained using RoM is 869 MPa, whereas that for intraply hybrid composites H1, H2 and H3 is 935 MPa, 964 MPa and 1024 MPa respectively. This higher experimental strength is because of synergistic effect obtained by hybridisation. For interply

hybrid I1 the experimental value of 898 MPa is slightly higher than the value obtained from the RoM.

Similarly, compressive strength for hybrid composite can be calculated from the RoM (as discussed in Appendix A), and this theoretical strength value for the hybrids is found to be 391 MPa. It can be seen from the Fig. 4.20b, intraply hybrids H1, H2 and H3 with mean strengths 484 MPa, 515 MPa and 535 MPa respectively, show a positive synergistic for compressive strength. Interply hybrid I1 shows no synergistic effect and its strength obtained experimentally coincides with the value obtained from RoM.

Further, the statistical uncertainties for the mean tensile strength values calculated using GUM [55] for H1, H2 and H3 at 90 % confidence level are: 58 MPa, 43 MPa and 49 MPa. This means, for example, for H3, out of 100 sampling tests, 90 % of the times, the mean strength of the samples will lie between the range of 975 to 1073 MPa (i.e. 1024 ± 49 MPa). The mean value for H3 in this range is still higher than the theoretical/RoM value for strength of hybrid and hence confirms a hybrid effect in tensile strength for H3 composite and this hybrid effect is about +17.8 %. Similar uncertainty analysis confirms the positive hybrid effect in tension for H1 and H2 and it comes to be +7.6 % and +10.9 % respectively. For I1 the uncertainty at 90 % confidence level is 44 MPa, which makes the range in which 90 % of the time the sample mean will lie to be 854 to 942 MPa; hence suggesting, though the mean strength for I1 is 3.3 % higher than RoM (869 MPa), but the mean sample strength is not significant to confirm positive hybrid effect in I1 interply composite.

Similar analysis of the mean compressive strengths and uncertainties confirm a positive hybrid effect for compressive strengths for intraply hybrid composites. This synergistic effect because of hybridisation is observed to be +23.8 %, +31.8 % and +36.9 % for H1, H2 and H3 intraply hybrids respectively. It can also be concluded that the synergistic hybrid effect by combining glass and carbon fibres for a composite is higher in compression than that in tension.

4.5 Conclusions

This chapter investigated the potential and mechanical performance of intraply and interply hybrid composites for newer light-weighting and structural applications. Using the analysis of the results and observations made during the fabrication and testing of the composite laminates, the following conclusions can be drawn.

- Among the three intraply hybrids H1, H2 & H3, the tensile modulus does not differ significantly, and similar trend is also observed for compressive and flexural modulus.

The interply hybrid I1 demonstrates lower stiffness of about 16.7 %, 9.4 % and 22.4 % lower than the average for intraply hybrids in respective loading conditions.

- Failure of composites in tension and compression was catastrophic, not only for reference carbon composites R1 but also for all the hybrids owing to a higher carbon composite volume fraction (V_c). In flexion, the failure was always on the compressive side and interply hybrid I1 showed largest delamination and damage region.

- Macroscopic and microscopic observations confirm the failure mode in tension is dominated by carbon fibre failure. For intraply hybrids, delamination of the glass tows from the surface after the carbon failure was distinctly observed, while for interply hybrid a brush like effect similar to carbon composite R1 was observed. The compression and flexural failure for interply hybrid I1 was observed to be most complex with several failure phenomenon occurring simultaneously leading to the final failure.

- In flexural loading, all hybrids show a positive improvement in failure strain when compared to reference R1 composite, and it was highest for I1 composite with a hybrid effect of $+59.7$ %. In tension only interply I1 shows positive hybrid effect of about $+7.4$ %; while in compression the hybrid effect for failure strain for I1 composite is -6.4 % .

- For hybrid composites a synergistic effect is observed for strength in tension and compression when compared to the strength obtained by the Rule of Mixtures. Results demonstrates a positive synergy / hybrid effect for all intraply hybrids.

- For intraply hybrids, effect of tow dispersion is demonstrated. It is observed that composite H3 (with 3 carbon and 3 glass tows blocked along width) has superior performance in tension and compression compared to H1 and H2. Hybrids H1, H2, H3 show a synergistic effect (deviation from RoM) of $+7.5$ %, $+10.9$ % and $+17.8$ % in tensile strength and $+23.8$ %, $+31.8$ % and $+36.9$ % in compressive strength.

- The ratio of tensile to compressive strength is similar for all intraply hybrids, and it is highest for ply per ply composite I1 and this can be attributed to diminished compression performance of I1 hybrid. For similar V_c, the tow level hybrids shows overall better performance in mechanical loading conditions when compared to the composites hybridised at ply level.

Partial replacement of carbon fibres by glass fibres in high volume applications such as wind blades or semi-structural automotive component offers prospects for use of composite

materials as a viable economic option. Along with cost savings in general, intraply hybrids such as those with 3C3G tow dispersion offers tremendous hybridisation potential for applications such as skies or other sports/leisure products. Tow level hybrids show synergistic effect in both tensile and compressive strengths while not adversely affecting the failure strain properties. Ply level hybrids can offer cost savings but may not prove to be a suitable choice for composites subjected to complex loading conditions. Interply hybrids though slightly improve failure strain in tension, but demonstrates negative synergy in all other properties, hence this configuration should not be chosen for structural applications.

Chapter 5

Mechanical performance of intermingled hybrids

Performances mécaniques des hybrides fibre à fibre

Ce chapitre traite de la fabrication et de la caractérisation d'une part des renforts hybrides, au niveau des fibres, fabriqués à partir de fibres de verre et de carbone et d'autre part de leurs composites. Pour cette étude, deux ensembles de composites hybrides fibre à fibre ont été réalisés ; sur la base d'UD cousus (utilisant des mèches comélées) et de la technologie d'étalement. Les renforts ont été caractérisés pour des propriétés mécaniques similaires à celles des hybrides inter-plis et intra-plis. Les objectifs de ce chapitre sont: (1) la fabrication des renforts, l'optimisation des procédé de fabrication et la caractérisation des hybrides fibre à fibre, (2) la caractérisation physique et mécanique des composites en traction, en compression et en flexion, et (3) la compréhension de l'effet de l'hybridation / l'effet synergique et l'équilibre des propriétés mécaniques des composites hybrides fibre à fibre réalisés par étalement simultané de verre et de carbone ou avec des mèches verre/carbone préalablement comélées.

La Section 5.2 présente l'état de l'art actuel des composites hybrides au niveau de la fibre, leur comportement mécanique et l'effet de l'hybridation. La Section 5.3 décrit les fibres et les configurations textiles utilisées, ainsi que les détails de la fabrication des composites et de la caractérisation mécanique. Enfin, la Section 5.4 examine les résultats obtenus à partir des tests des composites hybrides réalisés par étalement ou avec des mèches comélées et l'effet de l'hybridation est caractérisé.

Les conclusions des travaux expérimentaux sont présentées dans la Section 5.5. Le composite hybride réalisé par étalement a démontré des performances mécaniques supérieures en traction, flexion et compression par rapport aux hybrides comélés. Bien que le comélage soit un procédé de fabrication reconnu pour les fibres polymères, la présente étude montre que la méthode du mélange n'est pas appropriée pour produire des textiles et des composites hybrides à base de fibres techniques comme le verre et le carbone. La technologie d'étalement simultanée de fils de verre et de fils de carbone, en revanche, s'avère être une approche intéressante pour développer et étudier de nouveaux matériaux hybrides en fibres de carbone et de verre à haute résistance.

5.1 Introduction

This chapter discusses the fabrication and characterisation of fibre-level hybrid reinforcements made from glass and carbon fibres and their composites. Unidirectional textile reinforcements are developed using commingled rovings and spreading technique. The objectives of this chapter are: (1) fabrication, process optimisation and characterisation of intermingled hybrid composites, (2) physical, mechanical and damage characterisation of composites under tensile, compressive and flexural loading conditions, and (3) understanding hybrid/synergistic effect and balance of mechanical properties for carbon and glass composites hybridised at fibre level using commingled and spread tape hybrid reinforcements.

Section 5.2 reports in detail the current state of the art in hybrid composites specifically those based on intermingled level of hybridisation, their mechanical behaviour and their hybrid effect. Section 5.3 describes the fibre materials and the textile configurations used, along with the details of composite fabrication and mechanical characterisation. Finally, Section 5.4 discusses the results obtained from the testing of the hybrid composites made using commingled rovings and spread tapes. The significance and implications of the tests are discussed and the hybrid effect is characterised for the fabricated fibre hybrids. Conclusions of the study is reported in Section 5.5. The schematic overview of the experimental and scientific section of this chapter is presented in Fig. 5.1.

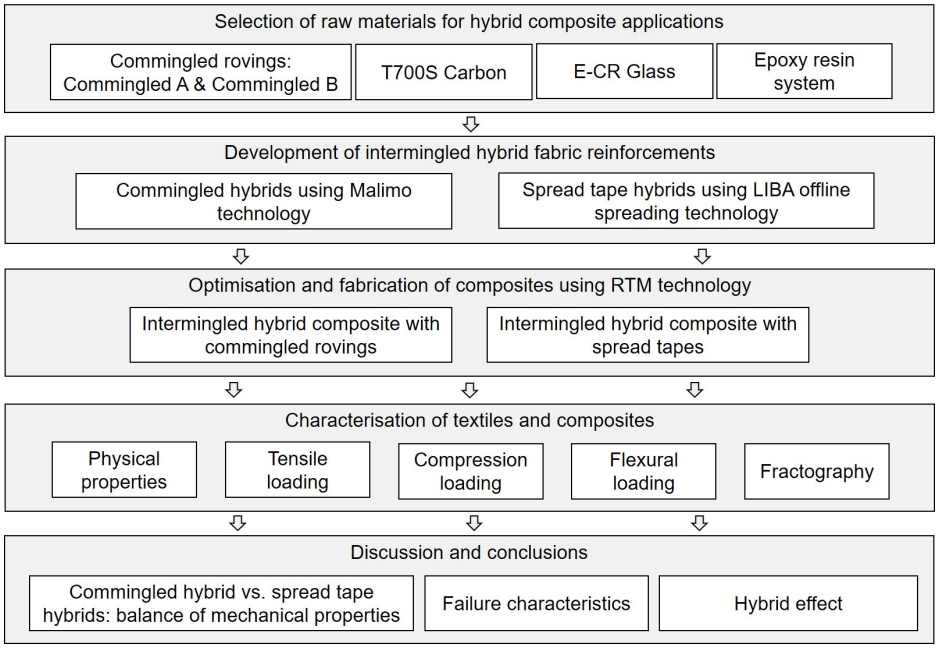

Fig. 5.1 Schematic overview of the experimental (Section 5.3) and scientific (Section 5.4) sections of this chapter.

5.2 State of the art

The main drawbacks of composite materials is their inherent brittleness, triggering a catastrophic failure mode with no damage warning further necessitating designers to over-designed structures. Large amounts of efforts are put-in to understand the mechanics of composites to develop more ductile composites with better balance of properties, which would not only allow a more efficient use of composites, but would also expand further their range of applications in industry. Hybridisation offers several advantages among which are the possibility to include a cheaper type of reinforcement, the ability to tailor the mechanical properties of the composite, enhanced fatigue life and improved impact resistance and the existence of various synergistic effects within a hybrid composite.

The potential advantages of hybridisation and hybrid effect has led to numerous studies on hybrid composites, mostly on the ply level hybrid and tow level hybrids and these studies are reported already in Section 4.2 in Chapter 4 of this thesis. Fibre level hybrids have been also studied widely, but the main objectives in these studies is to use one type of fibre which is a thermoplastic (PP or PEEK) polymer fibre which doubles as matrix in the hot compaction processes. Fibre hybrids, for two or more technical fibres hybridised at fibre levels have been very rarely reported. In fact, very few studies that have been reporting fibre hybrids with two technical fibres are by Yu et al. [170] demonstrating experimental work on discontinuous fibre carbon/glass hybrid and Makeev et al. [96] on carbon-carbon commingled hybrids. Studies on virtual characterisation framework on fibre level hybrids have also been reported Fukunaga et al. [49], Henry and Pimenta [60], Mishnaevsky Jr and Dai [102] and Swolfs et al. [144]. Hybrid composites are affected by non-linear hybrid effects (deviations from the Rule of-Mixtures), which are challenging to understand and predict, as recognised by several researchers [148, 143, 122, 121]. These effects are magnified with the use of intimately mixed fibre hybrid composites those made by intermingling or commingling.

The current work established the initial experimental and scientific framework for development of new generation of non-hybrid materials in the form of spreading processes for glass fibre. Furthermore, a first of its kind hybrid material in the form of carbon/glass commingled rovings was also studied. It was hence concluded based on experiences that processes such as tow spreading and commingling have reached a certain maturity for non-hybrid and needs further exploration for hybrid composites specifically involving two or more technical fibres such as carbon and glass, in agreement with what Swolfs et al. [143] report in their review. This chapter hence follows a natural progression to develop these fibre level hybrids in the form of dry reinforcements with higher dispersion and characterise their mechanical performance in different loading conditions and further understand the

hybrid effect in these fibre level hybrids vis-à-vis ply- and tow- level hybrids as reported in preceding chapters.

5.2.1 Fibre level hybrids

Fibre level hybrids are those where different types of fibre constituents are intimately mixed and the hybridisation is achieved within the yarn/tow/roving and therefore in the reinforcement ply and the composite itself. The term fibre level hybrids most of the times is synonymous with so called intermingled hybrid or commingled hybrids. Intermingled and commingled in these terms refers to the manufacturing process instead of the microstructure. Sometimes for unidirectional composites, the term fibre level hybrid is also used to refer to the interlaminated (interply) hybrids consisting of very thin plies, where the non-hybrid plies are brought together in alternating plies configuration, but due to thin layers, the cross sectional microstructure appears to be of a fibre level hybrid composite as seen in Fig. 5.2.

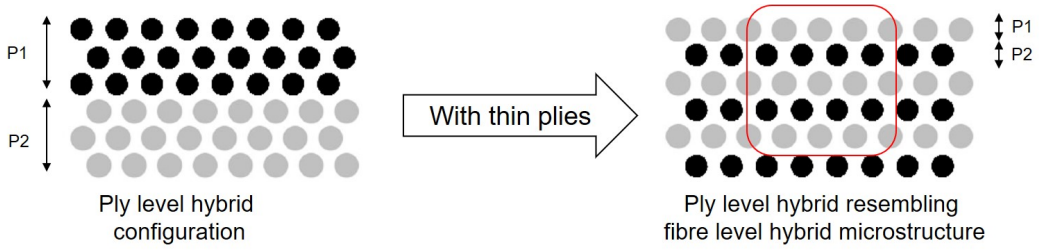

Fig. 5.2 Schematic of interlaminated thin ply hybrids.

The categorisation of terminologies proposed here is particularly common and useful, as it distinguishes one of the key features of fibre-hybrid composites, i.e. the degree of dispersion, which is a measure for how well the fibre types are mixed. The degree of dispersion is crucial for the magnitude of synergistic effects, for the way damage progresses and for challenges in manufacturing that involves with it. Despite its importance, the literature review does not show rigorous work on defining the dispersion. The most important reason for this, is that physically measuring the dispersion is not straight forward. Swolfs et al. [148] in their work proposed a definition saying, dispersion is the ratio of the fibre radius R for first type of fibre, over the average centre-to-centre distance d from the first type of fibre to the six nearest second type fibres. The centre-to-centre distance in this case measures how closely the first fibre type interacts with the second fibre type. This ratio then is averaged over all the fibres from the first type. Their proposed definition is schematically presented in Fig. 5.3. Though it has to be noted that in the definition, six fibres is arbitrary and that ideally not just the nearest fibres, but distance between each first type of fibre with every other second type of fibres is important to take into consideration.

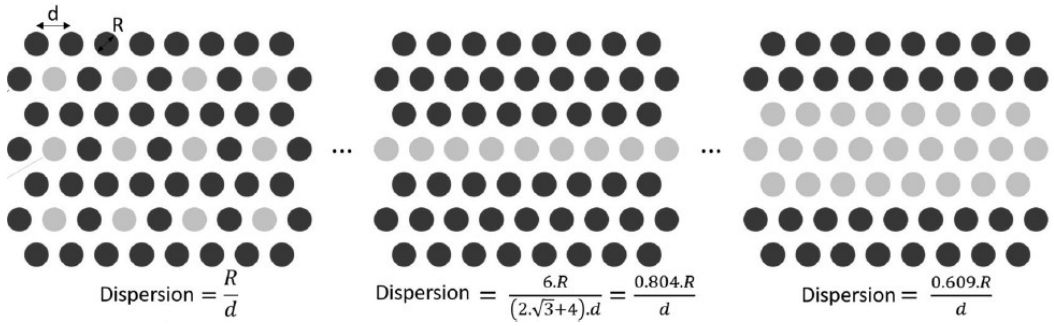

Fig. 5.3 Schematic illustration of different fibre dispersions and the newly proposed definition for this term. Adapted from Swolfs et al. [148].

Sections 3.2.1 - 3.2.3 already introduces the non-crimp fabric manufacturing technology and intermingled hybrid technology and reinforcements both using thin-ply and commingling process. Thin ply technology is a key preforming technology for high performance and structural composites and that it was nearly non-existent a decade ago. There is no strict definition, but, generally speaking, plies with a thickness below 100 µm are considered to be thin plies. The recent work by some also enables thin plies up-to 30 g m^{-2} using prepregging and about 50 g m^{-2} using dry reinforcements [131, 134] generating a single ply with about 4 to 10 fibre diameter thick. Standard thin plies have many advantages, they offer a greater versatility, have improved mechanical performance due to delayed onset of micro-damage and longer linear elastic regime, and offering better fatigue resistance along with suppression or delay of delamination. Though these advantages have been proven for non-hybrids, some of these advantages can also be exploited to achieve unique properties in fibre-hybrid composites through achieving a better dispersion in the hybrids. This dispersion allows strong interactions between fibres and can lead to synergistic effects for the initial failure strain in tension. Currently, there are many companies producing thin plies, such as Chomarat (France), Oxeon (Sweden), North Thin Ply Technology (Switzerland), TPCM (Germany), Mitsuya (Japan) and SK Chemicals (South-Korea), but there is no single work reported on fabrication of hybrid reinforcements (carbon/carbon or carbon/glass) using spreading process.

Commingling as a textile technology has been around for multiple decades, also as a reinforcement system for composites its use have been widely reported for a combination of a technical fibre and a polymeric fibre widely since a decade [130, 152]. In most of these studies, the polymer fibre is sacrificial and partially or completely melts in the composite forming process to become the matrix. Commingling even for polymeric fibres is not perfect and generally has a microstructure far away from an ideal fibre-to-fibre hybrid, and for technical fibres, this difference is more prominent. The main reason that the composite

designers have stayed away for commingled hybrids is the potential damage caused by the commingling process to the fibres and its uncontrolled orientation along with crimp. This further reduces the strength of the fibres, which negates any potential that may arise of positive hybridisation synergies.

Newer processes for intermingled hybrids using short fibres have also been introduced recently; a series of work on such hybrids is reported by Yu et al. [170] and their colleagues at University of Bristol. This work specifically also focuses on carbon/glass hybrids and through the process "HiPerDiF" achieving a fine dispersion is relatively straightforward. Similar work describing suspension of discontinuous fibres in water and producing aligned discontinuous composites using recycled carbon fibres has been reported by University of Nottingham [156]. As both these the technology produces composite reinforcements with discontinuous fibres only and not in the scope of the current thesis; hence these are not discussed in detail in the current work.

5.2.2 Hybrid / synergistic effect

The definition, the mechanisms controlling the mechanical properties of fibre-hybrid composites and hypothesis for hybrid/synergistic effect can be referred to in the Section 4.2 of Chapter 4. Synergies in fibre hybrid composites have been achieved for many different mechanical properties. For a basic mechanical property, such as tension in the fibre direction, the mechanisms are reasonably understood but for more complex properties, such as interlaminar fracture toughness or impact resistance, the level of understanding is very limited. It is also important to revisit Section 4.2.1.2 which explains the failure development process in a conventional unidirectional composite and how this changes for a hybrid composite; the key here is that these changes in failure development, and size effect are more prominent in case of fibre level hybrids, i.e. the intermingled or commingled hybrids.

5.2.3 Modelling tools

As experimentally verified in several studies presented in Section 4.2 and Section 5.2.4; the microstructure of a hybrid composite material governs the mechanical and functional properties of the fibre hybrid composite. The earlier models developed for conventional composites were found to not predict appropriately the mechanical properties of hybrid composites as they failed to predict the synergistic effects between fibres in hybrid composites. Since then lot of work has been reported for development of failure modelling tools specifically for fibre hybrid composites. It is interesting to note that while some of modelling and simulation tools

model the individual fibre breaks, cluster development and the final failure, others focus on damage development inside a ply and predict what happens when one or more plies fail.

Initial work on fibre break modelling for conventional composites were reported 6-8 decades ago in its simplest form not including stress recovery in broken fibres. Advanced models were later introduced by Rosen [127] and Zweben [175] that incorporated shear lag theories in the models. Models for fibre-hybrid composites were first reported 3-4 decades ago using 1D packings by Zweben [176] and Fukuda et al. [48] and were based non-hybrid model from Zweben [175]. Only in last two decades models for non-hybrids started using more realistic 2D packings combined with more accurate representation of the physical mechanism. Fibre break models for continuous fibre-hybrid composites only caught up recently with developments by Swolfs et al. [142], Swolfs [140]; and Mishnaevsky Jr and Dai [102]. Mishnaevsky Jr and Dai [102] model uses direct finite element simulations, which limits the number of fibres that can be modelled from 10 to 20. The main benefit of their model, however, is that it captures fibre misalignment as well as fatigue in tension and compression. Model developed by Swolfs [140] also uses finite element simulations, but only to capture stress concentrations around single fibre breaks in fibre-hybrid packing and further use this information in a numerical simulation with thousands of fibres.

Ply level models can be readily adapted from models for non-hybrid composites as these models ignore the micromechanical features, such as matrix cracking and fibre breaks, but investigate ply level features. The main focus for these hybrid models is predicting what happens after the first failure of the ply with the lowest failure strain. One such damage mode map by Jalalvand et al. [79] for carbon and glass hybrid is presented in Fig. 5.4. Damage model maps developed at University of Bristol [35, 79] and Dong and Davies [40] are prominent examples for ply level hybrid models.

No.	Order of required stress for damage modes	Expected damage process after the initial crack in the low strain material
1a	$\sigma_{@HF} < \sigma_{@LF} < \sigma_{@del}$	1. Failure in the high strain material
1b	$\sigma_{@HF} < \sigma_{@del} < \sigma_{@LF}$	1. Failure in the high strain material
2a	$\sigma_{@del} < \sigma_{@LF} < \sigma_{@HF}$	1. Catastrophic delamination 2. Failure in the high strain material
2b	$\sigma_{@del} < \sigma_{@HF} < \sigma_{@LF}$	1. Catastrophic delamination 2. Failure in the high strain material
3	$\sigma_{@LF} < \sigma_{@HF} < \sigma_{@del}$	1. Fragmentation of the low strain material 2. Failure in the high strain material
4	$\sigma_{@LF} < \sigma_{@del} < \sigma_{@HF}$	1. Fragmentation in the low strain material 2. Dispersed delamination 3. Failure of the high strain material

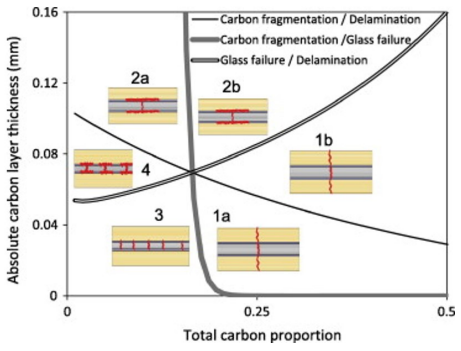

Fig. 5.4 Damage mode map of E-glass/TR30 carbon hybrid. Reprinted from Jalalvand et al. [79].

Further improvements in simulation tools along with accurately obtaining the input parameters such as fibre and resin properties is still needed so as to not just predict the

failure strain but the whole stress strain curve [146, 124, 71]. It is obvious from the review of literature that by combining the ply level and fibre level approaches and their features, i.e. by incorporating the micromechanical effects into ply level models it is possible to enable better predicting capability for the new models. Better and advanced modelling tools could push new developments in fibre hybrid composites and their application.

5.2.4 Mechanical properties of intermingled hybrids

Moving from ply level to fibre level hybrid is essentially increasing the degree of dispersion of two fibre constituents of the hybrid composites. This degree of dispersion, apart from the relative volume ratio is a very important parameter for comprehension of hybrid effect. Harlow [56] found an increase in the failure strain with increased dispersion, but in his study the relative fibre volumes of the constituents were not kept constant; this was also the case for several other studies. Studies by Fukunaga et al. [49] were the first ones to maintain a constant Fibre Volume Fraction and show that the hybrid effect increases when the bundle size decreases from four fibres to a single fibre. Fukunaga et al. [50] confirmed in their studies, both through modelling and experimental work that the hybrid effect is higher with better dispersion. Later, Swolfs et al. [144] showed for a 50 % hybrid volume fraction of carbon and glass fibres, the fibre dispersion to have an important influence on the hybrid effect. Random dispersion led to a hybrid effect of 9 % in tensile failure strain, while this effect was lower for tow level hybrid. The study also demonstrated highest hybrid effect of 16 % for an interlaminated hybrid with each layer having a thickness of a single fibre diameter, as seen in Fig. 5.2. Large amount of experimental data confirming the importance of dispersion now leaves no doubt that this is one of the most critical parameters.

Yu et al. [170] in their discontinuous fibre hybrids studies reported no pseudo-ductility or hybrid effect in tension for high strength carbon/E-glass intermingled composites, but pseudo-ductility was reported for the intermingled hybrid composites using high modulus carbon/E-glass fibres. The observed pseudo-ductile strain was a result of the fragmentation in the carbon fibre and was in good agreement with the simple analytical solution. They concluded that the extent of failure strain enhancement was related to the volume and moduli ratios and the failure strain of the low elongation constituent. Fibre direction compressive strength increases with the shear modulus to axial modulus ratio of composites across different fibre and resin combinations and considering this, Makeev et al. [96] studied a novel combination of hybrids containing intermediate-modulus (IM) and high-modulus (HM) carbon fibres by using commingling process. The new hybrid carbon/epoxy material is shown to approach fibre-direction compressive strength of IM carbon composites while having more than 30 % higher modulus compared to base IM carbon composites. Experimental results

presented by Wisnom et al. [165] showed hybrid effect for epoxy based thin ply carbon/glass interply hybrid composites. It was shown that there is an enhancement in strain at failure of up to 20 % for very thin plies, but no significant effect for thicker plies this was directly related to the dispersion of the carbon and glass fibres in the composites. Wisnom et al. [165] further conformed to the view presented by Manders and Bader [97] that, the hybrid effect is intimately linked to variability of strength and that "the hybrid effect arises from a failure to realise the full potential strength of the fibres in all-carbon fibre composites, rather than from an enhancement of their strength in the hybrid".

Commingling as a process for hybridisation and manufacturing has been vastly reported for a combination of technical fibre and a thermoplastic fibre, but it seems that no experimental studies have been reported on carbon and glass commingled hybrid composites. Apart from the unavailability of technology and know-how to process these fibres, the existing technologies tend to twist or disorient the fibres in the commingling process and hence is understood to defeat the idea of hybrid effect. One of the reason the thermoplastic fibre in commingling is popular is as it doubles as a matrix and hence solves the problems arising during the very critical step of infiltration during composite manufacturing [139, 2], however, commingled yarns may also be used in conjunction with thermoset matrix in order to improve damage tolerance [130, 61]. Almost any combination of glass or carbon fibres reinforcement and thermoplastic fibres can be mixed for structural applications using commingling method. A plethora of studies have been reported on such commingled rovings and their mechanical properties [88, 143, 95], but these are not in the scope of the current work and hence are not discussed in this section.

5.2.5 Reinforcements and composite manufacturing processes

Brief literature review and current state of the art on new material systems used in hybrid composites and fabrication of structural composite using RTM process relevant to this chapter is already presented in Sections 2.2.5, 3.2, 3.2, 3.2 and 4.2.3.

5.3 Experimental study

5.3.1 Materials

The raw materials chosen to study the fibre-level: intermingled hybrids were similar to the ones used in the interply and intraply hybrid study reported in Chapter 4. In terms of fibres, the T700S carbon and Advantex E-CR glass were the standard choice of fibres for reference baseline fabrics and also for the spread tape based intermingled hybrid fabric. For

the fibre-level hybrids made from commingled rovings, the choice of fibres was restricted. As the commingling process for 2 technical fibres have still not reached a desirable technological readiness levels, the choice of carbon and glass were influenced by the suitability of the process to specific types of fibres. As alternatives to the standard fibres selected, care was taken to choose the fibres with similar mechanical performances. The confirmation for using the selected alternative fibres came from the industrial experience of using these fibres receptively and from the technical data sheet provided by the respective manufacturers. 1400 tex commingled rovings from Supplier A contained HTS45 12 K carbon fibres and 2× 300 tex E-Glass from Toho Tenax Europe GmbH and PPG industries respectively. While the 2800 tex commingled rovings from Supplier B contained aerospace grade 2× 12 K AS4 carbon fibres and 1200 tex 111A E-CR Glass from Hexcel Corporation and Owens Corning respectively. For information, the mechanical properties of the fibres provided by their technical data-sheets is presented in Table 2.1.

5.3.2 Methods

5.3.2.1 Reinforcement manufacturing

Commingled rovings from Supplier A and Supplier B were used to manufacture unidirectional fabric reinforcements, Commingled-1 and Commingled-2, using Malimo UD stitching technology. The technology and the process parameters used for these fabrics were same as described in Section 4.3.2.1. For Commingled-1 fabric, made from Supplier A 1400 tex rovings, 2 rovings were passed through each dent to produce the required areal weight matching Commingled-2 fabrics made from 2800 tex Supplier B rovings. The stabilisation fabric and the stitching parameters for these fabrics were maintained constant and were the same as for the reference non-hybrid carbon and glass fabrics manufactured earlier. The stabilisation fabric used was a light woven fabric with an areal weight of $42\,\mathrm{g\,m^{-2}}$ made from fine glass yarns. The developed fabrics were further quality checked to confirm the compositions of the technical fibre, stitching thread and stabilisation fabrics. Photographs of the developed fabric reinforcements can be seen in the Fig. 5.5.

In this study, intermingled hybrid fabric in the form of a spread tape, S1, was developed by simultaneous glass and carbon spreading using a commercial technology based on “dynamic mechanical spreading” principle. The optimisation of the process to develop such fabrics is presented in Section 3.4.5. An epoxy based binder powder was applied on the surface of the fabric to impart cohesion to the parallel fibres and ensure the handle-ability of these reinforcements in subsequent processes. The difference in the dispersion of carbon and

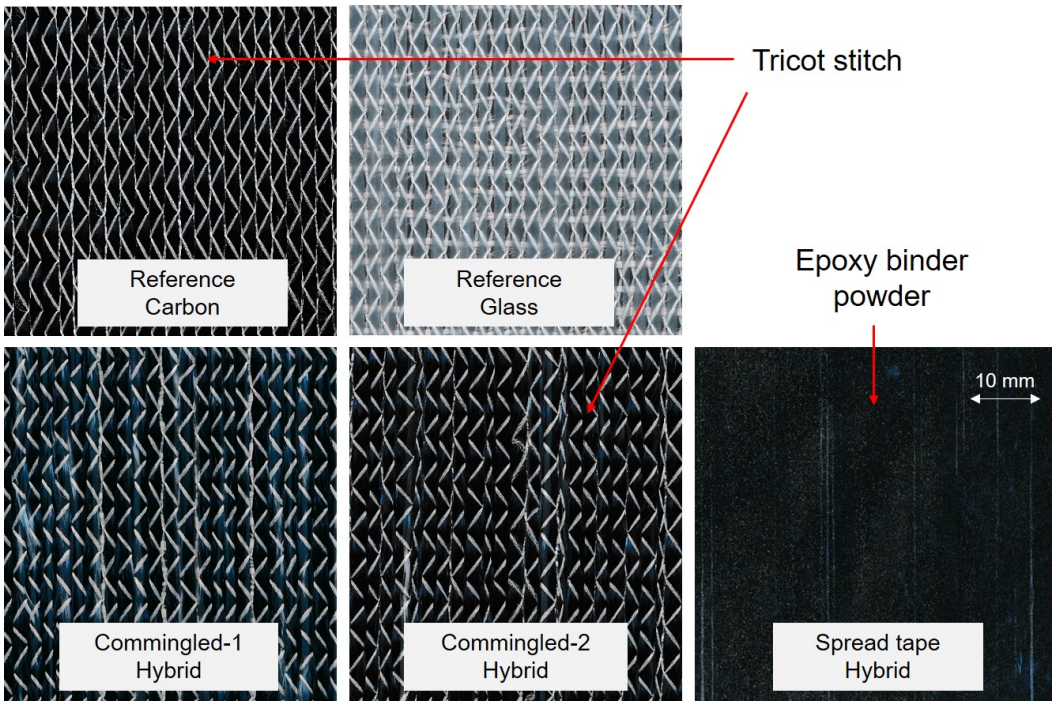

Fig. 5.5 Pictures of developed reference and hybrid reinforcements.

glass fibres can be visualised in the micro-graphs of the composites fabricated using these reinforcements as can be seen in Fig. 5.10.

5.3.2.2 Composite fabrication

All the composites fabricated for this study were made using RTM process. The composites made from commingled fabrics were fabricated using identical process and process parameters; the step-wise details of the composite manufacturing process utilised is described in Section 4.3.2.2 and photographically presented in Fig. 4.4, for this reason the composite fabrication is not repeated in this section. Each of these composites consisted of a cross-ply, symmetric layup $[0/90/0]_S$ consisting of 6 layers.

For composite made using the hybrid spread tape fabric an additional layer of glass stabilisation was added between each of the 6 reinforcement layers. This glass stabilisation was in the form of the same fine glass woven fabric that is present on the back side of each reference and commingled fabrics made using Malimo technology. The reason to use such glass stabilisation was two-fold: (1) it made possible a direct comparison between the spread tape composite S1 with commingled composites C1 and C2, and Reference composite R1 and R2, and (2) glass stabilisation improved the flow behaviour of resin in the otherwise not so permeable compact preform stack. Optimisation of preforming parameters such as

temperature and vacuum was essential for the spread tape fabrics. It was observed that a nominal vacuum of 0.3 bar was strong enough for these reinforcements producing a preform which was much finer than desired thickness. The consequences of finer thickness are lower permeability during infiltration and higher Fibre Volume Fraction, both of which are undesirable. An optimised setting of 0.15 bar vacuum and 80 °C preforming temperature was utilised for the intermingled fibre composites. Aligned fibres in spread tape fabric led to a significant reduction in permeability due to nesting and leading to higher FVF. The optimised parameters enabled fabrication of spread tape fabric based hybrid composites with comparable FVF similar to commingled hybrid composites. A layer of peel ply, was added to the preform on both the sides for assisting infiltration and this ply was removed after curing (Fig. 5.6). The curing conditions for this composite was similar to all other composites manufactured and is schematically presented in Fig. 4.4d.

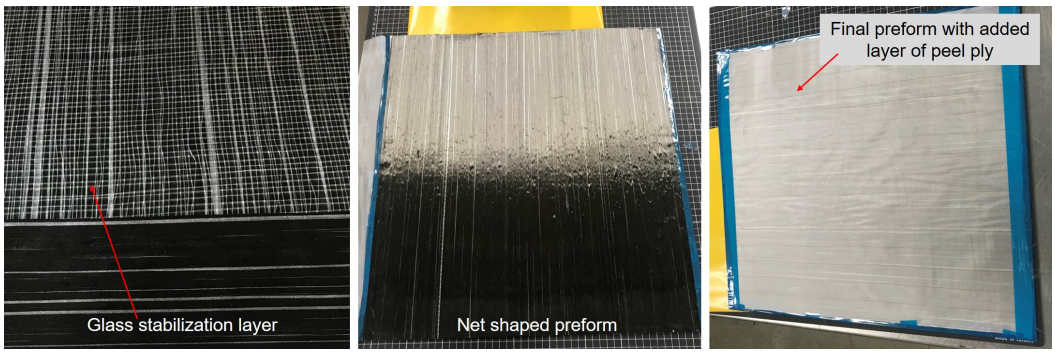

Fig. 5.6 Preform manufacturing for S1 intermingled hybrid.

The details of manufactured composites and their physical properties along with the Fibre Volume Fraction (FVF) is summarised in Table 5.1.

Table 5.1 Overview of manufactured composites.

	Composite name	Number of layers	Layup sequence	Thickness [mm]	Density [g/cc]	FVF [%]
Commingled	C1	6	$[0/90/0]_S$	2.81	1.65	52.2
	C2	6	$[0/90/0]_S$	2.88	1.66	52.8
Intermingled	S1	6	$[0/90/0]_S$	1.87	1.64	52.5

5.3.3 Characterisation of textile and composites

5.3.3.1 Physical properties of textiles and composites

Physical property characterisation for fabrics and composites is already discussed in detail in Section 4.3.3.1 and Section 4.3.3.2 respectively and hence not repeated in the current chapter. Table 5.2 presents the physical properties of textiles fabricated and used for composite manufacturing in this study.

Table 5.2 Physical properties of the manufactured fabric reinforcements.

Property	Units	Commingled-1	Commingled-2	Spread tape
Thickness @ 400 g load	[mm]	1.01	1.06	0.34
Thickness @28 kg load	[mm]	0.66	0.68	0.27
Areal density	[$g\,m^{-2}$]	527	555	321
Coverage	[%]	98.5	99.2	99.7
Stitch gauge	[stitches/inch]	10.1	9.8	–
Stitch pitch	[stitches/inch]	3.2	3.2	–

"Easyperm" 3D permeability measurement bench from IS Group, France, presented in Fig. 5.7 was utilised for permeability measurements of the developed fabrics in x- and y-directions. Easyperm allows evaluation of the capacity of reinforcement to be impregnated by a liquid resin. Permeability measurement is a crucial not only for performing and mould filling simulations for large and complex parts, but also for process optimisation for infiltration using liquid composite moulding process such as RTM.

Fig. 5.7 Permeability tests on reinforcement fabrics using Easyperm.

5.3.3.2 Mechanical properties

Tensile, compression and 3-point bending tests were carried out on the composite specimens, using a Zwick/Roell universal testing machine with a regularly calibrated 100 kN load cell and wedge type hydraulic grips as shown in Fig. 5.8. Tests in all the three loading conditions (Quasi-static tension, quasi-static compression and flexion) were performed using ISO norms, ISO 527-4 [73], ISO 14126 [75] and ISO 14125 [74] respectively. Sample dimension for each type of test and loading rates were selected as per the standard norms and presented in Fig. 4.8. Owing to limitations in composite plate size, for S1 composite the width for tensile test specimen was set to 15 mm instead of 25 mm, while standard gauge length of 150 mm was used for tensile tests. Though size effect for composite tests have been reported by several researchers [164], the effect in tension for similar gauge length and half the width is not expected to be significantly high and that this effect is considered in discussion of results. For tensile and compression samples, end tabbing of each specimen was carried out as described in Section 4.3.3.3 and Section 4.3.3.4. A test fixture that grips and loads the sample in compression as seen in Fig. 5.8 was used instead of an end loaded fixture (see Fig. 4.9). A minimum of 5 samples in tension and 6 samples in compression and flexion were tested for each type of tests and for each composite. The details of test procedures and methods for measuring the strengths, stiffness and strains in different loading conditions were similar to that described in Section 4.3.3.3. Strain measurements for all the three loading conditions were done using a 3D camera and digital image analysis setup from GOM Correlate.

5.3.3.3 Fractography

The fractured samples were analysed at macroscopic and microscopic level to understand typical fracture behaviour of the composites in different tests and loading conditions. The fractured samples were cut straight near the fracture location using a diamond saw. These samples were further embedded into a clear resin. After curing the samples embedded in resin were polished to provide clear images of the fracture surfaces. Optical microscopy was carried out using Zeiss AX10 Lab.A1 equipment with a magnification range from 50× to 1000×.

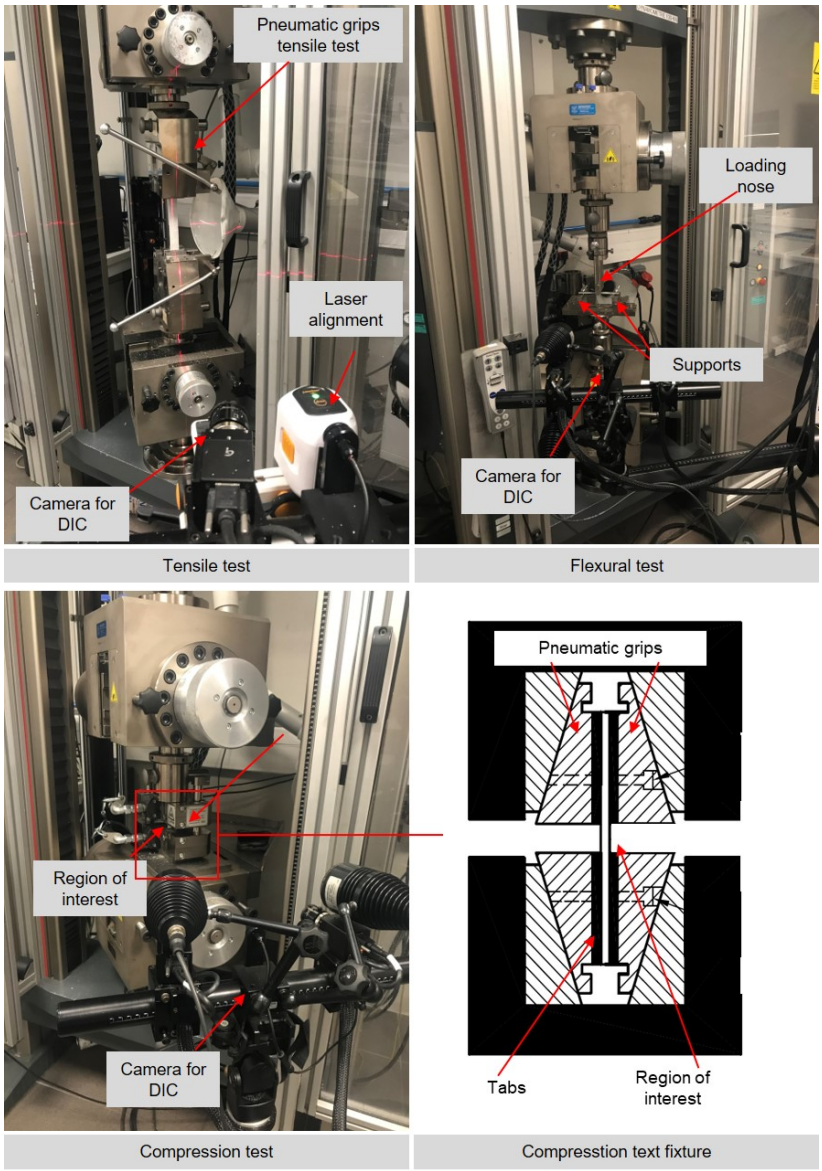

Fig. 5.8 Pictures of test-setups for tensile, compression and flexural testing of composites.

5.4 Results and discussions

5.4.1 Physical properties of textiles and composites

The fabric structural parameters such as thickness and areal weight for commingled roving fabrics were not significantly different from each other. For Commingled-2 hybrid fabric made from Supplier B roving, the areal weight was slightly higher than the Commingled-1 fabric. The difference was found to be originating from the input rovings, which had a linear

density 4.5 % higher than the expected 2800 tex. The stitching parameters for commingled hybrids were successfully maintained constant (See Table 5.2).

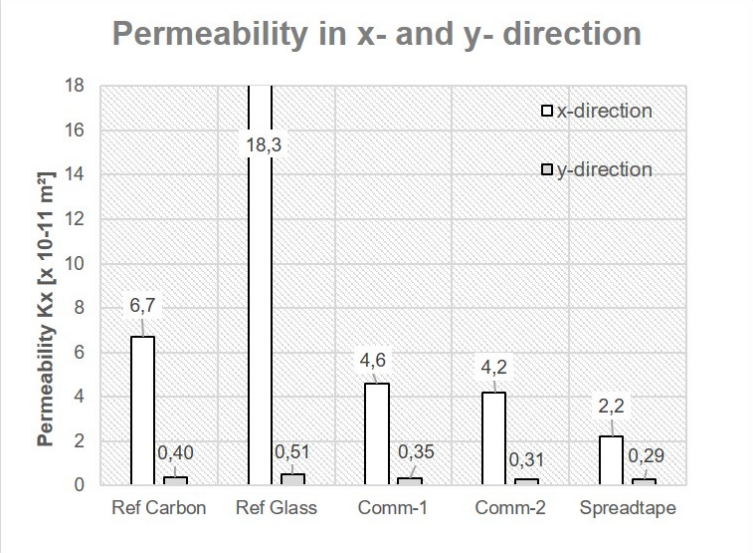

Fig. 5.9 Permeability: intermingled hybrids vs reference fabrics.

As seen in Fig. 5.9, for x-direction or (0°), the Commingled-1 and Commingled-2 hybrid fabrics have permeability of 4.6×10^{-11} m^2 and 4.2×10^{-11} m^2 respectively; the intermingled hybrid with highest dispersion of carbon and glass in the cross section has permeability equal to 2.2×10^{-11} m^2. The permeability in 0° for spread tape hybrids was observed to be half of the two commingled hybrid fabrics for similar Fibre Volume Fractions. Factors such as lower permeability, no channels because of absence of stitching and larger nesting behaviour in spread tape hybrids are responsible for lower permeability and cause difficulty in infiltration during composite manufacturing.

As expected, Fig. 5.9 shows that permeability of the fabrics in 0° is one order of magnitude higher than that in 90° direction. Reference carbon and glass fibre permeability measured during the earlier studies are added to the current graph as it was found that the permeability measured by the two different permeability measurement setups explained in Section 5.3.3.1 and Section 5.3.3.1 are comparable.

Fibre Volume Fraction and density of fabricated composite panels were evaluated to ensure the quality consistency of every composite specimen prior to subsequent mechanical tests. The density measurements and the fibre volume content from the burn-off tests are as presented in Table 5.1 and it can be seen the FVF for the three fibre level hybrid composites are comparable. Optical microscopy images detected presence of no voids with at a magnification of 200×. Cross-sections of the composite coupons from the composites C1, C2 and S1 are presented in Fig. 5.10a and the zoomed-in pictures showing the constituents

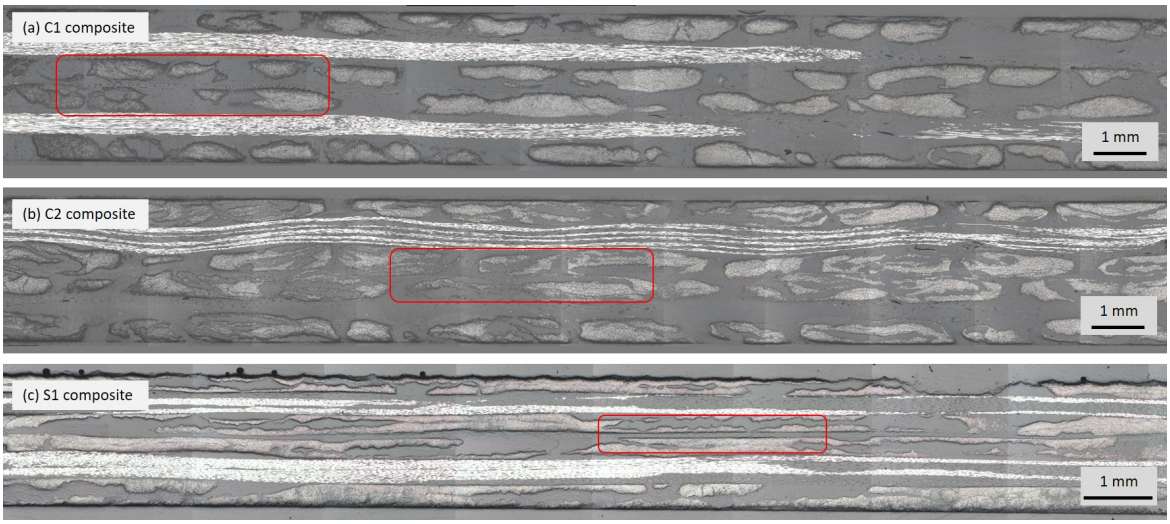

(a) Overview of cross-section

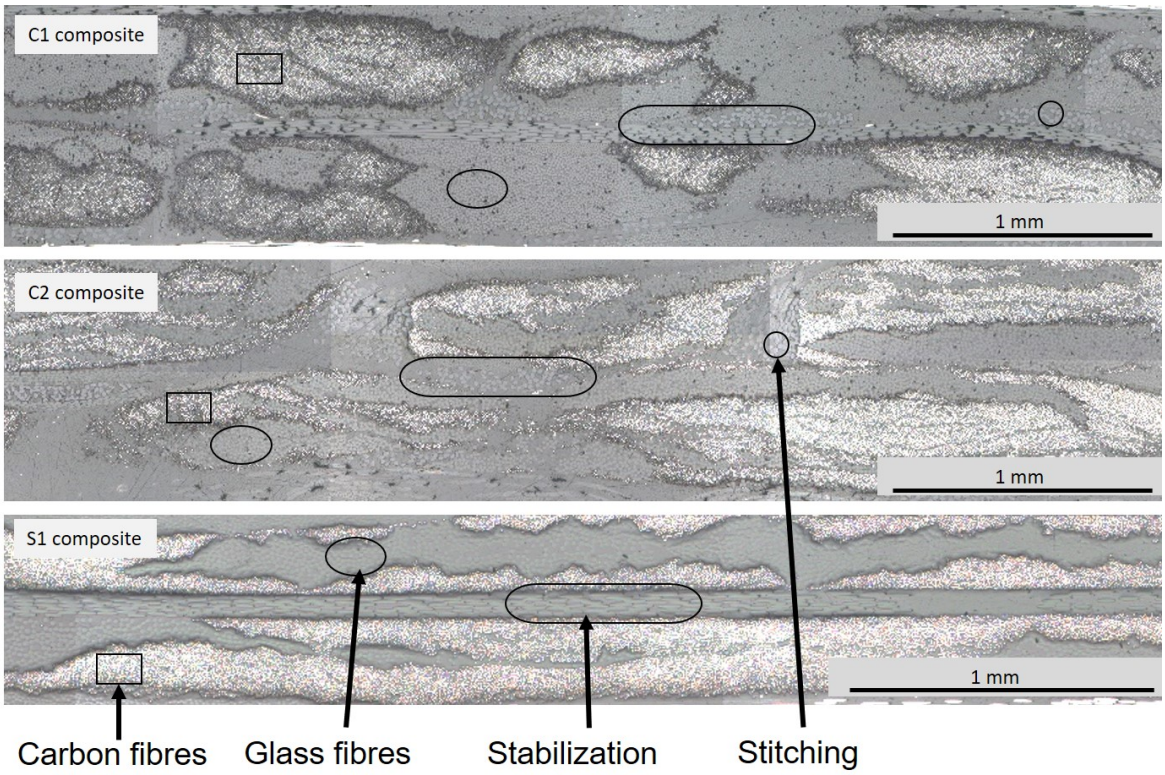

(b) Zoomed-in micro-graphs

Fig. 5.10 Optical microscopy images of commingled and intermingled hybrid composites a) overview of cross-section, and b) zoomed-in micro-graphs.

and dispersion of carbon and glass fibres is presented in Fig. 5.10b. Composite volume fraction (V_c) or hybrid ratio defined as the ratio of volume of one of the constituents of the

hybrid composite to the volume of hybrid composite was 0.62 for the three hybrid composites. For hybrid effect analysis, the reference carbon R1 (V_c = 1) and glass composite R2 (V_c = 0) from studies presented in Chapter 4 are used.

5.4.2 Mechanical properties of intermingled hybrids

5.4.2.1 Tensile properties

The last column in Table 5.3 provides the mean values (± standard deviation associated with 90 % confidence level) for Young's modulus for the developed intermingled composites. For these composites as expected, the tensile modulus is observed to be not significantly different, i.e. for similar hybrid composite volume fractions, the commingled and spread tape rovings have the same stiffness during the initial loading phase (Fig. 5.11a). This suggests that though in the composite microstructure, the dispersion of carbon and glass fibres is different it does not affect the stiffness of the composite. This stiffness for C1, C2 and S1 composites is on average 15 % lower than the stiffness for the reference carbon composite R1 (with stiffness 69.8 GPa) tested earlier also plotted in Fig. 5.11. The stiffness for three intermingled hybrids and three intraply hybrids is similar and it is about 15 % higher than interply hybrids or theoretical stiffness obtained using RoM.

Table 5.3 Tensile properties of intermingled composites along 0°; mean values for properties and standard deviation associated with 90 % confidence level are presented.

Composites	Ultimate tensile strength σ_t [MPa]	Tensile strain ε_t [%]	Tensile modulus E_t [GPa]
C1 - Commingled Composite	826 (± 32)	1.36 (± 0.06)	58.8 (± 0.6)
C2 - Commingled Composite	832 (± 29)	1.31 (± 0.05)	61.4 (± 1.5)
S1 - Spread tape Composite	1107 (± 50)	1.73 (± 0.06)	59.0 (± 2.4)

The hierarchy of tensile strength for intermingled hybrids is as follows: [S1 - Spread tape composite] > [C1 - Commingled composite] = [C2 - Commingled composite].

The hierarchy of tensile failure strain among intermingled hybrids follows the same trend as that of the tensile strength.

The failure strain of commingled hybrids C1 and C2 is 21 % and 24 % lower than the spread tape hybrid S1 respectively. The S1 hybrid has higher qualitative dispersion of carbon and glass fibres causing it to fail gradually, this was not quantitatively analysed but observed by carefully listening the fibre failure during testing. On the other hand, the commingled hybrids have fibres that are not straight and the carbon rovings are twisted to some extent, this twist in the fibres changes failure development in the composites. In other words,

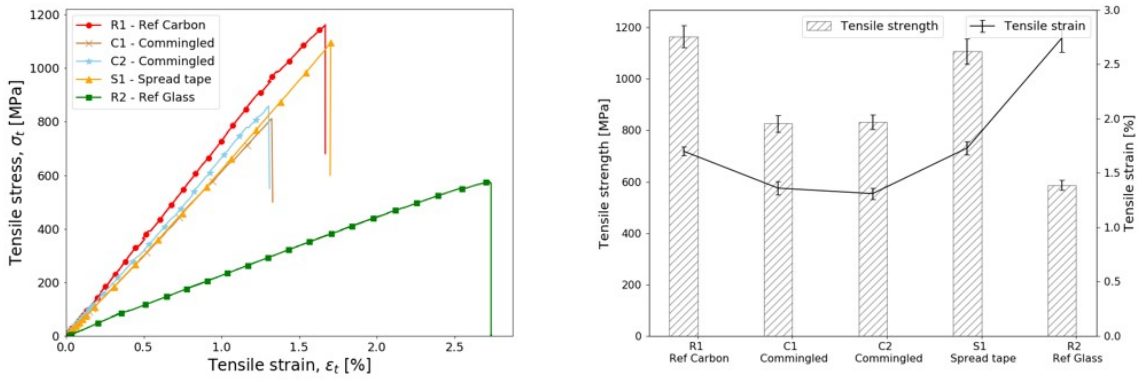

(a) Tensile stress - strain plot

(b) Tensile failure characteristics

Fig. 5.11 Tensile properties of intermingled hybrid composites alongside reference composites along 0°: (**a**) Stress-strain plot (**b**) Failure characteristics. (In (a) representative curves with failure characteristics closer to the average values reported in Table 5.3 for each composite type are presented.).

intermingled composites with commingled rovings fail earlier because of the twisted fibres and hence demonstrate lower tensile failure strain and tensile strength though their stiffness were identical because the measurements come from the initial part of the stress strain curve. This altered failure development also leads to an improvement of about 2 % (though it is not very significant) in failure strain for spread tape hybrid S1 over the reference carbon composite R1.

The tensile strength of C1 and C2 commingled composites is about 25 % lower than that for S1 spread tape hybrid. While S1 showed the strength of 1107 MPa, C1 and C2 showed tensile strength of 826 MPa and 832 MPa respectively. This can also be explained by gradual failure development in spread tape fibre level hybrids. The absence of stitching also enabled higher alignment of the fibres though out the width of the fabric and the length of the fibres. Higher strength observed for S1 composites can be attributed to not only to the effect of higher dispersion but also to some extent to the absence of stitching in S1 and the size effect (lower specimen width) for S1 composites samples. The two commingled roving composites did not show any significant difference in their stiffness or tensile failure behaviour. The failure in all three intermingled hybrid composites was catastrophic, and the stress-strain behaviour do not show pseudo-ductility owing to a higher carbon composite volume fraction in the hybrid composites in agreement with [35]. The overall behaviour is elastic-brittle because the glass fibres cannot carry the applied load after the carbon fibres fail and the stress–strain curve does not show any fragmentation plateau.

5.4.2.2 Compression properties

Table 5.4 provides the mean values (± standard deviation associated with 90 % confidence level) for compressive modulus for the developed intermingled composites. Composites C2 and S1 have similar stiffness in longitudinal compressive loading while C1 composite show a reduction of about 8 % when compared to C2 and S1. When compared to the theoretical stiffness (42.1 GPa) calculated using RoM (using the stiffness's of R1, R2 and hybrid ratio of 0.62), both configurations of intermingled hybrid composites show a significantly higher stiffness (6 to 15 %) in longitudinal compression. The stiffness in compression is more sensitive to the alignment of fibres, hence though C1, C2 and S1 showed similar tensile stiffness, in compression the stiffness of C1 composites with higher misaligned and twisted carbon fibre content was 8 % lower than C2 and S1.

Table 5.4 Compressive properties of intermingled composites along 0°; mean values for properties and standard deviation associated with 90 % confidence level are presented.

Composites	Ultimate compressive strength σ_c [MPa]	Compressive strain ε_c [%]	Compressive modulus E_c [GPa]
C1 - Commingled Composite	516 (± 27)	1.36 (± 0.08)	44.6 (± 3.2)
C2 - Commingled composite	528 (± 29)	1.20 (± 0.09)	48.6 (± 2.4)
S1 - Spread tape composite	580 (± 66)	1.65 (± 0.07)	48.5 (± 5.6)

The hierarchy of compressive strength for intermingled hybrids is as follows: [S1 - Spread tape composite] > [C2 - Commingled composite] > [C1 - Commingled composite].

The hierarchy of compressive failure strain among intermingled hybrids is as follows: [S1 - Spread tape composite] > [C1 - Commingled composite] > [C2 - Commingled composite].

Analogous to tensile tests, the S1 composite also shows highest failure strain in compressive loading as observed in Fig. 5.12a and Fig. 5.12b. In fact, the higher degree of dispersion in S1 composites and the thin-ply structure enables the compressive failure strain and the strength in these composites to reach 1.65 % and 580 MPa respectively. The twisted and misaligned structure affects the failure strain for commingled composites, C1 and C2 composite fails in compression at 1.36 % and 1.20 % of applied strain and is on an average 23 % lower than S1 composite with 1.65 % compressive failure strain. C1 and C2 composite compressive strengths were not significantly different from each other and though S1 shows an average compressive strength well above the strengths for C1 and C2 (516 MPa and 528 MPa respectively), but the difference between their strengths is not statistically significant. The compressive strengths for intermingled hybrids C1, C2 and S1 are very similar or higher than that for reference carbon composite R1. Such a trend for was observed for the intraply hybrid tested earlier and has also be reported by Pandya et al. [113] for their bidirectional composites.

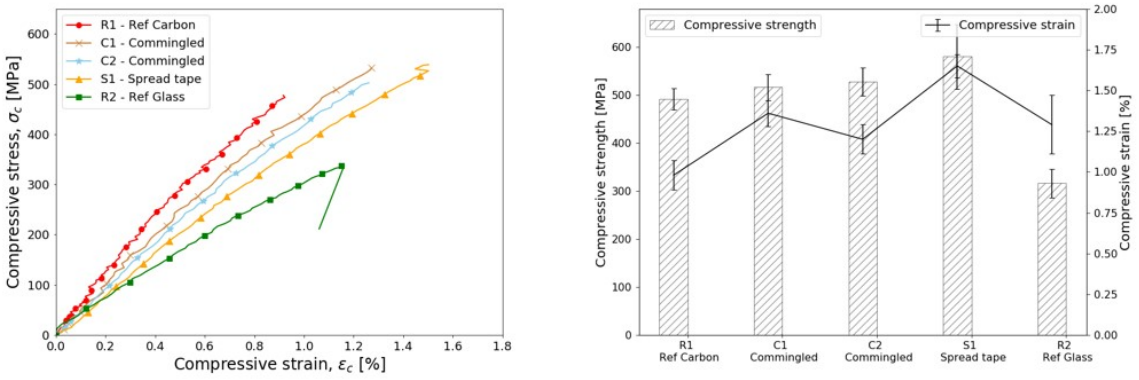

(a) Compressive stress - strain plot

(b) Compressive failure characteristics

Fig. 5.12 Compressive properties of intermingled hybrid composites alongside reference composites along 0°: (**a**) Stress-strain plot (**b**) Failure characteristics. (In (a) representative curves with failure characteristics closer to the average values reported in Table 5.4 for each composite type are presented.).

It has to be noted that, while in the current setup a pneumatic gripping and positive loading in compression was carried out, on the other hand, in the previous study the composites were loaded in an end-loaded test fixture described in Fig. 5.8 and Fig. 4.9 respectively. Confirmation tests were carried out on R1, R2 and H2 composites (from Chapter 4) using the current test set-up and it was found that the compressive modulus and strengths values are not significantly different, but the failure strains obtained using the end-loaded fixture were about 40 % lower than that obtained using current set up. Caution hence needs to be exercised when comparing the compressive failures strain results from the two studies.

5.4.2.3 Flexural properties

For the developed composites the hierarchy of flexural modulus is as follows: [C2 - Commingled composite] > [C1 Commingled composites] > [S1 - Spread tape composite]. The trend of modulus in flexion is similar to that of in tension. The mean stiffness values in flexural loading for the hybrids are similar to that in tensile loading (See Table 5.5 and Fig. 5.13a). These values suggest there is no effect of tow dispersion on the stiffness of hybrid composites.

The flexural strengths for the three intermingled hybrids C1, C2 and S1 are 796 MPa, 768 MPa and 812 MPa and that their strengths are observed to be statistically not significantly different from each other. It is observed that the initiation of failure in these hybrids is because of compressive stresses at the loading nose, which cause the carbon fibres to fail, but the final

Table 5.5 Flexural properties of intermingled composites along 0°; mean values for properties and standard deviation associated with 90 % confidence level are presented.

Composites	Ultimate flexural strength σ_{fl} [MPa]	Flexural strain ε_{fl} [%]	Flexural Modulus E_{fl} [GPa]
C1 - Commingled Composite	796 (± 19)	1.40 (± 0.08)	60.3 (± 0.6)
C2 - Commingled composite	768 (± 31)	1.29 (± 0.08)	62.6 (± 0.7)
S1 - Spread tape composite	812 (± 60)	1.70 (± 0.16)	57.8 (± 0.9)

failure shows for most of the intermingled composite a complex failure with fibre failure and delaminations both on the tension and the compression side of the specimen.

The hierarchy of flexural strain among these composites is: [S1 - Spread tape composite] > [C1 - Commingled composite] > [C2 - Commingled composite].

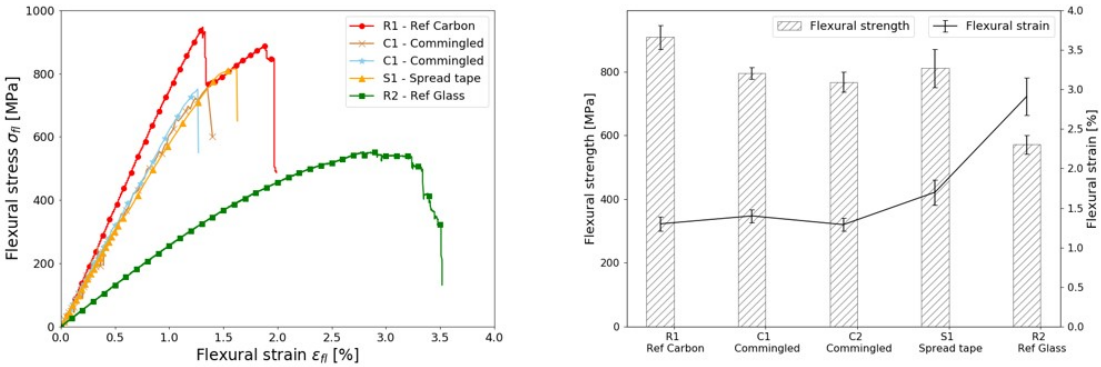

(a) Flexural stress - strain plot

(b) Flexural failure characteristics

Fig. 5.13 Flexural properties of intermingled hybrid composites alongside reference composites along 0°: (**a**) Stress-strain plot (**b**) Failure characteristics. (In (a) representative curves with failure characteristics closer to the average values reported in Table 5.5 for each composite type are presented.).

It is observed from plots in Fig. 5.13 that the reference glass fibre composite R2 has the highest failure strain (2.91 %) while the reference carbon composite has the lowest (1.30 %). The failure strain of C1 (1.40 %) and C2 (1.29 %) are similar to or slightly higher than the R1 composite, while the flexural strain for C1 composite (1.70 %) is significantly higher than that of R1. This shows that higher dispersion of fibres in S1 improves the flexural strain and the flexural strength of the hybrid composite.

It may be also noted that in flexural loading, compared to reference composite R1, for S1 composite the percentage gain in failure strain is about 31 % and is significantly higher than percentage loss in flexural strength which is just 11 %.

5.4.2.4 Fractography

Like the carbon composite R1 samples, all intermingled samples broke yielding two separate pieces or sometimes three pieces because of secondary failure induced by the shock of rapid elastic recovery (See Fig. 5.14). The failure in most of the samples was slightly away from the center. The composites failed catastrophically and this catastrophic failure in them can be attributed to a higher proportion of carbon fibres in the hybrid composite structure. Observations show that the three hybrid samples have very similar kind of failure surface. Single fibre failures in carbon fibres leads to stress concentrations and more fibre failures until a critical cluster is formed which cases the composite sample to fail catastrophically. While a brush like effect in the failure surface is not seen, excessive delamination and matrix failure is seen in the fracture surface of failed samples.

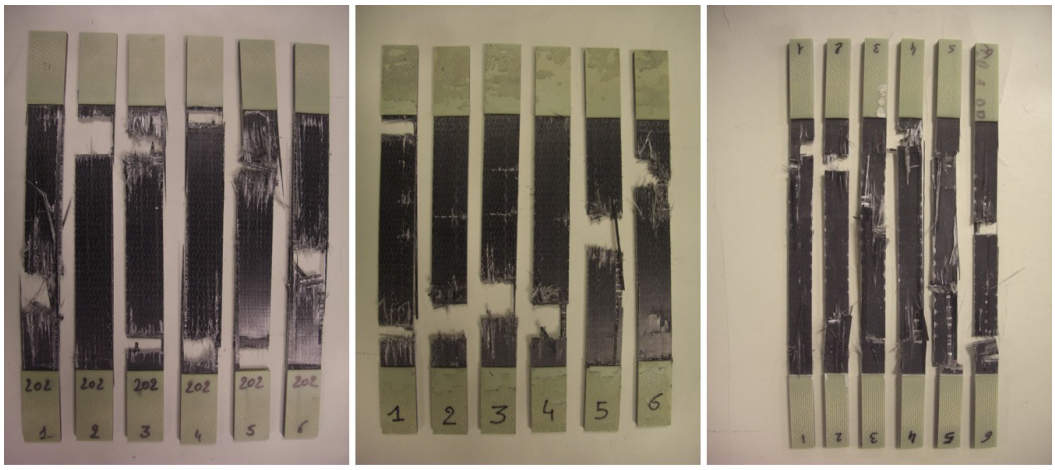

Fig. 5.14 Pictures of failed intermingled hybrid composite specimens in tensile tests.

All the samples loaded in longitudinal compression show catastrophic failure and the composite specimens after failure are observed to be completely separated into two halves. While the failure was similar for the three intermingled composites, the micro buckling, kinking and larger delaminations are observed specifically in large extent for S1 spread tape hybrid. Matrix cracking and though thickness crack through shearing is observed for all the three hybrids as seen in Fig. 5.15.

For the commingled hybrids, the final failure in 3-point bending corresponds to the fibre failure happening due to compressive load exerted by the loading nose. The failure is catastrophic and is accompanied sometimes by the delamination of the first layer (0°) from the second layer (90°). No further effect can be observed on the layers following or on the tension side of the coupon specimen as seen in Fig. 5.16 on the right. On the contrary

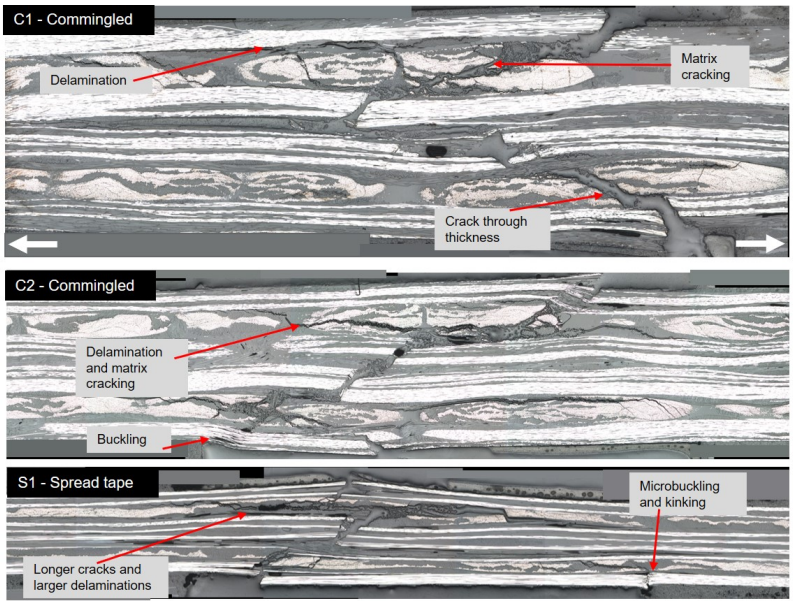

Fig. 5.15 Micrographs of failed intermingled hybrid composite specimens in compression tests.

for spread tape hybrid, the compressive failure was combined with the tensile failure and excessive delaminations and matrix cracking in the central layers. While carbon fibre failure on compression side is observed for all the hybrids, on the tensile side too, it is the carbon fibre which fails first owing to lower failure strain in carbon fibres.

It is observed that the most common failure mode is kinking or micro-buckling at the compression side, which can be found in all three intermingled hybrid composite specimens (Fig. 5.16). The details of failure modes for the tested composite types are summarised in Table 5.6.

Table 5.6 Composites and their failure modes in flexural tests.

Composite	Failure
C1 – Commingled hybrid	fibre buckling in compression (carbon), delamination in first ply
C2 – Commingled hybrid	fibre buckling in compression (carbon), delamination in first ply
S1 – Spread tape hybrid	fibre buckling in compression, larger delamination and shear, failure in tension (C). Complex.

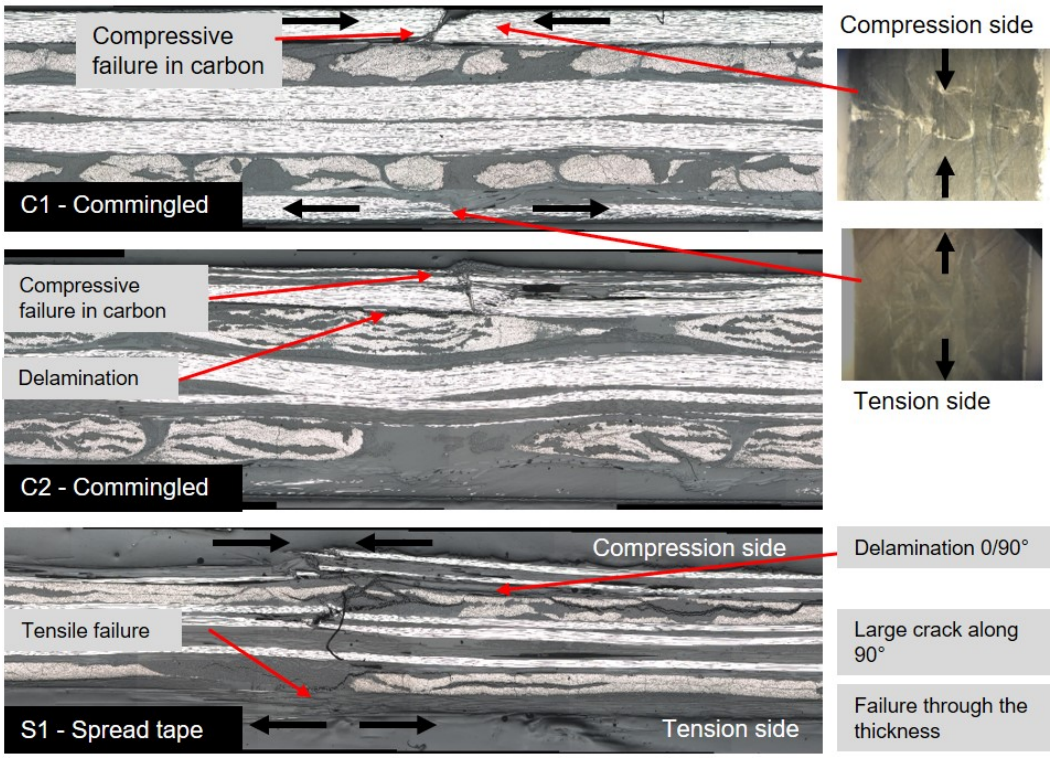

Fig. 5.16 Micrographs of failed intermingled hybrid composite specimens in flexural tests.

5.4.3 Hybrid effect

5.4.3.1 Improvement in failure strain

The failure strain in tension, compression and flexion normalised to the failure strain of low elongation reference carbon composites in respective loading conditions is presented in Fig. 5.17.

In tensile loading the commingled hybrids C1 and C2 demonstrate a sharp negative hybrid effect in failure strain. While the failure strain for spread tape intermingled hybrid is not significantly different than of R1 reference carbon fibre composite; C1 and C2 show a staggering reduction in tensile failure strain compare to R1. Among the three configurations for hybrids characterised, only interply hybrids showed a positive hybrid effect of $+7.4\,\%$ in tensile failure strain and commingled hybrids showed a negative hybrid effect of about $-19.8\,\%$ and $-22.9\,\%$ (See Fig. 4.19a and Fig. 5.17a). Intraply hybrid and intermingled hybrids showed no hybrid effect.

In compression though, all the three intermingled hybrids show positive hybrid effect in failure strain. It is to be noted that for characterisation of compression behaviour, slightly different test setups were used for intermingled hybrids and the reference composites char-

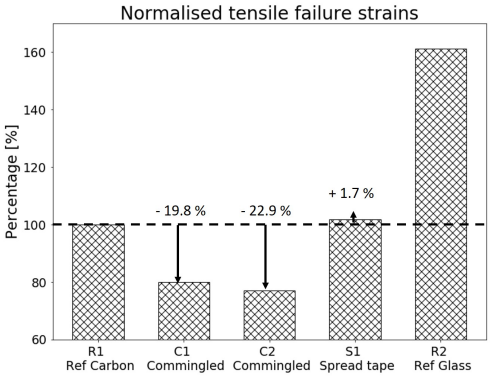

(a) Tensile failure strain

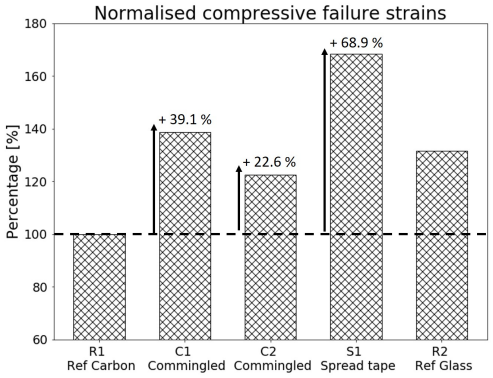

(b) Compressive failure strain

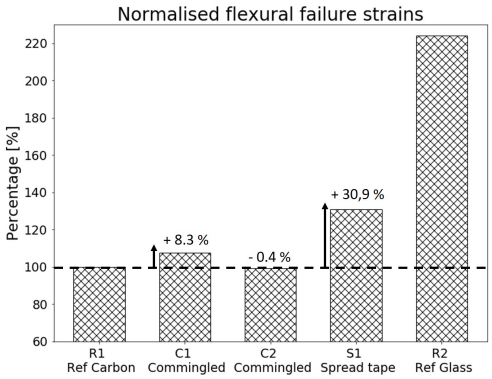

(c) Flexural failure strain

Fig. 5.17 Hybrid effect in failure strain for intermingled composites: Failure strains normalized to failure strain of carbon composite in different loading conditions.

acterised earlier. The two setups for a set of test composites measured similar stiffness and strengths but the failure strain measurements were significantly 30 to 40 % different. Caution has to be used in interpreting the compression failure strain results in Fig. 5.17b.

Interply hybrid on contrary to tensile failure strain showed a negative hybrid effect (-6.4 %) for compressive failure strain. H3 intraply hybrid and S1 spread tape intermingled hybrids confirms positive hybrid effect in compressive failure strain (See Fig. 4.19b and Fig. 5.17b).

In flexural loading, failure strain for S1 spread tape hybrid was $+30.9$ % higher than that of reference composite R1. Commingled hybrid C1 showed a positive hybrid effect of $+8.3$ %, while C2 showed no hybrid effect. In general all the three hybrid configurations demonstrated (see Fig. 4.19c and Fig. 5.17c) positive hybrid effect in failures strain when tested in flexural loading conditions.

Intermingled hybrids, specifically those from simultaneous spreading of carbon and glass fibres prove to provide best possible alternative for failure strain enhancements when compared to the low elongation composites in the three loading conditions. Commingling process on other hand is counterproductive for failure strain enhancement and it also affects adversely the strength due to inherently twisted fibre structure in multiple loading conditions.

5.4.3.2 Deviation from Rule of Mixtures

Tensile and compressive strength of hybrid composite as a function of carbon composite volume fraction (V_c) is presented in Fig. 5.18a and Fig. 5.18b respectively. These figures are plotted based on mechanics of materials approach to strength under quasi-static loading along the 0° direction and described in detail detail in Section 4.4.6.2. In Fig. 5.18a, the volume fraction of carbon composite at B is $V_c = 0.15$. Experimentally obtained mean strength values for hybrid composites C1, C2 and S1 are denoted by C1, C2 and S1 respectively in Fig. 5.18

The tensile strength obtained using Rule of Mixtures is 869 MPa, whereas the experimental values for tensile strengths for intermingled hybrids C1, C2 and S1 are 826 MPa, 832 MPa and 1107 MPa respectively. As can be seen from Fig. 5.18a, S1 shows a positive hybrid effect of +27.4 % in tensile strength while C1 and C2 hows slightly negative hybrid effect. Calculating the statistical uncertainties for the mean tensile strength values calculated using GUM [55]; it can be said that the positive hybrid effect for S1 is statistically significant, while C1 and C2 do not show significant hybrid effect and is in-line with the RoM predictions. Overall, hybridisation of carbon and glass at different levels of dispersion do not produce any negative deviation from RoM and for higher dispersion's, as in for H3 and S1, produces a positive synergy.

Similarly, compressive strength for hybrid composite can be calculated from the RoM, and this theoretical strength value for the hybrids is found to be 391 MPa. It can be seen in Fig. 5.18b, intermingled hybrids C1, C2 and S1 with mean strengths 516 MPa, 528 MPa and 580 MPa respectively, show a positive synergistic for compressive strength. Analysis of the mean compressive strengths and uncertainties confirm a positive hybrid effect for compressive strengths for intraply hybrid composites. This synergistic effect because of hybridisation is observed to be +32.1 % and +35.1 % for commingled composites C1 and C2, while it is highest +48.3 % for S1 spread tape intermingled hybrid. Only ply level hybrid I1 among all did not offer any positive synergy in compressive strength. Altogether the positive synergistic effect in hybrid composites is higher in compressive loading than in the tensile loading.

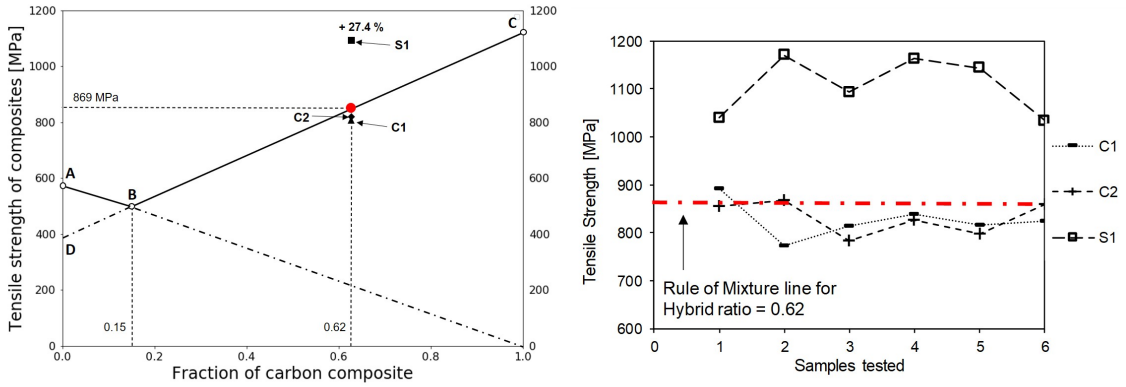

(a) Hybrid effect in tensile strength testing

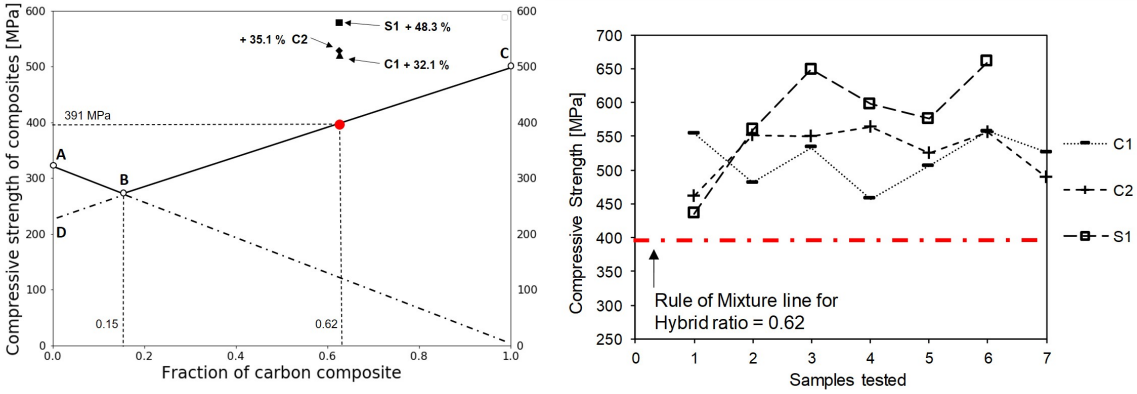

(b) Hybrid effect in compressive strength testing

Fig. 5.18 Synergistic hybrid effect on strength for intermingled hybrid composites under quasi-static loading.

5.5 Conclusion

This chapter investigated the fabrication of new generation of hybrid textiles and their composites fibre-level hybridised intermingled composites using carbon and glass fibres. Mechanical properties of the developed commingled composites and spread tape based intermingled hybrid composites were characterised and compared with the reference composites. Analysing the results and discussion, following conclusions from the study are drawn:

- Intermingled hybrid fabrics with higher dispersion than ply-level or tow-level composites containing technical fibres such were carbon and glass were successfully fabricated using commingling and spreading methods.

- Stiffness of intermingled hybrids in different loading conditions were similar to the stiffness for intraply hybrids with the same hybrid ratio in respective loading's.
- Failure of carbon /glass hybrid composites in tension and compression was catastrophic for the intermingled hybrids owing to a higher carbon composite volume fraction (V_c). In flexion, the failure for commingled hybrids (C1 and C2) was always on the compressive side and for spread tape hybrid (S1) the failure also included failure on tensile side and larger delaminations in plies in between.
- In tensile loading due to the twist in carbon fibres in the roving, the commingled fabric composites showed a negative hybrid effect in failure strain, it was observed to be $-19.8\,\%$ for C1 and $-22.9\,\%$ for C2 in the failure strain. In compressive and flexural loading, all three hybrids show either a positive improvement or no hybrid effect in failure strains when compared to reference R1 composite. The positive hybrid effect in failure strain in flexion was highest for S1 spread tape hybrid with a hybrid effect of $+30.9\,\%$.
- For spread tape intermingled hybrid S1, highest synergistic effect is observed for strength in tension ($+27.4\,\%$) and compression ($+48.3\,\%$) when compared to the strength obtained by the RoM. Commingled hybrids show no synergy in tensile loading but show a significant positive hybrid effect in compressive strength.
- Spread tape hybrid S1 demonstrates superior mechanical performance in tension, flexion and compression when compared to commingled hybrids.
- Commingling though being a popular reinforcement manufacturing process for polymeric fibres, this study of intermingled hybrid composites shows that the commingling method is not a suitable method to produce fibre hybrid textiles and composites based on two technical fibres such as glass and carbon.
- Spreading technology for fibre hybrid composites show tremendous potential due to its better dispersion capability without damaging or disorienting the fibres. Spreading is a powerful approach to develop and investigate new hybrid materials specifically those involving cost intensive fibre materials such as carbon and high strength glass fibres.
- Optimisation of simultaneous carbon/glass spreading parameters and possibility of manufacturing thin ply materials can open new horizons for hybrid composites in high performance structural applications.

For a similar carbon to glass volume fractions, carbon/glass fibres hybridised at fibre-level using spreading technology, can be used in several structural applications where high performance is key. Typically composite structural applications where complex loading conditions are applied over its service life, these thin-ply, spread tape, intermingled hybrids can offer tremendous potential for application and product development.

Chapter 6

Fracture toughness of thin-ply hybrids

Ténacité des composites hybrides à plis fins

Le défi de l'hybridation à l'échelle des fibres réside dans la compréhension, la prévision et finalement l'optimisation des comportements complexes observés aux échelles des constituants. Ces matériaux offrent l'accessibilité à de nouvelles propriétés au prix d'une plus grande complexité de conception, notamment du fait que les mécanismes coopératifs qu'ils présentent ne sont pas encore entièrement caractérisés et compris. Ce chapitre se concentre sur la caractérisation de la ténacité des composites hybrides à plis fins, fabriqués à partir de renforts hybrides intra-plis à base de carbone et de verre. L'effet d'hybridation est évalué par comparaison avec des matériaux de référence, constitués de renforts en verre et carbone purs.

La Section 6.2 de ce chapitre étudie et rend compte d'un état de l'art relatif à la caractérisation de la ténacité pour les matériaux composites et plus particulièrement de la ténacité translaminaire des matériaux composites et hybrides. La Section 6.3 décrit les matériaux et les configurations textiles étudiés dans le chapitre. Dans cette section, l'accent est mis sur la complexité que représente la fabrication de renforts plis fins puis de leur utilisation dans un procédé RTM pour l'obtention des composites. En Section 6.4, la caractérisation de la ténacité est obtenue à l'aide d'une éprouvette de type Compact Tension (CT). La Section 6.5 examine les résultats et montre un effet positif de l'hybridation sur la fissuration translaminaire. Bien que l'hybridation introduise des mécanismes dissipatifs supplémentaires par rapport aux matériaux de référence, l'effet n'est pas aussi important qu'espéré et une optimisation de ce type d'hybridation est nécessaire pour une ténacité accrue.

6.1 Introduction

The challenge of fibre hybridisation lies in understanding, predicting and eventually optimising the hybrid effect and associated complex behaviours. With the desirable properties offered by these material systems comes the associated penalty of increased design complexity and the fact that the failure mechanisms they exhibit are still not yet fully characterised and understood. This chapter focuses on the characterisation of the fracture toughness of thin-ply composites made from carbon and glass based intraply hybrid reinforcements. By testing and comparing properties of reference pure glass and carbon composites, the chapter gives insights on the possible hybrid effect for translaminar fracture toughness of hybrid intraply composites made from thin-ply reinforcements.

Section 6.2 investigates and reports in detail the current state of the art in fracture toughness characterisation for composite materials, composite failure modes and specifically translaminar fracture toughness of these composite materials and hybrids. Further, Section 6.3 describes in detail, the fibre materials and the textile configurations used in the chapter. Emphasis in this section is laid on the challenges in fabrication of thin-ply reinforcements and their composite manufacturing using RTM process. Physical and translaminar fracture toughness characterisation using Compact Tension (CT) test is described in detail in Section 6.4. Section 6.5 discusses the results obtained from the testing of the hybrid and non-hybrid composites in the compact tension test. Discussion on use of several data reduction schemes is reported in the section along with the hybrid effect in translaminar fracture toughness. The schematic overview of the experimental and scientific section of this chapter is presented in Fig. 6.1. Conclusions of the study is reported in Section 6.6.

6.2 Fracture toughness of composite materials

Fibre reinforced composites are attracting a significant interest for their weight-sensitive applications as their excellent stiffness and strength are combined with a low density. Unfortunately, higher stiffness and strength of these composites come at the expense of their limited toughness. Like most materials, fibre reinforced composites used for structural applications also face the strength versus toughness dilemma. Fracture toughness in material is a property that describes the capability of a material which contains a crack to resist break, and is one amongst the necessary properties of any material for several design applications. Fracture toughness can also be referred to as an approach to express a material's resistance to brittle fracture when a crack exists in its structure. Fracture in a material can occur even below its limiting load value, such brittle fractures have been reported earlier in composites in use (in

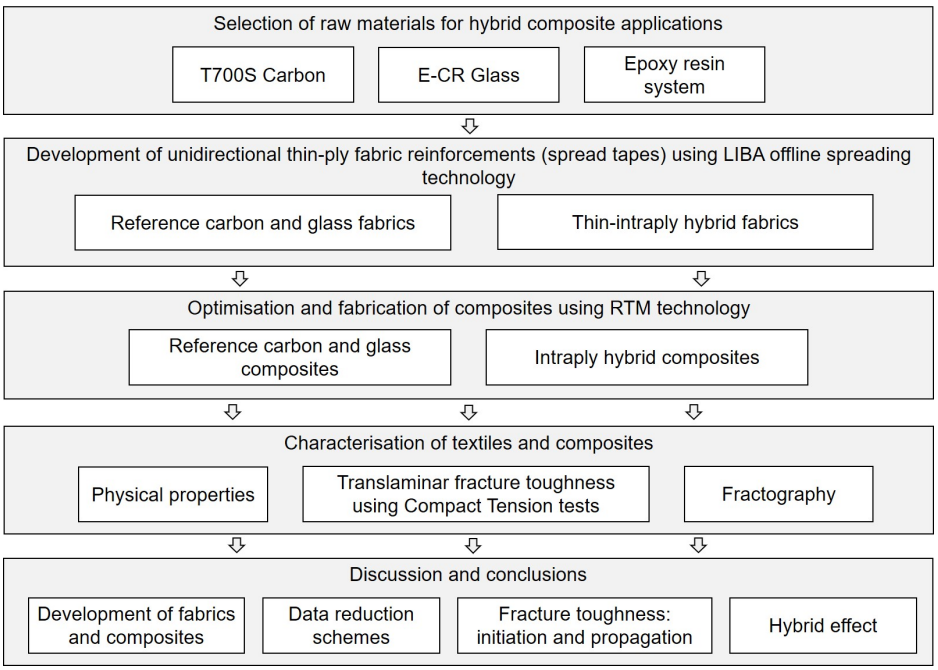

Fig. 6.1 Schematic overview of the experimental (Section 6.3) and scientific (Section 6.5) sections of this chapter.

vessels, ships and crafts) and the results sometimes can be catastrophic [172]. Newer materials are improved by increasing the strength, the trend is to also increase the stiffness of these materials. Increased stiffness in-turn increases brittleness. In fracture mechanics specimen geometry (pre-cracked specimen), one can study the evolution of the compliance and the fracture toughness as these properties are a key input for design of composite materials for specific applications.

Cracks may appear in laminated composites for several reasons. The main ones are the defects and damage caused during manufacturing processes and the damages occurring during the in-service period in the form of impact loading's, out-of-plane and in-plane unexpected overloading, cyclic loading's producing fatigue damage and structural discontinuities or stress concentration features. When a structure contains a flaw or some pre-existing damage, it is important to be able to predict the conditions under which a crack will begin to propagate and subsequently cause a failure of the structure. Characterisation of fracture mechanics hence addresses this problem by providing details in terms of critical stress intensity factors, which define the local state close to the crack tip at fracture and critical strain energy release rates which give a global description of the energy dissipated during the fracture process. The laminated nature of the composite material systems, produced by stacking layers of reinforcement (either pre-impregnated with resin or impregnated using liquid composite moulding processes), means that the fracture characteristics can be divided into three areas:

interlaminar, intralaminar and translaminar failure; as represented in the schematic in Fig. 6.2. The interlaminar fracture, is also called delamination (debonding of two successive plies). It is generally caused by out-of-plane loading and is one of the main weaknesses of laminated structures. The intralaminar fracture is where the crack propagates within the laminae of a laminate, parallel to the fibres. It can be caused by impact loading conditions and often appears together with interlaminar fracture. While, translaminar fracture is perpendicular to the fibres and it requires therefore much more energy to propagate than the inter- and intra-laminar fracture. Translaminar fracture is caused by excessive in-plane loading conditions or structural discontinuities such as cracks or holes. The translaminar fracture toughness governs the notch sensitivity of composite materials.

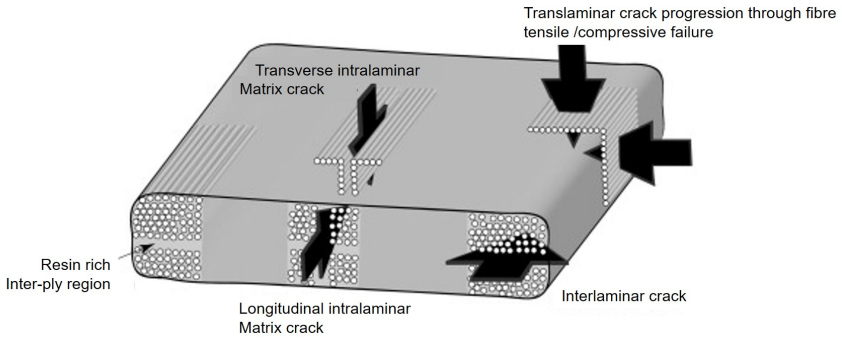

Fig. 6.2 Schematic of fracture characteristics of unidirectional composites Laffan et al. [90].

Over the last decade, toughening of fibre reinforced composites materials has been a highly active research area and several strategies have been proposed to make these materials more damage resistant, less brittle and tougher. While most researchers strategize toughening of the polymer matrix by modifying the polymer chemistry or by rubbers, thermoplastics or nano-scale reinforcements [13, 36]; in these strategies, the increased matrix toughness has a beneficial effect on the matrix dominated composite properties. New toughening mechanisms have been explored to better investigate the structure–property relations for high performance composites [136]. For example, the failure strain and toughness can be dramatically increased if brittle fibres are replaced by ductile fibres [148, 123, 121]. In this respect, metal fibres have been also explored by researchers [27], these hybrids posses high stiffness and large failure strain, but higher density of these fibres are a hindrance for this strategy. Polymer fibres such as Polypropylene, on the other hand, do have low densities and can be ductile, but are limited by their low stiffness and limited temperature resistance.

Owing to the drawbacks of these existing toughening strategies, hybridisation of different technical fibres with carbon fibres as a toughening mechanism is explored and is gaining a lot of attention in the research community. Among them, for example, carbon/epoxy

laminates made of particularly thin layers (from 0.030 to 0.150 mm) are particularly garnering larger interest because of the advantages these composites offer in terms of enlarging the design space. These composites made from thin layers of individual plies are referred to as thin-ply composites. These composites in general have outstanding strength and fatigue properties, thanks to a significant ply thickness effect reflected by a delayed onset of damage [133, 3]. However, this improvement in strength is also accompanied by higher brittleness and reduction of fracture toughness. This size effect is directly attributed to a change of failure mode, from accumulation of damage to brittle failure [14, 90].

6.2.1 Composite failure modes

The composite industry's approach for damage tolerant structures has been fuelled by the ever increasing understanding of composite failure and the desire for efficient design. Methods for predicting the onset and subsequent propagation of crack in composite components are therefore explored widely. According to the applied stress condition, a crack propagates under the three basic failure modes or the mixed-mode condition (see Fig. 6.3) . Mode I is the tensile opening mode, in which the crack faces separate in a direction normal to the plane of the crack. Mode II is the in-plane sliding or shear mode, in which the crack faces are mutually sheared in the direction normal to the crack front. Mode III is the tearing or out of plane mode, in which the crack faces are sheared parallel to the crack front. Though there are several approaches to model damage propagation, these models requires the fracture toughness for the failure mode they are simulating. Development of experimental techniques for an accurate characterisation of the toughness is therefore critical. As mentioned earlier, the failure modes exhibited by laminated composites can be divided into delamination, intralaminar fracture and translaminar fracture. Although delamination has been under extensive investigation for several years, recently, standardised procedures for measurement of different modes of crack propagation such as mode I [76], mode II [80] and mixed mode I/II [7] fracture toughness are established.

While the importance of translaminar fracture toughness measurement was recognised many years ago, until now it has received relatively little attention from the scientific community. It is envisaged that the fracture toughness associated with the translaminar failure modes will play an increasingly important role over the coming years. For a given loading condition, the fracture toughness and the formation and propagation of damage within a laminate is lay-up dependent and the final failure is governed by any one or a combination of the ply-level failure mechanisms presented schematically in Fig. 6.2. Important ply-level failures among them are: translaminar fibre tensile failure under tensile loading, translaminar fibre

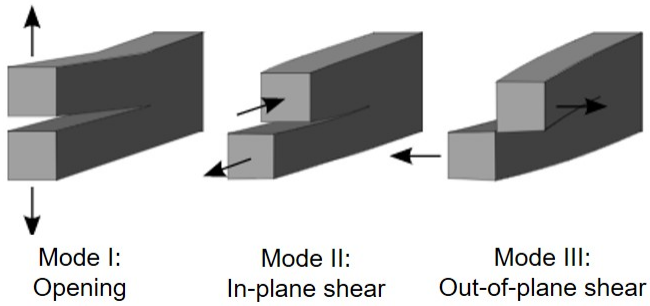

Fig. 6.3 The modes of crack propagation.

compressive failure under compressive loading and longitudinal or transverse interlaminar matrix failure.

6.2.2 Translaminar fracture toughness

This section reviews the Mode I translaminar tensile failure for composite materials.

6.2.2.1 Characterisation

Most of the studies to measure translaminar fracture of composites has been for multidirectional laminates manufactured either from unidirectional tapes or 2D woven material systems. The measured values of toughness is hence dependent on lay-up and will be the result of the constituent plies failing in a combination of the identified failure modes. Out of more than half a dozen test configurations found in literature, the compact tension, three or four point bend and extended compact tension specimens as presented in Fig. 6.4 exhibit stable crack growth and are widely used by researchers. Crack growth stability is the most important parameter to capture the change in critical strain energy release rate with the evolution of damage in the form of a resistance curve (R-curve).

CT Test:

The compact tension (CT) configuration, shown in Fig. 6.4a, is the most widely used specimen configuration for translaminar fracture toughness measurement of composites. A range of approaches to data reduction have also been developed for this test and includes schemes such as: (1) ASTM method, (2) Area method, (3) Compliance Calibration (CC method) (4) Modified Compliance Calibration (MCC method) and (5) J-integral method. By far the most widely used has been through the determination of the critical stress intensity factor, K_{Ic}, as recommended by the ASTM E399 for metallics [8]. The critical strain energy release

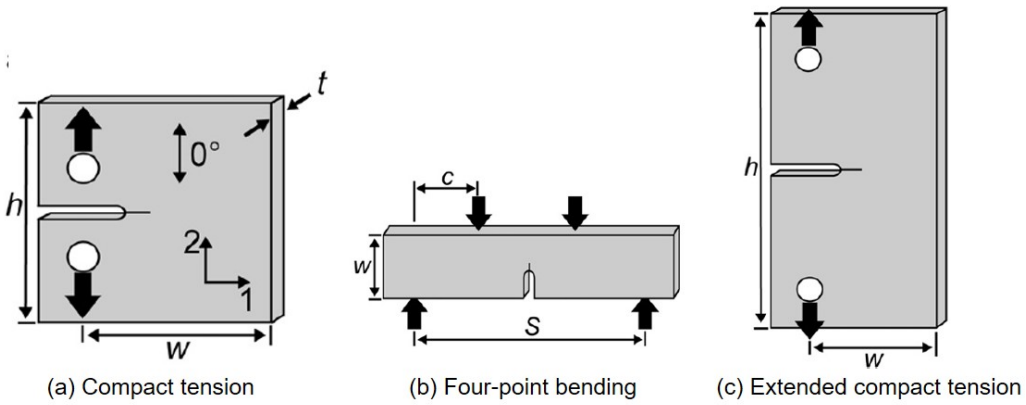

Fig. 6.4 Specimen configurations used for translaminar fracture toughness measurement: (a) compact tension, (b) four-point bending, (c) extended compact tension.

rate, G_{Ic}, can be obtained from the critical stress intensity factor as in equation below:.

$$G_{Ic} = \frac{K_{Ic}^2}{\sqrt{2E_{11}E_{22}}} \times \sqrt{\sqrt{\frac{E_{11}}{E_{22}}} + \frac{E_{11}}{2G_{12}} - \nu_{12}} \tag{6.1}$$

and,

$$K_{Ic} = \frac{P_c}{t\sqrt{w}} \times f(a/w) \tag{6.2}$$

where, P_c is the critical load causing crack extension, t and w are thickness and width of specimens, a is the crack length, $f(a/w)$ is a finite-width correction factor and E_{11}, E_{22}, G_{12} and ν_{22} are elastic moduli, shear modulus and Poisson's ratio respectively for the laminate.

In the area method, the energy dissipated during fracture is calculated by dividing the area underneath the specimen load-displacement curve by the fractured area associated with crack growth.

The critical strain energy release rate can be determined directly from experimental data, if the rate of change of compliance, C, with crack length a is known, the G_{Ic} for CC and MCC method can be calculated as follows:

$$G_{Ic} = \frac{P_c^2}{2t} \times \frac{\mathrm{d}C}{\mathrm{d}a} \tag{6.3}$$

The CC method makes use of direct measurement of the specimen compliance from load-displacement curves of tested specimens correlated with associated values of crack length that is measured optically; while the MCC uses measurement of the compliance of specimens with machined cracks of known length.

Data reduction using finite element method and the J-integral is also reported, where, the CT specimen is modelled with 1 mm thickness and a 1 N load applied at the point of the centre of the loading pin to obtain the J-integral, J, for a range of crack lengths. The energy release rate in this case can be defined as:

$$G_{Ic} = \frac{P^2}{t} \times f(a) \tag{6.4}$$

and,

$$f(a) = J. \left(\frac{1mm}{1N} \right)^2 \tag{6.5}$$

An extensive investigation of all of the aforementioned data reduction schemes by Laffan [89] found that the methods that relied on optical crack growth measurement were sensitive to errors in its measurement. This factor also led to the conclusion that the MCC method was the most appropriate of the data reduction.

The recently proposed technique by Catalanotti et al. [28] based on the identification of the crack tip location using Digital Image Correlation and then calculation of the J-integral directly from the test data is shown to be producing the crack resistance curves similar to MCC method for the same material system.

3-P bending Test:

Similar to the CT arrangement, the three-point bending specimen design also exists as an ASTM standardised specimen for metals and has been used for translaminar toughness characterisation of composites. There have been varied approaches to the data reduction process with this specimen, while Harris and Morris [57] using an FE based method of data reduction similar to that used for CT specimen; Underwood and Kortschot [157] presented a modified method by replacing $f(a/w)$ being replaced by $f(S/w, a/w)$, where S is the distance between bottom support as in Fig. 6.4b.

ECT Test:

Extended compact tension (ECT) specimen was further developed as an alternative configuration to the three or four point bending specimen so as to avoid the effect of sample damage caused by the loading nose in the later configurations. The ECT specimen configuration also originates from the tests earlier done for metals. It was adopted by Underwood and Kortschot [157] for testing of carbon/epoxy laminates, to resolve problems with undesirable failure modes.

0° ply fracture toughness, G_{Ic}^{0}:

The above mentioned test configurations and data reduction schemes along with others are currently used for fracture toughness calculation of laminates. The critical strain energy release rates, or stress intensity factors are essentially lay-up dependent properties and are of limited use as they are not representative of any property intrinsic to the material system. Several researchers later demonstrated that an in-situ 0° ply fracture toughness is a material property intrinsic to the material system, regardless of lay-up [158, 119]. Pinho et al. [119] used a Rule of Mixture type approach to obtain G_{Ic} for 0° plies. He assumed that the laminate fracture toughness can be partitioned into the separate contributions made by the 0° plies and 90° plies such that G_{Ic}^{0} could be obtained from the equation below:

$$G_{Ic}^{0} = \frac{t_{lam}}{t_0} \times G_{Ic}^{lam} - \frac{t_{90}}{t_0} \times G_{Ic}^{90} \tag{6.6}$$

where t_{lam} is the laminate thickness, and t_0 and t_{90} are the total thicknesses of 0° and 90° plies within the laminate respectively. G_{Ic}^{lam} is the critical energy release rate for the laminate and G_{Ic}^{90} represents the fracture toughness associated with mode I longitudinal intralaminar matrix failure.

6.2.2.2 Review of studies on hybrids

The hybrid effect in composites has been studied extensively in the literature [88, 143, 148] with reference to the deviation of a property of hybrid composite from the linear Rule of Mixtures. Many authors found synergistic effects in hybrid composites for tensile, compression and flexural loading conditions [143, 88]. The challenge of fibre hybridisation lies in understanding, predicting and eventually optimising the hybrid effect and associated complex behaviours such as impact or fracture toughness. With the advantageous properties offered by these material systems comes the associated penalty of increased design complexity and the fact that the failure mechanisms they exhibit are still not yet fully characterised and understood.

Numerous studies have characterised the translaminar fracture toughness of carbon epoxy composite laminates [119, 19, 20, 52, 22, 151], glass epoxy composite laminates [84, 82] and recently on carbon/glass hybrid composite laminates [141, 111, 110, 145, 85] in tension. A range of approaches in terms of both specimen configuration and data reduction schemes have been used [91, 89, 47, 28, 62]. The reported values in these studies for 0° carbon fibre/epoxy plies are in the range of 20 to 280 $\mathrm{kJ\,m^{-2}}$. The translaminar fracture toughness reported is significantly higher than interlaminar fracture toughness values, which typically range from 0.2 to 3 $\mathrm{kJ\,m^{-2}}$. The primary reason for this phenomena is that the translaminar

fracture is controlled by significant fibre/matrix debonding and pull-out, both of which can absorb large amounts of energy. The most commonly used specimen for the characterisation of fracture toughness of composite materials is the compact tension (CT). While most of the studies in the literature conducted on translaminar fracture toughness involved carbon or glass fibre reinforced composites, limited work out of them have focused on the investigation of the translaminar fracture toughness of hybrid composite materials and none of them has ever focused on the study of the effect of tow dispersion on the translaminar fracture toughness of intraply carbon/glass epoxy composites.

Donadon et al. [39] studied intralayer carbon/glass woven hybrids and found that the architecture of woven fabrics necessitates a more tortuous crack path for crack propagation. The improved toughness values reported by the study for hybrids can also be influenced by the in-plane shear effect added to primarily just the tensile opening mode I dominated test result. The study did not report hybrid effect as they did not characterise the reference carbon and glass laminates in their study. Ortega et al. [111, 110] in their studies conducted experiments on reference woven glass, woven carbon and unidirectional carbon plies and the hybrid made from these reinforcements. In their studies they reported no hybrid effect in the translaminar fracture toughness for the hybrid composites. Although for the hybrid configurations having blocked plies, a positive deviation was reported owing to increased matrix cracking and larger delamination. But this effect could also occur simply from the effect of higher thickness, as blocked plies operate as a single ply with double the thickness hence further tending to cause larger pull-outs during the tests as reported by Teixeira et al. [151] and Pimenta and Pinho [118].

Swolfs et al. [141] found for their woven carbon/glass interply hybrids that hybridisation influenced the pull-out lengths during the translaminar fracture toughness tests. They reported synergies up to $+15\,\%$ or $-15\,\%$ depending on the layup used for hybridisation. Like other studies for pure carbon composites, a positive effect was found for layups where the carbon plies were blocked together in the hybrid structures, which allowed longer pull-out lengths to be created.

The limited data on translaminar fracture toughness of fibre hybrid composites prompts that much work is still needed to be done on this topic. As of now, it is clear that increasing pull-out lengths contribute to increasing the translaminar fracture toughness for hybrid composites and that the hybridisation can have both negative and positive effects on these pull-out lengths. Hence it is important to consider an intelligent micro-structural design to achieve ideal toughness in composites for structural applications. This chapter focuses on the characterisation of the fracture toughness of thin-ply composites made from carbon and glass based intraply hybrid reinforcements. By testing and comparing properties of reference

pure glass and carbon composites; the current work gives insights on the possible hybrid effect for translaminar fracture toughness of hybrid intraply composites.

6.3 Materials fabrication

6.3.1 Materials

The experimental work in the current chapter is widening and supplementing the work carried out on intraply hybrid composites in the Chapter 4 of the thesis. Hence as a natural progression, similar carbon and glass fibres were utilised in the study; a T700SC 12 K carbon roving and a 111A 1200 tex, E-CR glass rovings were commercially procured from Toray Europe and Owens Corning respectively. A commercially available epoxy system from Huntsman Advanced Materials GmbH in Switzerland was used and it consisted of Araldite LY 564, a low viscosity epoxy resin and Aradur 2954, a cycloalophatic polyamine hardener. This system is used in a wide range of applications in industrial and aerospace composites owing to its excellent handling behaviour and suitability for various production processes. Some major properties of these fibres and cured matrix from their technical data sheets are provided in Table 4.1, in Chapter 4.

6.3.2 Fabrication of reinforcements

Considering the objective of characterising the translaminar fracture behaviour of composites using Compact Tension tests it was necessary that the thickness of the fabric plies be below 100 to 200 µm. To manufacture such thin-ply fabrics using the standard processes, it is essential to use finer rovings which in general for carbon are more expensive. It was established in Chapter 3 and Chapter 5 reported earlier in this thesis that thin-ply composite reinforcements including hybrid reinforcements can nevertheless be inexpensively manufactured using a fibre spreading technology. Hence, a novel set of fabrics both reference carbon and glass fabrics along with three intraply hybrids were manufactured using a fibre spreading technology optimised and described in detail in Chapter 3 of this thesis.

Spreading of E-CR glass fibres has been seldom reported in the literature. Therefore, the development of a novel spreading technique suitable for glass rovings is a challenge of high industrial impact that was addressed in this work. Additionally to the spreading of glass, efforts in this thesis were directed towards the development of a spreading technique that would allow the simultaneous spreading of glass and carbon rovings. Apart from spreading of the glass rovings being a novelty already, in this study efforts were successfully made

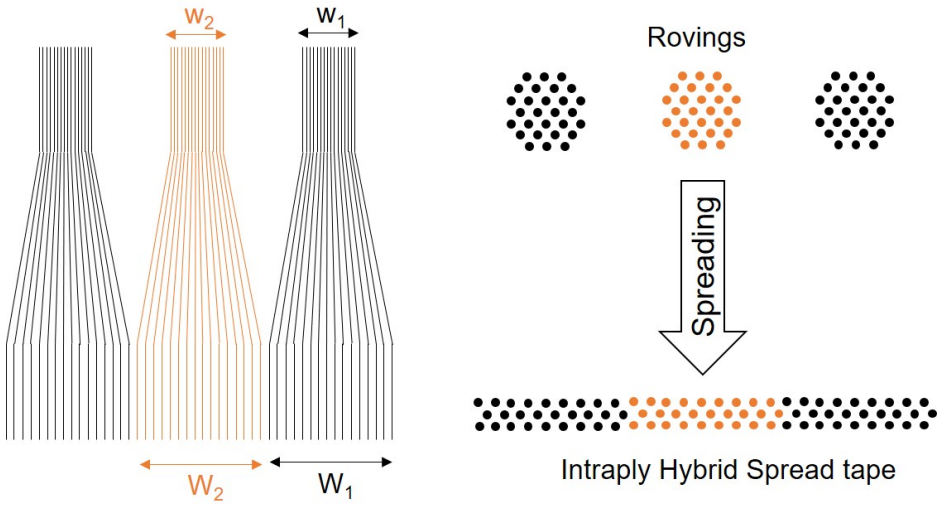

Fig. 6.5 Schematic of fibre spreading operation.

to develop a newer generation of intraply hybrids by simultaneous spreading of glass and carbon rovings in the spreading process as schematically presented in Fig. 6.5.

Necessarily, a spread tape is a non-cohesive bunch of parallel fibres in the form of a sheet and in the standard NCF manufacturing the spread tape is used as an intermediate product to manufacture a fabric, by stitching one or more layers together. For the current work, it was decided not to add stitching as an additional factor as researchers have reported ambiguity in their work on effect of stitching on the properties of NCF composites [4, 18]. In the current work, an epoxy powder binder, Epikote 05390 from Hexion Inc, ($4\,\mathrm{g\,m^{-2}}$) was evenly applied on face-side of the spread tape and cured on the fabric surface to impart handle-ability to the fabrics in subsequent processes. This binder was applied on both the reference fabrics and the hybrids and the microscopic image of the fabric and the binder can be seen in Fig. 6.6.

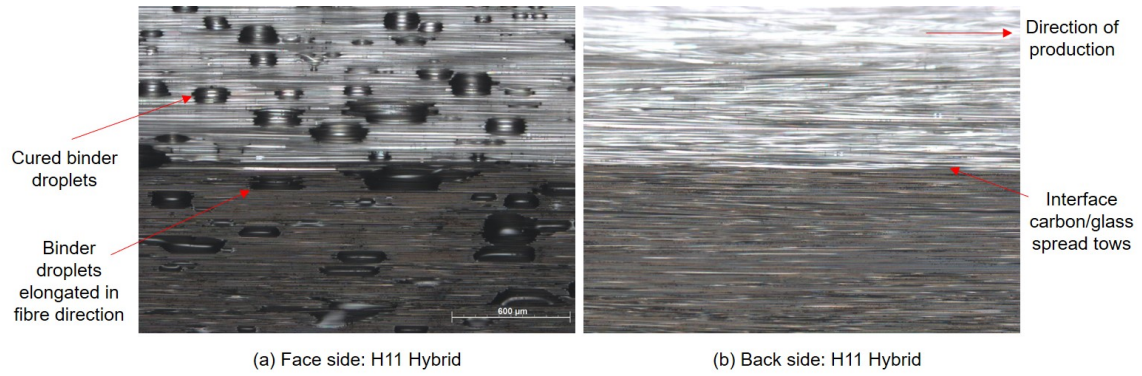

Fig. 6.6 Pictures of cured epoxy binder ($4\,\mathrm{g/m^2}$) on a hybrid spread tape.

The series of reference and hybrid fabrics had a thickness in between 0.11 to 0.13 mm and the pictographs of the developed fabrics is presented in the Fig. 6.7.

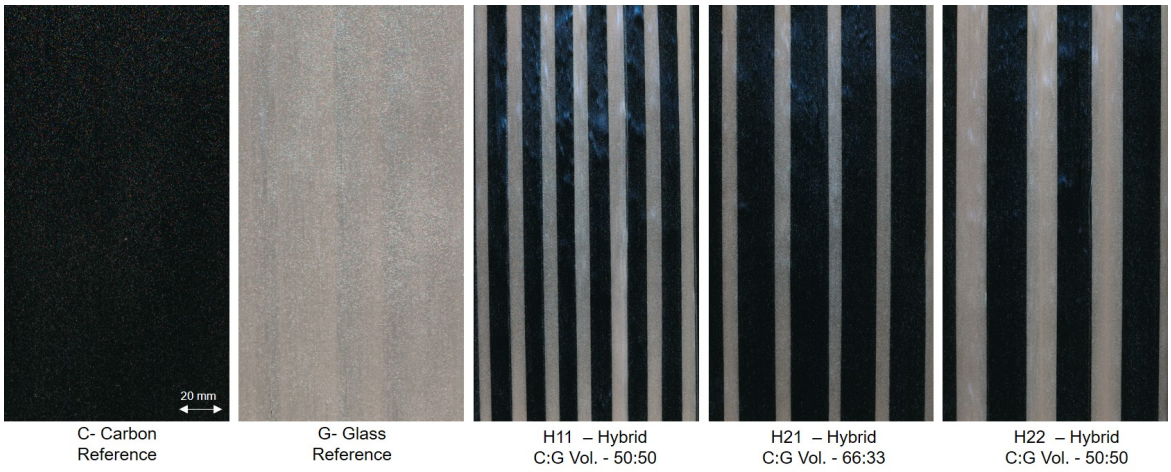

Fig. 6.7 Pictures of developed reference and hybrid reinforcements.

6.3.3 Composite fabrication using RTM

Fabrication of composite plates [500 mm × 500 mm × 5 mm] for the study was done using an epoxy based Resin Transfer Moulding (RTM) process. The used RTM process consisted of sequential preforming step, where a net shaped dry preform consisting of 50 layers in the sequence $[(90_2/0)_8/90]_S$] was first assembled as an intermediate step before resin injection. The stacked plies in each direction were randomly shifted by a few millimetres in subsequent layers. Pinho et al. [119] suggested that the 0° ply toughness is dependent on ply thickness, considering this, it was decided to place 2× 90° plies on either side of each 0° ply through the laminate symmetry plane to avoid blocking of 0° plies. The number of layers was determined by the individual ply thickness to enable a composite laminate with thickness of about 5 mm. Further, the laminate was designed to have 90° surface plies so that the crack could be optically monitored on the specimen surface during the tests.

The preforming step is described in detail in Section 4.3.2.2. This preform was laid into one of the mold half, the mold is then closed with over pressure of about 16 bar and vacuum in the cavity of about 0.9 bar and finally the resin is injected though a line injection gate at one of the side of the mold. The resin injection started at 2 bar and as the resin flowed through the preform the pressure was increased up to 6 bar. The resin was injected at 60 °C, and then cured in the mold for 1 h at 80 °C and further 6 h at 140 °C as per the recommendation of the resin supplier.

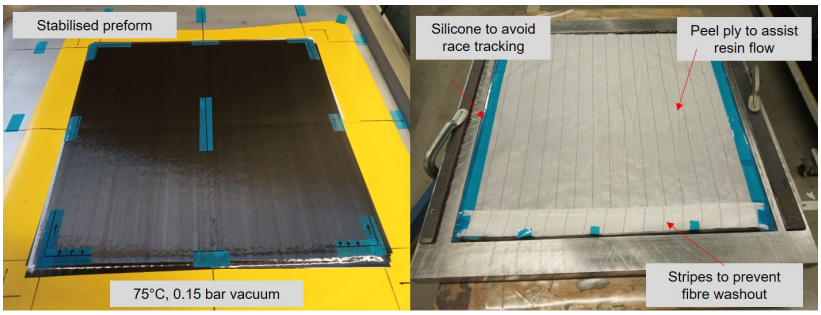

Fig. 6.8 Preforming for carbon composite manufacturing using thin ply spread tapes.

Composite manufacturing using the thin-ply, non-stitched spread tapes had several inherent challenges. The dry preforms fabricated using spread tapes were found to be thinner than the desired composite thickness, which rendered them unusable in the RTM process. Further these thin-ply preforms flowed along with the resin (Fibre Washing) when the cavity pressure increased. While the thickness of preforms was optimised by optimising the preforming parameters, namely, preforming temperature and vacuum pressure; the fibre washing was avoided by using additional stripes of peel ply near the injection line (see Fig. 6.8). Peel ply layers were also added to the preform on both the sides for assisting the flow and reducing the fibre washout, this was found to be more important for carbon composite.

Table 6.1 summarises the details of the composites manufactured for the study.

Table 6.1 Overview of manufactured thin-ply composites.

Fabric/ Composite	Layup 50 Layers	Hybrid ratio [%]	Thickness [mm]	Density [$g\,cm^{-3}$]	FVF [%]
C		100	4.5	1.5	60.9
G		0	4.9	2.0	58.5
H11	$[(90_2/0)_8/90]_S$	50	4.7	1.8	58.7
H21		66	4.6	1.7	63.0
H22		50	4.6	1.8	62.1

6.4 Experimental tests

6.4.1 Physical property characterisation

The central aim for this work was to characterise the translaminar fracture toughness using Compact Tension (CT) test. Before the tests, it was important for ascertaining experimen-

tal uncertainties and hence physical properties and other quality check's were performed on the composite plates and the test specimens. The Fibre Volume Fraction of the composites was measured using a modified Burn-Off method for composite coupon samples [5]. The thickness was measured using a standard micrometer, while the density of small composite samples from the plate was measured using the Buoyancy method [6]. These physical tests were done to confirm the initial properties of the fabricated plates and their comparability. Void content and infiltration quality in the composites was measured using Zeiss AX10 Lab.A1 equipment with a magnification range from 50× to 1000×.

Micrographs of the cross sections viewed from the direction of injection for carbon composites and the three hybrid composites H11, H21 and H22, are presented in the Fig. 6.9a-d respectively.

For all the test specimens to be tested in CT test, ultrasonic C-scans were performed in an immersion tank to check the quality of the samples. For some of the samples, X-Ray scans were performed before and after the test so as to see the damage in the sample after testing and that there are no other type of failure mechanism occurring other than expected linear crack propagation.

6.4.2 Compact tension test

The compact tension (CT) configuration, shown in Fig. 6.10a, is perhaps the most widely used specimen configuration for translaminar fracture toughness measurement of composites. The composite layup configurations, specimen dimensions and testing parameters in the current study were adapted to tests and studies by Pinho et al. [119] and Laffan et al. [91].

Compact tension tests were performed on an Instron universal testing machine with a 50 kN load cell. The CT test specimen design used is as shown in the Fig. 6.10a. The outer specimen dimensions were 60 mm × 65 mm with an initial crack length of 26 mm. The overall shape of specimen and the initial 4 mm wide and 30 mm long notch was cut out from the composite plate using a computer-controlled rotary cutter with rotor diameter of 2 mm. The final sharp tip in the notch was cut by extending the initial groove by 10 mm using a circular disc saw with tapered diamond tip producing an initial crack depth ratio (a/W=0.5) for all specimens. From the crack tip up to the other end of the specimen, a millimeter increment scale is marked (as seen in Fig. 6.10b) on a white background made using correction fluid, to monitor the crack propagation optically. This tapered diamond saw tip ensured the final crack tip radius of about 70 µm as can be seen in Fig. 6.10c. A minimum of six specimens were planned to be tested for each configuration. Linear Rule of Mixture based on reference carbon and glass fibre composites and the hybrid ratio is used to understand hybridisation effect as also reported in earlier studies by Swolfs et al. [141].

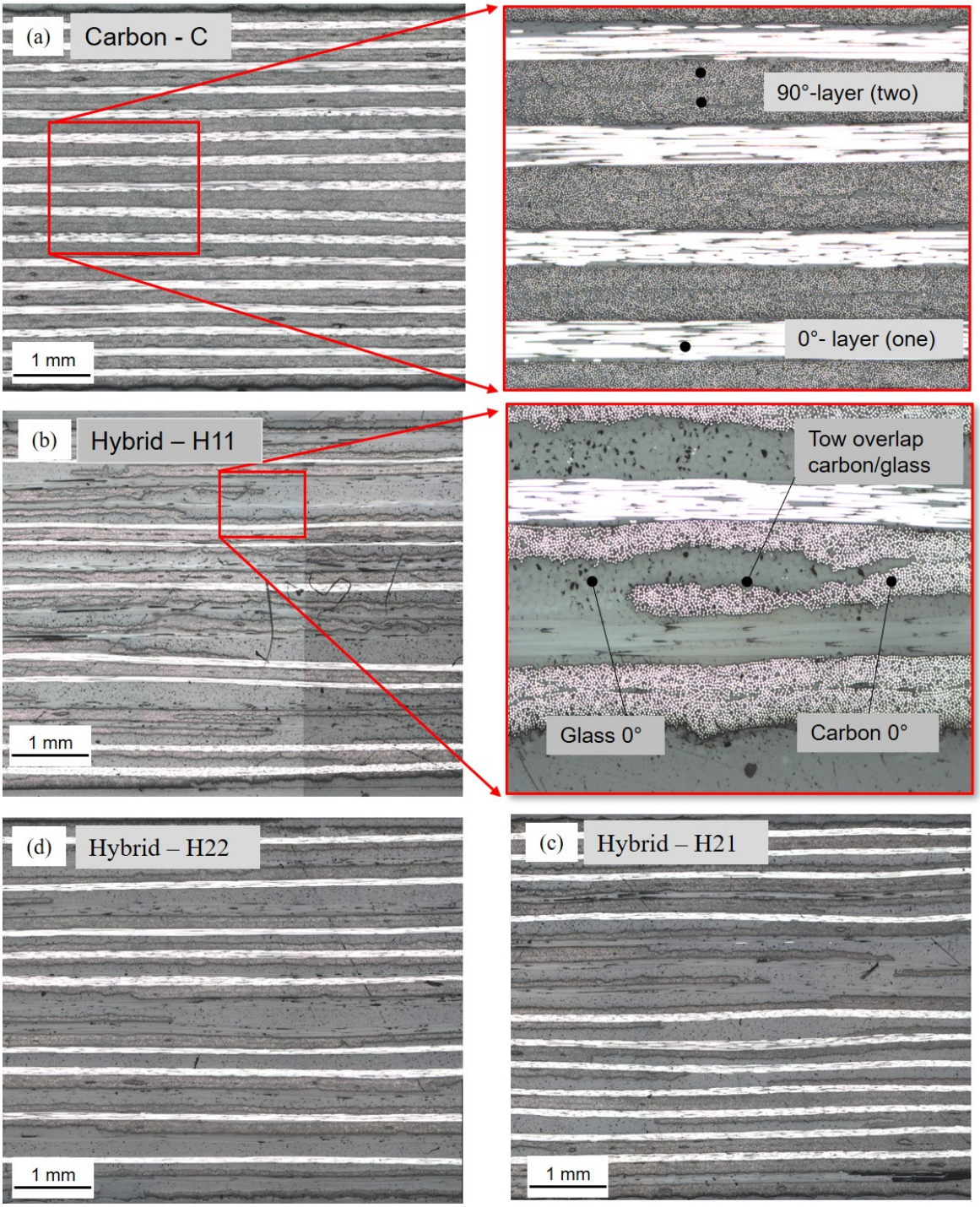

Fig. 6.9 Micrographs of the cross-section of the composites viewed from the direction of injection: (a) Carbon composite C, (b) Hybrid H11, (c) Hybrid H21 and (d) Hybrid H22.

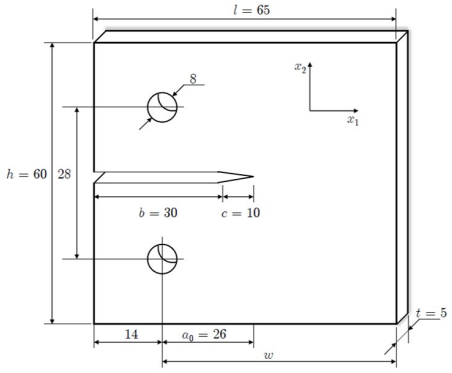

(a) Specimen dimension for CT test

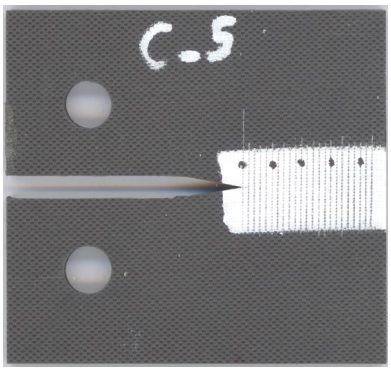

(b) Carbon CT test sample

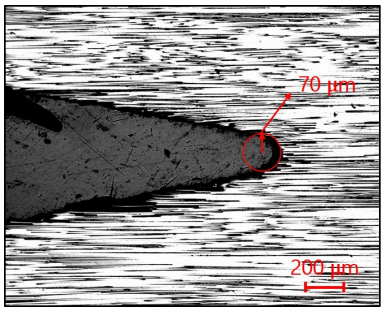

(c) magnified image of the crack tip

Fig. 6.10 Compact tension (CT) test sample preparation

6.4.3 Data reduction

Data reduction was performed using the standard ASTM E399 method (as described in [119]), compliance calibration (CC) method and the modified compliance calibration (MCC) method with finite element models (as described in [91]). Using ASTM method [8] of data reduction, G_{Ic} for the laminate is obtained using Eq. 6.1, while, G_{Ic} was calculated using Eq. 6.3 while utilising the CC and MCC methods of data reduction.

For CC method, the elastic compliance of the specimen was obtained at each optically measured crack length, a_{vis}, directly from the load displacement curve. The experimental C vs. a_{vis} data was plotted and fit with the following function:

$$C = (\alpha a + \beta)^{\chi} \tag{6.7}$$

where α, β, and χ were calculated to best fit the experimental data. Using Eq. 6.3 and Eq. 6.7 the critical strain energy release rate at each optically measured crack length was

then obtained from the following expression:

$$G_{Ic} = \frac{P_c^2}{2t} \times \alpha\chi(\alpha a + \beta)^{\chi-1} \tag{6.8}$$

MCC method on other hand eliminates the need to optically measure crack growth during testing and was used to calculate the fracture toughness. In this method a compliance calibration curve was obtained by using Finite Element Method. A half CT specimen was modelled using uniform square 8-noded elements (S8R5), with side l = 0.5 mm. Models were 1 mm thick and 1 N load was applied at the position of the loading pin. Table 6.2 summarises the engineering constants used in the finite element model for modelling the compliance curve using FEM. These constants were obtained from WiseTex-TexComp calculations.

Table 6.2 Engineering constants of the plies obtained from WiseTex-TexComp calculations and used as input for the compliance calibration using FEM.

	E_x [GPa]	E_y [GPa]	G_{xy} [GPa]	v_{xy} [-]
C	50.06	97.47	4.21	0.0227
G	22.40	37.02	4.07	0.066
H11	36.19	67.25	4.14	0.0345
H21	40.62	76.91	4.16	0.0293
H22	36.19	67.25	4.14	0.0345

The elastic compliance of the CT specimen was measured for several pre-crack lengths. These measurements were taken across the whole of the potential crack growth range, in 3 mm increments, to capture the full compliance versus crack length response. It is to be noted that this compliance versus crack length response can also be obtained testing specimens with various pre-machined and known crack lengths. The calibrated C vs. a data was plotted and fitted with Eq. 6.7 and an effective crack length, a_{eff}, could be determined using the elastic compliance measured from the load displacement curve of the test specimens, rearranging this equation:

$$a_{\text{eff}} = \frac{C^{\frac{1}{\chi}} - \beta}{\alpha} \tag{6.9}$$

The critical strain energy release rate was then determined using Eq. 6.8.

The energy release rate during propagation for all the data reduction schemes was calculated as the average energy release rate value over the plateau region of the R-curve.

The end region of the crack growth was avoided to prevent compressive failure at the back from interfering with the data.

6.5 Results and discussions

6.5.1 Crack growth analysis

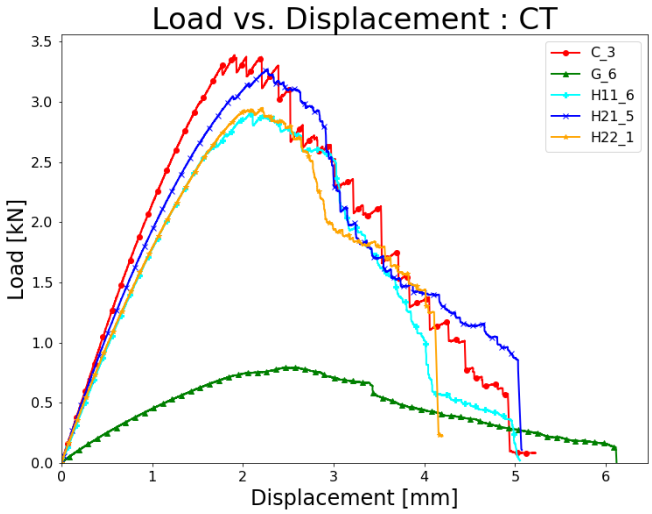

(a) All composites

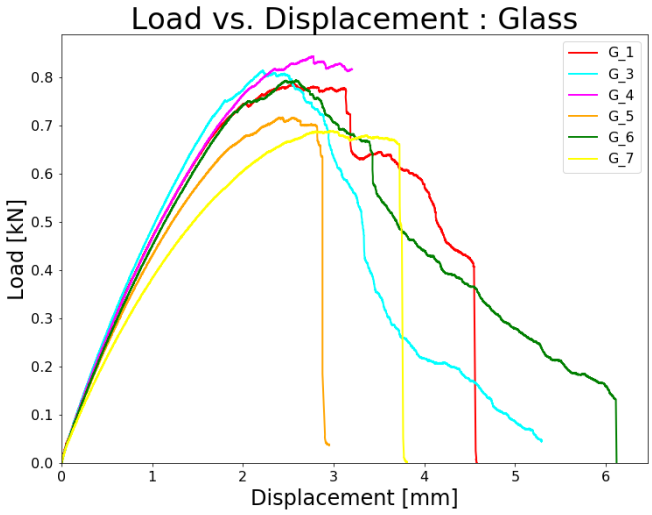

(b) Glass composite

Fig. 6.11 Representative load vs displacement curves for the tested composite samples

As seen in Fig. 6.11a[1], for all the CT specimens tested, crack growth demonstrated stick-slip effect and the curve was not smooth nor continuous. Each load drop in carbon and hybrid composites corresponded to about 0.5 to 1 mm increase in crack growth. The test and the crack propagation was recorded though a CCD camera and this magnified image containing crack growth was correlated to the load displacement values coming from the Instron data log thus providing the propagation load for each value of crack length where the crack had stopped. For carbon composite specimens, 2 out of 6 specimens on loading showed compressive failure before the crack propagation. This failure in compression was attributed to the incomplete infiltration of the composites and the presence of dry layers in the inner layers of the composite. This incomplete infiltration of composite was also recorded during composite fabrication as seen in Fig. 6.12, this was also confirmed by the C-scans of the specimens obtained before testing.

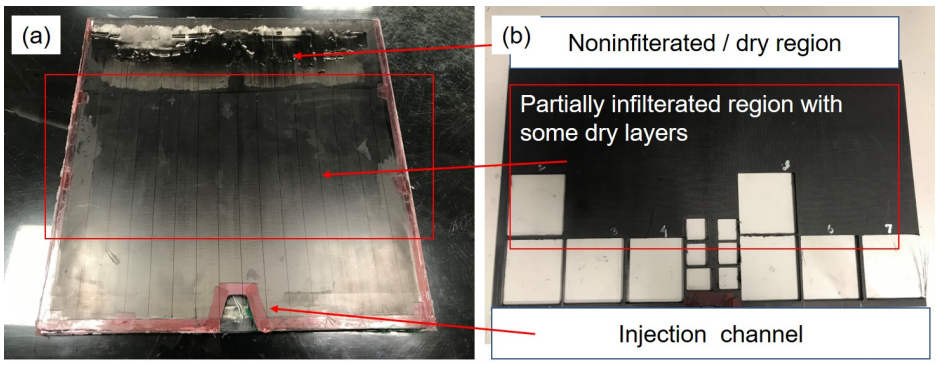

Fig. 6.12 Fabricated composite plate and specimen cutouts from Carbon composite plate C

Though there is extensive literature on translaminar fracture toughness for carbon fibre reinforced composites, data on glass fibre reinforced composites is observed to be scarce. In the current study, initial tests on glass specimens revealed that the specimens were prone to compressive failure on the opposite side of crack propagation front, before fracture initiation. To prevent this failure, the initial crack length for glass fibre composite was increased from 26 mm to 31 mm and further to 36 mm. This measure was not completely sufficient to prevent the compressive failure, but for increased initial crack length most of the samples showed crack initiation and propagation before the compressive failure occurred. The load for crack initiation of glass composite as seen in Fig. 6.11b was significantly lower than carbon also as a result of higher initial crack length for glass specimens.

[1]The curve for each composite type in Fig. 6.11a is a representative curve from 4 specimens tested for C and G composites and 6 specimens tested from H11, H21 and H22 respectively. The displacement presented here is the cross-head displacement measured from the optical images taken during the duration of test.

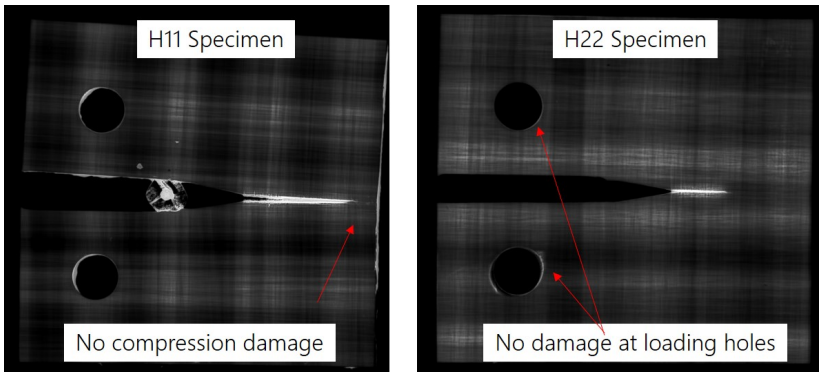

(a) scan of the samples after completion of test for H11 and at 80% of the displacement for H22

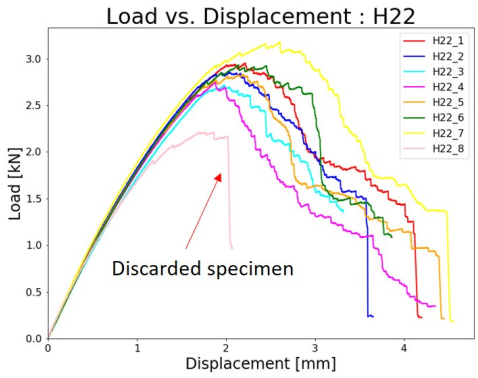

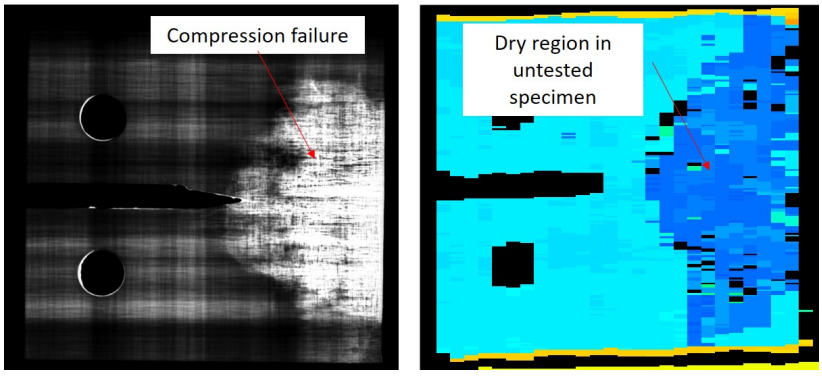

(b) Confirmation tests for discarding a particular specimen result using X-Ray and C-Scan

Fig. 6.13 CT test specimen observed in C-Scan images before testing and X-Ray scan images after completion of testing

All carbon and hybrid specimens with a 26 mm notch yielded a suitable failure; for some of the carbon specimens the crack propagation and failure on the compressive end was simultaneously observed. The load vs crack opening displacement curves are affected by the fibre hybridisation, after the linear-elastic response, the hybrid laminates exhibit a quasi-brittle failure as can also be seen in Fig. 6.11a. In both hybrid and non-hybrid cases,

the crack jumps were nearly similar, jumps in the range of 1 mm were observed in both cases on increasing the loads. The major difference here is the length of stable crack propagation for hybrids (approximately 15 mm for H11 and 10 mm for H21 and H22) was higher than that observed for carbon, which was just about 5 mm as can be seen in Fig. 6.16. The load drops in the curves for H11, H21 and H22 can be directly correlated with the crack propagation observed from the CCD camera recordings for all the three hybrids. There was no compressive failure observed for hybrids and this was confirmed by interrupting the test at 80 % of average displacement and performing X-Ray scan for the specimen as can be seen in Fig. 6.13a for H11 and H22. The maximum loads for carbon and hybrid H21 composites was more than 3 kN while those for H11 and H22 was between 2.5 to 3 kN hence the probable damage at loading point was checked in the X-Ray scan. No failure occurred around the loading holes for any of the tested specimens and this was also confirmed by the X-Ray images of the tested sample. The hybrid samples where the load displacement curves showed abnormality were excluded from the calculations after confirming the cause of it, by ultrasonic C-scan and X-Ray scan of the specimen, like presented in Fig. 6.13b for one of the H22 specimen.

6.5.2 Data reduction

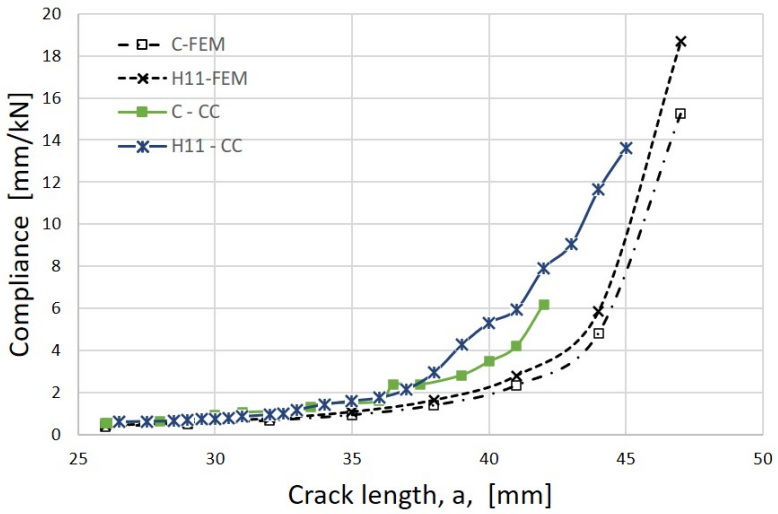

Fig. 6.14 Compliance vs. crack length curves obtained from FE, CC method and MCC method.

The difference in the critical energy release rate obtained using the data reduction from ASTM standard E399 [8] for metals (isotropic material) and the FE approach is found to

be very significant (55 to 60 % for the material, layup and geometry considered here). This difference is even higher for glass fibre specimens owing also to the excessive compressive damage. Therefore, the use of this standard for orthotropic composite materials is not recommended as also confirmed from other studies involving different materials, layups and geometries [119, 91]. The elastic compliance was measured directly from the load-displacement curve after each crack growth; the results are shown for a representative carbon and H11 hybrid composite in Fig. 6.14. The figure also shows the compliance versus crack length curves obtained from FE which was the root of the MCC method of data reduction. The strain energy release rate, G_{Ic} for initiation and during propagation is obtained from the CC method MCC were not significantly different.

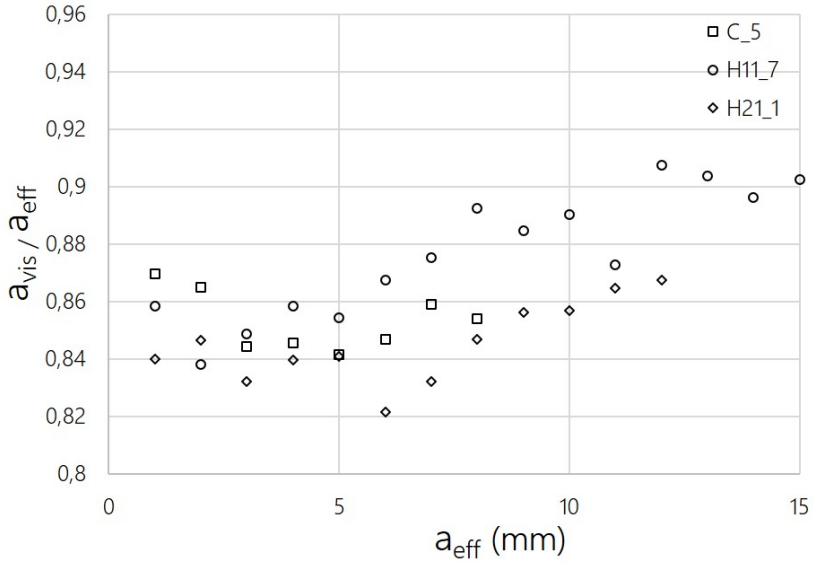

Fig. 6.15 Comparison of crack lengths: optically measured a_{vis} and effective a_{eff} from MCC method.

Fracture toughness was calculated from the MCC data using both the optically measured crack length, a_{vis}, and the effective crack length, a_{eff}, calculated from the measured FEM elastic compliance of the specimen. A comparison of the optically obtained crack length and effective crack length from MCC method is presented in Fig. 6.15. This difference between a_{vis} and a_{eff} leads to about 40 to 50 % difference in the energy release rate at initiation and propagation measured using the MCC method for the two crack length values.

6.5.3 R-curves

The R-curves obtained for all 5 composites using MCC method of data reduction are shown in Fig. 6.16a - e.

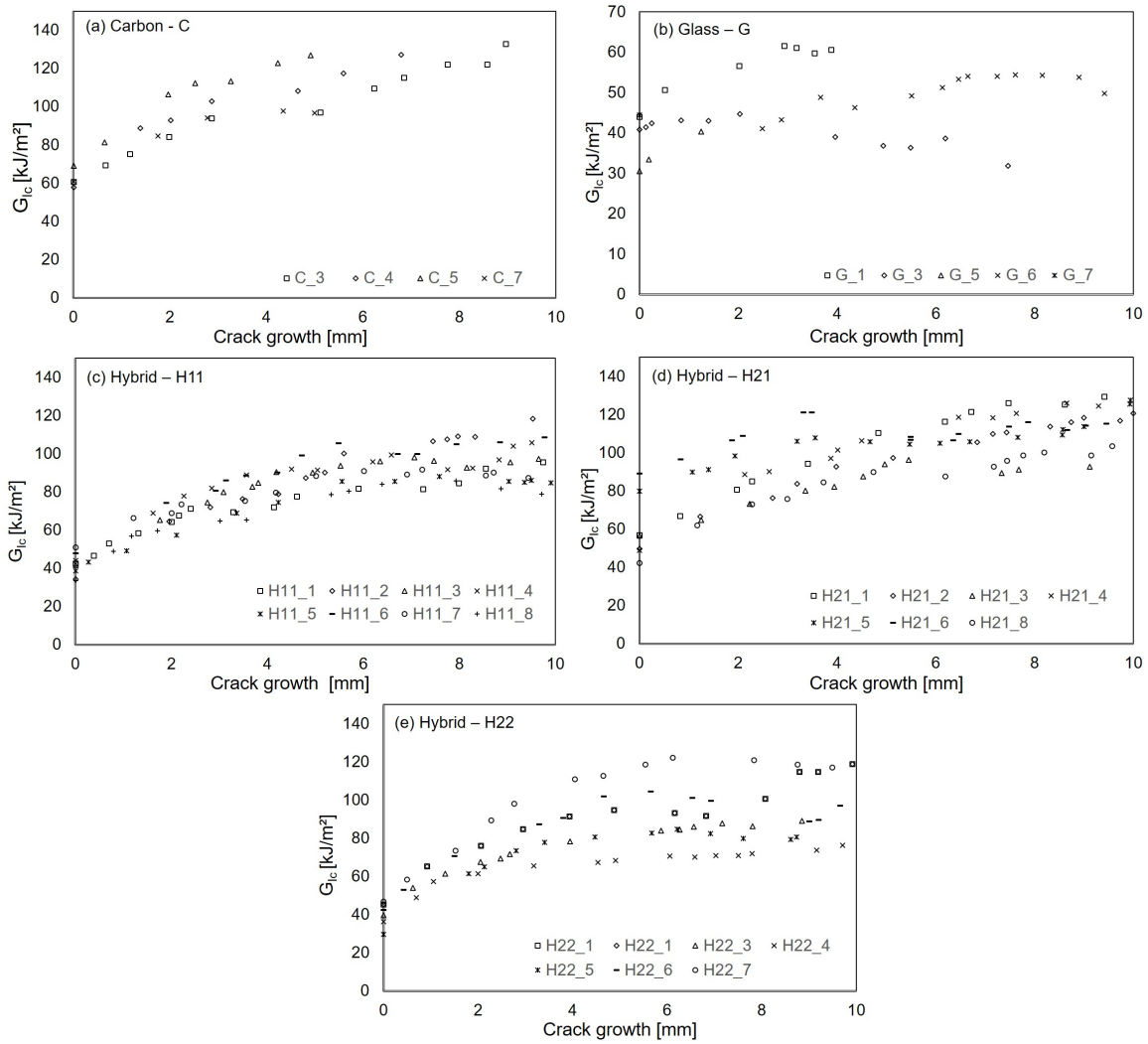

Fig. 6.16 R-curves obtained from CT testing and data reduction using MCC method: (a) Composite - C, (b) Composite - G, (c) Composite - H11, (d) Composite - H21 and (e) Composite - H22.

The scatter in the R-curves obtained from the other data reduction schemes, such as ASTM, area method and CC method was comparatively higher owing to use of optically measured crack length. Using this optical measurement method, the accuracy to which the crack length can be monitored is 0.5 mm only. The dC/da vs. a response obtained via FE for the CT specimen geometry was reported by Laffan [89] and it indicated the sensitivity of data reduction schemes to crack length measurement. The graph also suggested for a 65 mm wide specimen, with initial crack length of 26 mm, the measurements for a >40 mm should be avoided as the rate of change of dC/da becomes large, and also due to the proximity of the crack tip to the back edge of the specimen. Hence the propagation values and the R-curves

represent only the first 10 mm of crack growth. As mentioned above the ASTM E399 is strictly valid for isotropic materials and errors are introduced in the measurement by its application to orthotropic laminates. It is hence also found that the measured initiation value and average propagation is the lowest for this method among all the data reduction methods. Using the CC method, results were calculated using the compliance's measured at each optically measured crack length. It can be seen in Fig. 6.14 that for a <40 mm there is a very good agreement between the compliance values measured directly from the load displacement curve, and those obtained via FE and MCC methods.

A comparison of the measured initiation and propagation values of strain energy release rate using MCC method are presented in Fig. 6.17a and Fig. 6.17b respectively. The error bars in Fig. 6.17 represent the standard deviation of the mean values of energy release rates at 90 % confidence level as per the guidelines mentioned in Guidelines for Uncertainty Measurement (GUM) [55]. While, fracture toughness is the critical value of the energy release rate at initiation; the propagation values for the composites were defined as strain energy release value obtained for crack lengths greater than 0 mm up to the point where the R-curve may be rising, i.e up to 15 mm for hybrid composites and 5 mm for carbon and glass fibre composites. This ensured that exclusion of the strain energy release associated with the effect of compression damage, rapidly rising compliance and proximity of the crack to the edge. The average of these values presented in Fig. 6.17b.

6.5.4 Hybrid effect

The carbon fibre composite with energy release rate of 62.3 ± 5.4 kJ m^{-2} at initiation and 92.3 ± 10.9 kJ m^{-2} at propagation was found to be tougher than the glass fibre composite with energy release rate of 40.3 ± 5.7 kJ m^{-2} at initiation and 44.5 ± 8.8 kJ m^{-2} at propagation. This is in line with the results obtained by Swolfs et al. [141] and Ortega et al. [111, 110], which are among few authors that reported translaminar fracture toughness values of both carbon and glass fibre composites. This cannot be just attributed to the intrinsic fracture toughness of the fibres as this toughness contribution has been proved to be very limited [150]. The translaminar fracture toughness is predominantly also controlled by fibre pull-out and debonding [89, 118]. Carbon composite here has higher number of fibres with smaller diameter and higher total fibre surface per unit volume compared to glass and hence would have a system to create larger pullout lengths and requiring larger energy to be pulled apart even for similar pull out lengths. It has to be also noted that both previous studies were done on woven fabrics and not on thin-ply non-crimp fabrics used in the current study. While Ortega et al. [111, 110] had a huge difference between their glass and carbon

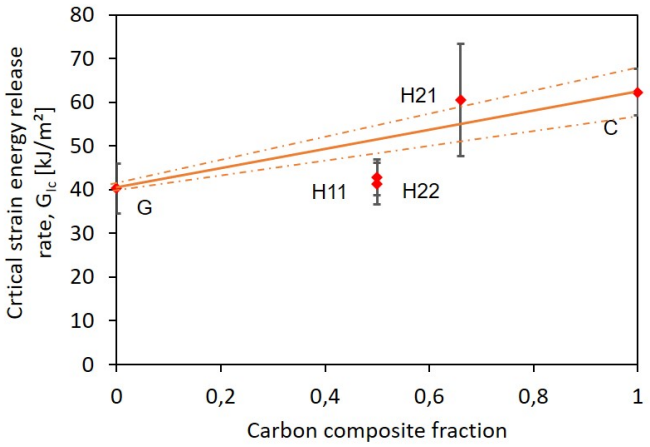

(a) Strain energy release rate: initiation

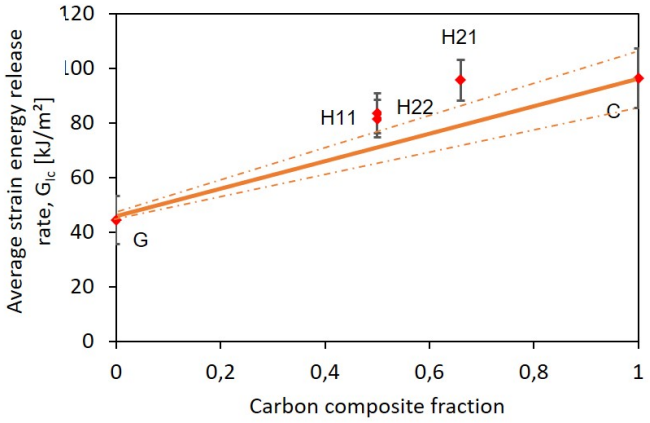

(b) Strain energy release rate: propagation

Fig. 6.17 Comparison of strain energy release rates and hybrid effect obtained via MCC method (a) initiation and (b) propagation.

fabric thicknesses, carbon being 50 % more thicker, made the interpretation of their results significantly more difficult.

For hybrids H11, H22 and H21, the fracture toughness at initiation was $42.9 \pm 4.1\,\mathrm{kJ\,m^{-2}}$, $41.4 \pm 4.8\,\mathrm{kJ\,m^{-2}}$ and $60.5 \pm 12.8\,\mathrm{kJ\,m^{-2}}$; while the average energy release rate for propagation was observed to be $81.5 \pm 6.9\,\mathrm{kJ\,m^{-2}}$, $83.5 \pm 7.4\,\mathrm{kJ\,m^{-2}}$ and $95.6 \pm 7.4\,\mathrm{kJ\,m^{-2}}$ respectively. The three hybrid layups deviated significantly from the linear Rule of Mixture behaviour. As can be observed in Fig. 6.17a, while the hybrids H11, H22 with 50 % carbon Fibre Volume Fraction showed a negative hybrid effect for initiation value, the H21 hybrid with 66 % carbon fibre volume ratio showed a significantly positive hybrid effect for initiation values. All the three hybrids, H11, H22 and H21, showed a significantly positive hybrid effect for critical energy release rate during propagation as can be seen in Fig. 6.17b.

Though the ply thickness effect is more relevant for cross ply laminates with unidirectional fibres [118, 151, 90], in the current study, both for initiation and propagation the hybrid effect observed is not attributed to the traditional ply thickness effect as the thickness of all the 5 fabrics were nearly similar. The hypothesis to explain the positive hybrid effect for translaminar fracture toughness of H21 is based on larger carbon bundle size and altogether to the larger proportion of carbon fibres (finer fibres) in the cross section. The results here hence agree with Pimenta and Pinho [118], who proved that larger bundles with more fibres lead to higher translaminar fracture toughness values. Swolfs et al. [141] reported in interply hybrids, if a carbon fibre ply is placed next to a glass fibre ply, the glass fibre ply will tend to reduce the pull-out lengths of the carbon. They further attributed owing to this reason a negative hybrid effect for a $(GC)_{4s}$ when compared to $(G_4C_4)_s$, because $(GC)_{4s}$ has more glass/carbon interfaces.

6.5.5 Fractography

Fractographic observations show pull out lengths of 0.5 to 2 mm for composite C as can be seen in Fig. 6.18a. The pullout lengths for carbon composite C were larger than that for the glass composite G, though they can not be compared directly as the stress state was not the same for these composites. For hybrids the pull-out lengths were more difficult to measure first because of intraply configuration and also due to random arrangement of positions of carbon or glass tows in the thickness direction. In the hybrid specimens the pull out lengths on average for carbon and glass fibres were similar (see Fig. 6.19a). Fibre bridging of 90° fibres was a dominant mechanism observed for hybrid composite (see Fig. 6.19b). Glass in the hybrids sometimes showed longer pullout lengths but these large pullouts were infrequent and not continuous unlike the continuous uniform pullouts in carbon fibres in the hybrid. The hybrid composite H21 altogether showed larger pullouts than the H11 or H22 composites and hence also demonstrating higher fracture toughness. This difference was higher in the middle of specimens compared to the rest of the specimen.

6.6 Conclusion

This study has investigated experimental work on carbon, glass and hybrid composites to obtain the fracture toughness associated with the fibre dominated failure modes using CT test method. It is shown that the data reduction process based on the stress intensity factor for isotropic materials should not be used for orthotropic materials and that the MCC or CC method are reliable alternative. Initiation and propagation energy release rate values for

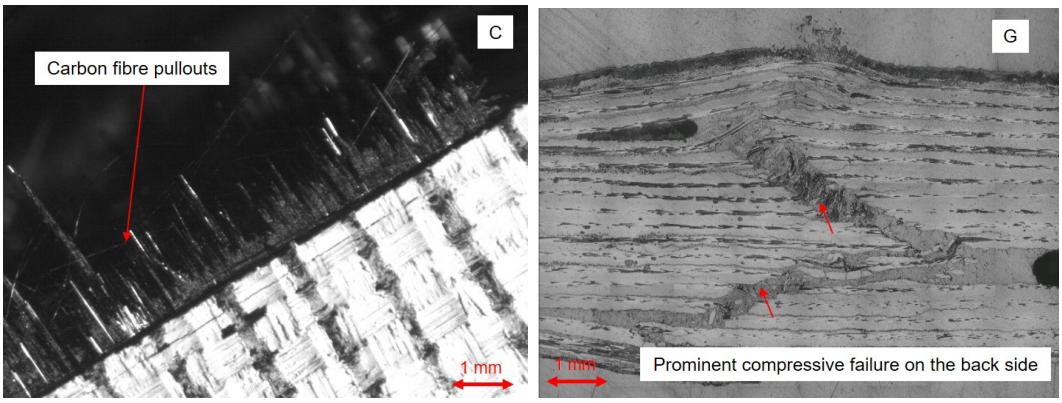

(a) Micrograph of the pullouts in composite C (b) Compressive failure in composite G

Fig. 6.18 Optical microscopy pictures of fracture surfaces for carbon and glass composite

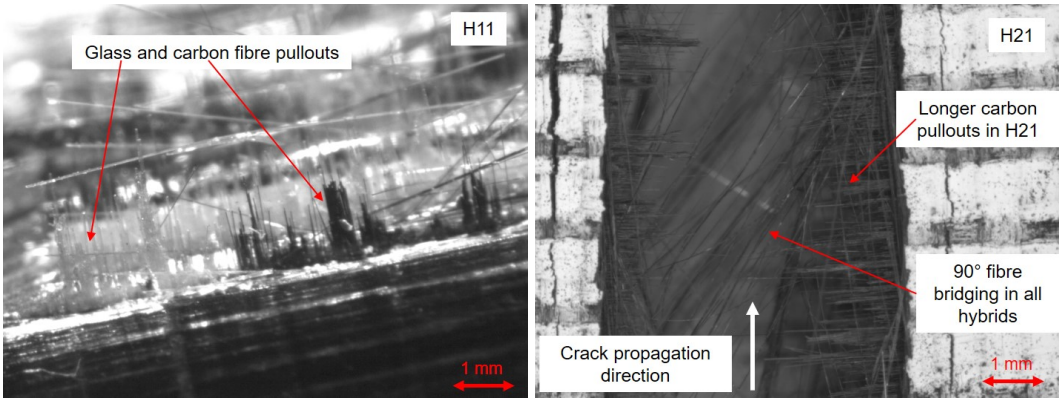

(a) Carbon and glass pullouts in H11 (b) Pullouts and bridging in H21

Fig. 6.19 Optical microscopy pictures of fracture surfaces for H11 and H21 hybrid composites.

hybrids H11 and H22 are not significantly different and hence for the same carbon fibre ratio, the changed microstructure due to altered tow dispersion did not affect the toughness of the composites. The hybrid H21 with higher carbon fibre fraction produced energy release rate values near the 100 % carbon composite C and demonstrated a positive hybrid effect both for energy release rates at initiation and propagation. For glass fibre composite a further optimisation of layup, specimen dimensions is essential to accurately characterise the fracture toughness using the CT method. The effect of fibre hybridisation on the translaminar fracture is hence demonstrated as it shows that hybridisation technique indeed triggers additional dissipative damage mechanisms; but the effect is not as large as expected and that further optimisation of the fibre hybridisation concept in terms of dispersion of fibres, types of fibres or for example hybrid ratios, is necessary.

Chapter 7

Conclusions and future work

Conclusions et travaux futurs

L'objectif de cette thèse était de développer une série de composites hybrides avancés utilisant des fibres de carbone et de verre et d'étudier leurs propriétés mécaniques. Plus précisément, il s'est agi de comprendre les comportements jusqu'à rupture de ces composites en conditions de traction, de flexion et de compression. Actuellement, la plupart des recherches sur les composites hybrides, y compris la thèse actuelle, s'intéresse au meilleur équilibre entre coûts et propriétés mécaniques. Il n'existe pas de composite idéal et universel qui pourrait correspondre à une multitude d'applications. Cela est également vrai pour les composites hybrides, pour lesquels une propriété est souvent améliorée au prix de la perte d'une autre. L'hybridation est essentiellement un compromis.

Le processus d'étalement des fibres a été identifié comme une étape intermédiaire essentielle pour la fabrication de renforts en carbone multiaxiaux plis fins à faible coût. Une étude expérimentale sur les mèches hybrides comélées a conclu que l'étalement de celles-ci est contre-productif. La technologie d'étalement permet de réaliser des hybridations à l'échelle des fibres à partir de mèches mono-matières à un coût raisonnable. Pour ces hybrides, une performance mécanique supérieure en traction, compression et flexion a été observée grâce à une meilleure dispersion du carbone et du verre. Par ailleurs, il a été montré via un test semi-automatisé de caractérisation monofilamentaire que le procédé sus-cité n'affecte pas de manière significative la distribution à rupture des renforts.

Les résultats présentés révèlent les avantages potentiels de l'hybridation à différents niveaux et dispersions. Ces résultats ouvrent une voie pour les futurs travaux sur les composites hybrides et leurs procédés de fabrication. Les futures études pourront s'intéresser de manière plus fine aux effets des fractions volumiques utilisées pour l'hybridation ainsi que l'incorporation d'autres natures de fibres. Cela pourra permettre le développement de nouveaux produits et offrir de nouvelles applications pour les composites hybrides. Tout cela ne pourra se faire sans investiguer les questions de durabilité et recyclabilité.

7.1 General discussion and critical reflection

The overall research objective in the current thesis was to develop a series of advanced hybrid composites using carbon and glass fibres and investigate their mechanical properties. More specifically, the plan was to understand the failure characteristics of non-hybrid and hybrid composites under tensile, flexural, and compressive loading conditions. Hybridisation in general offers an effective way of altering properties such as the failure strain of high modulus fibre composites, e.g. such as carbon fibre composites, while minimising its cost by adding some percentage of low modulus fibres, like glass or aramid. Such arrangement can lead to a possible decrease in in-plane strengths of hybrid composites compared with those of high modulus fibre composites. By combining two fibre types, it is possible to combine their advantages while simultaneously mitigating their less desirable qualities. Furthermore, such combination offers to designers and engineers a range of design options for specific applications. The design freedom that these hybrid composites provide is not only reflected in the choice of fibres and matrices, but also in aspects such as the hybrid configuration, fibre dispersion and orientations, stacking sequence and preform types.

Synergistic hybrid effects are achieved when the properties of the fibre hybrid composite are found to be higher or lower than expected. As an example, for properties such as failure strain, hybrid composite failure strain should remain constant irrespective of any other fibre type added to the low elongation fibre, but sometimes this is not the case. On the other hand, sometimes the expectation of the mechanical property is based on a Rule of Mixtures approach, based on the relative volume fraction of the two fibre types but the actual hybrid shows the mechanical property to be different than the expectation.

In the current thesis, T700S carbon fibres and E-CR glass fibres were selected to be the primary constituents for the hybridization study. These fibres were combined in three configurations: interply, intraply and intermingled (illustrated in Fig. 1.2). These configurations provided for the same hybrid volume fraction an altered dispersion and microstructure. Experimental studies were conducted in Chapter 2 on single fibre testing, in Chapter 3 on optimisation of the spreading technology, which paved a way to study reinforcement and composite fabrication, as well as the physical and mechanical characterisation of hybrid composites in Chapter 4, Chapter 5 and Chapter 6.

7.2 Main achievements and impacts

A composite that is ideal for all possible applications does not exist. This is also true for hybrid composites, where one property is often improved at the cost of another one,

therefore, hybridisation is essentially a compromise. The experimental results on loading of different configurations of hybrids provide a road map for optimising these composites for specific applications. In the process of achieving these insights several other tasks were performed, those include fibre characterisation, textile technology and its optimisation, composite fabrication, physical and mechanical characterisation of composite materials. Main achievements from of these studies are presented in the following sections.

The objective of experimental work in Chapter 2 was to understand the effect of textile processing on single fibre properties and to explore potential and challenges of single fibre tensile testing using a manual and an automated testing equipment setup. It was found that the automated testing can indeed overcome existing limitations and ensure consistent characterisation of single fibres with minimum human intervention. This further allows one to test statistically significant number of fibres. Pre-selection effect and strain induced stiffening of carbon fibres was proved to exist for carbon fibres. The results confirm a slight change in strength and distribution between fibres extracted from the as-received bobbin and the semi-finished textile preform, this effect is statistically not significant, considering the uncertainty associated with the measurement process.

Fibre spreading process was identified to be an essential intermediate step to manufacture low-cost thin-ply multiaxial carbon reinforcements. The optimisation study using glass fibres revealed that the spreading zone parameters such as Frequency, Temperature, Depth and Speed have significant effect on the spreading behaviour of glass fibres. It was also observed that the interaction effect among the parameters is critical for optimum spreading of glass fibres. This optimised setup from Chapter 3 further enables fabrication of a new generation of thin-ply reinforcements using glass along with other fibres. This strategy of hybridisation can be used to manufacture hybrids using different varieties of carbon fibres and opens vast possibilities in fibre hybrid composites and their applications. Experimental study on commingled rovings concluded that commingling affects the otherwise linear orientation of fibres and is a reason for a reduction of mechanical performance, furthermore, spreading of commingled rovings is counterproductive as it causes a lot of fibre breaks due to an inherent twist in the commingled roving structure.

Hybridisation tends to allow cost optimisation for composite materials for new application areas, where cost is a major factor. Direct material cost reduction is possible as for hybrids a costlier fibres are partially replaced by a relatively low cost fibres. On the other hand indirect reductions in material costs specifically using spreading technology based carbon fabrics is possible, owing to use of heavy tows (24 K or 50 K) which are one order of magnitude cheaper than finer tows to fabricate thin ply NCF's. Although the cost for raw material remains the same for a specific hybrid ratio, the processing of textiles and composite materials

for different dispersion can affect the final costs owing to use of different technologies. Intermingled hybrids fabricated from heavier carbon rovings allow cost savings, but the spreading process itself can add a significant amount to the processing cost, when compared to weaving or UD stitching. Furthermore, fabrication of composite materials using Resin Transfer Moulding process poses new challenges for hybrid composites, specifically when manufacturing composites that use thin-ply reinforcements. Higher injection pressure and adequate control of resin flow inside the mould by avoiding fibre-washing and race-tracking was observed to be critical for complete infiltration and obtaining a defect free part.

In terms of mechanical properties, tow level or intraply hybrids showed a synergistic effect in both tensile and compressive strengths while not reducing the failure strain. Macroscopic and microscopic observations confirm that the failure mode in tension is dominated by carbon fibre failure. In compression and bending, the failure of interply hybrid composite was observed to be more complex with several failure phenomena occurring simultaneously leading to the final failure. Although interply hybrids slightly increased the failure strain in tension, it demonstrated a negative synergy in all other properties. Ply level or interply hybrids, hence do not prove to be an ideal choice for composites subjected to complex loading conditions in structural applications. On the other hand, intraply hybrids for similar Fibre Volume Fractions showed a significantly positive synergistic effect in tensile and compressive strength while not reducing the failure strain in tension. This positive synergy was highest for intraply hybrids with 3 carbon and 3 glass tows blocked together.

The characterisation of translaminar fracture toughness in Chapter 6 for intraply hybrids and non-hybrids required manufacturing of thin-ply reinforcements for composites. It was shown that the data reduction process based on the stress intensity factor for isotropic materials should not be used for orthotropic materials and that the Modified Compliance Correction (MCC) or Compliance Correction (CC) method are reliable alternatives. For a similar hybrid volume fraction, altering the microstructure by tow blocking did not significantly affect the fracture toughness. For higher carbon volume fractions, the energy release rate for hybrid composites was observed to be closer to the reference carbon composite while also demonstrating a positive hybrid effect for energy release rates at initiation and propagation. The hybridisation technique indeed triggered additional dissipative damage mechanisms; however, the effect was not as large as expected and further optimisation of the fibre hybridisation concept is necessary for an enhanced toughness.

Intermingled hybrids based on commingling rovings demonstrated reduced stiffness and failure characteristics compared to other hybrid configurations. They demonstrated a negative hybrid effect in failure strain and no synergy in tensile and compressive strengths owing to their twisted microstructure. Spread tape based intermingled hybrids demonstrated a superior

mechanical performance in tension, bending and compression owing to the highest dispersion of carbon and glass fibres among all hybrid configurations. Spreading technology for fibre hybrid composites showed a tremendous potential due to its better dispersion capability without damaging or disorienting the fibres. Spreading can be a powerful approach to develop and investigate new hybrid materials, specifically those involving cost intensive fibre materials such as carbon and high strength glass fibres. The optimisation of simultaneous carbon/glass spreading parameters and the possibility of manufacturing thin ply materials can open new horizons for hybrid composites in high performance structural applications.

7.3 Limitations and future scope

Single fibre characterisation using an automated setup has now reached a technological level where statistically significant number of fibres can be tested to obtain statistically significant results. Single fibre testing can be a useful tool to characterise the effect of a physical or chemical environment during textile processing. However for these fibres, further characterising the geometry of the fibres becomes essential when to minimise uncertainties in strength measurements. Advanced techniques such as in-situ measurements of tensile strength can provide more information about the failure modes and flaws in the fibres.

Further studies on spreading of high strength glass fibres can enable fabrication of thin-ply glass reinforcements for high performance structural applications. In the future, the spreading technology can enable fabrication of intermingled hybrid composites with a higher dispersion. Future studies on simultaneous spreading of two technical fibres such as carbon and glass or a technical fibre along with a thermoplastic polymeric fibre can open new horizons for hybrid composite product and application development.

While in the current thesis the mechanical properties are characterised to evaluate stiffness and failure characteristics, future studies can focus on the mechanisms of failure under different loading conditions. In-situ characterisation of composites at the micro-scale and observing the failure mechanics through scanning electron microscopy or computer tomography can provide more insights into hybrid synergistic effects. Further, numerical modelling such as multi-scale modelling taking into consideration the damage and failure mechanisms at the level of each constituent can be addressed. These modelling tools at later stage can be extended for engineering components with real loading conditions (combined tension/compression, bending with multiaxial stress state).

Based on the mechanical performance results obtained in the thesis, a specific configuration can be selected for a suitable application and detailed studies of synergistic effect for a range of Fibre Volume Fractions can be carried out. These studies can further be extended to

other loading and performance conditions. Hybrid effect for composites containing carbon along with fibres such as Kevlar or Dyneema can be interesting for applications requiring a good ballistic and impact performance along with high strength. Studies on Cost economics of hybridization strategies should not be dissociated from studies enabling a better understanding of the intimate mechanisms of materials. Insights on materials and their mechanical behaviour along with associated costs can make it possible for industries to chose a specific hybrid material for actual product and applications.

Finally, sustainability and recyclability of hybrid composites needs to be addressed in future, as hybrid composites are now part of major industrial applications. Hybridisation can add complexity to the already highly complicated process chain of recycling of composite materials.

References

[1] AGY, S-2 glass (2016). S-2 glass reinforcement remains material of choice as vehicle armor evolves to meet higher threat levels. *Case History: Published on website*.

[2] Alagirusamy, R. and Ogale, V. (2004). Commingled and air jet-textured hybrid yarns for thermoplastic composites. *Journal of Industrial Textiles*, 33(4):223–243.

[3] Amacher, R., Cugnoni, J., Botsis, J., Sorensen, L., Smith, W., and Dransfeld, C. (2014). Thin ply composites: experimental characterization and modeling of size-effects. *Composites Science and Technology*, 101:121–132.

[4] Asp, L. E., Edgren, F., and Sjögren, A. (2004). Effects of stitch pattern on the mechanical properties of non-crimp fabric composites. *Proceeding of the 11 ECCM*, pages 31–05.

[5] ASTM (1999a). ASTM D3171-99 - Standard Test Methods for Constituent Content of Composite Materials. In *ASTM International*. ASTM Book of Standards.

[6] ASTM (1999b). ASTM D3800-16 - Standard Test Method for Density of High–Modulus Fibers. In *ASTM International*. ASTM Book of Standards.

[7] ASTM (2001). ASTM. D 6671/D 6671M-06 Mixed Mode I-Mode II Interlaminar Fracture Toughness of Unidirectional Fiber Reinforced Polymer Matrix Composites. In *ASTM International*. ASTM Book of Standards.

[8] ASTM (2003). ASTM E399-90 Standard Test Method for Linear-elastic Plane-strain Fracture Toughness of K_{lc} of Metallic Materials. In *ASTM International*. ASTM Book of Standards.

[9] ASTM (2014a). ASTM C1557-14 - Standard test method for tensile strength and young's modulus of fibers. In *ASTM International*. West Conshohocken, PA.

[10] ASTM (2014b). ASTM D3822 / D3822M-14 - Standard test method for tensile properties of single textile fibers. In *ASTM International*. West Conshohocken, PA.

[11] Aveston, J. and Sillwood, J. M. (1976). Synergistic fibre strengthening in hybrid composites. *Journal of Materials Science*, 11(10):1877–1883.

[12] AVK (September 2019). The Market for Glass Fibre Reinforced Plastics (GRP) in 2019. *Accessed on website*.

[13] Bajpai, A. (2018). *Modification of Epoxy Systems for Mechanical Performance Improvement*. PhD thesis, Technische Universität Kaiserslautern.

[14] Bazant, Z. P., Daniel, I. M., and Li, Z. (1996). Size effect and fracture characteristics of composite laminates. *Journal of engineering materials and technology*, 118(3):317–324.

[15] Beetz Jr, C. P. (1982). Strain-induced stiffening of carbon fibres. *Fibre Science and Technology*, 16(3):219–229.

[16] Bennett, S., Johnson, D., and Johnson, W. (1983). Strength-structure relationships in pan-based carbon fibres. *Journal of materials science*, 18(11):3337–3347.

[17] Berger, M.-H. and Jeulin, D. (2003). Statistical analysis of the failure stresses of ceramic fibres: Dependence of the weibull parameters on the gauge length, diameter variation and fluctuation of defect density. *Journal of materials science*, 38(13):2913–2923.

[18] Bibo, G., Hogg, P., and Kemp, M. (1997). Mechanical characterisation of glass-and carbon-fibre-reinforced composites made with non-crimp fabrics. *Composites science and technology*, 57(9-10):1221–1241.

[19] Blanco, N., Trias, D., Pinho, S., and Robinson, P. (2014a). Intralaminar fracture toughness characterisation of woven composite laminates. part i: Design and analysis of a compact tension (ct) specimen. *Engineering Fracture Mechanics*, 131:349–360.

[20] Blanco, N., Trias, D., Pinho, S., and Robinson, P. (2014b). Intralaminar fracture toughness characterisation of woven composite laminates. part ii: Experimental characterisation. *Engineering Fracture Mechanics*, 131:361–370.

[21] Borg, C. (2015). An introduction to spread tow reinforcements: Part 1–manufacture and properties. *Reinforced Plastics*, 59(4):194–198.

[22] Bullegas, G., Pinho, S. T., and Pimenta, S. (2016). Engineering the translaminar fracture behaviour of thin-ply composites. *Composites Science and Technology*, 131:110–122.

[23] Bunsell, A. and Harris, B. (1974). Hybrid carbon and glass fibre composites. *Composites*, 5(4):157–164.

[24] Bunsell, A. and Hearle, J. (1971). A mechanism of fatigue failure in nylon fibres. *Journal of Materials Science*, 6(10):1303–1311.

[25] Bunsell, A. R., Gorbatikh, L., Morton, H., Pimenta, S., Sinclair, I., Spearing, M., Swolfs, Y., and Thionnet, A. (2018). Benchmarking of strength models for unidirectional composites under longitudinal tension. *Composites Part A: Applied Science and Manufacturing*, 111:138–150.

[26] Busquets, G. G. (2016). *Improved delamination resistance of thin-ply based laminates: an experimental and numerical study*. PhD thesis, University of Girona.

[27] Callens, M., Gorbatikh, L., and Verpoest, I. (2014). Ductile steel fibre composites with brittle and ductile matrices. *Composites Part A: Applied Science and Manufacturing*, 61:235–244.

[28] Catalanotti, G., Camanho, P., Xavier, J., Dávila, C., and Marques, A. (2010). Measurement of resistance curves in the longitudinal failure of composites using digital image correlation. *Composites Science and Technology*, 70(13):1986–1993.

[29] Chamis, C., Lark, R., and Sinclair, J. (1981). Mechanical property characterization of intraply hybrid composites. In *Test Methods and Design Allowables for Fibrous Composites*. ASTM International.

[30] Chamis, C. C. (1983). Simplified composite micromechanics equations for hygral, thermal and mechanical properties. *Conf. of the Society of the Plastics Industry (SPI)*.

[31] Chi, Z., Chou, T.-W., and Shen, G. (1984). Determination of single fibre strength distribution from fibre bundle testings. *Journal of materials science*, 19(10):3319–3324.

[32] Choi, B., Diestel, O., and Offermann, P. (1999). Commingled cf/peek hybrid yarns for use in textile reinforced high performance rotors. *12th International Conference on Composite Materials (ICCM), Paris, France*, pages 796–806.

[33] Curtin, W. (2000a). Dimensionality and size effects on the strength of fiber-reinforced composites. *Composites Science and Technology*, 60(4):543–551.

[34] Curtin, W. A. (2000b). Tensile strength of fiber-reinforced composites: Iii. beyond the traditional weibull model for fiber strengths. *Journal of composite materials*, 34(15):1301–1332.

[35] Czél, G., Jalalvand, M., and Wisnom, M. R. (2016). Design and characterisation of advanced pseudo-ductile unidirectional thin-ply carbon/epoxy–glass/epoxy hybrid composites. *Composite Structures*, 143:362–370.

[36] De Greef, N., Gorbatikh, L., Godara, A., Mezzo, L., Lomov, S. V., and Verpoest, I. (2011). The effect of carbon nanotubes on the damage development in carbon fiber/epoxy composites. *Carbon*, 49(14):4650–4664.

[37] Deng, S., Ye, L., Mai, Y.-W., and Liu, H.-Y. (1998). Evaluation of fibre tensile strength and fibre/matrix adhesion using single fibre fragmentation tests. *Composites Part A: Applied Science and Manufacturing*, 29(4):423–434.

[38] Diao, H., Bismarck, A., Robinson, P., and Wisnom, M. (2012). Pseudo-ductile behaviour of unidirectional fibre reinforced polyamide-12 composite by intra-tow hybridization. In *Proceedings of ECCM*, volume 15.

[39] Donadon, M. V., Falzon, B. G., Iannucci, L., and Hodgkinson, J. M. (2007). Intralaminar toughness characterisation of unbalanced hybrid plain weave laminates. *Composites Part A: Applied Science and Manufacturing*, 38(6):1597–1611.

[40] Dong, C. and Davies, I. J. (2012). Optimal design for the flexural behaviour of glass and carbon fibre reinforced polymer hybrid composites. *Materials & Design*, 37:450–457.

[41] Dong, C. and Davies, I. J. (2013). Flexural properties of glass and carbon fiber reinforced epoxy hybrid composites. *Proceedings of the Institution of Mechanical Engineers, Part L: Journal of Materials: Design and Applications*, 227(4):308–317.

[42] Dong, C., Duong, J., and Davies, I. J. (2012). Flexural properties of s-2 glass and tr30s carbon fiber-reinforced epoxy hybrid composites. *Polymer Composites*, 33(5):773–781.

[43] Dorey, G., Sidey, G., and Hutchings, J. (1978). Impact properties of carbon fibre/kevlar 49 fibre hydrid composites. *Composites*, 9(1):25–32.

[44] Feih, S. and Mouritz, A. (2012). Tensile properties of carbon fibres and carbon fibre–polymer composites in fire. *Composites Part A: Applied Science and Manufacturing*, 43(5):765–772.

[45] Fischer, S. and Marom, G. (1987). The flexural behaviour of aramid fibre hybrid composite materials. *Composites science and technology*, 28(4):291–314.

[46] Flynn, J., Amiri, A., and Ulven, C. (2016). Hybridized carbon and flax fiber composites for tailored performance. *Materials & Design*, 102:21–29.

[47] Frossard, G. (2017). *Fracture of thin-ply composites effects of ply thickness*. PhD thesis, École polytechnique fédérale de Lausanne.

[48] Fukuda, H., Miyazawa, T., and Tomatsu, H. (1993). Strength distribution of monofilaments used for advanced composites. *ICCM/9. Composites: Properties and Applications.*, 6:687–694.

[49] Fukunaga, H., Chou, T.-W., and Fukuda, H. (1984). Strength of intermingled hybrid composites. *Journal of reinforced plastics and composites*, 3(2):145–160.

[50] Fukunaga, H., Chou, T.-W., and Fukuda, H. (1989). Probabilistic strength analyses of interlaminated hybrid composites. *Composites science and technology*, 35(4):331–345.

[51] Giancaspro, J. W., Papakonstantinou, C. G., and Balaguru, P. (2010). Flexural response of inorganic hybrid composites with e-glass and carbon fibers. *Journal of Engineering Materials and Technology*, 132(2):021005.

[52] Gigliotti, L. and Pinho, S. (2016). Translaminar fracture toughness of ncf composites with multiaxial blankets. *Materials & Design*, 94:410–416.

[53] González, E., Maimí, P., De Aja, J. S., Cruz, P., and Camanho, P. (2014). Effects of interply hybridization on the damage resistance and tolerance of composite laminates. *Composite Structures*, 108:319–331.

[54] Griffith, A. A. (1921). Vi. the phenomena of rupture and flow in solids. *Philosophical transactions of the royal society of london. Series A, containing papers of a mathematical or physical character*, 221(582-593):163–198.

[55] GUM (2008). GUM - Evaluation of measurement data – Guide to the expression of uncertainty in measurement. In *JCGM 100:2008*, page 134. *Published on website*.

[56] Harlow, D. (1997). Statistical properties of hybrid composites: asymptotic distributions for strain. *Reliability Engineering & System Safety*, 56(3):197–208.

[57] Harris, C. E. and Morris, D. (1986). A comparison of the fracture behavior of thick laminated composites utilizing compact tension, three-point bend, and center-cracked tension specimens. In *Fracture Mechanics: Seventeenth Volume*. ASTM International.

[58] Hayashi, T. (1972). On the improvement of mechanical properties of composites by hybrid composition. *8th Reinforced Plastics Group Conference*, 22:149.

[59] Hedgepeth, J. M. and Van Dyke, P. (1967). Local stress concentrations in imperfect filamentary composite materials. *Journal of composite materials*, 1(3):294–309.

[60] Henry, J. and Pimenta, S. (2018). Virtual testing framework for hybrid aligned discontinuous composites. *Composites Science and Technology*, 159:259–272.

[61] Hogg, P. J. (2005). Toughening of thermosetting composites with thermoplastic fibres. *Materials Science and Engineering: A*, 412(1-2):97–103.

[62] Hou, F. and Hong, S. (2014). Characterization of r-curve behavior of translaminar crack growth in cross-ply composite laminates using digital image correlation. *Engineering Fracture Mechanics*, 117:51–70.

[63] Hwang, S.-F. and Mao, C.-P. (1999). The delamination buckling of single-fibre system and interply hybrid composites. *Composite structures*, 46(3):279–287.

[64] Hwang, S.-F. and Mao, C.-P. (2001). Failure of delaminated interply hybrid composite plates under compression. *Composites Science and Technology*, 61(11):1513–1527.

[65] Ikbal, H., Wang, Q., Azzam, A., and Li, W. (2016). Effect of hybrid ratio and laminate geometry on compressive properties of carbon/glass hybrid composites. *Fibers and Polymers*, 17(1):117–129.

[66] Ikbal, M. H., Ahmed, A., Qingtao, W., Shuai, Z., and Wei, L. (2017). Hybrid composites made of unidirectional t600s carbon and e-glass fabrics under quasi-static loading. *Journal of Industrial Textiles*, 46(7):1511–1535.

[67] Irfan, M., Machavaram, V., Mahendran, R., Shotton-Gale, N., Wait, C., Paget, M., Hudson, M., and Fernando, G. (2012). Lateral spreading of a fiber bundle via mechanical means. *Journal of Composite Materials*, 46(3):311–330.

[68] Islam, F. (2020). *Probabilistic single fibre characterisation to improve stochastic strength modelling of unidirectional composites*. PhD thesis, Mines ParisTech, PSL University.

[69] Islam, F., Bucknell, S., Leray, Y., Bunsell, A., Laiarinandrasana, L., and Joannès, S. (2018a). Improvements in determination of carbon fibre strength distribution using automation and statistical data analysis. In *Fiber Society's Spring Conference 2018*, page 3 p., Tokyo, Japan.

[70] Islam, F., Joannès, S., Bucknell, S., Leray, Y., Bunsell, A., and Laiarinandrasana, L. (2018b). Towards accurate and efficient single fibre characterization to better assess failure strength distribution. In *ECCM18 European Conference on Composite Materials*.

[71] Islam, F., Joannès, S., and Laiarinandrasana, L. (2019). Evaluation of critical parameters in tensile strength measurement of single fibres. *Journal of Composites Science*, 3(3):69.

[72] ISO (1996). ISO 11566:1996 - Carbon fibre – Determination of the tensile properties of single-filament specimens. In *ISO Standards*. *Published on website*.

[73] ISO (1997). ISO 527-4:1997 - Determination of tensile properties – Part 4: Test conditions for isotropic and orthotropic fibre-reinforced plastic composites. In *ISO Standards*. *Published on website*.

[74] ISO (1998). ISO 14125:1998 - Fibre-reinforced plastic composites – Determination of flexural properties. In *ISO Standards*. *Published on website*.

[75] ISO (1999). ISO 14126:1999 - Fibre-reinforced plastic composites – Determination of compressive properties in the in-plane direction. In *ISO Standards*. *Published on website*.

[76] ISO (2001). ISO 15024:2001 Determination of mode I interlaminar fracture toughness, GIC, for unidirectionally reinforced materials. In *ISO standards*. book.

[77] ISO (2012). ISO 527-2:2012 - Plastics — Determination of tensile properties — Part 2: Test conditions for moulding and extrusion plastics. In *ISO Standards*. *Published on website*.

[78] ISO (2019). ISO 178:2019 - Plastics — Determination of flexural properties. In *ISO Standards*. *Published on website*.

[79] Jalalvand, M., Czél, G., and Wisnom, M. R. (2015). Parametric study of failure mechanisms and optimal configurations of pseudo-ductile thin-ply ud hybrid composites. *Composites Part A: Applied Science and Manufacturing*, 74:123–131.

[80] JIS (1993). JIS. K 7086-1993 Testing methods for interlaminar fracture toughness of carbon fibre reinforced plastics. In *Japanese Standards Association*. *Published on website*.

[81] Jones, F. and Huff, N. (2009). The structure and properties of glass fibres: Natural regenerated, inorganic, and specialist fibres. *Handbook of Textile Fiber Structure*, 2.

[82] Jose, S., Kumar, R. R., Jana, M., and Rao, G. V. (2001). Intralaminar fracture toughness of a cross-ply laminate and its constituent sub-laminates. *Composites Science and Technology*, 61(8):1115–1122.

[83] Kafi, A., Huson, M., Creighton, C., Khoo, J., Mazzola, L., Gengenbach, T., Jones, F., and Fox, B. (2014). Effect of surface functionality of pan-based carbon fibres on the mechanical performance of carbon/epoxy composites. *Composites Science and Technology*, 94:89–95.

[84] Kamiya, S. and Sekine, H. (1996). Prediction of the fracture strength of notched continuous fiber-reinforced laminates by interlaminar crack extension analysis. *Composites science and technology*, 56(1):11–21.

[85] Katafiasz, T., Iannucci, L., and Greenhalgh, E. (2019). Development of a novel compact tension specimen to mitigate premature compression and buckling failure modes within fibre hybrid epoxy composites. *Composite Structures*, 207:93–107.

[86] Kawabe, K. (2009). New carbon tow-spread technology and applications to advanced composite materials. *SAMPE journal*, 45(2):6–17.

[87] Kim, M., Choe, J., et al. (2016). Development of the fire-retardant sandwich structure using an aramid/glass hybrid composite and a phenolic foam-filled honeycomb. *Composite Structures*, 158:227–234.

[88] Kretsis, G. (1987). A review of the tensile, compressive, flexural and shear properties of hybrid fibre-reinforced plastics. *Composites*, 18(1):13–23.

[89] Laffan, M. (2011). *Development of translaminar fracture toughness testing methods for composite materials*. PhD thesis, Imperial College London.

[90] Laffan, M., Pinho, S., Robinson, P., and Iannucci, L. (2010). Measurement of the in situ ply fracture toughness associated with mode i fibre tensile failure in frp. part ii: Size and lay-up effects. *Composites Science and Technology*, 70(4):614–621.

[91] Laffan, M., Pinho, S., Robinson, P., and McMillan, A. (2012). Translaminar fracture toughness testing of composites: A review. *Polymer testing*, 31(3):481–489.

[92] Lee, B., Leong, K., and Herszberg, I. (2001). Effect of weaving on the tensile properties of carbon fibre tows and woven composites. *Journal of reinforced plastics and composites*, 20(8):652–670.

[93] LM Wind Power (April 2019). Extreme Measures: At 107 Meters, The World's Largest Wind Turbine Blade Is Longer Than A Football Field. Here's What It Looks Like. *Published on website*.

[94] Lucintel (March 2019). Composites market report: Trends, forecast and competitive analysis. *Published on website*.

[95] Mäder, E., Rausch, J., and Schmidt, N. (2008). Commingled yarns–processing aspects and tailored surfaces of polypropylene/glass composites. *Composites Part A: Applied Science and Manufacturing*, 39(4):612–623.

[96] Makeev, A., Ghaffari, S., and Seon, G. (2019). Improving compressive strength of high modulus carbon-fiber reinforced polymeric composites through fiber hybridization. *International Journal of Engineering Science*, 142:145–157.

[97] Manders, P. W. and Bader, M. (1981). The strength of hybrid glass/carbon fibre composites. *Journal of materials science*, 16(8):2246–2256.

[98] Markets and Markets (August 2017). Composites market by fiber type (glass, carbon), resin type (thermoset, thermoplastic), manufacturing process (layup, filament winding, pultrusion), application (transportation, aerospace and defense, wind energy), region - global forecast to 2022. *Published on website*.

[99] Markov, A., Fiedler, B., and Schulte, K. (2006). Electrical conductivity of carbon black/fibres filled glass-fibre-reinforced thermoplastic composites. *Composites Part A: Applied Science and Manufacturing*, 37(9):1390–1395.

[100] Matsuhisa, Y. and Bunsell, A. (2009). Tensile failure of carbon fibers. In *Handbook of Tensile Properties of Textile and Technical Fibres*, pages 574–602. Elsevier.

[101] Mencattelli, L., Tang, J., Swolfs, Y., Gorbatikh, L., and Pinho, S. T. (2019). Bio-inspired design for enhanced damage tolerance of self-reinforced polypropylene/carbon fibre polypropylene hybrid composites. *Composites Part A: Applied Science and Manufacturing*, 121:341–352.

[102] Mishnaevsky Jr, L. and Dai, G. (2014). Hybrid carbon/glass fiber composites: Micromechanical analysis of structure–damage resistance relationships. *Computational Materials Science*, 81:630–640.

[103] Mochane, M., Mokhena, T. C., Mokhothu, T., Mtibe, A., Sadiku, E., Ray, S. S., Ibrahim, I., and Daramola, O. (2019). Recent progress on natural fiber hybrid composites for advanced applications: A review. *Express Polymer Letters*, 13(2):159–198.

[104] Mordor Intelligence (2018). Thermoplastic Composites Market - Growth, trends and forecast (2019-2024). *Published on website*.

[105] Naik, N., Ramasimha, R., Arya, H., Prabhu, S., and ShamaRao, N. (2001). Impact response and damage tolerance characteristics of glass–carbon/epoxy hybrid composite plates. *Composites Part B: Engineering*, 32(7):565–574.

[106] Naito, K., Yang, J.-M., Tanaka, Y., and Kagawa, Y. (2012). The effect of gauge length on tensile strength and weibull modulus of polyacrylonitrile (pan)-and pitch-based carbon fibers. *Journal of Materials Science*, 47(2):632–642.

[107] Nedele, M. and Wisnom, M. (1994). Stress concentration factors around a broken fibre in a unidirectional carbon fibre-reinforced epoxy. *Composites*, 25(7):549–557.

[108] Nunna, S., Chandra, P. R., Shrivastava, S., and Jalan, A. (2012). A review on mechanical behavior of natural fiber based hybrid composites. *Journal of Reinforced Plastics and Composites*, 31(11):759–769.

[109] Okuda, H., Young, R. J., Tanaka, F., Watanabe, J., and Okabe, T. (2016). Tensile failure phenomena in carbon fibres. *Carbon*, 107:474–481.

[110] Ortega, A., Maimí, P., González, E., de Aja, J. S., de la Escalera, F., and Cruz, P. (2017). Translaminar fracture toughness of interply hybrid laminates under tensile and compressive loads. *Composites Science and Technology*, 143:1–12.

[111] Ortega, A., Maimí, P., González, E., and Ripoll, L. (2014). Compact tension specimen for orthotropic materials. *Composites Part A: Applied Science and Manufacturing*, 63:85–93.

[112] Pandya, K. S., Pothnis, J. R., Ravikumar, G., and Naik, N. (2013). Ballistic impact behavior of hybrid composites. *Materials & Design*, 44:128–135.

[113] Pandya, K. S., Veerraju, C., and Naik, N. (2011). Hybrid composites made of carbon and glass woven fabrics under quasi-static loading. *Materials & Design*, 32(7):4094–4099.

[114] Peijs, A., Catsman, P., Govaert, L., and Lemstra, P. (1990). Hybrid composites based on polyethylene and carbon fibres part 2: influence of composition and adhesion level of polyethylene fibres on mechanical properties. *Composites*, 21(6):513–521.

[115] Perry, A., Ineichen, B., and Eliasson, B. (1974). Fibre diameter measurement by laser diffraction. *Journal of Materials Science*, 9(8):1376–1378.

[116] Phillips, L. (1976). The hybrid effect-does it exist? *Composites*, 7:7–8.

[117] Phillips, M. (1981). Composition parameters for hybrid composite materials. *Composites*, 12(2):113–116.

[118] Pimenta, S. and Pinho, S. T. (2014). An analytical model for the translaminar fracture toughness of fibre composites with stochastic quasi-fractal fracture surfaces. *Journal of the Mechanics and Physics of Solids*, 66:78–102.

[119] Pinho, S. T., Robinson, P., and Iannucci, L. (2006). Fracture toughness of the tensile and compressive fibre failure modes in laminated composites. *Composites science and technology*, 66(13):2069–2079.

[120] Rajpurohit, A. and Henning, F. (2017). Bio-fiber thermoset composites. In *Lightweight and Sustainable Materials for Automotive Applications*, pages 39–92. CRC Press.

[121] Rajpurohit, A., Joannès, S., Singery, V., Sanial, P., and Laiarinandrasana, L. (2020). Hybrid effect in in-plane loading of carbon/glass fibre based inter-and intraply hybrid composites. *Journal of Composites Science*, 4(1):6.

[122] Rajpurohit, A., Singery, V., Joannès, S., Sanial, P., and Laiarinandrasana, L. (2018a). Manufacturing and performance of hybrid fabric reinforcements and their composites. *ECCM18, European Conference on Composite Materials, Athens, Greece*.

[123] Rajpurohit, A., Singery, V., Joannès, S., Sanial, P., and Laiarinandrasana, L. (2019). Development and performance evaluation of inter-ply and intra-ply hybrid fabric reinforcements and their composites. *ICRACM2019, International Conference on Recent Advances in COmposite Materials, Varanasi, India*.

[124] Rajpurohit, A., Singery, V., Joannès, S., Sanial, P., Laiarinandrasana, L., Islam, F., and Bucknell, S. (2018b). Characterization and statistical analysis of single fibre strength of fibres at various processing stages. *ICCM 22, International Conference on Composite Materials, Melbourne, Australia*.

[125] Ren, P., Zhang, Z., Xie, L., Ren, F., Jin, Y., Di, Y., and Fang, C. (2010). Hybrid effect on mechanical properties of m40-t300 carbon fiber reinforced bisphenol a dicyanate ester composites. *Polymer Composites*, 31(12):2129–2137.

[126] Rojek, J., Joannès, S., Teissedre, J.-C., Laiarinandrasana, L., and Bunsell, A. (2019). Effect of through-thickness compressive stress and porosity on the tensile strength of carbon-fibre reinforced composites. *ICCM 22, International Conference on Composite Materials, Melbourne, Australia*.

[127] Rosen, B. W. (1964). Tensile failure of fibrous composites. *AIAA journal*, 2(11):1985–1991.

[128] Sanial, P. (2013). How c-ply can change the way we design and manufacture. *Innovative composites summit, Singapore*.

[129] Schnabel, A. and Gries, T. (2011). Production of non-crimp fabrics for composites. In *Non-Crimp Fabric Composites*, pages 3–41. Elsevier.

[130] Selver, E., Potluri, P., Hogg, P., and Soutis, C. (2016). Impact damage tolerance of thermoset composites reinforced with hybrid commingled yarns. *Composites Part B: Engineering*, 91:522–538.

[131] Shahidi, E. (2015). C-ply sp (thin plies) usage for aerospace applications : potential benefits. *Franco-British Symposium on Composite Materials*.

[132] Shokrieh, M. M. and Omidi, M. J. (2005). Reinforcement of metallic plates with composite materials. *Journal of composite materials*, 39(8):723–744.

[133] Sihn, S., Kim, R. Y., Kawabe, K., and Tsai, S. W. (2007). Experimental studies of thin-ply laminated composites. *Composites Science and Technology*, 67(6):996–1008.

[134] Singery, V. (2016). *C-Ply (Trademark) Ultra light CarbonNCF : Study of the manufacturing process and textile reinforcement optimization*. PhD thesis, Université de Haute-Alsace.

[135] Soares, C. G. (1997). Reliability of components in composite materials. *Reliability Engineering & System Safety*, 55(2):171–177.

[136] Studart, A. R. (2012). Towards high-performance bioinspired composites. *Advanced Materials*, 24(37):5024–5044.

[137] Sudarisman, S., San Miguel, B. D., and Davies, I. J. (2009). The effect of partial substitution of e-glass fibre for carbon fibre on the mechanical properties of cfrp composites. *International Conference on Materials and Metallurgical Technology 2009 (ICOMMET 2009)*.

[138] Summerscales, J. (1983). *The mechanical properties of carbon fibre with glass fibre hybrid reinforced plastics*. PhD thesis, University of Plymouth.

[139] Svensson, N., Shishoo, R., and Gilchrist, M. (1998). Manufacturing of thermoplastic composites from commingled yarns-a review. *Journal of Thermoplastic Composite Materials*, 11(1):22–56.

[140] Swolfs, Y. (2015). *Hybridization of self reinforced composites. Modelling and verifying a novel hybrid concept*. PhD thesis, KU Leuven.

[141] Swolfs, Y., Geboes, Y., Gorbatikh, L., and Pinho, S. T. (2017). The importance of translaminar fracture toughness for the penetration impact behaviour of woven carbon/glass hybrid composites. *Composites Part A: Applied Science and Manufacturing*, 103:1–8.

[142] Swolfs, Y., Gorbatikh, L., Romanov, V., Orlova, S., Lomov, S. V., and Verpoest, I. (2013). Stress concentrations in an impregnated fibre bundle with random fibre packing. *Composites Science and Technology*, 74:113–120.

[143] Swolfs, Y., Gorbatikh, L., and Verpoest, I. (2014). Fibre hybridisation in polymer composites: a review. *Composites Part A: Applied Science and Manufacturing*, 67:181–200.

[144] Swolfs, Y., McMeeking, R. M., Verpoest, I., and Gorbatikh, L. (2015a). The effect of fibre dispersion on initial failure strain and cluster development in unidirectional carbon/glass hybrid composites. *Composites Part A: Applied Science and Manufacturing*, 69:279–287.

[145] Swolfs, Y. and Pinho, S. T. (2019). 3d printed continuous fibre-reinforced composites: Bio-inspired microstructures for improving the translaminar fracture toughness. *Composites Science and Technology*, 182:107731.

[146] Swolfs, Y., Verpoest, I., and Gorbatikh, L. (2015b). Issues in strength models for unidirectional fibre-reinforced composites related to weibull distributions, fibre packings and boundary effects. *Composites Science and Technology*, 114:42–49.

[147] Swolfs, Y., Verpoest, I., and Gorbatikh, L. (2016). A review of input data and modelling assumptions in longitudinal strength models for unidirectional fibre-reinforced composites. *Composite Structures*, 150:153–172.

[148] Swolfs, Y., Verpoest, I., and Gorbatikh, L. (2018). Recent advances in fibre-hybrid composites: materials selection, opportunities and applications. *International Materials Reviews*, pages 1–35.

[149] Taketa, I. (2011). *Analysis of failure mechanisms and hybrid effects in carbon fibre reinforced thermoplastic composites*. PhD thesis, KU Leuven, Belgium.

[150] Tanaka, F., Okabe, T., Okuda, H., Kinloch, I. A., and Young, R. J. (2014). Factors controlling the strength of carbon fibres in tension. *Composites Part A: Applied Science and Manufacturing*, 57:88–94.

[151] Teixeira, R., Pinho, S., and Robinson, P. (2016). Thickness-dependence of the translaminar fracture toughness: experimental study using thin-ply composites. *Composites Part A: Applied Science and Manufacturing*, 90:33–44.

[152] Thanomsilp, C. and Hogg, P. (2005). Interlaminar fracture toughness of hybrid composites based on commingled yarn fabrics. *Composites science and technology*, 65(10):1547–1563.

[153] Thomason, J. (2013). On the application of weibull analysis to experimentally determined single fibre strength distributions. *Composites Science and Technology*, 77:74–80.

[154] Todinov, M. (2009). Is weibull distribution the correct model for predicting probability of failure initiated by non-interacting flaws? *International journal of Solids and Structures*, 46(3-4):887–901.

[155] Toray Industries, Inc. (2014). Toray Develops High Tensile Strength and Modulus Carbon Fiber TORAYCA T1100G and High-performance TORAYCA Prepreg. *Accessed on website*.

[156] Turner, T., Warrior, N., and Pickering, S. (2010). Development of high value moulding compounds from recycled carbon fibres. *Plastics, Rubber and Composites*, 39(3-5):151–156.

[157] Underwood, J. and Kortschot, M. (1994). Notch-tip damage and translaminar fracture toughness measurements from carbon/epoxy laminates. Technical report, Army Armament Research Development and Engineering Center, Watervliet, NY BENET Labs.

[158] Vaidya, R. S. and Sun, C. (1997). Fracture criterion for notched thin composite laminates. *AIAA journal*, 35(2):311–316.

[159] Wang, F., Ma, X., Zhang, Y., and Jia, S. (2018a). Lightning damage testing of aircraft composite-reinforced panels and its metal protection structures. *Applied Sciences*, 8(10):1791.

[160] Wang, Q., Wu, W., Gong, Z., and Li, W. (2018b). Flexural progressive failure of carbon/glass interlayer and intralayer hybrid composites. *Materials*, 11(4):619.

[161] Wang, Q., Wu, W., and Li, W. (2018c). Compression properties of interlayer and intralayer carbon/glass hybrid composites. *Polymers*, 10(4):343.

[162] Watson, A. S. and Smith, R. (1985). An examination of statistical theories for fibrous materials in the light of experimental data. *Journal of Materials Science*, 20(9):3260–3270.

[163] Weibull, W. et al. (1951). A statistical distribution function of wide applicability. *Journal of applied mechanics*, 18(3):293–297.

[164] Wisnom, M., Khan, B., and Hallett, S. (2008). Size effects in unnotched tensile strength of unidirectional and quasi-isotropic carbon/epoxy composites. *Composite Structures*, 84(1):21–28.

[165] Wisnom, M. R., Czél, G., Swolfs, Y., Jalalvand, M., Gorbatikh, L., and Verpoest, I. (2016). Hybrid effects in thin ply carbon/glass unidirectional laminates: accurate experimental determination and prediction. *Composites Part A: Applied Science and Manufacturing*, 88:131–139.

[166] Witik, R. A., Payet, J., Michaud, V., Ludwig, C., and Månson, J.-A. E. (2011). Assessing the life cycle costs and environmental performance of lightweight materials in automobile applications. *Composites Part A: Applied Science and Manufacturing*, 42(11):1694–1709.

[167] Xia, Y. and Ruiz, C. (1991). Analysis of damage in stress wave loaded unidirectional composites. *Computers & Structures*, 38(3):251–258.

[168] Yerramalli, C. S. and Waas, A. (2003). Compressive behavior of hybrid composites. In *44th AIAA/ASME/ASCE/AHS/ASC Structures, Structural Dynamics, and Materials Conference*, page 1509.

[169] You, Y.-J., Park, Y.-H., Kim, H.-Y., and Park, J.-S. (2007). Hybrid effect on tensile properties of frp rods with various material compositions. *Composite structures*, 80(1):117–122.

[170] Yu, H., Longana, M. L., Jalalvand, M., Wisnom, M. R., and Potter, K. D. (2015). Pseudo-ductility in intermingled carbon/glass hybrid composites with highly aligned discontinuous fibres. *Composites Part A: Applied Science and Manufacturing*, 73:35–44.

[171] Zhang, J., Chaisombat, K., He, S., and Wang, C. H. (2012). Hybrid composite laminates reinforced with glass/carbon woven fabrics for lightweight load bearing structures. *Materials & Design (1980-2015)*, 36:75–80.

[172] Zhang, W. (2016). Technical problem identification for the failures of the liberty ships. *Challenges*, 7(2):20.

[173] Zinck, P., Pay, M., Rezakhanlou, R., and Gerard, J. (1999). Mechanical characterisation of glass fibres as an indirect analysis of the effect of surface treatment. *Journal of materials science*, 34(9):2121–2133.

[174] Zion Market Research (October 2019). Global industry perspective, comprehensive analysis and forecast, 2017 – 2024.

[175] Zweben, C. (1968). Tensile failure of fiber composites. *AIAA journal*, 6(12):2325–2331.

[176] Zweben, C. (1977). Tensile strength of hybrid composites. *Journal of Materials Science*, 12(7):1325–1337.

Appendix A

A.1 Theoretical calculation for strength of hybrid composite

Tensile strength for unidirectional composites can be assessed using the Rule of Mixtures involving fibre and matrix properties and volume fractions. The basic assumptions used for these calculations are: both matrix and fibres are linearly elastic, isotropic, and homogeneous, fibres are perfectly aligned and spaced, matrix is void free, and bonding between matrix and fibres is perfect. A similar approach is used for assessing the strength of hybrid composites using the Rule of Mixtures involving the properties of carbon fibre composite and glass fibre composite and composite volume fraction. It has to be noted that, at lower carbon composite volume fractions, the property of hybrid composites would be governed by glass fibre composite properties, whereas at higher carbon composite volume fractions, it would be governed by carbon fibre composite properties. Hence, at lower carbon composite volume fractions (in tension):

$$\sigma^h_{\max} = \sigma^g_{\max} \times (1 - V_c) \tag{A.1}$$

and, at higher carbon composite volume fractions (in tension):

$$\sigma^h_{\max} = \sigma^c_{\max} \times V_c + (\sigma^g)_{\varepsilon^c_{\max}} \times (1 - V_c) \tag{A.2}$$

where $\sigma^h_{\max}$ is the tensile strength of hybrid composite; $\sigma^c_{\max}$ is the tensile strength of carbon composite; $\sigma^g_{\max}$ is the tensile strength of glass composite; $(\sigma^g)_{\varepsilon^c_{\max}}$ is the stress in glass composite corresponding to ultimate strain of carbon composite; and V_c is the carbon composite volume fraction.

Point B in the figures (for synergistic effects) is obtained by using these two equations (A.1) and (A.2) for a range of carbon composite volume fractions. It represents the minimum strength that can be obtained by combining the two fibres and the carbon composite volume ratio associated with it.

Sample calculations for hybrid composite under in–plane tensile loading can be done using: $V_c = 0.62$; $\sigma^c_{\max} = 1165$ MPa, $\varepsilon^c_{\max} = 1.7$ %, and $\sigma^g = 386$ MPa Now, using Eq. A.2,

$$\sigma^h_{\max} = 869 \text{ MPa}$$

Similar calculations can be done for in-plane compressive strength of hybrid composites.

A.2 Calculation of hybrid effect

For change in failure strain (in tensile, compression and flexural loading) in hybrids, the hybrid effect (λ) is calculated from Eq. A.3 below. Here an increase in the failure strain of hybrid composites over failure strain of reference low elongation composite is considered to be positive hybrid effect.

$$\lambda_{\text{failure strain}} = \frac{\varepsilon_H}{\varepsilon_{LE}} - 1 \tag{A.3}$$

where, ε_H is the failure strain for hybrid composite and ε_{LE} is the failure strain for low elongation composite (carbon composite in the current work).

For the tensile and compressive strengths, the hybrid effect is calculated by the Eq. A.4. A positive hybrid effect here is defined as a positive deviation of a certain mechanical property from the Rule of Mixture behaviour.

$$\lambda_{\text{strength}} = \frac{\sigma_H}{\sigma_{\text{RoM}}} - 1 \tag{A.4}$$

where, σ_H is experimentally obtained strength of hybrid composite and σ_{RoM} is theoretically obtained value for hybrid composite using Rule of Mixture (equal to the $\sigma^h_{\max}$ from Eq. A.2).

For instance, for tensile test of intraply hybrid H3, $\varepsilon_H = 1.67$ %, $\varepsilon_{LE} = 1.7$ %, $\sigma_H = 1024$ MPa and $\sigma_{\text{RoM}} = \sigma^h_{\max} = 869$ MPa. Hence, using above equations,

$$\lambda_{\text{failure strain}} = +1.8 \text{ \%}$$
$$\lambda_{\text{strength}} = +17.8 \text{ \%}$$

Appendix B

B.1 Specimen preparation and characterisation

Mechanical behaviour of selected resin system (Araldite LY 564 & Aradur 2954) was characterised by testing pure resin samples in tension and flexion. Using RTM process pre-mixed resin and hardener (100:35) was injected in a closed mould (500 mm × 500 mm) with cavity thickness of 4 mm. The resin was then cured in the mould in accordance to the curing cycle that was used for the all the composites fabricated in this thesis and presented in Fig. 4.4d. The samples were then cut from the neat resin plate in the flow direction (0°) and transverse to the flow direction (90°) and characterised in the mechanical tests.

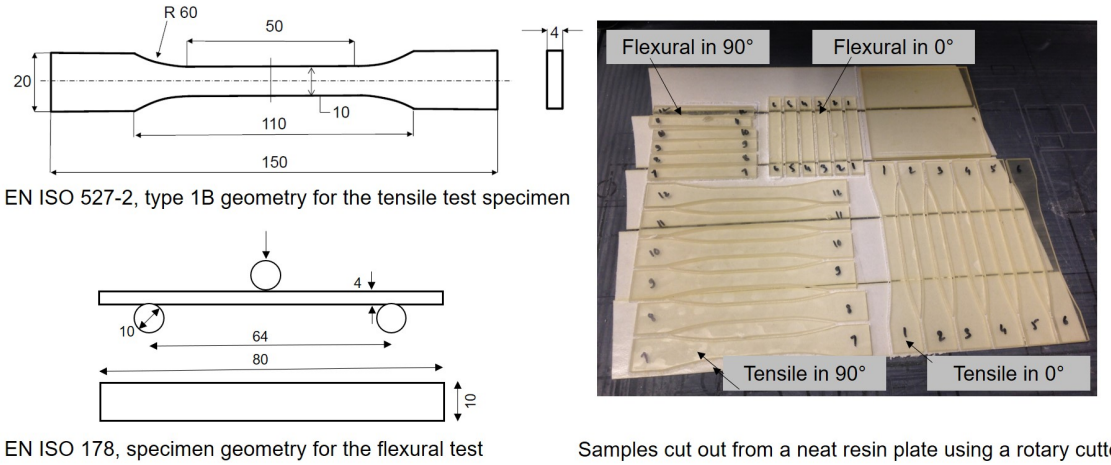

Fig. B.1 Specimen dimensions and orientation of samples.

Quasi-static tensile and flexural tests were conducted using a Universal Testing Machine (UTM) from Instron using a load cell with maximum capacity of 10 kN. Five samples for each orientation were tested according to ISO 527-2 standard [77] for tensile and ISO 178 standard [78] for flexural loading. The schematic of specimen dimensions is presented in Fig. B.1. The loading step was controlled with a cross-head speed of 2 mm min^{-1} for both loading

conditions. The strain in the composite was measured using optical strain gauge setup, namely, Advanced Video Extensiometer attached to the Instron UTM. The tensile and flexural strength was determined using the stress-strain curve and the modulus was determined by calculating the slope of the initial linear portion (from 0.05 to 0.25 % of strain values) of the obtained curve.

B.2 Mechanical properties

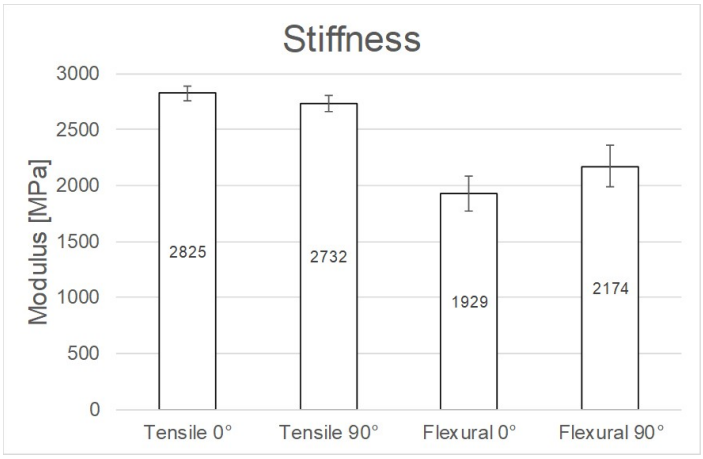

(a) Stiffness

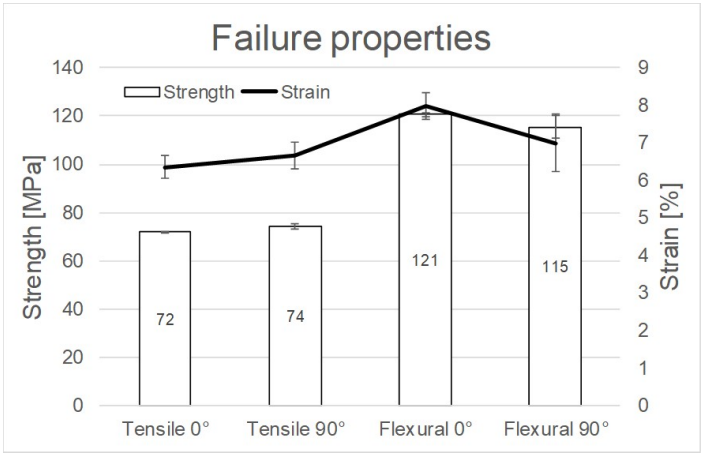

(b) Failure characteristics

Fig. B.2 Properties of neat resin along 0° and 90° in tension and compression: (**a**) Stiffness (**b**) Failure characteristics.

The density of neat cured resin samples were measured using buoyancy method as per ASTM standard D3800-16 [6] was found to be 1.13 $\mathrm{g\,cm^{-3}}$.

It was found that the stiffness of neat resin in tension is significantly higher than in the flexural loading. Stiffness for the neat resin tested is not dependent on the flow behaviour, i.e. the stiffness in both tension and compression in longitudinal and transverse direction were not significantly different. The average strength and failure strain in tension are observed to be lower than the flexural strength and failure strain. The actual measured tensile properties are in-line with the properties for the resin in the technical data sheet and the coefficient of variation for the measure values is less than 5 %; this confirms the curing parameters used in the current study are reliable.

Appendix C

C.1 Additional composite cross-sectional pictures

The cross-section of all the reference, interply and intraply composites developed in Chapter 4 can be seen in Fig. C.1.

The cross-section of all intermingled hybrid composites developed in Chapter 5 can be seen in Fig. 5.10a and Fig. 5.10b.

The cross-section of all thin-ply composites developed in Chapter 6 for translaminar fracture toughness study can be seen in Fig. 6.9 (a)-(d).

C.2 Additional microscopic images of fracture surfaces in different loading conditions

Microscopic images of fracture surfaces in tensile, compression and flexural loading of interply and intraply hybrids are presented in Fig. 4.16, Fig. 4.17 and Fig. 4.18. Additional images of failure of carbon fibres in reference carbon composite is presented in Fig. C.2.

Microscopic images of fracture surfaces in tensile, compression and flexural loading of intermingled hybrids are presented in Fig. 5.14, Fig. 5.15 and Fig. 5.16 respectively.

For thin-ply hybrids tested in the Compact Tension test, the failure micrographs are presented in Fig. 6.18 and Fig. 6.19. For H11 hybrid the bridging and pullout of fibres in the CT test is presented in Fig. C.3.

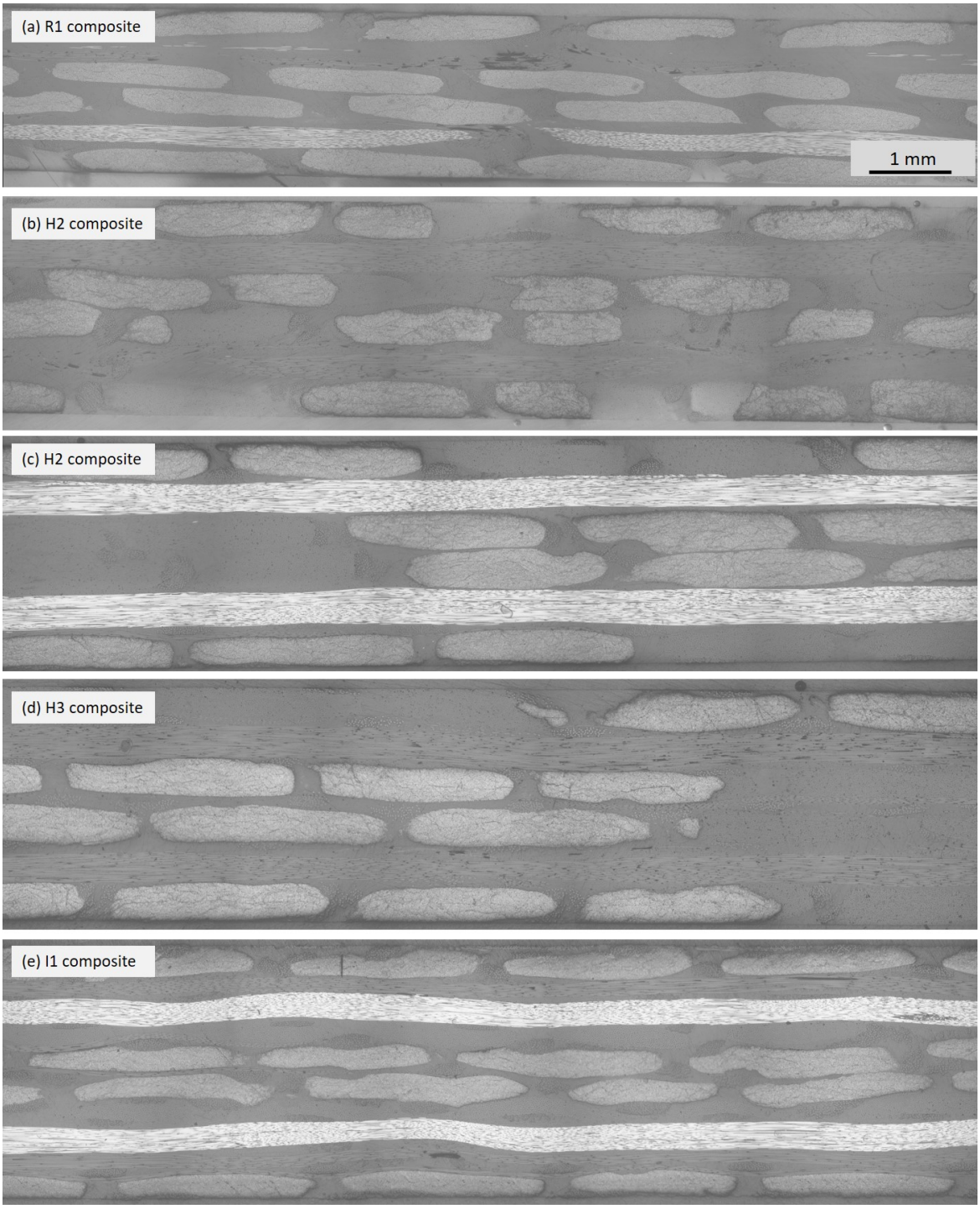

Fig. C.1 Optical microscopy images of reference, interply and intraply composites.

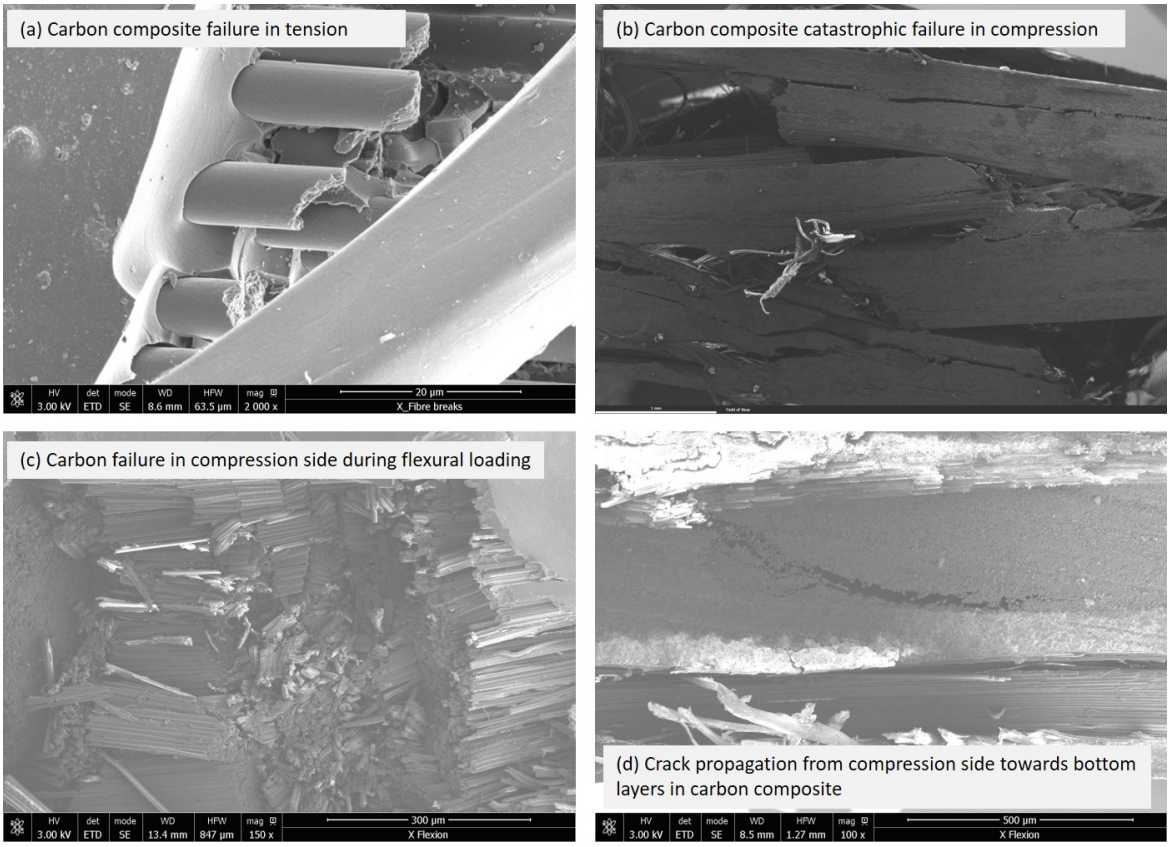

Fig. C.2 Carbon fibre failure in different loading conditions.

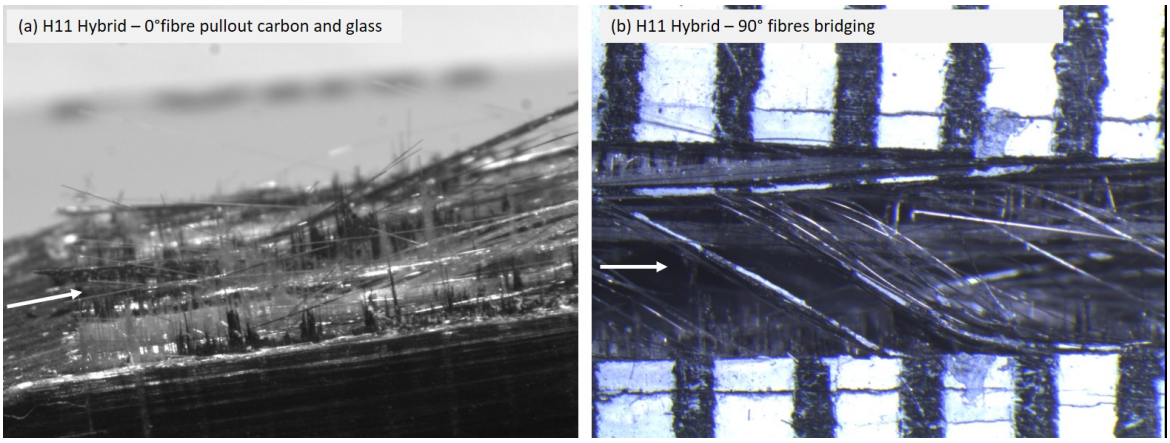

Fig. C.3 Fracture surface of H11 composite sample tested in CT test

RÉSUMÉ

Les composites hybrides offrent un moyen efficace d'améliorer les propriétés mécaniques des matériaux composites. Cette thèse vise à comprendre le comportement mécanique et l'effet synergique offerts par de tels composites hybrides sous plusieurs conditions de chargement. L'accent est mis, non seulement sur la caractérisation mécanique, mais également sur le développement et l'optimisation de nouvelles générations de renforts hybrides, permettant ainsi une hybridation aussi bien au niveau des nappes, qu'au niveau des mèches et des fibres. Dans ce travail, les fibres de carbone et de verre sont choisies comme les deux types de renforts pour les composites hybrides. Les propriétés de ces fibres unitaires sont d'abord caractérisées pour étudier l'impact des procédés textiles. De nouveaux renforts unidirectionnels ont été fabriqués après avoir optimisé les procédés, tels que la technologie UD cousu et l'étalement des fibres. Les composites ont été fabriqués via RTM basse pression en utilisant une résine époxy. Les caractéristiques en raideur et en résistance des composites de référence, des hybrides inter-plis, intra-plis et fibre à fibre ont ensuite été caractérisées dans des conditions de charge quasi-statique en traction, compression et flexion. L'effet d'hybridation (synergique) a été évalué pour ces composites en comparant les propriétés du composite hybride avec un composite de référence en carbone. Afin de comprendre le comportement à rupture de ces composites dans différentes conditions de charge, une étude de fractographie a été réalisée. Les hybrides inter-plis font apparaître une légère augmentation de la déformation à rupture en traction mais présentent une synergie négative pour toutes les autres conditions. Les hybrides intra-plis montrent eux, un effet synergique pour les résistances à la traction et à la compression, sans réduire leur déformation à rupture. Un composite hybride fibre à fibre réalisé par étalement montre une performance mécanique supérieure par rapport à d'autres hybrides. Les résultats présentés révèlent les avantages potentiels de l'hybridation à différents niveaux et dispersions. Les résultats ouvrent une voie pour les futurs travaux sur les composites hybrides et leurs procédés.

MOTS CLÉS

Renforts textiles hybrides, composites structurels, hybrides inter/intra-plis, hybrides fibre à fibre (comélés), propriétés mécaniques, effet d'hybridation/synergique.

ABSTRACT

Hybrid composites offer an effective way of enhancing mechanical properties of composite materials. This thesis aims to understand the mechanical behaviour and synergistic effect offered by such hybrid composites in several loading conditions. The focus not only lies on mechanical characterisation but also on development and optimization of new generation of hybrid reinforcements thus allowing hybridization both at ply levels and at tow and fibre levels. In this work, carbon and glass fibres are chosen as the two types of reinforcements for hybrid composites. Single fibre properties of these fibres were first characterised to study the effect of textile processes. Novel unidirectional reinforcements have been fabricated after optimising the processes such as unidirectional stitching and spreading technology. Composites were manufactured via low pressure RTM process using an epoxy resin. Stiffness and failure characteristics of reference, interply, intraply and intermingled hybrid composites were then characterised in quasi-static tensile, compression and flexural loading conditions. The hybrid (synergistic) effect were evaluated for these composites by comparing the hybrid composite properties with a carbon reference composite. To understand the failure behaviour under different loading conditions, a fractography study was conducted. Interply hybrids slightly increase the failure strain in tension but demonstrate negative synergy in all other properties. On the other hand, intraply hybrids show a synergistic effect in both tensile and compressive strengths, while not reducing the failure strain. A spread tape intermingled hybrid composite demonstrates a superior mechanical performance when compared to other hybrids. The presented results reveal the potential benefits of hybridisation at different levels and dispersions. The results provide a driving force for future work on hybrid composites and their processing.

KEYWORDS

Hybrid textile reinforcements, structural composites, inter/intraply hybrids, intermingled hybrids, mechanical properties, hybrid/synergistic effect.